THE APPLICATION OF MOIRE INTERFEROMETRY TO AUTOMATED 3-DIMENSIONAL INSPECTION

by

Joseph M. Wander
B.S.M.E. Virginia Polytechnic Institute and State University
(1982)

Submitted in partial fulfillment of the
degree of

MASTER OF SCIENCE in MECHANICAL ENGINEERING

at the

MASSACHUSETTS INSTITUTE OF TECHNOLOGY

January, 1985

Signature of Author _____
Department of Mechanical Engineering
January 18, 1985

Certified by _____
Steven Dubowsky
Thesis Advisor

Accepted by _____
Ain A. Sonin
Chairman, Departmental Graduate Committee

The Application of Moire Interferometry to
Automated 3-Dimensional Inspection

by

Joseph Wander

Submitted to the Department of Mechanical Engineering on
January 18, 1985 in partial fulfillment of the requirements
the degree of Master of Science in Mechanical Engineering

Abstract

Moire Interferometry is a technique which utilizes interference fringes produced by two repeating patterns to gain information about an object. This thesis is concerned with developing tools for the application of moire interferometry specifically to automated inspection of the shape of manufactured parts. In this thesis analytical models for moire interferometry for both diffusely and specularly reflecting objects are developed to be useful for designing and evaluating the characteristics of moire interferometers. Also developed is an analytical method for constructing the moire fringe pattern observed on diffusive objects. Verification of the analytical developments are offered through both experimentation and computer aided design (CAD) based simulations. Finally, the utility of the analytical models are demonstrated through the design of moire interferometers for hypothetical inspection tasks.

Thesis Supervisor: Steven Dubowsky, Professor
Mechanical Engineering Department

Table of Contents Page

Acknowledgements

I would like to thank my thesis advisor, Prof. Steven Dubowsky, for his efforts and support. I would also like to thank my colleague, Ron Leonard, for his support and friendship. To my friends who have helped me I express sincere thanks. To my parents, my deepest appreciation, and it is to my parents that I dedicate this work.

Chapter 1 The Application of Moire Interferometry to Automated 3-Dimensional Part Inspection

1.1 Introduction

Inspection of the shape of manufactured parts is to a large extent still performed manually. An automated process which could rapidly inspect the 3-dimensional features of parts would be of great value in industrial processes and quality control. Automated inspection systems could offer high precision inspection with tireless consistency. On line inspection systems could be used to adaptively control manufacturing processes to maintain part quality and thereby avoid costly scrap and rework. It is widely agreed that vision systems have great potential for providing rapid, non-contact, automated part inspection with limited part fixturing and part preparation. Vision based automated parts inspecton systems currently exist [34,35], but these systems have a number of limitations for inspection tasks that require direct determination of the true 3-dimensional shape of an object.

A common method employed by current vision based inspection systems is to extract information from the easily recognized outline features of a part. These features, which contain only 2-dimensional information, are used to imply 3-dimensional part quality. Unfortunately, only flaws that effect the observable outlines on the object can be detected. A serious drawback to this technique is that for defects in the part to be detectable the flaws must be large

for application to automated 3-dimensional inspection [1,2]. The primary advantages of moire interferometry are:

1) direct 3-dimensional information about object shape can be obtained over the entire field of view from a single measurement operation,

2) the accuracy of the method is not directly limited by the spacial resolution of the vision system employed,

3) the system parameters of the moire interferometer can be designed to suit the the inspection requirements and the capabilities of the vision system employed.

The work of this thesis is an initial study in a program dedicated to applying moire interferometry specifically to 3-dimensional automated part inspection. In this study current moire methods are expanded to be more useful in the specific role of 3-dimensional shape inspection. Analytical techniques for predicting and designing the capabilities of moire inspection systems are developed and verified experimentally. The the usefulness of the developed techniques are then demonstrated through a design example for hypothetical inspection tasks.

1.2 Moire Interferometry

Moire interferomety is a structured light technique, and a very general representation of the process is illustrated in Figure 1-1. As shown, moire interferometry is applicable to both diffusely reflecting (like white paper) and specularly reflecting (mirror like) objects. The application of moire interferometry to diffusive or specular objects is fundamentally different, and in both this work and

enough to be directly resolvable to the vision system employed. For many systems this requires that defects must be about 1/2 % of the dimension of the part contained in the field of view, which is too coarse a measurement capability for many applications.

Structured light techniques are used to directly obtain 3-dimensional information about an object. Conventional structured light techniques commonly extract 3-dimensional information about an object by analysing the intersection between the object and a known ray or a plane of light. However, with these techniques the information obtained is limited to a point or a line on the object, and as with 2-dimensional inspection, the accuracy of the system is directly limited by the resolution of the vision system. Structured light can be used to examine shape of the entire object by moving the object in the structured light field, although such techniques require extensive computation time.

Stereo vision techniques can be used to compute the spatial location of points on an object that are common to the field of view of two cameras. Stereo vision is severly limited for general shape inspection by the need for the common point to be recognizable to the vision system software in both fields of view. Also, the accuracy of the system is again directly limited by the vision system resolution.

Moire interferometry, which is a structured light technique utilizing a field of structured light, posseses several potential advantages over the methods prevously described for direct 3-dmensional optical inspection of the shape of objects. Because of theses advantages, moire interferometric methods have been suggested

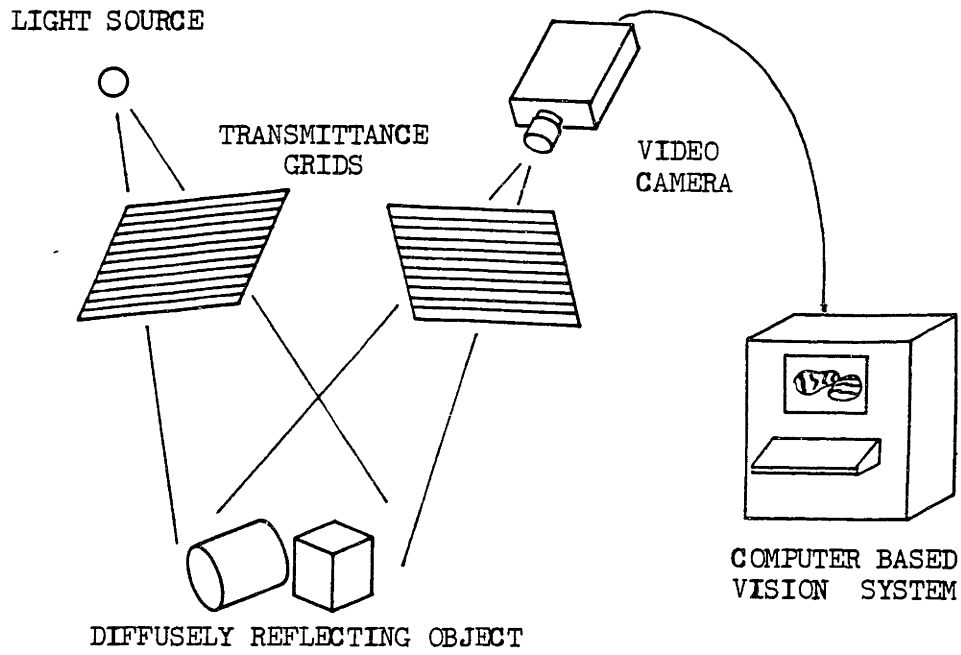

1-1 (a) Diffuse Moire Interferometery

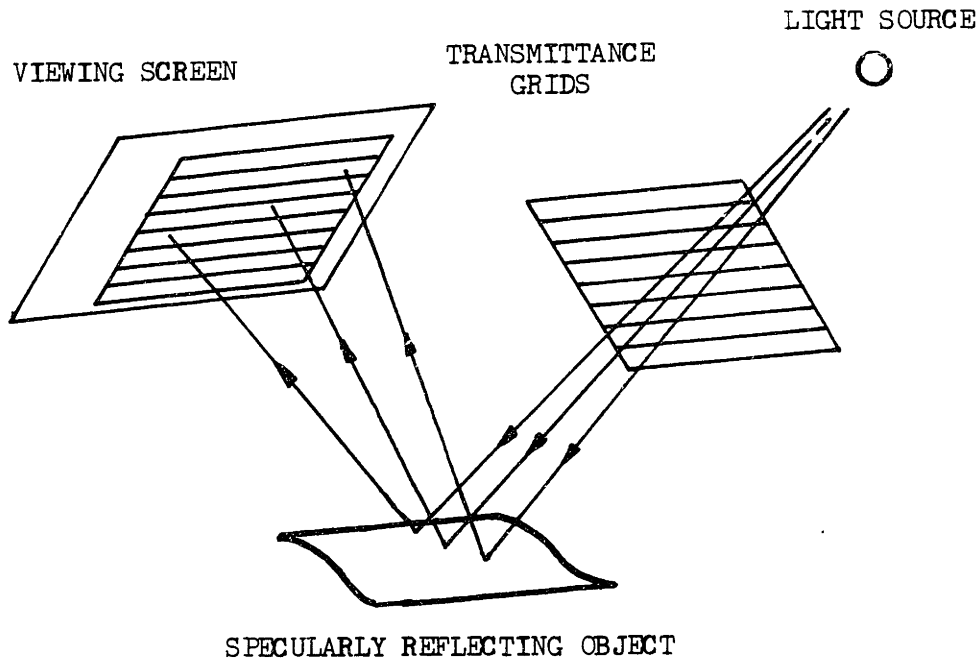

1-1 (b) Specular Moire Interferometry

FIGURE 1-1 General Representations for Moire Interferometry

in the literature there is a clear division between the two.

Moire interferometric techniques for diffusive objects usually involve projecting a field of structured light onto an object, creating alternating lines of light and shadow. Almost exclusively the structured light field consists of alternating planes of light and shadow obtained by passing a beam of light through a grid which consists of alternating straight dark (low light transmittance) and light (high light transmittance) lines. To clarify what is meant by light transmittance, clear glass has high light transmittance while tinted glass has a lower light transmittance.

The light pattern reflecting off the object is then viewed from some known perspective. Note, the lines of light and shadow on the object will in genaral appear curved as the shadows follow the shape of the object. Thus, the shape of the reflecting pattern depends on the hape of the object. At some point in the viewing process the light intensity pattern imaged from the object is combined with a second alternating light and dark pattern. Most often the reflected pattern is passed through a second transmittance grid. Provided the patterns are similar but slightly different this interference will produce moire fringes. The shape of the object can be inferred from the information contained in the shape of the fringe lines in the moire pattern and the known projection and viewing geometries.

Examples of simple moire patterns produced by the interference (overlap) of two similar but slightly different staight line patterns are illustrated in Figure 1-2. In part a of the figure the spatial frequency of the two patterns are slightly different. In part b the

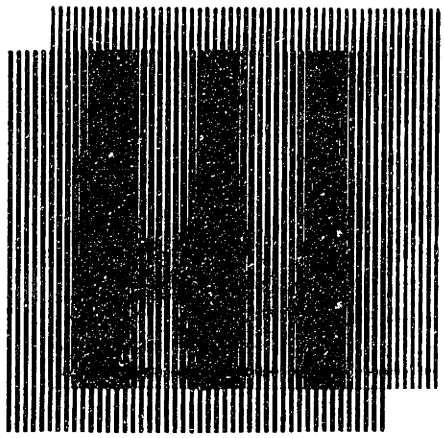

1-2 (a)
Different Spatial
Frequencies

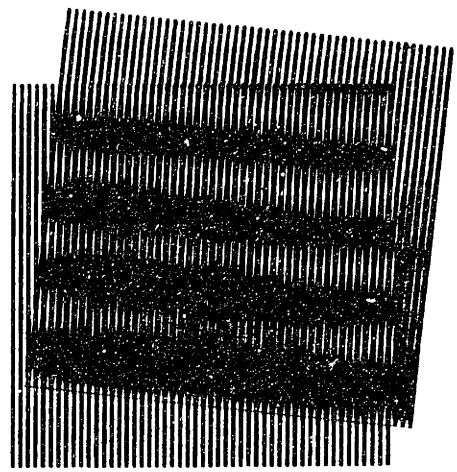

1-2 (b)
Skewed by Small
Angle

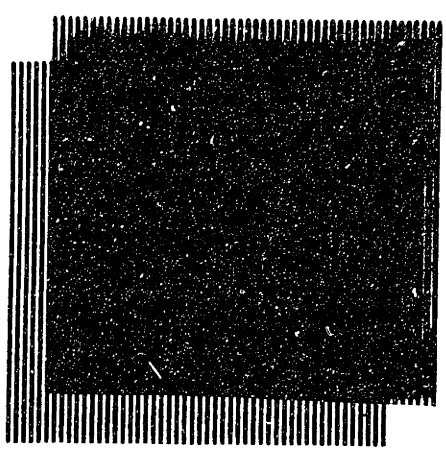

1-2 (c)
Slight Shift

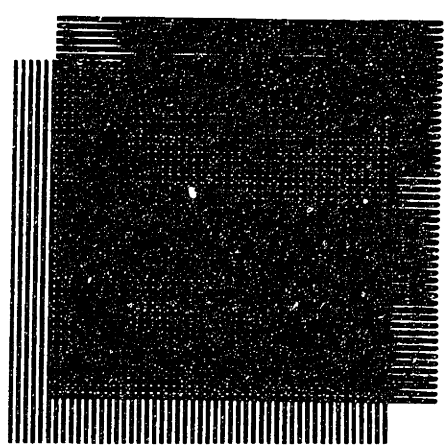

1-2 (d)
Skewed by Large
Angle

FIGURE 1-2 Example Moire Fringe Patterns

two patterns are of equal spatial frequency, but they are skewed by a small angle. Part c and d illustrate two special cases. In c the patterns are identical except for a slight shift in one pattern, and for this case the interference pattern can be interpreted as consisting of one broad moire fringe. In d the patterns are so dissimilar (.e.g. perpendicular) that no moire pattern is visible.

As observed in Figure 1-2, moire fringes are recognizable by changes in the average intensitiy of the combined line patterns. These changes in intensity are caused by changes in the relative orientation of the two interfering patterns. For instance, where the dark lines of the patterns overlap the intensity is a maximum. Where the dark lines of one pattern overlap the light lines of the other pattern the intensity is a minimum. This is important as the relative orientation of two patterns will be used as a means of predicting the changes in the average intensity, and hence the occurance of moire fringes, caused by the combination of the two paterns.

It can be observed in Figure 1-2 that two similar but slightly different high spatial frequency patterns cause the appearence of moire fringes of much lower spatial frequency. Also, small changes in the high frequency patterns result in dramatic changes in the moire pattern. By measureing the large distortions of the low frequency moire pattern the small distortions of the high frequency patterns can be determined. The shape of the high frequency pattern is in turn related to the shape of the object. It is this amplifying effect that enhances the accuracy of moire interference methods.

1.3 Past Work

Moire interferometry has been developed primarily as a laboratory tool. Moire interferometry for diffuseive objects has been used for the measurement of mechanical strain [3,4,9,10] and object shape [1,2,5-9,11-29]. Moire interferometry for specular objects is often called moire deflectometry, as it has been used to measure object properties that are manifested by the deflections of light rays [22-26]. Of concern in this thesis are the moire methods used for object shape measurement, and the potential of these methods for application to automated inspection schemes.

1.3.1 Diffusive Objects

For measurement of the shape of diffusely reflecting objects, moire interferometers have usually been arranged to produce moire fringes that approximate the contour lines (lines of equal depth, as in a geological map) of the object [1-12]. Commonly, the shape of the object is computed from the measured coordinates (usually by hand from a photograph) of points on the observed fringes. The shape of the object is reconstructed using the change in depth (contour interval) between adjecent fringe line centers. As discussed further in section 1.4, this approach is not well suited to object inspection. Reconstructing the gross shape of the object makes no use of the known nominal object shape and limits the accuracy of the technique. Also, contour like fringe maps generally contain complex shapes that are not easily processed by computer vision systems.

Several configurations of diffuse moire interferometers exist and these systems have almost exclusively been used to reconstruct the shape of the object from the countour like fringes. Shadow moire

interferometry [5-8] produces moire fringes using a single grid directly in front of the object. The grid is used to both structure the light incident onto and to interfer with the light intensity (light and shadow) pattern reflected from the object. Provided both the lines of the grid and the structured light pattern on the surface of the object are in the depth of focus of the viewing system, moire fringes will be observed.

Projection moire interferometry [1,11,12] , which is the arrangement illustrated in Figure 1-1(a), uses imaging optics to project structured light onto the object and to view the resulting light intensity pattern on the object. Moire fringes are produced by interfering the image of the intensity pattern on the object (produced by the viewing system) with a second alternating light and dark pattern. Idewsawa [1] and Tou [2] point out that the Projection arrangement is superior for several reasons to the Shadow moire arrangement. The need in Shadow moire interferometry for a light structuring grid as large as the object is elliminated, as well as reducing the depth of field required for the viewing system. By having the patterns used for projecting and viewing indepentent of each other the flexibility of the Projection technique is increased. Also, the components used in the Projection arrangement make the process more suitable for the introduction of computer basesd methods for producing and analysing the moire fringe pattern.

In past work the patterns used to structure the light field and interfer with the intensity pattern on the object have almost exclusively consisted of straight evenly spaced lines. An exception is Double Exposure moire interferometry [15,16], which has been used

to measure the difference in shape between two similar objects. In Double Exposure moire a reference line pattern is produced by photographing the nominal object in a structured light field. Interference between the reference pattern and the pattern produced on a similar object in the same structured light field produces moire fringes that approximate contours of the difference in shape between the two objects. Unfortunately this techqnique also produces fringe patterns with complex shapes, and is sensitive to fixturing errors.

Work has been done to automate moire interferometry for shape measurement, and this work has centered around developing techniques to process contour like fringe patterns. Both interactive [17] and more fully automated [1,2,18,19,20] schemes have been developed for fringe pattern aquisition, recognition, and fringe pattern interpretation. A three-color technique for resolving the depression/elevation ambiguity associated with object countours has been developed, and automated reconstruction of the crossection of objects has been achieved [1].

The object of past moire methods has focused on reconstruction of the object shape as opposed to part inspection. Tou [2], however, describes an automated part inspection technique which determines part quality by a direct comparison of the processed moire contour fringe maps. While this technique eleminates the computational burden of computing the object shape it is still based on the complex and relatively insensitive contour like fringes that represent the gross shape of the object.

1.3.2 Specular Objects

Moire interferometry for specular objects (deflectometry) has been used primarily as a laboratory tool for measuring the slope of nearly flat surfaces [22-25]. Moire deflectometry for shape measurement has not been as extensively developed as moire interferometry for diffusive objects, and automated methods have yet o be developed. As with diffuse moire methods, moire deflectometry has been developed for shape measurement as opposed to part inspection. Also, the only case of moire techniques being applied specifically to measure the shape of a specular object uses an arrangement similar to that shown in Figure 1-1 (b) to detect the slope and small displacements in thin nearly flat membranes [22,23]. The technique is limited to detecting only one component of the surface slope, and the method requires two measurement operations , each for a different system configuration.

Moire deflectrometric techniques have also been developed for phase objects, and these methods seem to have greater potential for automated inspection [24-26] of specular objects. Phase objects are clear (transparent) objects that will deflect rays of light that pass through them. Current moire methods for phase objects pass a collimated beam (parallel light rays) through an object, causing the emerging rays to be deflected a small amount. The deflected rays then pass through two transmittance grids (straight, evenly spaced dark lin patterns) that are spaced by a small distance and then onto an image plane (a screen or a plate of film). Interference between the intensity pattern created by the first grid and the second grid produces a moire pattern on the image plane. The variations in the direction of the rays cause distortions in the nominally (i.. for no

ray deflection) straight evenly spaced moire fringe lines. While the moire methods for phase objects have not been directly applied to specular objects the techniques are directly applicable.

1.4 Current Limitations for Automated Part Inspection

As discussed above in section 1.3, a great deal of work has been dedicated to moire interferomtric methods. The potential for automated part inspection has been suggested, and automated shape measurement and inspection systems have been applied in the laboratory. When considered specifically for automated inspection, however, the methods posses several deficiencies, and these are disussed in this section.

1.4.1 Diffuse Moire

The development of moire interferometry for diffuse objects has been directed toward shape measurement via the contour fringe map of the object. Consequently the methods, with the exception of Double Exposure moire, have been developed to obtain the gross shape of an object. Shape reconstruction, or even the direct comparison of contour like fringes is a poor utilization of the information available from knowlege of the nominal object. Even for simple fringe maps a great deal of computational effort (and time) could be expended to verify that an object is of nominal shape. Also, in general the contour map like moire fringe pattern will not be easily recognizable to the vision system due to the complex shape of the contour like fringes. A more desireable situation would be one in which the fringes have some regular simple shape for the nominal object, and in

which object deformations of interest produce clear and easily recognized deformations in the fringe pattern. However, the analytical tools required to predict or design such a situation have not yet been developed.

While the fundamentals for relating the moire fringe pattern to object shape have been developed, current analyses provide no analytical technique for predicting the observed fringe pattern for a specified object and specified system parameters. The fringe producing characteristics of a specific moire interferometer need to be modeled in a way that is useful for evaluating and designing the shape of the fringe pattern produced on a specific object.

Also, the need for contour fringes to be insensitive enough to map the gross shape of the part restricts the sensitivity of the fringes to small errors in the shape of the object. Double Exposure moire is an important exception since fringes appear only when the object under inspection is different from the nominal object. However, even for Double Exposure moire, the accepted measure of sensitivity (contour depth) only indirectly measures the sensitivity of the fringes as observed from the perspective of the vision system. In order to design of evaluate the capabilities of a moire inspection system the analysis needs to be expanded to directly yield the observable fringe sensitivities to specific object deformations.

1.4.2 Specular Moire

The current methods for moire deflectometry are not capable of general 3-dimensional shape measurement of specular objects. The current methods for speculr objects and phase objects, as outlined above, are only capable of measuring one component of ray deflections caused by the object, and hence one component of the object surface. This limitation is fundamental to the moire process employed (specifically the use of straight line grid patterns). Complete information can be obtained by performing at least two inspections operations, each for different system orientations, but the methods for doing this have not been developed.

Given the limitations above, the moire methods developed for phase objects seem promising for automated inspection of the shape of nearly flat specular objects. The current analyses are, however, developed in terms of variables that are suitable for manual analysis, but not for automated inspection. Specifically, the method is deficient of expressions for the nominal fringe lines. Furthermore, current methods only measure one component of the variation of the rays deflected (or reflected in the case of specular objects) from the object.

1.5 Development Goals

The overall research goals of our ongoing program at MIT are the development of an automated 3-dimensional part inspection technique based on moire interferometry that will be very accurate, high speed, compatible will the limitations of modern conventional vision systems, and which will exploit the design power of computer aided design (CAD) techniques. Unlike most previously developed moire methods, the

techniques will be specifically directed to the design and evaluation of part inspection systems.

The research currently being persued to accomplish these goals can be separated into three areas.

1) Analytical development (for both diffuse and specular moire configurations) of relations capable of directly predicting the observed fringe pattern shape and properties, including sensitivities.

2) Development of CAD simulations for the diffuse and specular moire interferometers which utilize the part representation and inspection requirements to evaluate and design inspection stations [29].

3) Experimental demonstrations to evaluate the validity and practicallity of the developing methods.

The work of this thesis contributes in areas 1 and 3. Moire methods for both diffusive and specular objects are reconsidered specifically for inspection, and the methods are extended when appropriate. Work in area 2 was developed in tandem with the work of this thesis by Ron Leonard [29], and the CAD generated fringe patterns presented here are from his work.

In Chapter 2 the phenomena of moire fringes is explained and modeled mathematically. The relations developed in Chapter 2 involve a quantity called the 'fringe order', which has appeared under various titles in much of the literature on moire interferometry. This quantity is explained in physical terms.

In Chapter 3 the basic relations for Projection moire interferometry for diffusive objects are rederived and extended. Contributions to diffuse moire methods include a scheme for

analytically constructing the observed fringe pattern for a given object (section 3.3), and an approximate closed form method for directly computing local geometric fringe properties as observed from the perspective of the viewing system (section 3.5). The fringe properties, which are calculated based on the equiorder surface concept of Idewsawa [1], include fringe spacing, angle, spacing and angular sensitivities to object orientation, and fringe position sensitivity (fringe shift) to object position.

The analysis of Chapter 3 was developed for a Projection type moire arrangement which utilizes real imaging type optics. In Chapter 4 the analysis for diffusive objects is repeated for the special case of collimated imaging.

In Chapter 5 experimental verification is offered for the analysis of Chapter 3. Moire fringe patterns obtained experimentally are used to verify the analytical fringe construction technique of section 3.3 and the approximate relations for the geometric properties of the fringe pattern of section 3.5. Also, a CAD based emulation of the moire process is used to produce simulated moire fringe patterns which are also compared against the analytical results [29]. In general there is good agreement between the analytical, the experimental, and the CAD generated results.

In Chapter 6 the usefulness of the closed form relations for fringe properties and the fringe construction tequniques as design and evaluation tools for diffuse moire inspection systems is demonstrated. Moire interferometers for two hypothetical inspection tasks are designed using the analytical tools developed in Chapter 3, and the

moire fringe patterns associated with the inspection tasks are analytically constructed.

In Chapter 7 the basic relations for moire interferometry for specular objects are developed. In the analysis the current moire techniques for phase objects are extended to allow the calculation of at least one component of the object surface slope from the coordinates and fringe order of a point on the moire fringe pattern. Also, relations that are useful in scaling the parameters of a moire interferometer to yield a specified sensitivity are developed.

In Chapter 8 the analysis for specular moire interferometry of Chapter 7 is verified experimentally. Moire fringe patterns produced on a thin polished steel disk deflected at its center are analysed using the relations of Chapter 7. The experimatal results for the deflection angls of the rays reflected off the disk are compared with theoretically predicted values. Also, CAD generated simulations of the moire fringe pattern produced with the disk are analysed, and the results compared against the theoretical values [29]. In general the results are positive and indicate that the analysis of Chapter 7 is valid.

Chapter 2 Modeling Moire Fringe Patterns

As illustrated in Figure 1-2, moire fringes are produced by the interference of two similar but slightly different repeating patterns. In this chapter the phenomenon of moire fringes is discussed in detail. A mathematical model for the phenomena, which is used in subsequent chapters of this thesis, is developed. In the process of modeling moire fringes a quantity called the 'fringe order' is developed. This quantity is important because it relates the intensity of the moire fringe pattern to the orientation of the interfering patterns. The fringe order has appeared in several forms and under several titles in the literature, and seems to be fundamental to modeling the occurence of moire fringes. Unfortunately, clear explaination of this quantity and its physical significance is not given in the literature, and this chapter tries to fill that void.

2.1 Pattern Interference

For all of the moire interferometer arrangements considered in this thesis an intensity pattern coming from a structured light pattern on the object and a transmittance grid consisting of alternating high and low light transmittance combine (interfere) to produce the moire fringe pattern. Interference between the two patterns occurs as the intensity pattern from the object passes through (i.e. is modulated by) the transmittance grid. Thus, the

local intensity of the resulting light pattern on the image plane, which is behind the transmittance grid in the viewing system, is the product of the local intensity and the transmittance. For simplicity the repeating light intensity pattern coming from the object will be called simply the intensity pattern. Also, the repeating and alternating transmittance grid that interfers with the intensity pattern will be called the transmittanc grid, and the resulting intensity pattern will be rightfully called the moire pattern.

2.2 Relative Pattern Alignment

It was stated above that changes in the relative pattern alignment cause the changes in the average intensity that are recognized as the moire pattren. By average intensity it is meant that the intensity variations in the moire pattern are of a spatial frequency that is significantly lower than the spatial frequency of either the intensity pattern or the transmittance grid. What is recognized as the moire pattern consists of the low frequency intensity variations that would remain if the high frequency intensity fluctuations were averaged (or filtered) out.

To illustrate what is meant by the relative pattern alignment and how this effects the average intensity, consider Figure 2-1. Figure 2-1 shows in cross section interference between an intensity pattern and a transmittance pattern for two different relative alignments. As represented the transmittance pattern alternates between complete transmittance (transmittance of 1) and complete opacity (transmittance of 0). The alternating intensity pattern is modulated by the

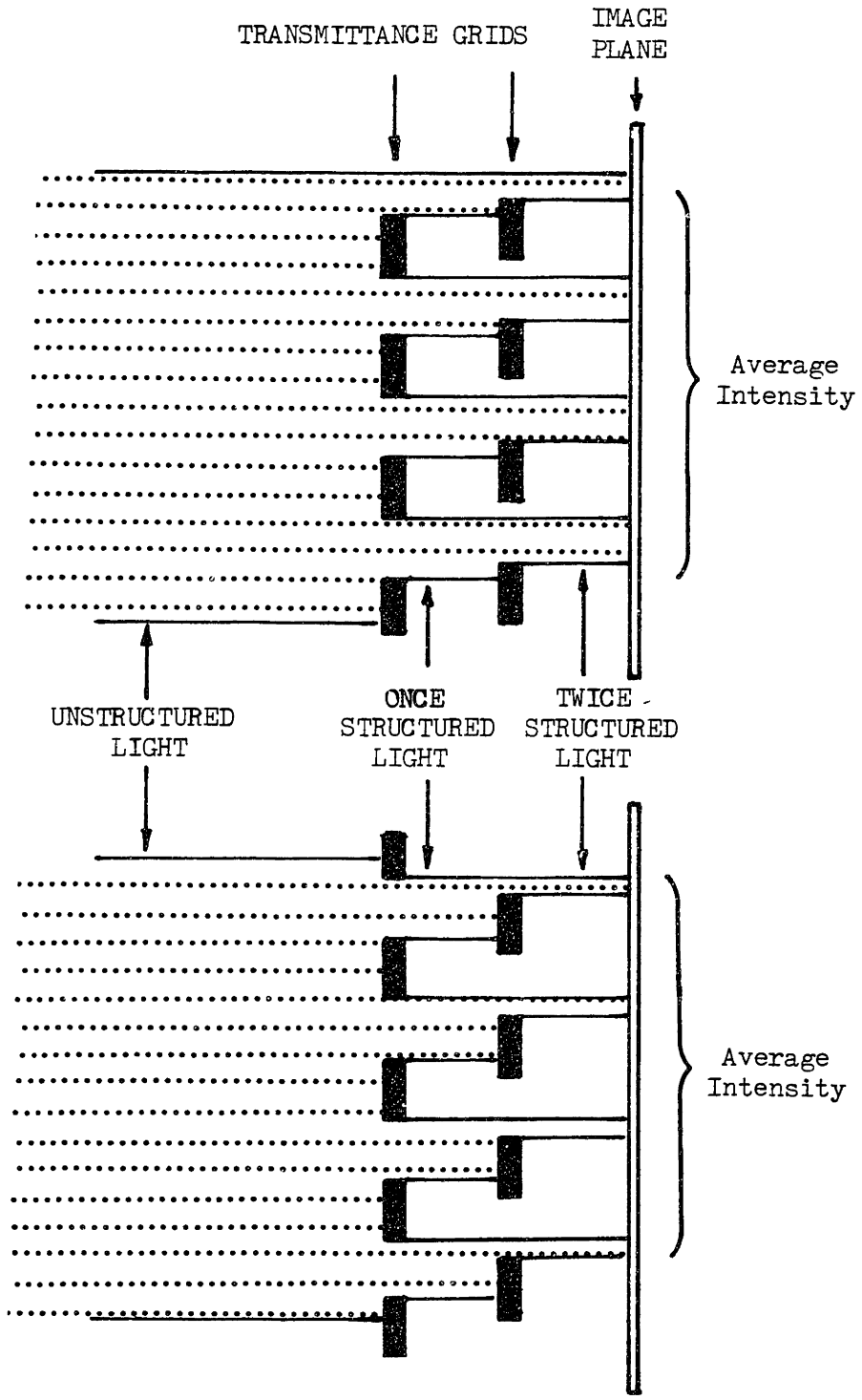

FIGURE 2-1 The Effect of Relative Alignment of the Transmittance Grids

transmittance grid on its way to the image plane. For the two cases shown the alignment between the lines of the intensity pattern and the transmittance pattern changes. It should be clear from Figure 2-1 that the average intensity on the viewing plane is effected by the change in alignment between the patterns.

2.3 Mathematical Model for Patterns, and Fringe Order

As illustrated above, a specific state of alignment between the intensity pattern and the transmittanc grid can be associated with a specific average intensity on the image plane. Consequently, changes in the relative alignment of the intensity pattern and the transmittance grid will produce changes in the average intensity on the image plane. It is this variation in the average intensity that is recognized as a moire fringe pattern.

A mathematical expression for the relative alignment of the interfering intensity pattern and transmittance grid can be used to predict the average intensity and, hence, the moire fringe pattern. In developing such an expression it is first neccessary to consider the intensity pattern and the transmittance grid separately

In all of the Figures presented thus far the patterns that interfer to produce moire fringes have been straight and evenly spaced line patterns. For this discussion the condition that the lines need to be straight will be relaxed. This is appropriate because the lines of the intensity pattern that come from a 3-dimensional object in a structured light field will in general not be straight when viewed from the perspective of the viewing system. The lines of the

transmittance grid are also considered to be curved. The intensity pattern and the transmittance grid are still be assumed to be alternating, that is consisting of alternating maximum and minimum intensity or transmittance. Note the term 'lines' of the intensity pattern or transmittance grid implies the lines of constant minimum or constant maximum intensity or transmittance since it is these lines that are most naturally recognized by the observer. It is important to realize that the intensity and transmittance are in general contiuously changing across the field between maximum and minimum values.

More concisely stated, the intensity pattern and the transmittance grid can be represented as periodic functions of planar position (i.e. spatialy periodic in 2-dimensions). A general expression for the intensity pattern, I, and the transmittance grid, T, as a function of cartesian coordinates Xv and Yv on the viewing system image plane can be written:

$$I = f(n_i) \; ; \; n_i(X_V, Y_V) \qquad (2\text{-}1\ a)$$

$$T = g(n_t) \; ; \; n_t(X_V, Y_V) \qquad (2\text{-}1\ b)$$

where f and g are periodic functions of the variable n_i and n_t (called the profile number), and where the subscripts i and t simply denote the intensity pattern and the transmittance grid, respectively. The profile number is in turn a function of the image plane coordinates, Xv and Yv.

The profile number can be thought of as simply an alternate coordinate in which the intensity and transmittance functions can be expressed. The relationship between the profile number and the image plane coordinates is such that lines in the image plane of constant profile number coincide with lines of constant intensity or transmittance. Also, the profile numbers are defined such that intergral values of the profile number correspond to points of minimum intensity or minimum transmittance. Thus, the profile number of adjecent lines of minimum intensity or transmittance would differ by one.

Figure 2-2 illustrates an intensity pattern and a transmittance grid in the image plane. The lines in the figure represent lines of minimum intensity and minimum transmittance. This means that the lines also represent lines of integral intensity profile number and transmittance profile number. Figure 2-3 illustrates the arbitararily assumed profile of the intensity and transmittance patterns along the cross sections indicated in Figure 2-2. Figure 2-4 shows the intensity and transmittance profiles along the same cross section as in Figure 2-3 except plotted as a function of profile number. As shown in Figure 2-3, while the profile expressed as a function of cartesian distance along the crossection is alternating but not periodic. However, as shown in Figure 2-4, the profile expressed as a function of profile number is periodic (regularly repeated profile) with a period of unity.

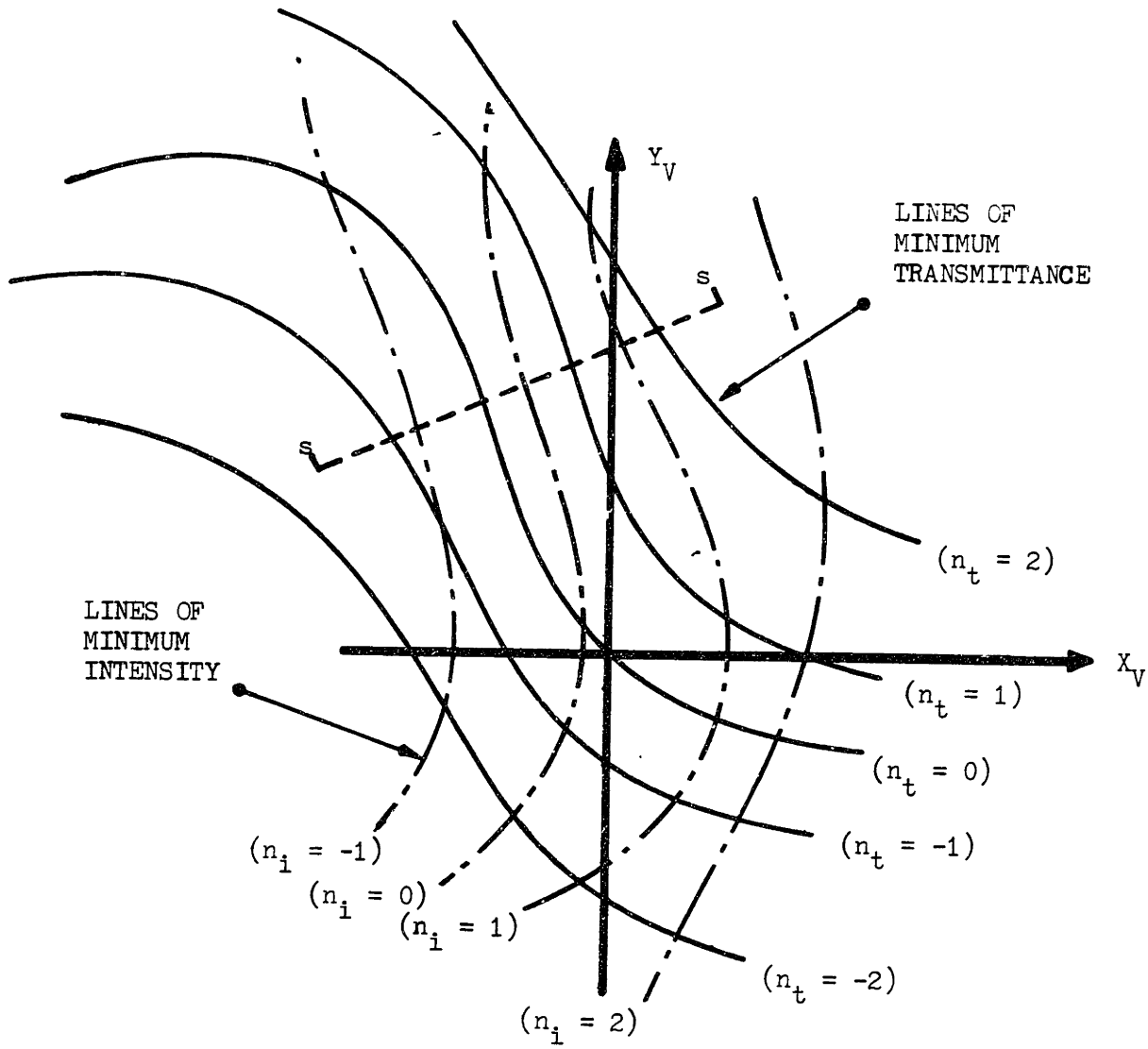

n_i : Profile number for intensity pattern

n_t : Profile number for transmittance pattern

FIGURE 2-2 General Representation for Interfering Patterns

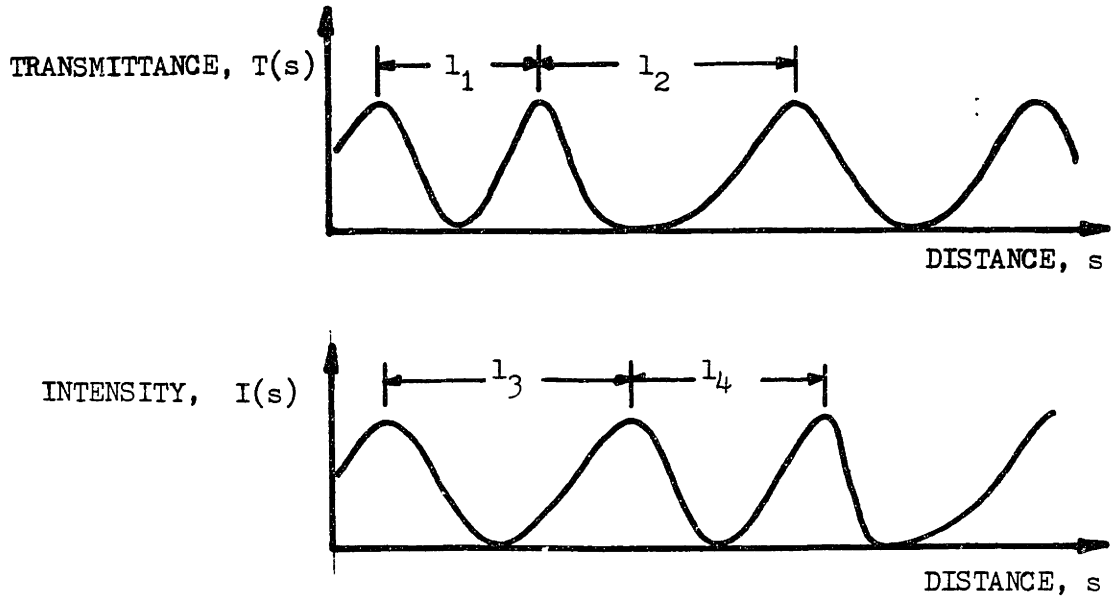

$$l_1 = l_2 = l_3 = l_4$$

FIGURE 2-3 Intensity and Transmittance Profiles as a Function of Distance on the Image Plane

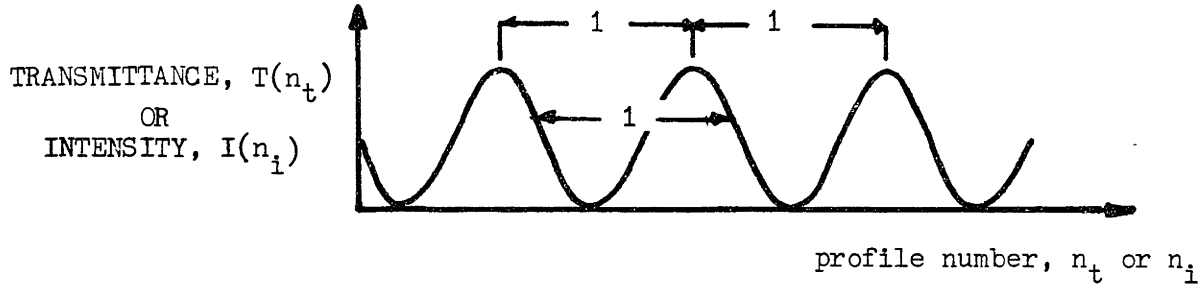

FIGURE 2-4 Intensity and Transmittance Profiles as a Function of Profile Number

As indicated in Figure 2-4 the profile number is, by definition, related to a specific point (i.e. intensity or transmittance value) on the profile. Thus, any two points that have the same profile number or that have profile numbers that differ by an integer will have the same intensity(I) or transmittance(T). Note, the transformation between the profile number and the viewing plane coordinates $n_t(X_V,Y_V)$ and $n_i(X_V,Y_V)$ of equation 2-1 will in genaral not have a simple analytical expression. Straight and evenly spaced patterns are an important exception, and are discussed later in this chapter.

With the profile numbers for the intensity pattern (n_i) and the transmittance grid (n_t) defined as described above, the difference between the profile numbers (n_t - n_i) indicates the relative alignment between the two patterns. To illustrate this consider Figure 2-3 again. As can be seen, changes in the alignment betwween the patterns is reflected by a change in the difference in the profile numbers. This leads to the defining expression for the relative alignment, R.A.:

$$R.A. = n_t(X_V, Y_V) - n_i(X_V, Y_V) \qquad (2\text{-}2)$$

It was previously stated that the relative alignment determines the average intensity (high spatial frequencies averaged). To show this consider the case of an intensity pattern and a transmittance grid with sunusouidal cross section (alternating between 0 and 1) when ploted as a function of profile number. This case corresponds to

Figure 2-4. The expressions for the intensity (I) and (T) along the crossections can be expressed as a function of profile number as follows:

$$I = \tfrac{1}{2} \text{ SIN } \{(2n_i (X_V, Y_V) - 1)\pi\} + \tfrac{1}{2} \qquad (2\text{-}3\ a)$$

$$T = \tfrac{1}{2} \text{ SIN } \{(2n_t (X_V, Y_V) - 1)\pi\} + \tfrac{1}{2} \qquad (2\text{-}3\ b)$$

Interference along the crossection occurs as the intensity pattern is modulated by the transmittance grid. The resulting intensity (Im) along the crossection is, therefore:

$$\begin{aligned} Im = I \times T = {} & \tfrac{1}{4} + \tfrac{1}{4} \text{ SIN } \{(2n_t - 1)\pi\} \\ & + \tfrac{1}{4} \text{ SIN } \{(2n_i - 1)\pi\} \\ & - 1/8 \text{ COS } \{2(n_t + n_i)\pi\} \\ & + 1/8 \text{ COS } \{2(n_t - n_i)\pi\} \end{aligned} \qquad (2\text{-}4)$$

where n_t and n_i represent $n_t(X_V, Y_V)$ and $n_i(X_V, Y_V)$

The moire pattern is due to the low frequency intensity (i.e. due to the $n_t - n_i$ term) fluctuations, or the last term in equation 2-4. The moire is then, for this simple case at least, a periodic function of the relative alignment, R.A..

An important point is that the high frequency terms of equation 2-4 do not contribute to the moire pattern. What this means physically is that the lines of the interfering patterns, which will have a high spatial frequency, do not need to be resolved to observe the moire fringe pattern.

To show this try this simple experiment. Open the document to Figure 1-2, which shows moire fringe patterns. Prop the document open so that you can walk accross the room and see the figure. Doing so you should find that even though the individual lines of the patterns are too closely spaced to be resolved, the moire fringe pattern is still visible. This is important since it means that a vision system that uses moire fringes for inspection need only resolve the low frequency moire and not the high frequency interfering patterns.

Although never rigorously explained, equations of the form of 2-2 have been used in most previous analyses for moire interferometry. Hopefully, this discussion more clearly explains the physical significance of such relations. To be consistent with the terminology of previous work the relative alignment will hencefourth be refered to as the 'fringe order', and will be denoted Fo. Accordingly equation 2-2 will be rewritten:

$$Fo = n_t(X_V, Y_V) - n_i(X_V, Y_V) \qquad (2\text{-}5)$$

The fringe order, as indicate by the average intensity of the moire fringes on the image plane of a moire interferometer, will be used in in subsequent chapters to determine the relative alignment of the two interfering patterns.

2.4 Representing Straight Line Patterns

The special case when the intensity pattern and or the transmittance grid consist of straight evenly spaced lines is useful to consider in detail for several reasons. First, because straight grids are easy to manufacture (relative to curved grids) almost all moire interferometers use straight grids. This is true of the interferometer analysed in the next chapter. Second, a curved grid could be considered to consist of a collage of small elemental areas which consist of straight line patterns. Thus, an understanding of the simpler case of straight grids may be extendable to curved grids as well.

Figure 2-5 illustrates the minimum lines of either an intensity pattern or a transmittance grid in a plane with cartesian coordinates X an Y. The lines are assumed to be straight and evenly spaced. The equations of the lines of constant minimum intensity or transmittance can be expressed as a function of profile number as follows:

$$X = -Y \tan \alpha + \frac{(n + \Phi)}{\cos \alpha} P \qquad (2\text{-}6)$$

where, α is the angle (positive counter clockwise) of the lines with the Y axis, ϕ is the fraction of a period that the zero profile number line is offset from the origin, and P is the pitch (wavelength) between the lines on the coordinate plane. Equation 2-6 can be rearranged to give the profile number as a function of plane position, yielding:

$$n = (X \cos \alpha + Y \sin \alpha)\frac{1}{P} - \Phi \qquad (2\text{-}7)$$

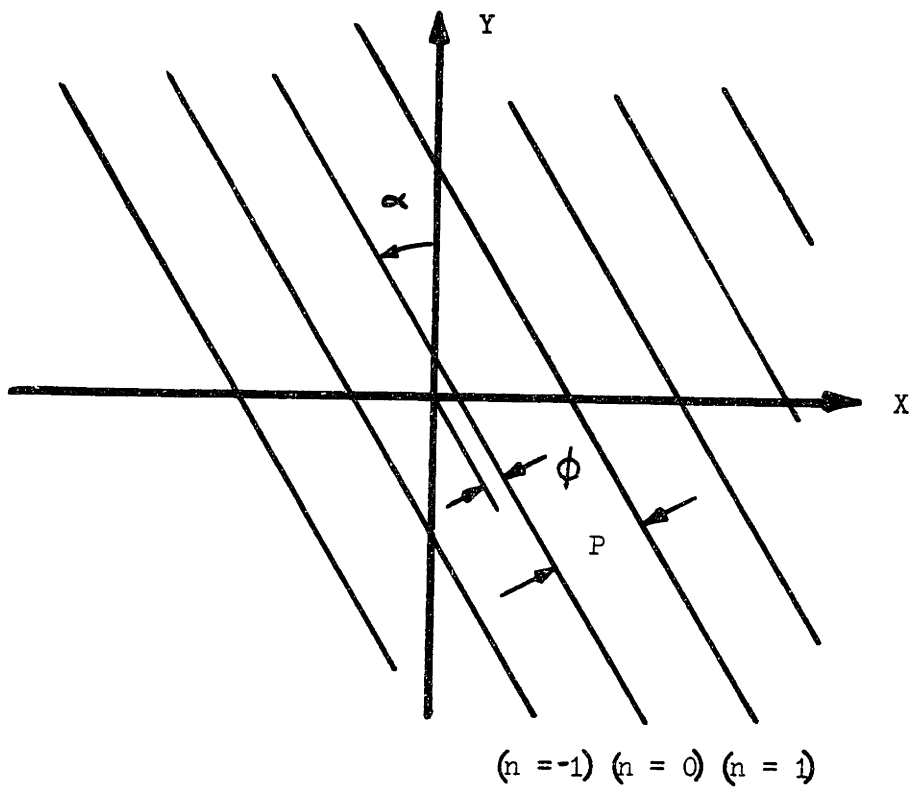

FIGURE 2-5 Straight Line, Evenly Spaced Patterns

Equation 2-7 is of the functional form $n(X_V, Y_V)$ of the mapping (or coordinate transform) indicated for n_i and n_t in equation 2-4. Equation 2-7 expresses the mapping from planar cartesian coordinates X,Y to profile number space, n. Given any plane coordinates, the corresponding profile number coordinate can be determined. The profile number can, in turn, be related to the local intensity or transmittance, provided the profile of the repeating periodic patterns are known (for instance the sinusiodal profile in Figure 2-3 b).

The utility of equation 2-7 will become more apparent through the analysis for a diffuse moire interferometer presented in the next chapter.

Chapter 3. Moire Interferometry for Diffusive Objects.

3.1 Introduction

In this chapter the basic equations for modeling moire interferometry for diffusely reflecting objects are developed. As discussed in Chapter 1, the goal of the relations developed is to expand moire techniques for diffuse objects to be more useful for automated inspection. Before outlining the developments in this chapter, current moire techniques and their deficiencies for automated inspection will be discussed further. This discussion was delayed until this point as it relys on the reader having some understanding of the material presented in Chapter 2.

As discussed in section 1.3, projection type moire interferometry seems to be the most promising configuration for application to automated part inspection. Therefore, it is this configuration that will be analysed. In subsequent chapters if a diffuse moire interferometer is discussed it can be assumed to be of the projection type.

A general schematic for the projection arrangement is illustrated in Figure 3-1. For this arrangement the structured light field (that illuminates the object) is produced using a real imaging projection system, such as an ordinary slide projector. An intensity pattern that is created by illuminating the back of a transmittance grid is projected onto the object. For the analysis, the transmittance grid

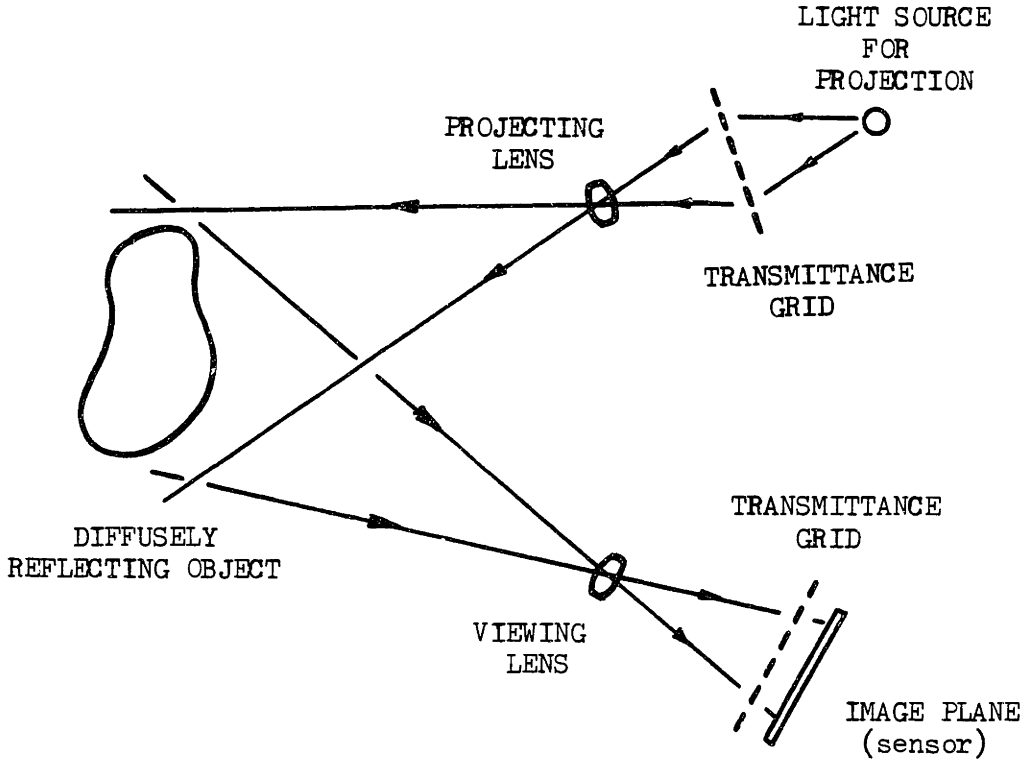

FIGURE 3-1 General Schematic for Projection Type Moire Interferometry

will be assumed to consist of straight evenly spaced dark and light lines. The light and shadow pattern produced on the object, which appears warped as the light follows the contours of the object, is then viewed with a real imaging vision system (like an ordinary camera). The image of the intensity pattern on the object passes through a straight line transmittance grid placed just in front of the image plane of the viewing system. Interference between the image of the intensity pattern from the object and the transmittance grid produces a moire fringe pattern on the image plane.

The moire fringe pattern formed on the image plane contains information about the shape of the object. Specifically, as several authors have shown (eg. [1]), the fringe order, as defined in Chapter 2, and position of the fringes on the viewing plane can be related to the coordinates of the corresponding point on the object. Given complete knowledge of the fringe pattern (and this is not always practical) the shape of the object can be reconstructed.

As discussed in Chapter 1, at present moire interferometry is most commonly used as a laboratory tool for reconstructing the gross shape of an object. This is done by configuring the moire interferometer such that the moire fringes produced for the object approximate the normal contour lines (lines of equal depth) of the object. The positon and order of points on the fringes are then used to calculate the coordinates of points on the object. In this way the shape of the object can be reconstructed.

As discussed in Chapter 1, object reconstruction is not well suited to shape inspection since the need for the fringe lines to be insensitive enough to represent the gross shape of the object limits the sensitivity of the fringes to small errors in the shape of the object. For the purposess of inspection it is only important that the fringes to be a clear measure of the errors in the shape of the object.

Unfortunately, current analyses are oriented toward object reconstuction and the interpretation of moire fringe lines as contour lines. Current analyses are capable of reconstructing the object from the order and position of the fringe lines, but not the reverse. That is, presently there are no analytical techniques for predicting the moire fringe pattern (which means predicting the fringe order and the position of point in the fringe pattern) from knowlege of the object. Such techniques would make it possible to analytically predict the shape of the fringe pattern for a given object, and predict how the fringe pattern would change with changes in the shape of the object.

Relations that are capable of predicting the moire fringe pattern are developed in section 3.3. More specifically, relations are developed that are capable of predicting the location on the viewing plane and the fringe order of a specific point on the moire fringe pattern provided the object coordinates and the system parameters are known.

The relations of section 3.3 are essentially the inverse of the relations that currently exist for object reconstruction. For completeness the relations for the forward problem of computing the

object coordinates from the moire fringe pattern are also developed, and this derivation is presented in section 3.2.

A second major defficiency of current analyses for moire interferometry is that current analyses do not provide a measrue of the sensitivity of the moire interferometer that is well suited to the task of part inspection. The current measure for the sensitivity of an interferometer is based on the interpretation of the moire fringe lines resembling the contour lines of an object. Thus, the current measure for sensitivity is the 'contour interval', or the change in depth associated with the transition from one fringe line to another.

The reason that this is not a good measure of the sensitivity is that it is not a direct mesure of the parameters of concern. What is of concern for part inspection are the visible changes in the fringe pattern associated with small changes in the shape of the object.

When any pattern is analysed information is extracted from the geometric properties of the entities in the pattern. For a moire fringe pattern information is conveyed by the shape and position of the moire fringe lines. For part inspection it is the changes in these geometric features that will be used to gain information about the object. A more suitable measure of sensitivity for part inspection would be, therfore, a direct relation between the features of the fringe pattern and the shape of the object.

With such a relation the capabilities of a particular interferometer, including the resolution and sensitivity, could be evaluated directly in terms of the parameters of interest; the changes in the object and the observable changes in the fringe

pattern. Also, such a relation would be useful in designing the parameters of a moire interferometer to suit a specific inspection task.

The relations for analytically constructing the fringe pattern that are developed in section 3.2 do constitute a direct relation between the object and the observed moire fringe pattern. However, to use such relationships to evaluate sensitivities would require first construction of a fringe pattern for both the nominal and varied object, and then a comparison of the two fringe patterns. Such a procedure could be computationally burdensome. Consequently, a closed form relation to predict the geometric features of the moire fringe pattern from the shape of the object is developed.

The derivation of the closed form relations for the geometric features of the moire fringe pattern is presented in section 3.5. The form of the relations are such that if the parameters of the moire interferometer, the location of the point on the object and the local orientation of the surface of the object are specified, the local geometric properties of the fringe pattern can be calculated. The local geometric properties of the fringe pattern that are calculated include:

1) the direction of the moire fringe line,

2) the spacing between adjecent moire fringe lines,

3) the sensitivity of the direction and the spacing of the fringe lines to changes in the orientation of the object,

4) the sensitivity of the position of the fringe lines to changes in the position of the object.

The relations developed in section 3.5 rely on the concept of the equiorder surfaces of a moire interferometer developed by Idewsawa [1]. Section 3.4 is dedicated to explaining the equiorder surface concept and how the concept is useful. Also, the closed form relations are only approximate relations. To calculate the geometric features of the fringe pattern in closed form it is neccessary to make some simplifying assumptions, and these are explained in section 3.5.

3.2 Computing Object Point Coordinates from Fringe Patterns

Idewsawa [1], among others, shows that from knowledge of the fringe order and coordinates on the image plane of a point on the moire fringe pattern and knowlege of the interferometer geometry one can compute the coordinates of the associated point on the object. Relations capable of performing this calculation are derived in this section. The results are similar to those of Idewsawa. The relations are derived here to give completeness to the analysis for moire interferometry.

3.2.1 Model for Projection Moire Interferometer.

Figure 3-2 shows the analytical model for a moire interferometer. As illustrated in the figure, the reference coordinate frame (X,Y,Z) is located at the node of the optical system used for viewing. The Z axes of the viewing system coincides with the optical axis of the viewing optics, with positive Z values extending toward the object under inspection. The image plane of the viewing system (called the viewing plane) is perpendicular to the optical axis and located a

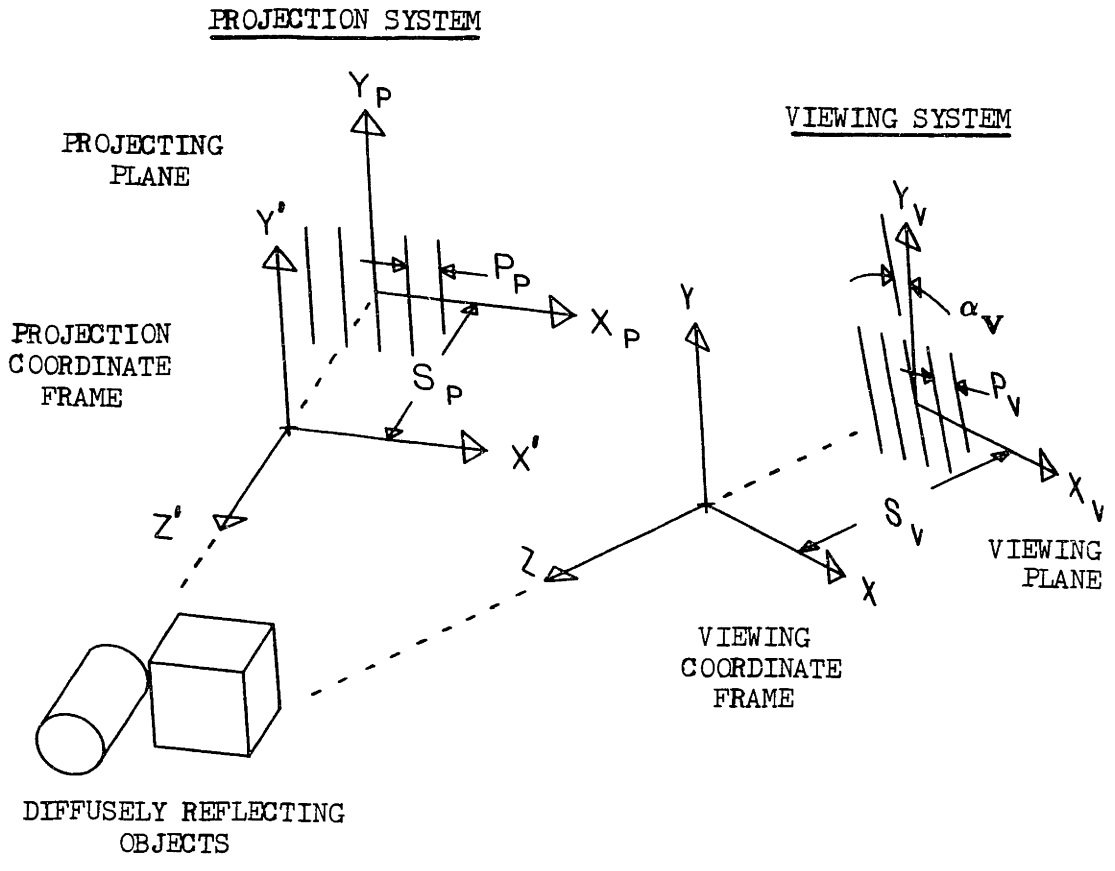

FIGURE 3-2 Analytical Model for Diffuse Moire Interferometry

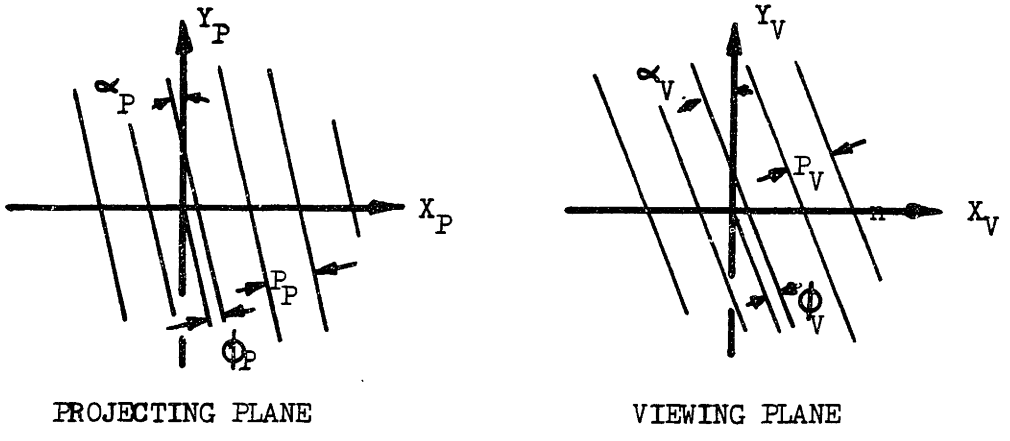

FIGURE 3-3 Transmittance Grids on the Projecting and Viewing Planes

distance S_V along the negative Z axis. Coordinate axes X_V, Y_V on the viewing plane are oriented parallel to the X and Y axis, respectively.

Similar to the viewing system, the origin of the projecting system coordinate frame (X',Y',Z') is located at the node of the optics used for projection, with the optical axis for the projection system coincident with the Z' axes. Also, the image plane of the projection system (called the projecting plane) is perpendicular to the Z' axes and located a distance S_p along the negative Z' axis. The coordinate axes X_p and Y_p on the projecting plane are parallel to the X' and Y' axes, respectively.

The transmittance grids used for projecting structured light onto the object and for interfering with the intensity pattern viewed on the object are modeled as exsting in the projecting and viewing planes, respectively. The mathematical representation for the patterns, which is illustrated in Figures 3-3, is developed as described in Chapter 2. Accordingly, the equations for lines of constant intensity or transmittance become:

$$X_V = - Y_V \tan \alpha_V \div \left(\frac{n_V + \Phi_V}{\cos \alpha_V}\right) P_V \qquad (3\text{-}1\ a)$$

$$X_p = (n_p + \Phi_p) P_p \qquad (3\text{-}1\ b)$$

(for $\alpha_p = 0$)

where the subscripts v and p refer to the viewing and projecting systems, P is the pitch of the pattern, n is the profile number (as defined in Chapter 2), ϕ is the fraction of period that the zero profile number grid line is offset from the origin, and α is the angle measured positive counterclock wise of the pattern lines relative to the Y axes in the image plane. Note that for the projecting system α_p is always assumed to be zero.

The orientation of the projection system coordinate frame is specified relative to the viewing system (reference) coordnate frame. The origin of the projecting frame is located at viewing frame coordinates Xo,Yo,Zo, as shown in Figure 3-4 (a). The orientation of the projecting frame is represented by the three sequential current frame rotations θ , ξ , ψ, about the X,Y, then Z axes (resectively) that would bring the viewing frame into the same orientation as the projecting frame. That is, the viewing frame could be placed into the orientation of the projecting frame by first rotating the viewing frame about its X axis through an angle θ, then by rotating through an angle ξ about the new (current) Y axis, and finally by rotating through and angle ψ about the new (current) Z axis. This process is illustrated in Figure 3-4 (b). By locating the projecting system coordinate frame in this way the coordinate transformation between the viewing frame to the projecting frame can be determined using homogeneous (or 4 by 4) transforms. This transformation can be written:

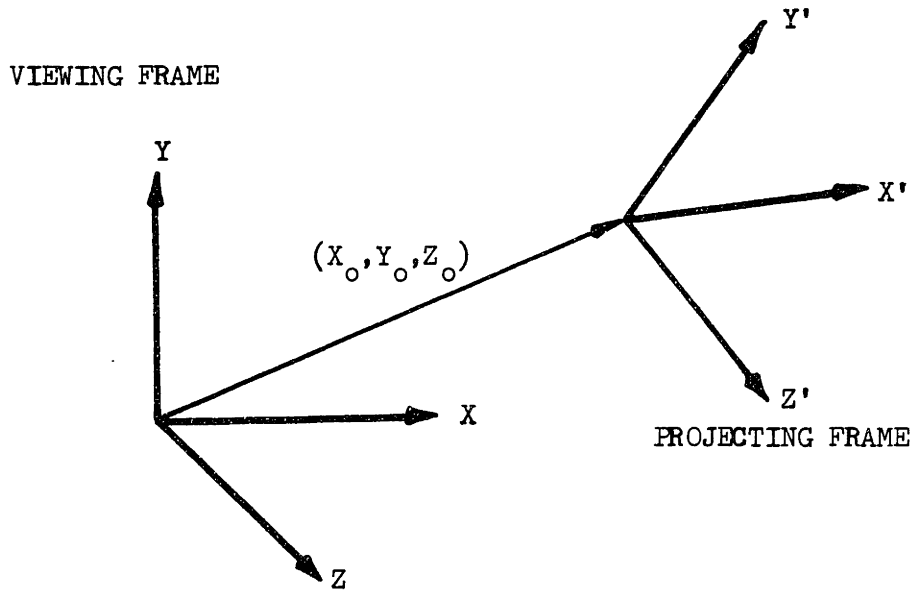

3-4 (a) Relative Positioning of Coordinate Frames

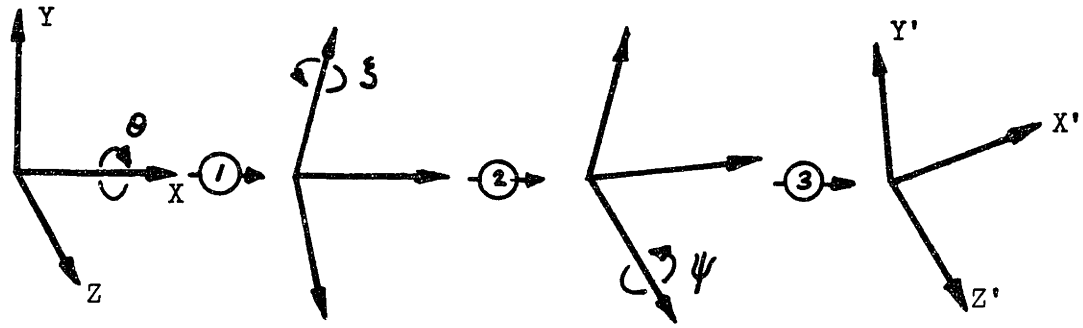

1: Rotate θ about X axis
2: Rotate S about new (current) Y axis
3: Rotate ψ about new (current) Z axis

3-4 (b) Relative Orientation of Coordinate Frames

FIGURE 3-4 Parameters for Orienting the Projecting Frame Relative to the Viewing Frame

$$\begin{bmatrix} X' \\ Y' \\ Z' \\ 1 \end{bmatrix} = \begin{bmatrix} T_1 & T_2 & T_3 & T_X \\ T_4 & T_5 & T_6 & T_Y \\ T_7 & T_8 & T_9 & T_Z \\ 0 & 0 & 0 & 1 \end{bmatrix} \begin{bmatrix} X \\ Y \\ Z \\ 1 \end{bmatrix} \qquad (3\text{-}2)$$

where

$$\begin{aligned}
T_1 &= \cos\Psi \cos\zeta \\
T_2 &= \sin\Psi \cos\Theta + \cos\Psi \sin\zeta \sin\Theta \\
T_3 &= \sin\Psi \sin\Theta + \cos\Psi \sin\zeta \cos\Theta \\
T_4 &= -\sin\Psi \cos\zeta \\
T_5 &= \cos\Psi \sin\Theta + \sin\Psi \sin\zeta \sin\Theta \\
T_6 &= \cos\Psi \sin\Theta + \sin\Psi \sin\zeta \cos\Theta \\
T_7 &= \sin\zeta \\
T_8 &= -\cos\zeta \sin\Theta \\
T_9 &= \cos\zeta \cos\Theta \\
T_X &= -(T_1X_O + T_2Y_O + T_3Z_O) \\
T_Y &= -(T_4X_O + T_3Y_O + T_4Z_O) \\
T_Z &= -(T_YX_O + T_8Y_O + T_9Z_O)
\end{aligned}$$

The method of developing the transformation, which involves using matricies to represent translations and rotations, can be reviewed in Hartenberg and Denavit[30] or Paul[31].

It is assumed for this derivation that both the fringe order, Fo, as defined in Chapter 2, and the exact position (X_V, Y_V) on the viewing system image plane (viewing plane) are known for a point in the moire fringe pattern.

3.2.2 Analysis

What is sought in this analysis are the object coordinates (X,Y,Z) corresponding to the observation of a moire fringe of a known order at a known point on the viewing plane. Also, it is assumed that the parameters of the interferometer are known, as are the the fringe order and the coordinates on the viewing plane.

The fringe order can be related to the two patterns that interfere on the image plane to form the moire fringes via the equation for fringe order developed in Chapter 2 (equ. 2-2). Refering to Figure 3-2, the two patterns that interfer in this case are the pattern of the viewing grid and the intensity pattern from the object that was illuminated by the shadow pattern of the projecting grid. Consequently the profile numbers that belong in the equation for fringe order are the profile numbers of the viewing grid and the profile number of the intensity pattern. The profile number of the viewing grid is n_V, as appears in the equation for the lines of the profile grid (Equation 3-1 a). The profile number for the intensity pattern, n_p, is the profile number of the projecting grid, as appears in the equation for the lines of the projecting grid (Equation 3-1 b).

Note that the profile number of the projecting grid is associated with the intensity pattern on the viewing plane. This simply implies that a line in the intensity pattern with a given profile number is the image of a point on the object that was illuminated by a line in the projecting grid with the same profile number.

The equation for fringe order can then be written for this case as:

$$Fo = n_V - n_P \qquad (3\text{-}3)$$

Because the viewing plane coordinates X_V and Y_V are known, the profile number for the transmittance grid, n_V, is determinable from Equation 3-1 a. Thus, the profile number of the projecting grid is the only unknown quantity in Equation 3-3. Rearranging Equation 3-1 a and substituting into Equation 3-3 yields:

$$n_P = [(X_V \text{ COS } \alpha_V) + (Y_V \text{ SIN } \alpha_V)] \frac{1}{P_V} - \Phi_V - Fo \qquad (3\text{-}4)$$

At this point the geometric constraints imposed by the projecting and viewing optics are considered. Knowing that the object point was imaged to the point X_V, Y_V constrains the object point to be on the ray (line) that passes through the point X_V, Y_V and the node of the viewing system coordinate frame. Furthermore, having determined the profile number of the projecting grid constrains the point on the object that is imaged to the point X_V, Y_V to having been illuminated by the n_p profile number line of the projecting grid. Geometrically this can be interpreted as constraining the object to be in a plane defined by the n_p profile line of the projecting grid and the node of the projecting system coordinate

frame.

To isolate the object point coordinates it is then neccessary to find the point that satisfies both these constraints. Interpreted geometrically this means that the intersection point between the plane and the line that have been described needs to be determined.

The profile number of the projecting grid is related to the projecting plane coordinates by Equation 3-1 b. If the profile number, n_p, is fixed Equation 3-1 b constraines X_p to be a certain value. Rearranging Equation 3-1 b to yield the projecting plane X coordinate as a function of projecting grid profile number yields:

$$Xp = np/Pp \qquad (3\text{-}5)$$

(where Op is assumed to be zero)

The line containing the point X_V, Y_V and the origin of the viewing system coordinate frame can be expressed in viewing system coordinates by the following set of equations:

$$X_V = -S_V(\frac{X}{Z}) \qquad (3\text{-}6\ a)$$

$$Y_V = -S_V(\frac{Y}{Z}) \qquad (3\text{-}6\ b)$$

The equation of the plane defined by the n_p profile line of the projecting grid and the origin of the projection system can be expressed in projection system coordinates as follows:

$$X_p = -S_p\left(\frac{X'}{Z'}\right) \tag{3-7}$$

To combine Equations 3-5 and 3-6 a and b with the constraint expressed in Equation 3-7 it is first neccessary to transform Equation 3-7 from projection system coordinates, X',Y',Z', to viewing system coordinates, X,Y,Z. This can be accomplished using Equation 3-2. The expressions for X' and Y' in terms of X, Y, and Z can be determined from the first and third rows of Equation 3-2, respectively. Using these relations to replace X' and Z' in Equation 3-7 yields:

$$X_p = -S_p\left[\frac{T_1X + T_2Y + T_3Z + T_X}{T_7X + T_8Y + T_9Z + T_Z}\right] \tag{3-8}$$

Equations 3-5, 3-6 a and b, and 3-8 can be solved simultaneously for the Z coordinate of the object point coordinates (in viewing sytem coordinates). The X and Y coordinates of the point can then be found by rearranging Equations 3-6 a and b to yield the X and Y, respectively, and then back substituting Z. Carrying out these steps you obtain:

$$Z = \frac{AX_V + BY_V + C}{DX_V^2 + EY_V^2 + F(X_V Y_V) + G(X_V) + HY_V + I} \quad (3\text{-}9\ a)$$

$$X = -\left(\frac{X_V}{S_V}\right) Z \quad (3\text{-}9\ b)$$

$$Y = -\left(\frac{Y_V}{S_V}\right) Z \quad (3\text{-}9\ c)$$

where

$$A = -T_Z \cos \alpha_V \frac{P_P}{S_P P_V}$$

$$B = -T_Z \sin \alpha_V \frac{P_P}{S_P P_V}$$

$$C = T_Z Fo \frac{P_P}{S_P} - T_X$$

$$D = -T_7 \cos \alpha_V \frac{P_P}{S_P S_V P_V}$$

$$E = -T_8 \sin \alpha_V \frac{P_P}{S_P S_V P_V}$$

$$F = -(T_7 \sin \alpha_V + T_8 \cos \alpha_V) \frac{P_P}{S_P S_V P_V}$$

$$G = (T_7 Fo + T_9 \cos \alpha_V) \frac{P_P}{S_P P_V} - \frac{T_1}{S_V}$$

$$H = (T_8 Fo + T_9 \sin \alpha_V) \frac{P_P}{S_P P_V} - \frac{T_2}{S_V}$$

$$I = T_3 - T_9 Fo \frac{P_P}{S_P}$$

Note that all of the terms on the right hand side of Equations 3-9 a b and c are known from the geometry of the moire interferometer except for X_V, Y_V, and Fo, which are assumed to be determined from analysing the fringe pattern.

3.3 Computing the Fringe Pattern from Object Coordinates

3.3.1 Introduction

Moire interferometry has been used primarily as a tool for measuring the gross shape of objects. Consequently, the relations of section 3.2, which determine the object coordinates from the known moire fringe pattern, are representative of current analyses for moire interferometry. Because shape measurement has been the primary concern the inverse problem of determining the fringe pattern from the known object shape has not been developed.

In this section relations are developed that are suitable for determining the moire fringe pattern from the known object shape. Specifically, relations are developed which can be used to determine the position and fringe order of a point on the moire fringe pattern (on the viewing plane) from the known coordinates of a point on the surface of the object, and the known interferometer geometry. These relations are suitable for analytically constructing the moire fringe pattern produced by an object in a point by point manor.

The need for the capability to analytically construct the moire fringe pattern arises from considering moire interferometry as an tool for object inspection. Because any vision system used to interpret

the moire fringe pattern will have limited powers of resolution and pattern recognition it is important that the moire fringe pattern be sufficiently simple in shape and sufficiently sensitive to indicate changes in the object. If the fringe pattern could be analytically constructed then the shape and sensitivity of the moire fringe lines for various interferometer and object configurations could be explored analytically. Thus, the relations developed in this section are valuble as a tool to evaluate and design the configuration of the interferometer and object.

3.3.2 Analysis

The equations for predicting the fringe pattern will be derived in this section. The analysis uses the same system models as in section 3.2 for the moire interferometer. The derivation is the inverse of that in Section 3.2 in that for this case it is assumed that the coordinates of the point on the object (X,Y,Z,) are known and the location and fringe order of the associated point on the viewing plane is sought.

The first step is to determine what location on the viewing plane corresponds to the object point. Since the object coordinates X, Y, Z (in the viewing system coordinate frame) are assumed to be known, the perspective transformation (i.e. the equation of the viewing rays) represented by Equations 3-6 a and b can be used to determine the viewing plane coordinates, X_V and Y_V.

Next, the fringe order (Fo) at this point on the viewing plane needs to be calculated. To compute the fringe order it is first necessary to determine the profile number of the viewing grid (n_V) and the profile number of the point on the projecting grid (n_p) that illuminates the object point (X, Y, Z).

The profile number of the viewing grid can be calculated from the viewing plane coordinates X_V and Y_V (as given by Equation 3-6 a and b) using the equation of the viewing grid lines (Equation 3-1 a). Substituting for X_V and Y_V in Equation 3-1 a using Equations 3-6 and solving for the profile number yields:

$$n_V = [(\frac{X}{Z}) \text{ COS } \alpha_V + (\frac{Y}{Z}) \text{ SIN } \alpha_V] \frac{S_V}{P_V} - \Phi_V \qquad (3\text{-}10)$$

To calculate the profile number of the projecting grid (n_p) the X_p coordinate of the point on the projecting plane that illuminates the object point (X,Y,Z), needs to be determined. This can be calculated with Equation 3-7 provided the object coordinates X', Y', and Z' are first expressed in viewing system coordinates. This is done by expressing the projection system coordinates X', Y', Z' in terms of the viewing system coordinates X, Y, Z using Equation 3-2.

Using the expressions for X' and Z' that are given by the first and third rows of Equation 3-2 to replace X' and Y' in Equation 3-7, and solving for the profile number, n_p , yields:

$$n_P = \left[\frac{T_1X + T_2Y + T_3Z + T_X}{T_7X + T_8Y + T_9Z + T_Z}\right]\left(\frac{S_P}{P_P}\right) - \Phi_P \qquad (3\text{-}11)$$

Note that the Op term, that had been assumed zero in equations 3-5 and 3-7, was included in equation 3-11.

The fringe order can now be evaluated by substituting the expressions for the profile numbers (3-10 and 3-11) into the equation for fringe order, Equation 3-3. This yields the following expression for fringe order:

$$\begin{aligned} Fo = &\left[\frac{T_1X + T_2Y + T_3Z + T_X}{T_7X + T_8Y + T_9Z + T_Z}\right]\left(\frac{S_P}{P_P}\right) \\ &- \left[\left(\frac{X}{Z}\right)\cos\alpha_V + \left(\frac{Y}{Z}\right)\sin\alpha_X\right]\frac{S_V}{P_V} \\ &+ (\Phi_V - \Phi_P) \end{aligned} \qquad (3\text{-}12)$$

which expresses the fringe order of a point on the moire fringe pattern in terms of the known object point coordinates and the known geometric parameters of the moire interferometer.

3.3.3 Implimenting the Relations

As discussed in Chapter 2 the fringe order can be related to the intensity of the moire fringe pattern. For instance, points in the moire fringe pattern that have intergal fringe orders will be points of minimum intensity while points in the fringe pattern with intergal + 1/2 fringe order will be points of maximum intensity. Thus, Equation 3-6 and 3-12 can be used to compute the intensity of a point on the fringe pattern. By computing the intensity at many points on the fringe pattern the moire fringe pattern could be analytically constructed.

As a design tool and as a method of verification for this analysis a computer program capable of point by point construction of the fringe pattern was developed. The program uses the relations developed in this section to construct the fringe pattern produced by a flat, diffusely reflecting object for arbitrary interferometer parameters and object orientation. The program, which is described in Chapter 5 (listing in appendix B) uses the calculated fringe order to isolate and draw the lines of minimum and maximum intensity of the moire fringe pattern. Examples of these analytically constructed fringe patterns are shown in Chapters 5 and 6, where they are compared against actual moire fringe patterns.

3.4 The Equiorder Surface Concept

The concept of equiorder surface, introduced by Idewsawa[1], leads to a concise and intuitive way to characterize the fringe producing properties of a moire interferometer. Because of this, the

concept of equiorder surfaces is used as the basis for the closed form analytical relations for the geometric properties of a moire fringe pattern developed in the next section. As the concept is fundamental to work in section 3.5 it will be reviewed in this section.

An equiorder surface is a 3-dimensional locus in the object (viewing) space of a moire interferometer such that any intersections between the locus and the surface of an object will lead to the observation of a moire fringe of a particular order. Alternately, if an equiorder surface of order Fo was to physically exist (which it does not) then one broad fringe of order Fo would be observed on the viewing plane.

To further understand what an equiorder surface is it is helpful to consider how an equiorder surface would be calculated. Equations 3-9 a, b and c give the coordinates of a point as a function of the viewing plane coordinates X_V, Y_V and fringe order, Fo. With the fringe order held constant at Fo you can interpret Equations 3-9 as the three components of the equation of a surface parameterized in the variables X_V and Y_V. This is the equation of an equiorder surface of order Fo. By varying X_V and Y_V over the viewing plane the coordinates of the equiorder surface (X, Y, Z) at different points on the surface can be calculated.

Equiorder surfaces represenatative of two configurations of a moire interferometer are illustrated in Figures 3-5 and 3-6. For each configuration two equiorder surfaces, each for a different value of the fringe order, are shown. Also indicated in the figure are the parameters of the coordinate transformation (i.e. eq. 3-2) that

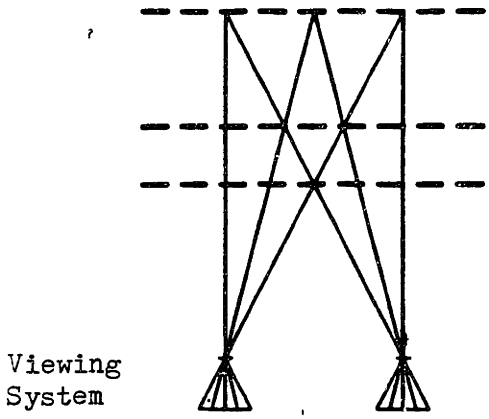

3-5 (a)
Top View of
Equiorder Surfaces

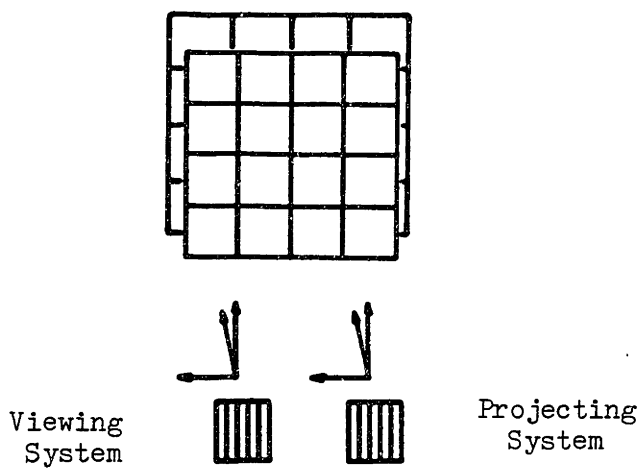

3-5 (b)
3-D Sketches of
Equiorder Surfaces

Case One

$$\psi = 0 \qquad x_o \neq 0$$
$$\varsigma = 0 \qquad y_o = 0$$
$$\theta = 0 \qquad z_o = 0$$
$$\alpha = 0$$

3-5 (c)
Interferometer
Configuration
Parameters

FIGURE 3-5 Example Equiorder Surfaces, Case One

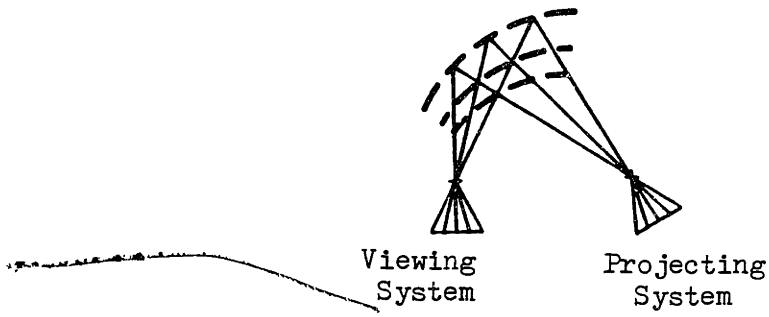

3-6 (a)
Top View of
Equiorder Surfaces

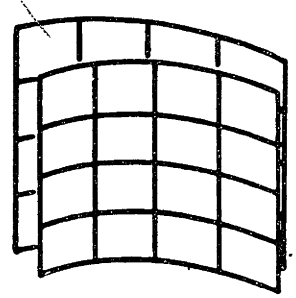

3-6 (b)
3-D Sketch of
Equiorder Surfaces

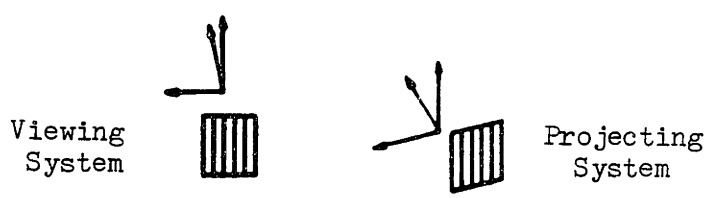

Case Two

$$\psi = 0 \qquad x_o \neq 0$$
$$\varsigma \neq 0 \qquad y_o = 0$$
$$\theta = 0 \qquad z_o \neq 0$$
$$\alpha = 0$$

3-6 (c)
Interferometer
Configuration
Parameters

FIGURE 3-6 Example Equiorder Surfaces, Case Two

determines the geometry of the moire interferometer. Note that for the special case of having the optical axes parallel ($\theta = 0$, $\zeta = 0$), having the viewing and projecting planes coplaner ($Zo = 0$), and having the projecting and viewing grid lines parallel ($\psi = 0$), the equiorder surfaces are flat and parallel. This case is illustrated by Figure 3-5. However, as shown for the more general case of Figure 3-6, the equiorder surfaces are in general curved surfaces.

The value of the equiorder concept arises from the interpretation that the intersection between an object and an equiorder surface of a particular order leads to the observation of a moire fringe of that order on the viewing plane. The corresponding fringe line (curve) in the viewing plane is just the perspective view of the line (curve) defined by the object/equiorder surface intersection.

The concept clearly provides an intuitive method of understanding the fringe pattern produced on a given object, and how that pattern will be changed as the object changes. If the equiorder surfaces for a particular interferometer are determined it is then relatively easy to visualize the object/equiorder surface intersections and the perspective view of those intersections (which is the moire fringe pattern). It is also relatively easy to visualize the effect of changing the shape or orientation of the object. In contrast, it would be very difficult to visualize the moire fringe pattern by trying to visualize the viewing grid pattern and the intensity pattern from the object an then interpret the resulting moire fringe lines.

Because of its intuitive interpretation and concise characterization for moire interferometers, the equiorder surface concept is used as the basis for developing approximate closed form relations for the local geometric properties of the moire fringe pattern. These relations, which are developed in section 3.5, are based on computing the fringe lines via the object/equiorder surface intersections.

3.5 Approximate Closed Form Solution for Fringe Properties.

3.5.1 Overview of Analysis

As discussed in section 3.3, in evaluating or designing a moire interferometer for an inspection task it is desireable to be able to analytically predict the shape of the moire fringe pattern for a specific object. Also, it is desireable to be able to predict the sensitivity of the moire fringe lines to changes in the shape of the object.

One way to evaluate the shape and sensitivity of the moire fringe pattern would be to use the relations of section 3.3 to analytically construct the fringe pattern for the specific object and interferomerter configuration of concern. The fringe properties and their sensitivity could be determined directly from the analytically constructed fringe patterns. However, this approach involves a great deal of computation since the fringe pattern for every object and interferometer configuration considered needs to be constructed. To avoid the burden of repeated fringe pattern construction, and to gain a more intuitive method of designing projection moire systems, closed

form, but approximate, relations for the fringe properties will be developed in this section.

The relations developed in this section are capable of computing the approximate local geometric properties of the moire fringe pattern produced by a specific interferometer and object. Relations, which are in closed form, are developed to compute the folowing properties at a point on the moire fringe pattern:

1) the direction of the moire fringe line,

2) the spacing between adjacent moire fringe lines,

3) the sensitivity of the direction and the spacing of the fringe lines to changes in the orientation of the object,

4) the sensitivity of the position of the fringe lines to changes in the position of the object.

The closed form relations developed in this section are based on the concept of object/equiorder surface intersections. As discussed in section 3.4, fringes observed on the viewing plane can be interpreted as the perspective view of the intersections between the object and the equiorder surfaces of the moire interferometer. Unfortunately, as shown in section 3.4, the the equiorder surfaces are in general not of a simple shape. For this reason, and because objects will also be of a complicated shape, it is very difficult to calculate the curves of intersection between even a simple object and the equiorder surfaces.

To simplify the object/equiorder surface intersections so that the intersections can be calculated in closed form the equiorder surfaces are assumed to be locally planar, parallel, and that distance between surfaces is a linear function of fringe order. It is also assumed for simplicity that locally the object is planar.

With these assumptions the equiorder surface model for fringe production reduces to the intersections of planes, as illustrated in Figure 3-7. Accordingly, the fringe lines simplify to be the perspective view of the straight line of intersection of two planes. Once the representations for the object and equiorder plane are developed, the equation of the fringe lines can easily be calculated in closed form. Unfortunately, by assuming that the equiorder surface and the object surface are planer errors are introduced.

The analysis to develop the approximate closed form relations for the local geometric properties of a moire fringe pattern has been divided up into eight separate tasks and each task is discussed in one of the eight subsections that follow.

3.5.2 Equiorder Surface and Object Normal Vectors

As shown in Figure 3-7, the planar approximation for the equiorder surface and the object surface is based on the local surface normals at a point of interest. The point of interest is simply the point in the object space of the moire interferometer (X,Y,Z) at which the fringe properties are desired. As the point of interest will be on an object/equiorder surface intersection of some order (but not

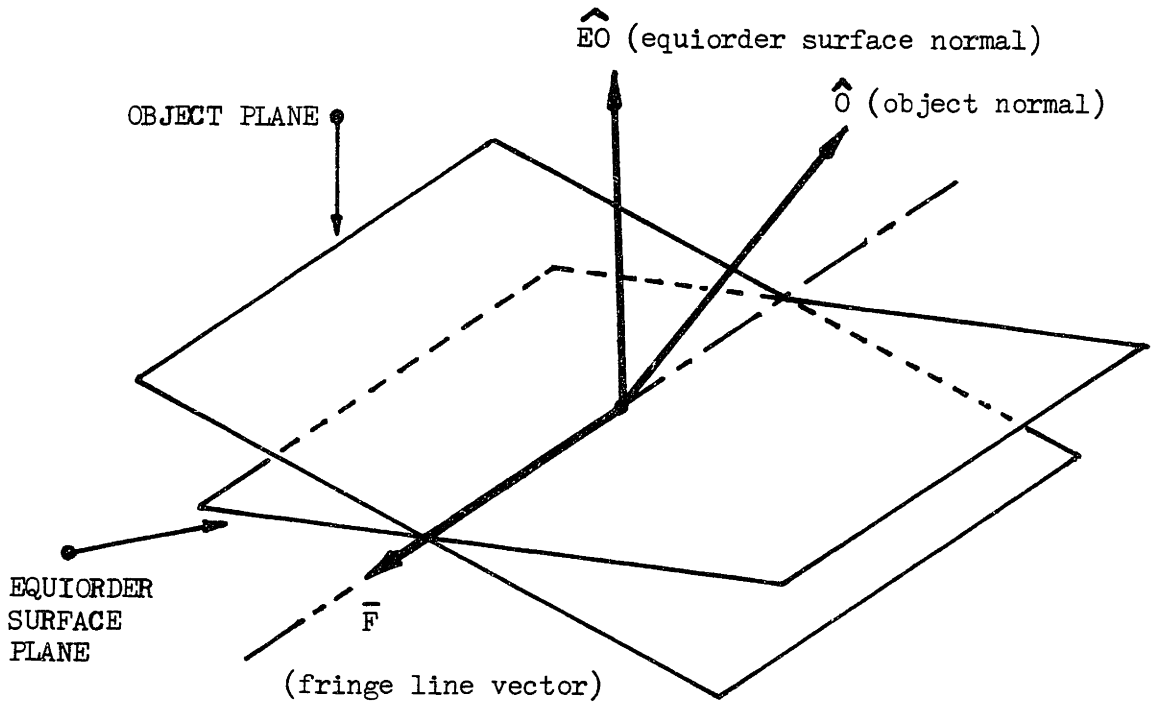

FIGURE 3-7 Local Intersection Between the Object Plane and an Equiorder Surface Plane

necessarily integral fringe order) the point of interest is taken to be the base of the object and equiorder surface unit normal vectors.

The local unit normal vector of the equiorder surfaces is calculated using Equation 3-9. Calculation of the local equiorder surface normal at the point of interest is based on the following partial differential vector equation:

$$\hat{N} = \frac{\frac{\partial \bar{R}}{\partial a} \times \frac{\partial \bar{R}}{\partial b}}{\left| \frac{\partial \bar{R}}{\partial a} \times \frac{\partial \bar{R}}{\partial b} \right|} \qquad (3\text{-}13)$$

where $\hat{N}$ is the local normal vector of the 3-dimensional surface given by $\bar{R} = f(a,b)$, which is the equation of a surface parameterized in the variables a and b. To calculate the equiorder surface unit normal, Equation 3-13 is applied to Equation 3-9, which can be interpreted as the components of a surface parameterized in X_V, Y_V (i.e. $a = X_V$ and $b = Y_V$). The resulting equation for the local unit normal vector (EO) is given below:

$$\hat{EO} = \begin{bmatrix} EO_X \\ EO_Y \\ EO_Z \end{bmatrix} = \begin{bmatrix} \left(\frac{\partial Y}{\partial X_V}\right)\left(\frac{\partial Z}{\partial Y_V}\right) - \left(\frac{\partial Y}{\partial Y_V}\right)\left(\frac{\partial Z}{\partial X_V}\right) \\ \left(\frac{\partial Z}{\partial X_V}\right)\left(\frac{\partial X}{\partial Y_V}\right) - \left(\frac{\partial Z}{\partial Y_V}\right)\left(\frac{\partial X}{\partial X_V}\right) \\ \left(\frac{\partial X}{\partial X_V}\right)\left(\frac{\partial Y}{\partial Y_V}\right) - \left(\frac{\partial X}{\partial Y_V}\right)\left(\frac{\partial Y}{\partial X_V}\right) \end{bmatrix} \frac{1}{Mag} \qquad (3\text{-}14)$$

where mag above is the square root of the sum of the squares of the components. The partial derivatives in equation 3-14 can be written in terms of the parameters of equation 3-9 as follows:

$$\frac{\partial \bar{R}}{\partial X_V} = \begin{bmatrix} \frac{\partial X}{\partial X_V} \\ \frac{\partial Y}{\partial X_V} \\ \frac{\partial Z}{\partial X_V} \end{bmatrix}$$

$$= \begin{bmatrix} \frac{1}{S_V} \{(AX_V^2 + BX_VY_V + CX_V)(2DX_V + FY_V + G) - (2AX_V + BY_V + C)V\} \\ \frac{1}{S_V} \{(AX_VY_V + BY_V^2 + CY_V)(2DX_V + FY_V + G) - (AY_V)V\} \\ \{AV - (AX_V + BY_V + C)(2DX_V + FY_V + G)\} \end{bmatrix} \quad (3\text{-}15\ a)$$

$$\frac{\partial \bar{R}}{\partial Y_V} = \begin{bmatrix} \frac{\partial X}{\partial Y_V} \\ \frac{\partial Y}{\partial Y_V} \\ \frac{\partial Z}{\partial Y_V} \end{bmatrix} \quad (3\text{-}15\ b)$$

$$= \begin{bmatrix} \frac{1}{S_V} \{(AX_V^2 + BX_VY_V + CX_V)(2EY_V + FX_V + H) - (BX_V)\ V\} \\ \frac{1}{S_V} \{(AX_VY_V + BY_V^2 + CY_V)(2EY_V + FX_V + H) - (AX_V + 2BY_V + C)\ V\} \\ BV - (AX_V + VY_V + C)(ZEY_V + FX_V + H) \end{bmatrix}$$

where

$$V = \cdot (DX_V^2 + EY_V^2 + FX_VY_V + GX_V + HY_V + I)$$

To evaluate the parameters A through I it is neccessary to know the viewing plane coordinates (X_V, Y_V) and the fringe order, Fo (which will be constant on a given equiorder surface, associated with the point of interest X,Y,Z. Since the point of interest will be specified, X_V, Y_V, and Fo corresponding to that point can be

calculated using the relations of section 3.3.

The object plane will also be represented using its unit normal vector. How the object normal is specified is not presumed, and the components of a unit normal are simply defined as:

$$\hat{O} = \begin{bmatrix} O_X \\ O_Y \\ O_Z \end{bmatrix} \qquad (3\text{-}16)$$

3.5.3 Fringe Line Vector

The straight line of intersection between the object plane and the equiorder surface plane corresponds to the moire fringe line passing through the point of interest X,Y,Z (see Figure 3-7). This fringe line coincides with the intersections of the planes represented by $\hat{EO}$ and $\hat{O}$. A vector along this intersection line can be calculated from their cross product. Thsi vector, which is called the fringe line vector, $\bar{F}$, is given by the following equation.

$$\bar{F} = \hat{O} \times \hat{EO} = \begin{bmatrix} O_Y\, EO_Z - O_Z\, EO_Y \\ O_Z\, EO_X - O_X\, EO_Z \\ O_X\, EO_Y - O_Y\, EO_X \end{bmatrix} \qquad (3\text{-}17)$$

3.5.4 Spacing Between Adjecent Equiorder Surfaces

To calculate the spacing between adjecent fringe lines it is necessary to know a point on an object/equiorder surface intersection adjecent to the intersection at the point of interest. Adjacent means of an order that is increased or decreased by one. For instance, if the point of interest corresponds to a point on a dark fringe a point corresponding to an adjacent dark fringe would be needed.

Since the object and the equiorder surfaces are assumed to be planar, and the orientations have been determined (subsection 3.5.2) only the distance between adjacent equiorder surfaces is needed to find a point on an adjacent object/equiorder surface intersection.

The distance between adjecent equiorder surfaces can be calculated using Equation 3-9 provided X_V, Y_V and the fringe order Fo corresponding to the point of interest have been determined. First, the Z coordinate of the point on the Fo + 1 equiorder surface that lies on the viewing ray through the point of interest is calculated with Equation 3-9. This is done by holding all other values constant in 3-9 a and increasing the fringe order to Fo +1. The difference in Z values, Z(Fo +1) - Z(Fo), is the Z component of a vector connecting the point of interest to a point in an adjacent equiorder plane. An expression for Z(Fo +1) - Z(Fo) was developed from Equation 3-9 a, yielding the result:

$$\Delta Z = \frac{JM - KL}{K^2 - KM(2(FO + \Phi_p - \Phi_V)+1) + M(FO + \Phi_p - \Phi_V)^2 + (FO + \Phi_p - \Phi_V))} \qquad (3\text{-}18)$$

where

$$J = -T_X - T_Z \left(X_V \cos \alpha_V + Y_V \sin \alpha\right) \frac{P_P}{P_V S_P}$$

$$K = \left(T_3 - T_1 \left(\frac{X_V}{S_V}\right) - T_2 \left(\frac{Y_V}{S_V}\right)\right) + \frac{P_P}{S_P P_V} \left(T_9 - T_7 \left(\frac{X_V}{S_V}\right)\right.$$

$$\left. - T_8 \left(\frac{Y_V}{S_V}\right)\right) \left(X_V \cos \alpha_V + Y_V \sin \alpha_Y\right)$$

$$L = -T_Z \frac{P_P}{S_P}$$

$$M = \frac{P_P}{S_P} \left(T_9 - T_7 \left(\frac{X_V}{S_V}\right) - T_8 \left(\frac{Y_V}{S_V}\right)\right)$$

The distance between the equiorder surfaces is best expressed by the distance along the local equiorder surface normal. As illustrated in Figure 3-8, this distance can be calculated approximately from the equiorder surface normal vector, the Z component along the viewing ray from Equation 3-18, and the direction of the viewing ray .

The direction of the viewing ray throught the point of interest can be determined from Equation 3-6. Provided the coordinates X_V and Y_V the direction of a unit vector along the direction of this ray can be expressed as follows:

$$\hat{VR} = \begin{bmatrix} VR_X \\ VR_Y \\ VR_Z \end{bmatrix} = \begin{bmatrix} -X_V \\ -Y_V \\ S_V \end{bmatrix} \frac{1}{mag} \qquad (3\text{-}19)$$

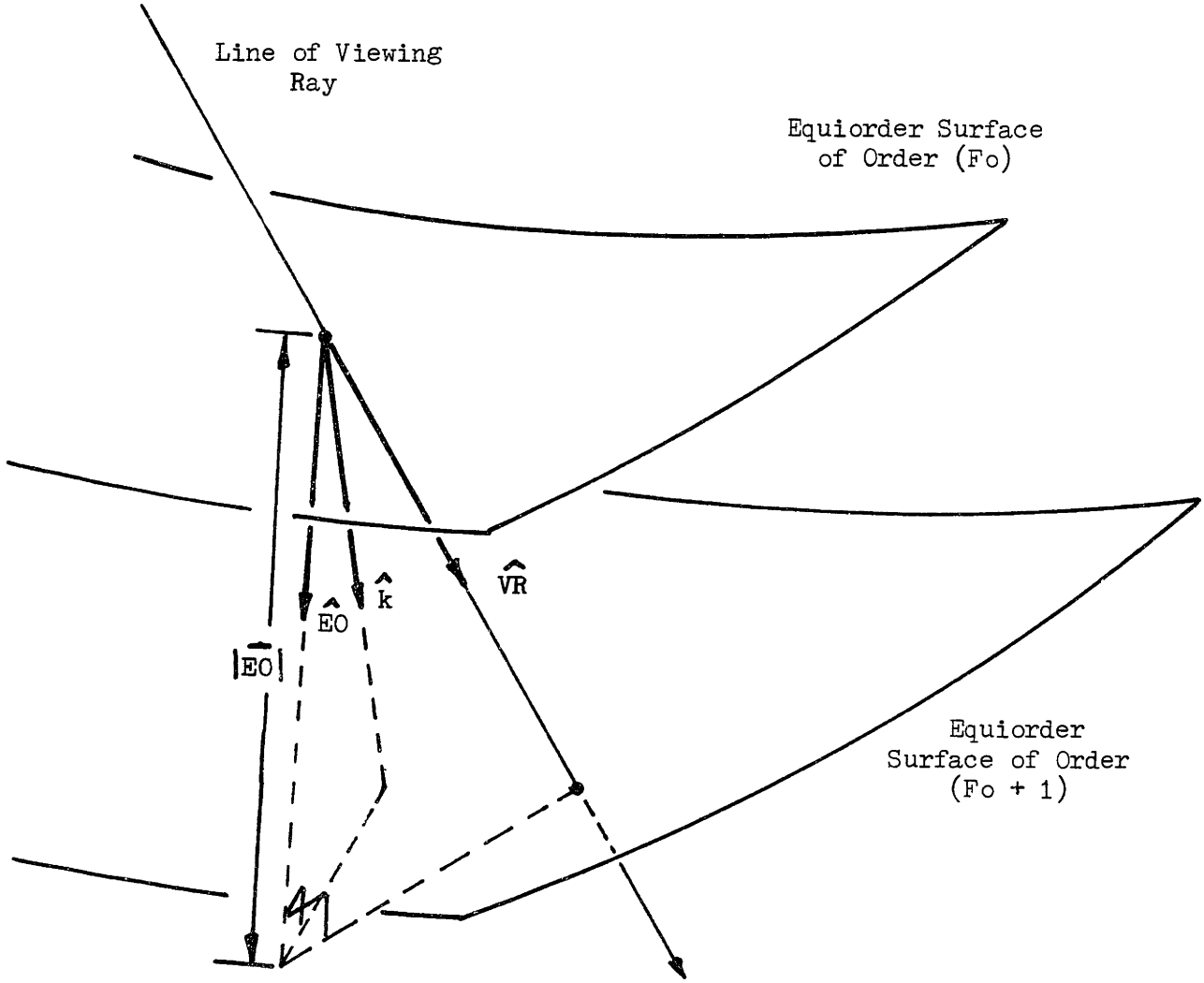

FIGURE 3-8 Scheme for Calculating theLocal Distance Between Adjecent Equiorder Surfaces

where

$$mag = \sqrt{X_V^2 + Y_V^2 + S_V^2}$$

The local spacing between the equiorder surfaces in the direction of the unit normal, $|\bar{EO}|$, can be calculated using the direction of the unit normal ($\bar{EO}$ from Equation 3-14), the direction of the viewing ray (VR from Equation 3-19), and the change in Z along the viewing ray between adjecent equiorder surfaces (ΔZ from Equation 3-18). The appropriate vector relation is:

$$|\bar{EO}| = \Delta Z \left[\frac{\hat{VR} \cdot \hat{EO}}{\hat{VR} \cdot \hat{k}} \right] \qquad (3\text{-}20)$$

where $\hat{k}$ is the Z axis unit vector. For curved equiorder surfaces, which will generally be the case, this equation is only approximate.

3.5.5 Fringe Spacing Vector

The spacing between adjacent fringes can be determined from a vector in the object plane connecting points on adjecent object/equiorder surface intersections, as illustrated in Figure 3-9. This vector, $\bar{A}$, can be calculated using the following constraints :

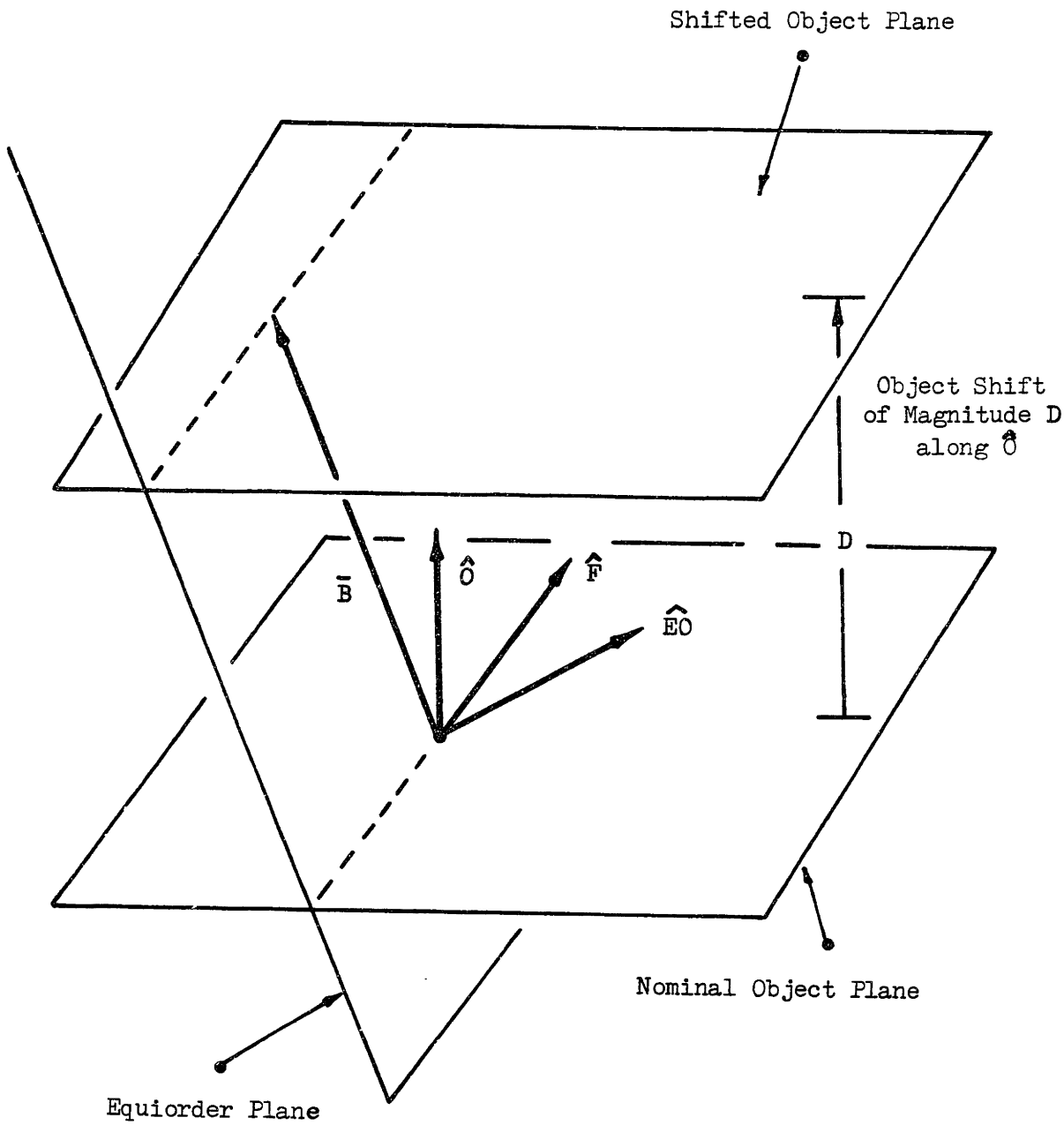

FIGURE 3-9 Illustration of the Fringe Shift Vector, $\bar{B}$

1) the vector $\bar{A}$ lies in the object plane and is therefore perpendicular to the object normal,

2) since the vector $\bar{A}$ connects adjacent equiorder surface planes, the component of $\bar{A}$ along the direction of the equiorder surface normal must be equal to the equiorder surface spacing of Equation 3-20,

3) the arbitrary conditon that $\bar{A}$ is perpendicular to the direction of the fringe line vector of Equation 3-17.

These constraints can be expressed respectively in vector form as:

$$(\hat{O} \cdot \bar{A}) = 0 \qquad (3\text{-}21\ a)$$

$$(\bar{A} \cdot \hat{EO}) = |\bar{EO}| \qquad (3\text{-}22\ b)$$

$$(\bar{A} \cdot \bar{F}) = 0 \qquad (3\text{-}23\ c)$$

When written in component form the vector Equations of 3-21 through 23 can be solved simultaneously to determine the components of $\bar{A}$. The results are listed below:

$$A_Z = \frac{|\bar{EO}|\ (F_Y O_X - F_X O_Y)}{(F_Z O_Y - F_Y O_Z)\ EO_X + (F_X O_Z - F_Z O_X)\ EO_Y + (F_Y O_X - F_X O_Y)\ FO_Z} \qquad (3\text{-}24\ a)$$

$$A_Y = \left[\frac{F_X O_Z - F_Z O_X}{F_Y O_X - F_X O_Y}\right] A_Z \qquad (3\text{-}24\ b)$$

$$A_X = -\left[\frac{O_Y}{O_X}\right] A_Y - \left[\frac{O_Z}{O_X}\right] A_Z \qquad (3\text{-}24\ c)$$

Since the solution for $\bar{A}$ depends on solving for one component of $\bar{A}$ and then back computing the other components, the solution will possess singularities for system configuration that cause this first component not to exist. For the configurations considered in subsequent chapters this does not occur. If this problem is encountered it can be corrected by simply changing the order of solution for the components.

3.5.6 Fringe Shift Vector

The shift, or position sensitivity, of the observed fringes produced by a shift in the position (but not orientation) of the object can be determined from a vector in the equiorder plane of order Fo that connects a point on the nominal and displaced object plane. Figure 3-10 illustrates the model for the shifted object plane and the vectors used in solving for the fringe shift.

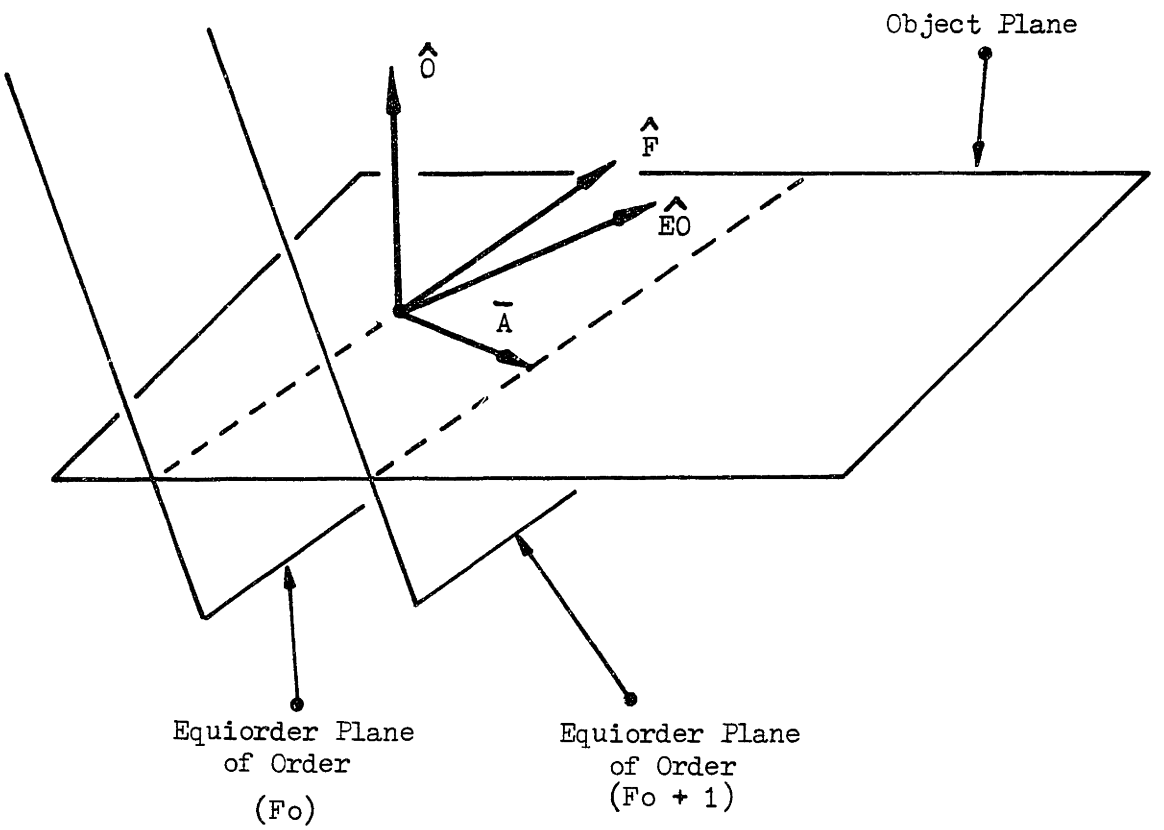

FIGURE 3-9 Illustration of the Fringe Spacing Vector, $\bar{A}$

The solution for $\bar{B}$, the fringe shift vector that connects points on the nominal and shifted object plane, is similar to the solution for $\bar{A}$. The three constraints used to isolate $\bar{B}$ are:

1) the vector $\bar{B}$ lies in the equiorder plane that passes throught the point of interest,

2) the component of $\bar{B}$ along the direction of the object normal must be equal to the magnitude of the displacement, $|\bar{D}|$,

3) the arbitrary condition that $\bar{B}$ is perpendicular to the fringe line direction.

These conditions can be expressed in vector form as:

$$1) \qquad \bar{B} \cdot \hat{EO} = 0 \tag{3-25}$$

$$2) \qquad \bar{B} \cdot \hat{O} = |\bar{D}| \tag{3-26}$$

$$3) \qquad \bar{B} \cdot \bar{F} = 0 \tag{3-27}$$

Solving the above equatioins simultaneously for the components of $\bar{B}$ yields:

$$B_X = \frac{|\bar{D}| \ (F_Y EO_Z - F_Z EO_Y)}{(O_Y F_Z - O_Z F_Y) \ EO_X + (O_Z F_X - O_X F_Z) \ EO_Y + (O_X F_Y - O_Y F_X) \ EO_Z} \tag{3-28 a}$$

$$B_Y = \left(\frac{F_Z EO_X - F_X EO_Z}{F_Y EO_Z - F_Z EO_Y} \right) B_X \tag{3-28 b}$$

$$B_Z = -\left(\frac{EO_X}{EO_Z} \right) B_X + -\left(\frac{EO_Y}{EO_Z} \right) B_Y \tag{3-28 c}$$

3.5.7 Perspective View of 3-D Fringe Vectors

The fringe line, fringe spacing and the fringe shift vectors are 3-dimensional vectors in the object spcae of the moire interferometer (in viewing system coordinates). However, what is really of concern is the direction, the fringe spacing, and the shift of the moire fringe lines as seen on viewing system image plane. To compute these quantities it is necessary to compute the perspective view of the vectors $\overline{F}$, $\overline{A}$, and $\overline{B}$. Accordingly, a general expression for the perspective view, $\overline{PV}$, of a vector with base at X,Y,Z and with components ΔX, ΔY, and ΔZ was developed.

The expression for the perspective view of a 3-dimensional vector is based on knowing that the base and tip of the vector are imaged along viewing rays that pass throught the node of the viewing system. Using the equations of the viewing rays (Equations 3-6 a and b) it is possible to compute the viewing plane coordinates of the base and tip of the 3-dimensional vector. By subtracting the viewing plane coordinates of the base from the viewing plane coordinates of the tip the components of the 2-dimensional vector, $\overline{PV}$, on the viewing plane are determined. An expression for $\overline{PV}$ is:

$$\overline{PV} = \begin{bmatrix} PV_X \\ PV_Y \end{bmatrix} = \begin{bmatrix} \dfrac{X\Delta Z - Z\Delta X}{Z^2 \quad Z\Delta A} \\ \dfrac{Y\Delta Z - Z\Delta Y}{Z^2 + Z\Delta Z} \end{bmatrix} \qquad (3\text{-}29)$$

Using Equation 3-29 the perspective views of the fringe direction vector, $\bar{F}$, and the fringe spacing vector, $\bar{A}$, and the fringe shift vector, $\bar{B}$, can be written in terms of the point of interest X,Y,Z and the components of the 3-dimensional vectors. The perspective views of the vectors $\bar{F}$, $\bar{A}$, and $\bar{B}$ will be called $\bar{FP}$, $\bar{AP}$, and $\bar{BP}$, respectively. Writing out the expressions for $\bar{FP}$, $\bar{AP}$, and $\bar{BP}$, produces:

$$\bar{FP} = \begin{bmatrix} FP_X \\ FP_Y \end{bmatrix} = \begin{bmatrix} \dfrac{XF_Z - ZF_X}{Z^2 + ZF_Z} \\ \dfrac{YF_Z - ZF_Y}{Z^2 + ZF_Z} \end{bmatrix} \qquad (3\text{-}30)$$

$$\bar{AP} = \begin{bmatrix} AP_X \\ BP_Y \end{bmatrix} = \begin{bmatrix} \dfrac{XA_Z - ZA_X}{Z^2 - ZA_Z} \\ \dfrac{YA_Z - ZA_Y}{Z^2 - ZA_Y} \end{bmatrix} \qquad (3\text{-}31)$$

$$\bar{BP} = \begin{bmatrix} BP_X \\ BP_Y \end{bmatrix} = \begin{bmatrix} \dfrac{XB_Z - ZB_X}{Z^2 + ZB_Z} \\ \dfrac{YB_Z - ZB_Y}{Z^2 - ZB_Z} \end{bmatrix} \qquad (3\text{-}32)$$

3.5.8 Evaluating the Observed Fringe Properties

FRINGE ANGLE

The direction of the fringe lines on the image plane is indicated by the vector $\bar{FP}$. The fringe angle is taken as the angle of FP with respect to the positive X_V axis, with positive angles counter-clockwise.

FRINGE SPACING

The fringe spacing in the viewing plane is the perpendicular distance between adjacent fringe lines as seen on the viewing plane. Although the vectors $\bar{F}$ and $\bar{A}$ are neccessarily perpendicular, this is not true of their perspective views, $\bar{FP}$ and $\bar{AP}$. Thus, the component of $\bar{AP}$ that is perpendicular to FP needs to be calculated. The perpendicular direction to $\bar{FP}$, denoted by the vector $\hat{SP}$, is established by computing the cross product of a unit vector along $\bar{FP}$ and the Z axis unit normal, $\hat{k}$.

$$\hat{SP} = \begin{bmatrix} -FP_X \\ FP_Y \end{bmatrix} \frac{1}{mag} \qquad (3\text{-}33)$$

where

$$mag = \sqrt{FP^2 + FP_Y{}^2}$$

The magnitude of the fringe spacing, SPC, in the viewing plane can then be calculated by finding the component of $\bar{AP}$ along the direction of $\hat{SP}$ using the dot product.

$$SPC = (\bar{AP} \cdot \hat{SP}) \qquad (3\text{-}34)$$

FRINGE SHIFT

Since the vector $\bar{BP}$ is no longer necessarily perpendicular to the fringe direction, the component of $\bar{BP}$ that is perpendicular to the observed fringe lines needs to be computed. This component is the fringe shift, SFT, and can be calculated by the dot product of $\bar{BP}$ with $\hat{SP}$.

$$SFT = (\bar{BP} \cdot \hat{SP}) \qquad (3\text{-}35)$$

3.5.9 Fringe Spacing, Angle and Shift Sensitivities

For a particular projection moire configuration, object position, and object orientation the local fringe properties of fringe angle and fringe spacing can be determined as described in subsection 3.5.7. Equally important to design or evaluate a moire interferometer are the observable sensitivity the fringe fringe spacing to changes in the interferometer perameters and object orientation.

The angular and spacing sensitivity of the fringes can be determined by computing the finite differences in the fringe properties produced by a finite change in the object orientation or system parameter. This can be done by using the equations presented previously in this section to compute the fringe properties before and after the object or system is varied. The sensitivities can then computed using the following defining equations:

$$\text{FRINGE ANGLE SENSITIVITY} = \frac{\Delta \text{ FRINGE ANGLE}}{\Delta \text{ PARAMETER}} \qquad (3\text{-}36)$$

$$\text{FRINGE SPACING SENSITIVITY} = \frac{\Delta \text{ FRINGE SPACING}}{\Delta \text{ PARAMETER}} \qquad (3\text{-}37)$$

Where the change in fringe spacing is evaluated from SP, the change in

fringe angle is computed from $\overline{FP}$ and ' Parameter' is the change in the object orientation angle or system parameter of interest. Note that computing the sensitivities using partial derivatives of the perspective view vectors would be more accurate, but very complex.

Similarly, the fringe shift sensitivity, or alternately the sensitivity of the position of the fringes to the postion of the object, can be calculated by the following defining equation:

$$\text{Fringe Shift Sensitivity} = \frac{\text{Fringe Shift}}{\text{Object Shift}} \qquad (3\text{-}33)$$

Since the fringe direction, fringe spacing, fringe angle, spacing and angle sensitivities, and the fringe shift are all computed under the assumption that the equiorder surfaces are flat, parallel and evenly spaced, a condition which is in general not true, the properties will only be approximately correct. The closer the moire interferometer and object approximate these assumptions, the closer the equations can model the actual properties of the observed fringes.

3.6 Implementing the Closed Form Relations for Fringe Properties

The relations for the local fringe properties developed in section 3.5 were implemented on a digital computer and subsequently used for two purposses. The purposses include:

1) Verificatioin that the relations can be used to predict the fringe properties for a real moire interferometer.

2) To demonstrate the usefulness of the approximate relations as a tool for

designing the properties of a moire interferometer

The validity of the approximate relations will be verified by comparing the actual fringe properties, obtained experimentally, to those predicted using the approximate relations. The verification of the approxomate relations is discussed in Chapter 5 . The usefullness of the approximate relations for interferometer design will then be demonstrated via a hypothetical design task. The design calls for choosing the parameters for a moire interferometer that produce specific local fringe properties (i.e. fringe spacing and fringe sensitivities) using the approxomate relations. The hypothetical design example is presented in Chapter 6. In this section the operation of the program implementation of the approximate relations is discussed and sample output is provided. A listing of the program is provided in appendix A.

3.6.1 Program Operation

As presented above, the approximate relations for fringe properties are applicable for:

- a specific interferometer configuration,
- a specific point on an object of known shape and orientation,
- a specific variation in the object orientation (for fringe spacing and angle sensitivity calculations),
- a specific shift of the object (for fringe shift calculation).

What will most often be of interest is the change in the fringe properties as one of the parameters above is varied. For instance, for the pupose of desinging the configuration of a moire interferometer what is of interest is how changes in the configuration of the interferometer and the orientation of the object will effect the fringe properties. Accordingly the computer program used to impliment the approximate relations of section 3.5 was developed to compute and plot the fringe properties as either a parameter of the interferometer or the orientation of the object was varied.

To limit the scope of the parameters to be varied were limited to:

1) the spacial frequencies of the projecting and viewing grids, with the ratio of the frequencies of the two grids maintained constant,

2) the angle of rotation of the object about a single axis that is parallel to the Y axis of the viewing coordinate frame.

Although, the programs that were developed allow rotation of the object about any desired axis.

To clarify the variations in the object orientation considered in this thesis, consider Figure 3-11. The orientation of the object normal is limited (in viewing system coordinate) to always be in a plane parallel to the X,Z plane. The orientation of the object normal in the X,Z plane could then be specified by only the angle ($\S_{OBJ}$) between the object normal and the Z axis. Equivilently, this angle can be thought of as the rotation of the object about an axis parallel to the Y axis of the viewing system coordinate frame which passes through the point on the object being considered. This is the axis

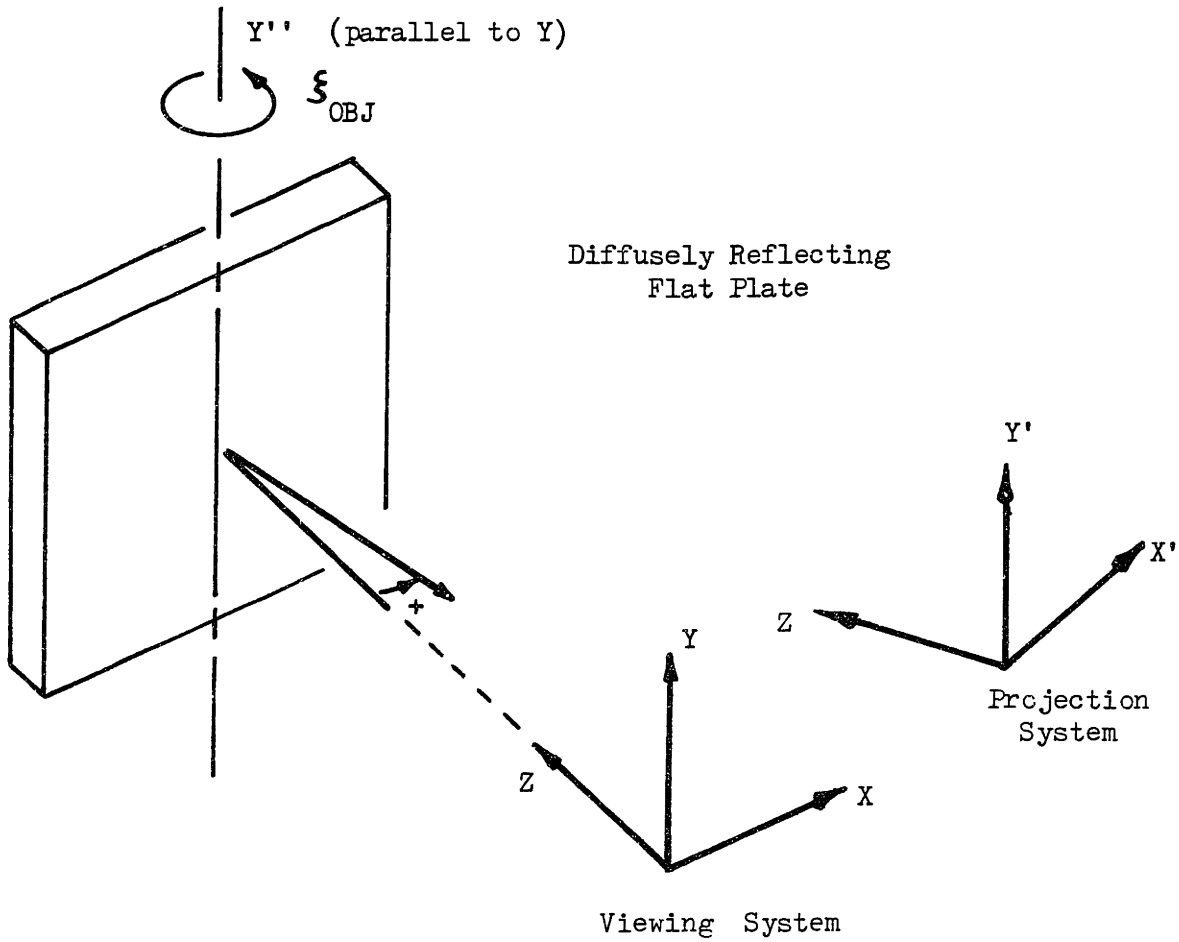

FIGURE 3-11 Object Rotation Considered For Program Demonstration

Y'' illustrated in the figure, and which is refered to in the part 2 above. With the exception of these two parameters all of the parameters for the interferometer and the object were held constant.

3.6.2 Sample Output

As mentioned above, to be useful for the work of Chapters 5 and 6 the program implementation of the approximate relations was developed to compute and plot the fringe properties. Example output of the program is given in Figures 3-12 and 3-13.

Figure 3-12 illustrates the relation between the fringe properties and the object orientation. For the plots of Figure 3-12 the spatial frequency of the projecting and viewing grids are held constant at .3987 lines/mm (100 lines/inch) and the object orientation (ξ_{OBJ}) is varied from -60 to 60 degrees.

Figure 3-13 illustrates the relationship between the fringe properties and the spatial frequency of the projecting and viewing grids. For the plots of Figure 3-13 the orientation of the object is fixed at ξ_{OBJ} = 0.05 rad and the spatial frequency of the projecting and viewing grids are simaltaneously varied from 1 to 20 lines/mm.

In both Figures 3-12 and 3-13 the five local fringe properties calculated using the approximate relations are shown in parts a through e of the figures. Specifically, as shown in the figures the five fringe properties are:

a) The spacing in the viewing plane between adjecent fringe lines. The spacing is the the perpendicular distance between the fringe lines, and is expressed in mm.

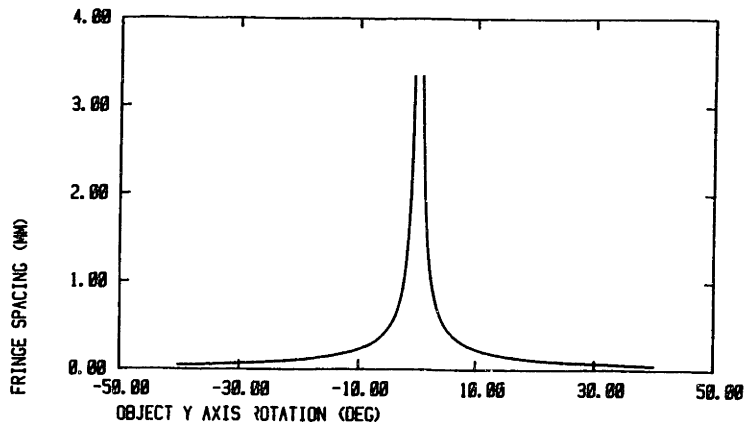

3-12 (a) Fringe Spacing vs. Object Angle

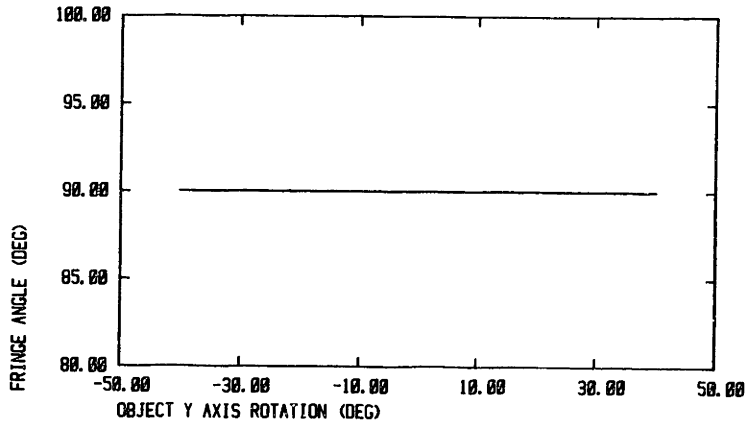

3-12 (b) Fringe Angle vs. Object Angle

FIGURE 3-12 Sample Output from Program Implimentation of Approximate Relations for Local Fringe Properties

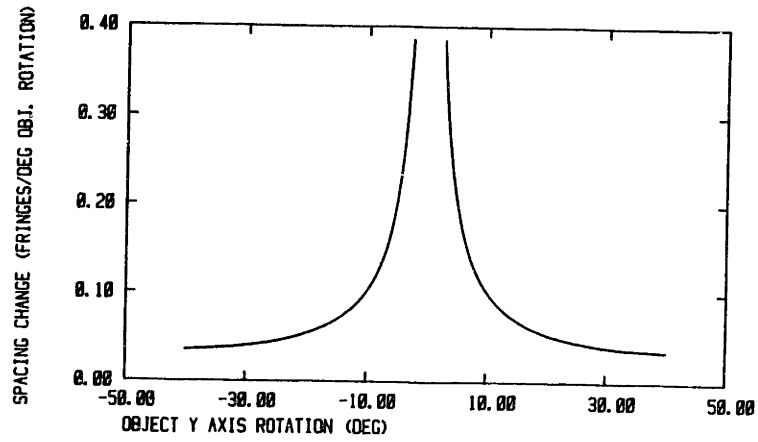

3-12 (c) Sensitivity of Fringe Spacing vs.Object Angle

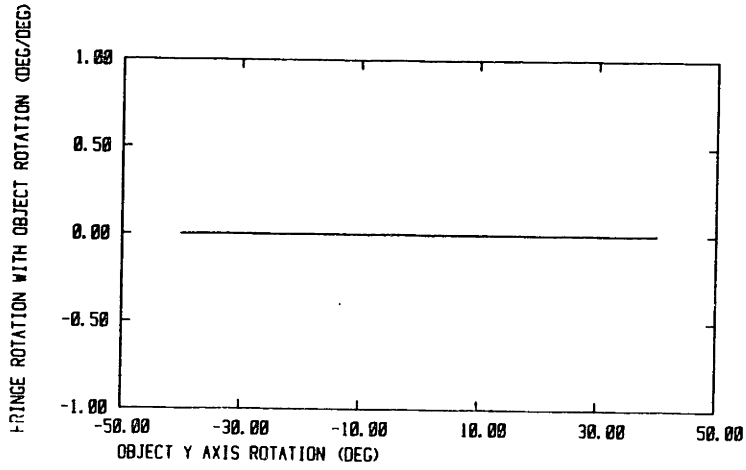

3-12 (d) Sensitivity of Fringe Angle vs. Object Angle

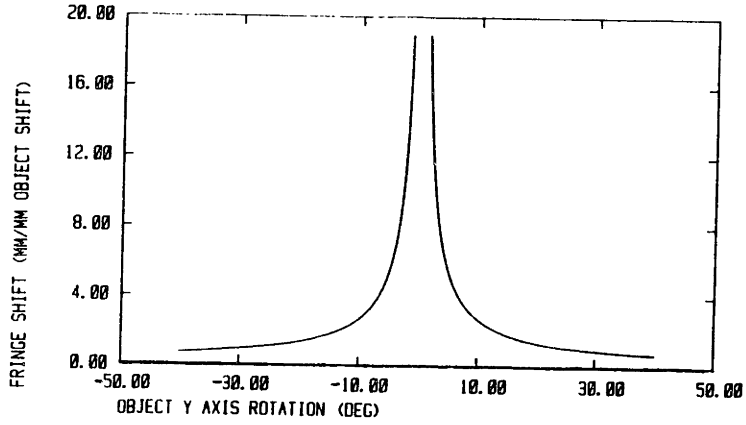

3-12 (e) Sensitivity of Fringe Position vs.Object Angle

FIGURE 3-12 (continued)

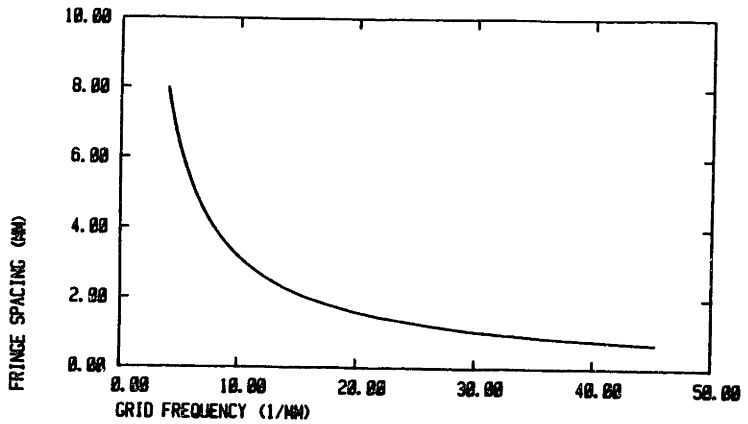

3-13 (a) Fringe Spacing vs. Grid Frequency

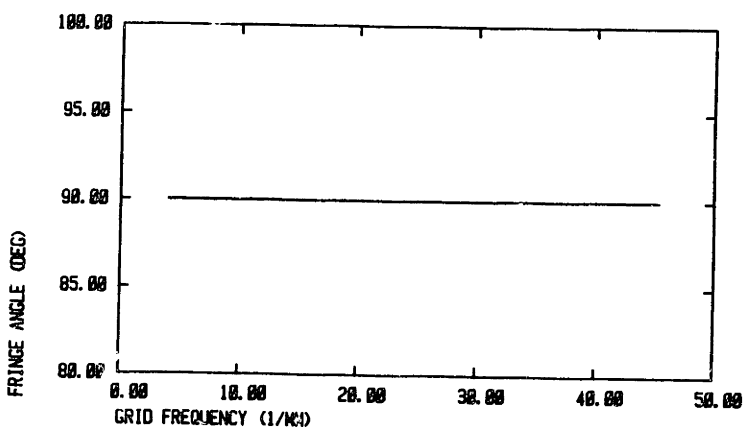

3-13 (b) Fringe Angle vs. Grid Frequency

FIGURE 3-13 Sample Output from Program Implimentation of the Approximate Relations for Local Fringe Properties

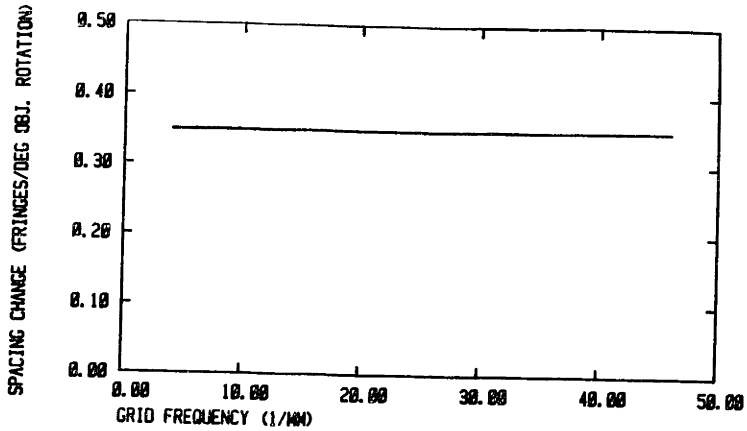

3-13 (c) Sensitivity of Fringe Spacing vs.Grid Frequency

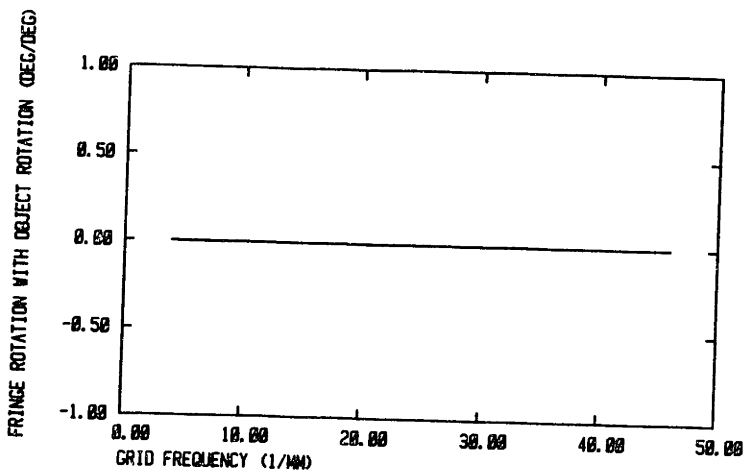

3-13 (d) Sensitivity of Fringe Angle vs.Grid Frequency

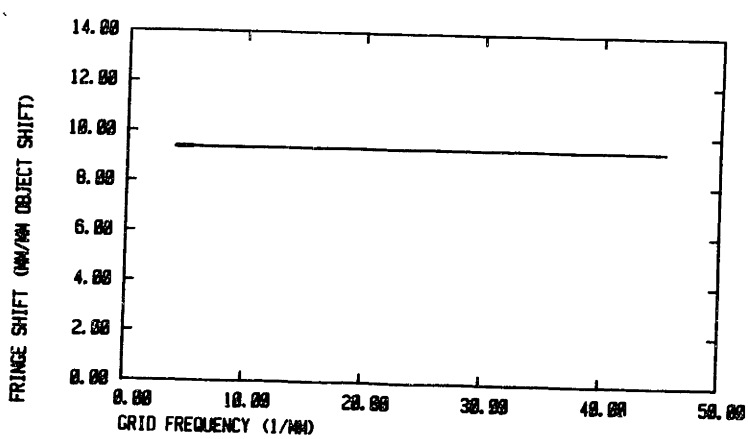

3-13 (e) Sensitivity of Fringe Position vs. Grid Frequency

FIGURE 3-13 (continued)

b) The angle of the fringe lines on the viewing plane. The angle is measured from the positive X_V axis (positive counterclockwise) and is expressed in degrees.

c) The sensitivity of the spacing between the fringes on the viewing plane to a small rotation (0.0005 rad is used in the program) of the object about the Y'' axis. The sensitivity is expressed as the change in the fringe spacing (in fractions of the nominal fringe spacing) per degree object rotation.

d) The sensitivity of the angle (i.e. direction) of the fringe lines on the viewing plane to a small rotation in the object (same as in c). The sensitivity of the fringe angle is expressed as the change in angle (rotation) of the fringe divided by the rotation of the object, in deg. per deg..

e) The sensitivity of the position of the fringe lines (or fringe shift) to a small displacement of the object along the object normal vector (a one mm displacement is used in the program). The sensitivity of the fringe position is expressed as the shift of the fringe lines divided by the displacement of the object, in mm per mm.

As mentioned above, with the exception of the object orientation and the grid frequencies the parameters of the interferometer and the object are fixed. The fixed parameters that were used for the plots of both Figure 3-12 and 3-13 can be summarized as follows:

Elements of the Transfomation which specifies the Projecting Coordinate frame:

Xo = 100 mm	$\Theta = 0$
Yo = 0	$\xi = 0$
Zo = 0	$\psi = 0$

Image distances for the projecting and viewing systems:

$$S_p = 35.5 \text{ mm}$$

$$S_V = 35.5 \text{ mm}$$

Location of the point of interest on the object, expressed in viewing frame coordinates:

$$X = 0$$

$$Y = 0$$

$$Z = 100 \text{ mm}$$

The orientation of the viewing grid:

$$\alpha = 0$$

The parameter listed above were choosen so that the configuration of the moire interferometer matches the special case configuration that leads to flat equiorder surfaces. This special case is discussed in section 3.4, and is illustrated in Figure 3-6. This configuration, which will also be used in Chapter 6, was choosen for two reasons. First, having flat equiorder surfaces makes it easier to visualize the object/equiorder surface intersections. Second, this configuration for the moire interferometer will match the assumptions of the approximate relations closely. That is, the equiorder surfaces will be flat as assumed for the approximate relations for fringe properties. This configuration should, therefore, produce good agreement between the actual fringe properties and those predicted with the approximate relations.

Chapter 4. Diffuse Moire with Collimated Imaging.

4.1 Introduction

The relations of Chapter 3 were developed for a projection moire interferometer with real imaging optics (i.e. like a slide projector and camera). In this chapter the special case of projection and viewing with collimated light is analysed. This special case is important since, for straight evenly spaced transmittance grids, collimated imaging leads to planar, equally spaced equiorder surfaces. Thus, such a system will yield the true, as opposed to approximate for real imaging, contour fringes of an object.

A further motivation for analysing collimated imaging relates to the elemental interpretation for a moire fringe pattern. If only a small area on the moire fringe pattern is considered, then even for real imaging the rays going to or from this small area are nearly parallel. (In fact, the assumption in Chapter 3 that the equiorder syrfaces were locally flat implies that the viewing and the projecting rays are parallel). Also, because the relations for collimated imaging are more simple than those for real imaging, the closed form analysis for the fringe properties will be simlified.

Similar to the analysis for real imaging, the relations developed in this analysis for collimated imaging include :

1) the relations for computing the object coordinates from the coordinates and fringe order at a point

on the observed fringe pattern,

2) the relations for computing the fringe order and location of a point on the moire fringe pattern from object coordinates,

3) relations for the locally observed fringe line direction and fringe spacing (which are suitable for computing the fringe spacing and angular sensitivities,

4) relations for the observed fringe shift due to a shift in the object.

As the following analysis is very similar to the analysis of Chapter 3, the explaination of the steps involved in the analysis is somewhat cursory. Chapter 3 will serve to suppliment the expainations given here, and the appropriate section for review will be noted.

4.1.1 Collimated Imaging

Collimated imaging requires that the light rays incident onto the object and the rays reflectedfrom the object are parallel. Presently, true collimated projection and viewing can only be approximated. This is because any real light source is finite in size. A schematic for how collimated projection moire interferometry with collimated imaging can be approximated is given in Figure 4.1. In Figure 4.1 the collimated beam used to produce the structured light field approximates a point light source oriented at the focal length of a real imaging optical system. An alternate method of producing a collimated source is to expand the already well collimated beam of a laser.

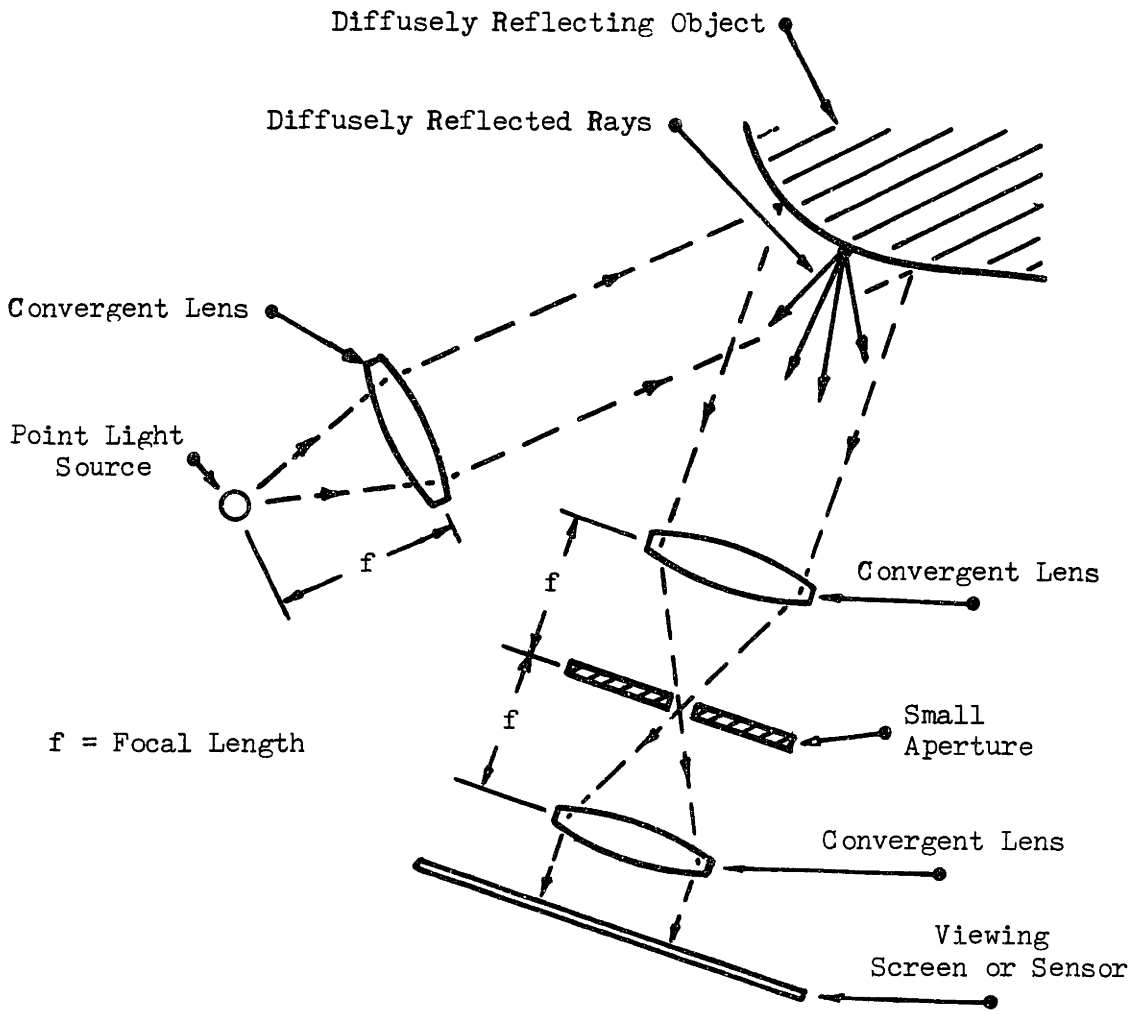

FIGURE 4-1 Scheme for Collimated Projection and Viewing

Collimated viewing of the intensity pattern on the object can be approximated by collecting only the rays that reflected through some small, but finite, solid angle. One optical arrangement for doing this is shown in Figure 4.1 and consists of a positive lense, a small aperture at the back focal plane of this lense, and a second identical lense placed one focal length behind the small aperture. With the components arranged as shown, only the rays of light that are reflected nearly parallel to the optical axis of the viewing system pass through the apparture.

System Model

As with the real imaging configurations for collimated imaging, moire fringes are produced when an intensity pattern that is reflected from the object passes through (is modulated by) a transmittance grid. The interference between the intensity pattern and the transmittance grid will produce moire fringes on an image plane placed behind the transmittance grid. The image plane can itself be a sensing device, such as a plate of photographic film or a photosensitive array of a video camera, or it can be mearly a translucent screen (diffuser) on which the moire pattern will be viewed.

The system model for the analysis is illustrated in Figure 4-2. As in the analysis of Chapter 3, the Z and Z' axes coincide with the optical axes of the viewing and projecting systems, respectively. For collimated viewing this means that the direction of the Z and Z' axes coincide with the direction of the projection and viewing rays, respectively. As the model for collimated viewing has no lens node, the location of the image planes for the projection and viewing

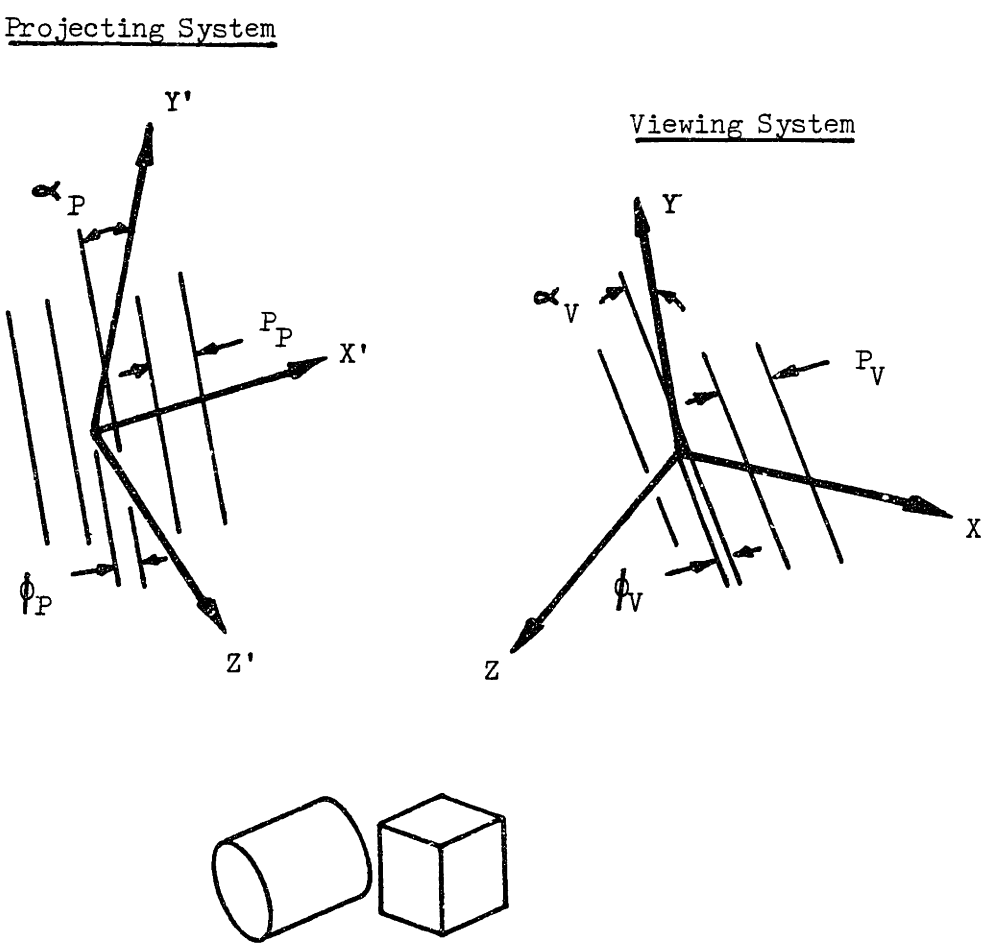

FIGURE 4-2 Analytical Model for Collimated Moire Interferometer

systems can be choosen for convenience, and are taken to be coincident with the X,Y and the X',Y' planes, respectively. Again the titles viewing plane and projecting plane, with the associated subscripts v and p, will be use to denote the image planes of the viewing and projecting systems

The primary difference between the analysis for real and collimated imaging are the expressions for the viewing and projecting rays. Since for collimated imaging the light rays are parallel to the optical axes for each system, the equations for the projecting and viewing rays can be written in the following simple form:

$$X = X_V \qquad (4\text{-}1\ a)$$

$$Y = Y_V \qquad (4\text{-}1\ b)$$

$$X' = X_P \qquad (4\text{-}2\ a)$$

$$Y' = Y_P \qquad (4\text{-}2\ b)$$

It is because relations 4-1 and 4-2 are so simple that the analysis for collimated imaging is more simple than the analysis for real imaging.

As in Chapter 3, the transmittance grid of the projection and viewing systems are assumed to consist of straight and evenly spaced lines. As shown in Figure 4-2, for collimated imaging the projection and viewing grids lie in the X,Y and the X',Y' planes, respectively. The relations for the profile numbers of the transmittance grids as a function of position can be developed as in Chapter 2, and are given

below:

$$n_Y = (X_1 \text{ COS } \alpha_V + Y_V \text{ SIN } \alpha_V) \frac{1}{P_V} - \Phi_V \qquad (4\text{-}3\ a)$$

$$n_P = \frac{X_P}{P_P} - \Phi_P \qquad (4\text{-}3\ b)$$

(α_P assumed zero)

As for the case of real imaging, the projection system coordinate frame is located relative to the viewing system frame by the 4 by 4 coordinate transformation developed in Chapter 3. The transformation between the projection and viewing coordinates can, therefore, again be written (see Equation 3-2):

$$\begin{bmatrix} X' \\ Y' \\ Z \\ 1 \end{bmatrix} = \begin{bmatrix} T_1 & T_2 & T_3 & T_X \\ T_4 & T_5 & T_6 & T_Y \\ T_7 & T_8 & T_9 & T_Z \\ 0 & 0 & 0 & 1 \end{bmatrix} \begin{bmatrix} X \\ Y \\ Z \\ 1 \end{bmatrix} \qquad (4\text{-}4)$$

where the elements of the transform are defined as in Chapter 3.

The above equations can be used in conjunction with the expression for fringe order developed in Chapter 2, which is repeated below, to analyse the fringe producing characteristics of the collimated imaging system illustrated in Figure 4-2. Recalling the relation for fringe order:

$$Fo = n_V - n_P \qquad (4\text{-}5)$$

4.2 Object Coordinates from Moire Fringe Pattern

As stated above, except for the expressions for the viewing rays, the derivation of the relations for the object coordinates as a function of fringe order and position is identical to the derivation of section 3.2. Assuming that the fringe order (Fo) and coordinates on the viewing plane (X_V, Y_V) of a point on the observed moire fringe pattern are known, the assocated object coordinates (X,Y,Z) can be calculated.

The first step is to apply Equation 4-5 to point of interest in the moire fringe pattern on the viewing plane. Substituting for the profile numbers of the projecting and viewing patterns in 4-5 using Equations 4-3 a and b gives:

$$Fo = (X_V \text{ COS } \alpha_V + Y_V \text{ SIN } \alpha_V)\frac{1}{P_V} - \frac{X_P}{P_P} + (\Phi_P - \Phi_V) \qquad (4\text{-}6)$$

where, X_V and Y_V are the viewing plane coordinates of a point on the moire pattern, which has a fringe order Fo. X_P is the point of origin on the projecting plane for the ray that illuminates the point X,Y,Z on the object. X_P from Equation 4-6 is next transformed into the viewing system coordinate frame using Equations 4-4 and 4-2 a. The expression for X_P in terms of viewing frame coordinates, taken

from the first row of Equation 4-4 and Equation 4-2 a, is:

$$X_P = T_1X + T_2Y + T_3Z + T_X \qquad (4\text{-}7)$$

Substituting Equations 4-1 and 4-7 into Equation 4-7 yields an equation which can be solved for the Z coordinate of the point on the object associated with the known X_V, Y_V and Fo. Solving this equation gives:

$$Z = \left(\frac{P_P}{P_V T_3}\cos\alpha_V - \frac{T_1}{T_3}\right) X_V + \left(\frac{P_P}{P_V T_3}\sin\alpha_V - \frac{T_2}{T_3}\right) Y_V - \left(\frac{(Fo - \Phi_P + \Phi_V)\,P_P + T_X}{T_3}\right) \qquad (4\text{-}8)$$

The above equation gives the Z coordinate (in the viewing frame) of the object point associated with the observation of a moire fringe of order Fo at the point X_V, Y_V on the viewing plane. The other two coordinates of the object point, X and Y, are simply X_V and Y_V since for collimated viewing the viewing rays are parallel to the Z axis (see Equation 4-1).

As with the results of Section 3.2, the relations of Equations 4-1 and 4-8 are suitable for point by point object reconstruction from the observed moire fringe pattern provided the coordinates and fringe order can be determined.

4.3 Fringe Pattern from Object Object Coordinates.

As discussed in Chapter 3, if the object surface and the system parameters are known, the fringe pattern can be analytically constructed. As suggested, point by point construction of the fringe pattern could be accomplished by calculating the viewing plane coordinates and fringe order corresponding to a particular object point. Relations suitable for calculating the fringe order, Fo, and the viewing plane coordinates (X_V, Y_V) of the point on the moire fringe pattern from the the object coordinates X,Y,Z will be derived below for the case of collimated imaging.

Similar to section 3.3, given knowledge of the object coordinates in the viewing frame (X,Y,Z), the associated viewing plane coordinates, X_V, Y_V, are given by 4-1 a and b. Also, the projecting plane X coordinate (X_V) corresponing to the object coordinates can be determined using Equation 4-2 with X' calculated from Equation 4-7.

Substituting the image plane coordinates (X_V, Y_V, and X_P) into Equations 4-3 a and b allows calculation of the viewing and projecting pattern profile numbers. The profile numbers can then be substituted into Equation 4-5 to calculate the fringe order.

By combining Equations 4-7, 4-3, and 4-5 the fringe order can be exressed in terms of the known object coordinates as:

$$Fo = (X \cos \alpha_V + Y \sin \alpha_V)\frac{1}{P_V} - (T_1X + T_2Y + T_3Z + T_X)\frac{1}{P_P} + (\Phi_P - \Phi_V) \quad (4\text{-}9)$$

As discussed in Chapter 2, the local average intensity, which can be used to reconstruct the fringe pattern, is indicated by the fringe order. Thus, Equations 4-1 a and b and 4-9 can be used to determine the fringe pattern at one point provided the interferometer geometry and the object coordinates are known. By repeated application of these equations at many points on an object the moire fringe pattern produced by the object could be constructed.

4.4 Closed Form Relationships for Fringe Properties.

As for the case of real imaging, closed form relations for the local geometric properties of the fringe pattern are desireable for designing or eveluating the characteristics of a moire interferometer. Approximate closed form relations for certain local geometric properties of the fringe will be derived in this section for the case of collimated imaging.

The local geometric properties of the fringe pattern that will be calculated include:

1. the fringe spacing,
2. and fringe angle,
3. the sensitivity of the spacing and angle to changes in the orientation of the object,
4. the sensitivity of the fringe position to the object position, i.e. the fringe shift.

Because the derivation is so similar to the work in section 3.5 the presentation is somewhat terse.

Recall from section 3.4 that the observed fringe pattern can be thought of as the perspective view of the intersections between the object and the equiorder surfaces of the moire interferometer. While the equiorder surfaces for the case of collimated imaging are simple (planar) an object of general 3-dimensional shape has no simple analytical representation. It is not possible, therefore, to calculate the object/equiorder surface intersections in closed form.

As discussed in Chapter 3, the approximate local geometric fringe properties can be calculated if locally the object is assumed to be planar. Under this assumption the object/equiorder surface intersection reduces to the intersection of two planes, which has a simple analytical representation. The approximate local fringe properties can then be determined from the perspective view on the viewing system image plane of this line of intersection.

To show that for collimated imaging the equiorder surfaces are truely planar, consider Equation 4-8 rewritten in the standard form of a plane:

$$AX + BY + CZ + D = 0 \qquad (4\text{-}10)$$

where

$$A = \left(\frac{P_P}{P_V T_3} \cos \alpha_V - \frac{T_1}{T_3} \right) \qquad B = \left(\frac{P_P}{P_V T_1} \sin \alpha_V - \frac{T_2}{T_3} \right)$$

$$C = -1 \qquad D = -\left(\frac{(Fo - \Phi_P + \Phi_V) P_P + T_X}{T_3} \right)$$

Note that the position of the equiorder surface plane is dependent only on D, which is a linear function of the fringe order.

The local fringe properties are calculated at some specified point of interest, X,Y,Z. To calculate the object/equiorder surface intersection at this point it is again necessary to know both the object plane and the equiorder surface plane normal vectors at the point X,Y,Z. The object normal is again arbitrarily defined, and is represented as:

$$\hat{O} = \begin{bmatrix} O_X \\ O_Y \\ O_Z \end{bmatrix} \qquad (4\text{-}11)$$

The local normal vector of the equiorder surface is determined using Equations 4-1 a and b and 4-3. Considered together Equations 4-1 a and b and Equation 4-8 constitute the components of the equation for the equiorder surface parameterized in X_V and Y_V. The equiorder surface normal is calculated by applying Equation 3-13 to Equations 4-8 and 4-1. The equiorder surface unit normal, $\hat{EO}$, can be written:

$$\underset{\wedge}{EO} = \begin{bmatrix} EO_Y \\ EO_Y \\ EO_Z \end{bmatrix} = \begin{bmatrix} \left(\frac{T_1}{T_3} - \frac{P_P}{P_V T_3} \text{ SIN } \alpha_V\right) \frac{1}{mag} \\ \left(\frac{T_2}{T_3} - \frac{P_P}{P_V T_3} \text{ SIN } \alpha_V\right) \frac{1}{mag} \\ \frac{1}{mag} \end{bmatrix} \qquad (4\text{-}12)$$

where

$$mag = \sqrt{\left(\frac{P_P}{P_V T_3} \text{ COS } \alpha_V - \frac{T_1}{T_3}\right)^2 + \left(\frac{P_P}{P_V T_3} \text{ SIN } \alpha_V - \frac{T_2}{T_3}\right)^2 + 1}$$

4.4.1 Fringe Angle

As in section 3.5, the object plane is defined such that it contains the point of interest X,Y,Z. This is done by choosing the point X,Y,Z as the base of the object normal vector. The intersection between the object plane and the equiorder surface (plane) that passes through the point X,Y,Z corresponds to a moire fringe line. It is this line of intersection that is used to determine the observed fringe direction. A vector along this line of intersection can be determined from the cross product of the unit normal vectors for the object and the equiorder surface. This vector is illustraded in Figure 3-7. The appropriate vector relation (repeated from Section 3.5) is:

$$\overline{F} = \hat{O} \times \hat{EO} = \begin{bmatrix} F_X \\ F_Y \\ F_Z \end{bmatrix} \qquad (4\text{-}13)$$

The fringe line vector, $\overline{F}$, is a 3-dimensional vector expressed in viewing frame coordinates. What is of interest, however, is the fringe direction as observed on the viewing plane, or the perspective view of $\overline{F}$. Since the fringe lines are observed along collimated rays

parallel to the Z axes, the perspective views of the vector $\overline{F}$ on the viewing plane (which is the XY plane) is given simply by the X and Y components of the 3-dimensional vector. Accordingly, the perspective view of $\overline{F}$, denoted $\overline{FP}$, can be written in terms of the components of $\overline{F}$ as:

$$\overline{FP} = \begin{bmatrix} FP_X \\ FP_Y \end{bmatrix} = \begin{bmatrix} F_X \\ F_Y \end{bmatrix} \qquad (4\text{-}14)$$

The angle of the fringes is simply the angle of the vector FP on the viewing plane.

4.4.2 Fringe Spacing

As in section 3.5, the fringe spacing on the viewing plane is determined using the fringe spacing vector, $\overline{A}$, which lies in the object plane and connects adjacent fringe lines. Figure 3-9, which illustrates the vector $\overline{A}$, applies for collimated imaging as well. The solution for $\overline{A}$ proceeds in the same manner as in Section 3.5, except the components of $\hat{\overline{EO}}$ are defined as by 4-12. Also, the distance between the equirder surfaces, $|\overline{EO}|$, is evaluated directly from the last term in the equation for the equiorder surface, or 'D' in Equation 4-10. The equiorder surface spacing is equal to the change in the last term caused by increasing the fringe order from Fo to Fo + 1. Thus, the spacing can be written as:

$$|\overline{EO}| = D\,(Fo + 1) - D\,(Fo) = \frac{P_p}{T_3} \qquad (4\text{-}15)$$

Using the same methods as in section 3.5, the components of $\bar{A}$ can be expressed in terms of the vectors $\hat{EO}$, $\bar{F}$, and $\hat{O}$, and the expressions for the components of $\bar{A}$ are repeated below (see section 3.5):

$$A_Z = \frac{|\bar{EO}|\ (F_Y O_X - F_X O_Y)}{(F_Z O_Y - F_Y O_Z)\ EO_X + (F_X O_Z - F_Z O_X)\ EO_Y + (F_Y O_X - F_X O_Y)\ EO_Z} \qquad (4\text{-}16\ a)$$

$$A_Y = \left[\frac{F_X O_Z - F_Z O_X}{F_Y O_X - F_X O_Y}\right] A_Z \qquad (4\text{-}16\ b)$$

$$A_X = -\left[\frac{O_X}{O_Y}\right] A_Y + -\left[\frac{O_Z}{O_X}\right] A_Z \qquad (4\text{-}16\ c)$$

The observed fringe spacing is determined from the perspective view of the fringe spacing vector. As above, the perspective of $\bar{A}$, which is called $\bar{AP}$, on the viewing plane is given by the X and Y components of $\bar{A}$.

$$\bar{AP} = \begin{pmatrix} AP_X \\ AP_Y \end{pmatrix} = \begin{pmatrix} A_X \\ A_Y \end{pmatrix} \qquad (4\text{-}17)$$

As for the case of real imaging, the fringe spacing is given by the component of $\bar{AP}$ that is perpendicular to the direction of the fringe lines (i.e perpendicular to $\bar{FP}$). Equations 3-33 and 3-34 of section 3.5 can be used to compute the fringe spacing for collimated viewing as well, yielding the following relations for the observed fringe spacing, SPC:

$$SPC = \left(AP_Y FP_Y - AP_X FP_X \right) \frac{1}{mag} \qquad (4\text{-}18)$$

where

$$mag = \sqrt{(FP_X)^2 + (FP_Y)^2}$$

4.4.3 Fringe Angle and Spacing Sensitivity

As in section 3.5, the fringe angle and the fringe spacing sensitivities are evaluated from the finite changes in the fringe spacing and fringe angle produced by a known variation in the orientation of the object or parameter of the moire interferometer. The general relations offered in Chapter 3 still apply for the case of collimated imaging and the relations are repeated below:

$$\text{Fringe Angle Sensitivity} = \frac{\Delta \text{ Fringe Angle}}{\Delta \text{ Parameter}} \qquad (4\text{-}19)$$

$$\text{Fringe Spacing Sensitivity} = \frac{\Delta \text{ Fringe Spacing}}{\Delta \text{ Parameter}} \qquad (4\text{-}20)$$

4.4.4 Fringe Shift

As in section 3.5, the fringe shift caused by a shift in the position of the object along the object normal is again calculated using the fringe shift vector. The fringe shift vector, $\bar{B}$, is a vector in the equiorder surface plane that connects the nominal object plane and a parallel plane that is a distance $|D|$ along the object

normal. The illustration of Figure 3-10 applies to this analysis as well, and illustrates the vectors $\overline{D}$ and $\overline{B}$. The conditions for calculating the fringe shift, are the same as for the real imaging case. The solution given by Equation 3-23 still applies provided that the equiorder surface normal is calculated with Equation 4-12. The expressions for the components of the fringe shift vector are repeated below:

$$B_X = \frac{\left|\overline{D}\right| (F_X EO_Z - F_Z EO_X)}{(O_Y F_Z - O_Z F_Y) EO_X + (O_Z F_X - O_X F_Z) EO_Y + (O_X F_Y - O_Y F_X) EO_Z} \qquad (4\text{-}21\ a)$$

$$B_Y = \left[\frac{F_Z EO_X - F_X EO_Z}{F_Y EO_Z - F_Z EO_Y}\right] B_X \qquad (4\text{-}21\ b)$$

$$B_Z = -\left[\frac{EO_X}{EO_Z}\right] B_X - \left[\frac{EO_Y}{EO_Z}\right] B_Y \qquad (4\text{-}21\ c)$$

The vector $\overline{B}$ is a three dimensional vector representing the shift of the fringe lines. What is sought, however, is the apparent fringe shift seen on the viewing plane. The perspective view of the vector $\overline{B}$ on the viewing plane, denoted $\overline{BP}$, is determined by simply the X and Y components of $\overline{B}$.

$$\overline{B_P} = \begin{bmatrix} BP_X \\ BP_Y \end{bmatrix} = \begin{bmatrix} B_X \\ B_Y \end{bmatrix} \qquad (4\text{-}22)$$

The component of $\overline{BP}$ that is perpendicular to the fringe line vector $\overline{F}$ is the apparent fringe shift, and is denoted SFT. As in section 3.5, the fringe shift can be calculated by the dot product of the vector $\overline{BP}$ with a vector in the viewing plane that is perpendicular to the fringe line vector, $\overline{F}$. The appropriate expression for SFT is as follows:

$$SFT = \left[B_Y FP_Y - B_X FP_X \right] \frac{1}{mag} \qquad (4\text{-}23)$$

where

$$mag = \sqrt{(FP_X)^2 + (FP_Y)^2}$$

The fringe position sensitivity can then be evaluated by simply dividing the magnitude of the fringe shift by the magnitude of the object displacement.

Chapter 5. Experimental Verification for Diffuse Analysis.

5.1 Introduction

In this chapter experimental verification is presented for the analysis of moire interferometry for diffusive objects that was developed in Chapter 3. The verification relys on experimentally obtained moire fringe patterns obtained with a projection type moire interferometer and a flat diffusely reflecting object. The developments of Chapter 3 that are verified through the experiments include:

1) the relations for analytically constructing the moire fringe pattern (section 3.3),

2) the closed form relationships of section 3.5 thet yield the approximate local geometric properties of the moire fringe pattern (section 3.5).

The apparatus used for the experiments is described in section 5.2. In section 5.3, fringe patterns constructed analytically using the relations of section 3.3, are compared with experimentally obtained fringe patterns. The experimental and analytical results are also compared against moire fringe patterns obtained from a CAD (computer aided design) emulation of the moire interferometer. The analytical, experimental and CAD generated fringe patterns compare very well. In section 5.4 the closed form relations for local geomteric fringe properties (of section 3.5) are verified by comparing analytically predicted local fringe properties (including fringe angle, spacing, and fringe sensitivities) against experimentally determined fringe properties. The results show a good correlation between the

experimental and the analytical results, although systematic errors do appear. These errors represent a fundamental limitation of the of the closed form relations, and the source of these errors is discussed.

5.2 Experimental Apparatus and Procedures.

5.2.1 Description of Apparatus

A schematic of the diffuse moire interferometer used in the experiments is given in Figure 5-1. Consistant with the analysis of Chapter 3, the moire interferometer employs real imaging type projection and viewing. The components of the moire interferometer are discussed in detail in this section.

The projection system is a standard slide projector. The projector was equipped with a 4 inch, f = 4 air spaced doublet lens. It was necessary to stop the lense down to f = 10 to obtain the required 1.5 inch depth of focus. As with any slide projector, the intensity pattern projected onto the object was formed by back illumination of a transmittance pattern (like an ordinary film slide). For the experiments the transmittance pattern was a one inch glass square, 100 line/inch, ronchi ruling. A ronchi ruling consists of evenly spaced straight, dark lines etched into glass. The profile of the transmittance pattern created with the ronchi ruling is approximately that of a square wave, alternating between high and low levels of light transmittance.

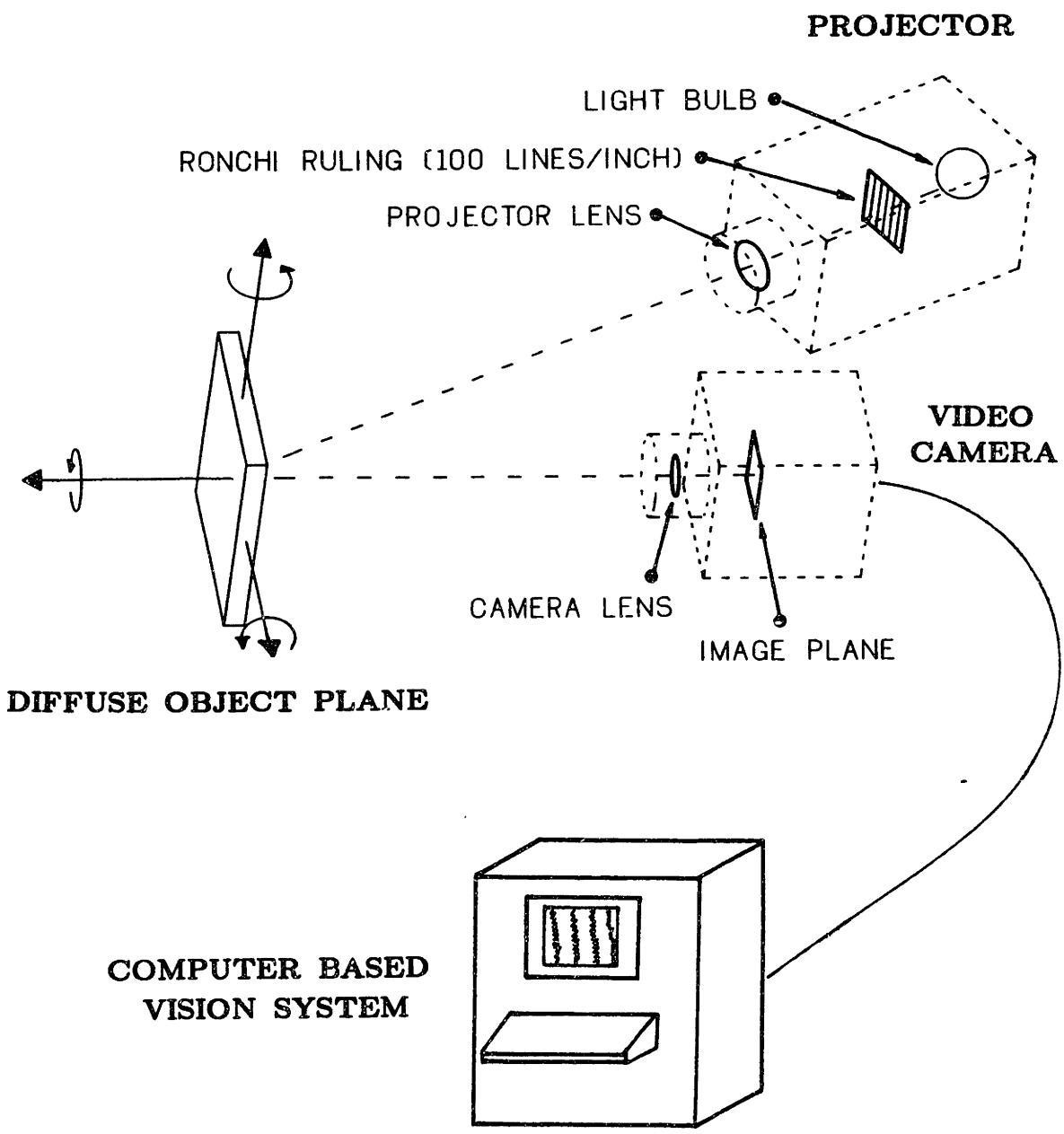

FIGURE 5-1 Schematic of Experimental Apparatus

The diffusive object used in the experiments was a 4 inch square aluminum plate covered with white paper. The plate was held by a mechanism that allowed the orientation of the plate to be changed while keeping the center of the plate at a fixed position.

The viewing system of the experimental moire interferometer made use of a computer based vision system (Automatix Inc., Autovision II). The computer vision system uses a Panasonic CCD (charge coupled device) solid state video camera, equipped with a 25 mm lens. The lens was typically operated at f numbers of 5 through 8. The resolution of the CCD pixel (picture element) array on the camera backplane is 404 horizontally and 256 vertically, with 16 levels of resolution in intensity. The spatial resolution on the camera backplane, if considered to be equal to the size of the pixels, is approximately 0.025 mm (0.001 inch). An entire video frame can be stored in a memory buffer and is then available for processing and display on a monitor. The camera was aligned so that the horizontal and vertical rows of the image plane pixel array coincided with the X_V and Y_V axes of the viewing system.

The viewing grid that interferes with the intensity pattern viewed on the object to produce moire fringes was created in software using the computer vision system. A stored video frame containing the digitized picture of the structured light pattern on the object was processed by setting alternate columns in the picture buffer array to zero intensity. This had the effect of drawing equally spaced zero intensity lines parallel to the Y_V axis. The result was the same as would be observed if an evenly spaced transmittance pattern of the same pitch and with a square wave profile (alternating between 0 and

1) were placed directly in front of the pixel backplane. The resulting intensity pattern contained the moire fringe pattern, and the moire pattern was clearly visible when displayed on the monitor.

5.2.2 Disadvantages to System Configuration

It is important to note that because the columns of the pixel array are used as the viewing grid, the spatial resolution of the viewing grid is limited to being equal to or lower than the frequency of the pixel array. The sensitivity of the moire fringes to object shape depends strongly on the grid frequencys. Thus, producing the viewing grid with the pixel array will severely limit the sensitivity of the interferometer with respect to the field of view. Recall that having the moire process limited by the resolution of the vision system is exactly contrary to the purposes for developing the moire technique. To take full advantage of the moire technicue the spatial frequency of the grids should not be directly coupled to the resolution of the vision system used to interpret the moire fringes. However, for the experiments, which did not require great sensitivities, it was simpler to form the moire pattern using the video camera array.

Instead, the fringes should be formed through a separate imaging process in front of the vision system. A possible scheme for doing this is depicted in Figure 5-2. If such a scheme were employed the vision system would only need to have sufficient resolution to resolve the moire fringe lines. In general (but not always) the moire will have a spatial frequency much lower that the interfering grids.

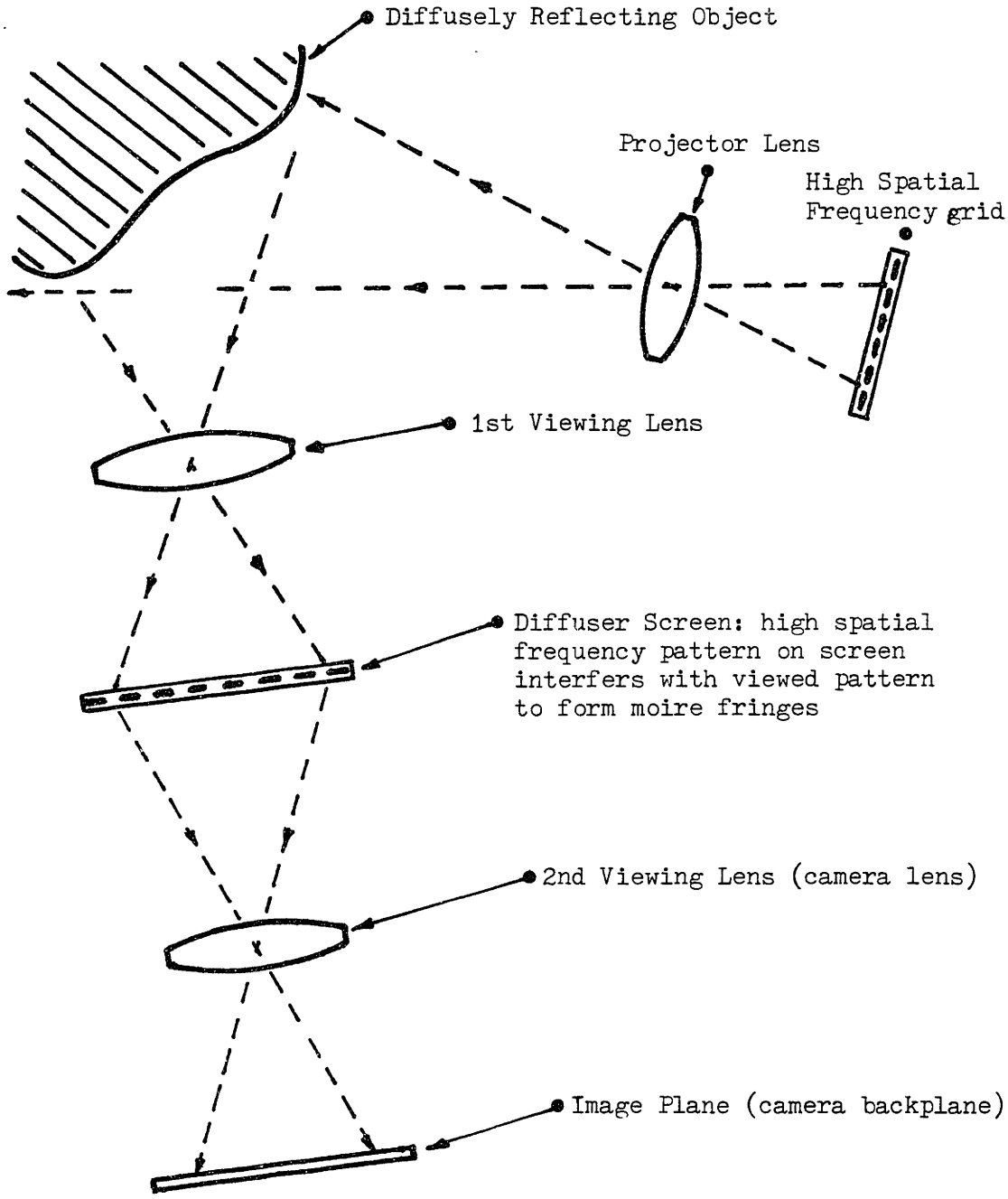

FIGURE 5-2 Schematic for Directly Viewing the Moire Fringe Pattern

5.2.3 Interferometer Parameters

The parameters for the experimental system shown in Figure 5-1 were either measured directly or calculated from the manufacturer's specifications for the components. The origin (i.e. lens node) for the projection system lens was determined by measuring the combined object and image distances and the projector magnification (using the projected ronchi ruling). The object (756 mm) and image (119 mm) distances were then computed using paraxial (i.e simple) lens equations. The location of the origin of the viewing system was estimated by assuming that the node for the lens is at the geometric center of the lense. The image distance for the viewing system (26.7 mm) was then calculated using the measured object distance (393 mm). The rotations that described the orientation of the projecting system relative to the viewing system (i.e. the angles in the coordinate transformation) are were zero except for the rotation about the Y axis, τ . This angle was measured to be 18 degrees (.314 rad). The offsets of the origin of the projecting system relative to the viewing system origin (Xo,Yo,Zo) were computed from the measured angles and object distances. In summary, the parameters used in the transform (see Equation 3-2) representing the interferometry geometry can be listed as follows:

$\theta =$ $\quad X_o = -236$ mm

$\zeta =$ $\quad Y_o = 0$

$\psi =$ $\quad Z_o = 334$ mm

Computing the effective pitch of the software generated patterns required calibration of the vision system. Specifically, the relation between the software units and real distances on the camera image plane was required. First, a scale factor (assumed constant over the field of view) between pixel measurements and distances on the object was determined by measuring known distances with the vision system. The pitch of the software generated pattern was computed using this scale factor, the calculated viewing system magnification (from object and image distances) and the pitch of the software generated pattern in software units, to be 0.115 mm. This value was later modified by trial and error to 0.113 mm since the later was found to produce closer agreement between the analytically constructed and experimentally observed fringe patterns. This small (1.7 %) but necessary adjustment in pitch was attributed to measurement and specification errors of the system parameters used to calculate the pitch.

5.2.4 Experimental Procedures

For both the verification of the relations for fringe pattern construction (presented in section 5.3) and the verification of the relations for the local geometric fringe patterns (presented on section 5.4), moire fringe patterns for several object orientations were obtained experimentally. To simplify the procedures variations in the object orientation were restricted to rotations of the object plate about a single axis. Specifically, the object (plane) was restricted to being parallel to the Y'' axis shown in Figure 5-3, which is in turn parallel to the Y axis of the viewing system. The

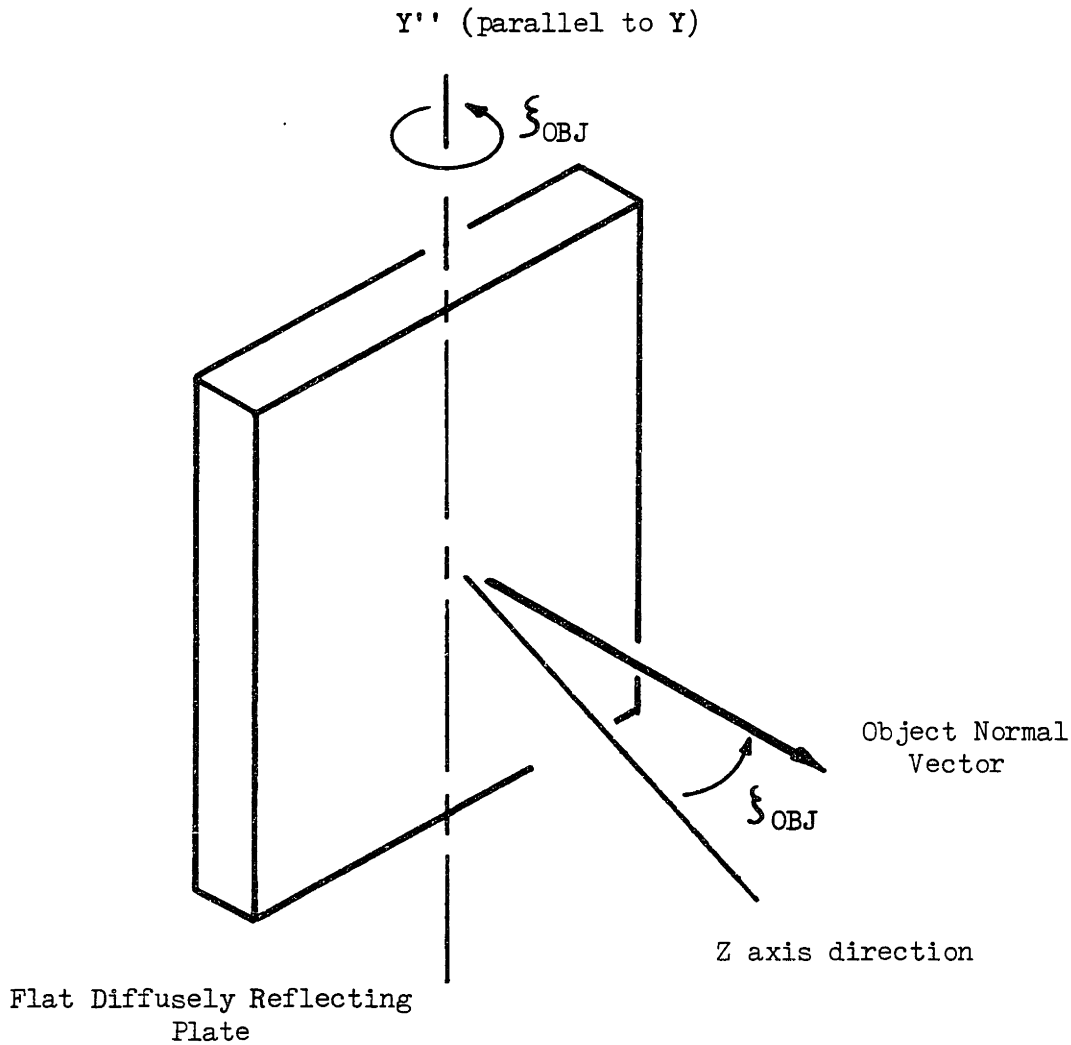

FIGURE 5-3 Object Rotations Considered in the Experiments

rotation of the object about the Y'' axis is denoted by the angle ζ_{OBJ}, measured from the Z axis direction (positive counter clockwise).

To facilitate comparing the experimentally obtained fringe patterns against analytically constructed ones (for section 5.3) it was necessary to record the fringe patterns displayed on the Autovision II monitor. To obtain hard copies of the moire fringe patterns the moire fringe patterns were simply photographed using a 35 mm camera.

The verification of the relations for the local geometric properties of the fringe pattern (section 5.4) involes comparing specific properties of the moire fringe lines (e.g. the angle, spacing, and sensitivities of the fringe lines) with analytically predicted values. The experimental fringe properties of angle and position were evaluated for individual fringe lines using the pattern analysis software of the computer vision system. However, before this software could be used, the high spatial frequency intensity fluctuations (i.e the individual lines of the patterns) in the moire pattern needed to be filtered out to make the moire fringe lines pattern recognizable to the vision system software. Filtering was accomplished by reassigning the local pixel values in the picture memory buffer to be equal to the average intensity level of the immediate surrounding area. After filtering, only the low spatial frequency intensity pattern of the moire (i.e the fringe lines) remained. The maximum and minimum intensity lines could then isolated using intensity thresholding techniques, and the angle and position of the fringe lines could be measuresd. The angular and spacing

sensitivities of the fringe lines were calculated from the changes in angle and position of the fringe lines. The procedures for determining the fringe properties will be described in more detail section 5.4.

5.3 Experimental Verification of Analytical Fringe Pattern Construction Techniques.

The derivation presented in section 3.3 provides relations for the coordinates and fringe order of the moire fringe pattern on the viewing system image plane as a function of object coordinates and the parameters of the moire interferometer. As discussed in Chapters 2 and 3, the image plane coordinates and fringe order represent complete information about the local (at a point) moire fringe pattern. Thus, it is suggested in Chapter 3 that by applying the relations of section 3.3 point by point over the object, the observed fringe pattern could be analytically constructed.

To demonstrate this technique a computer program was developed (listed in Appendix B) that determines and plots the moire fringe pattern produced on a flat, diffusely reflecting object. For simplicity the program is only capable of plotting points that fall on minimum (integral fringe order) or maximum (integral + 1/2 fringe order) intensity lines of the moire fringe pattern. Briefly, the object is scanned in a regular pattern, with small steps between points that are considered. At each point the fringe order and viewing plane coordinates are calculated using the relations of section 3.3. The points that fall within a small tolerance of being

integral or integral + 1/2 are plotted as a light or dark fringe centers.

The fringe patterns constructed using this program for four object orientations are presented in part a of Figures 5-4 through 5-7. Part b of these figures are the actual moire fringe patterns produced on the object, obtained by photographing the vision system monitor. The analytical and experimental fringe patterns are clearly very similar.

Part c of Figures 5-4 through 5-7 shows the moire fringe patterns produced using a computer aided design (CAD) based simulation for the projection moire interferometer. The simulation, which was developed by a collegue at MIT, Ron Leonard, is being explored as a design tool for moire interferometers [29]. The simulation computes and draws individual dark lines of the intensity pattern reflected off the object. The lines of the viewed intensity pattern are drawn in proper perspective, and appear as they would on the viewing system image plane. The moire pattern is then produced by drawing lines corresponding to the minimum transmittance lines of the transmittance grid on top of the lines representing the intensity pattern. The overlap of the two patterns is analogous to the interference of the actual intensity and transmittance patterns, and leads to the simulated moire pattern. From the figures it is seen that the CAD produced fringe patterns also compare favorably with the experimental results.

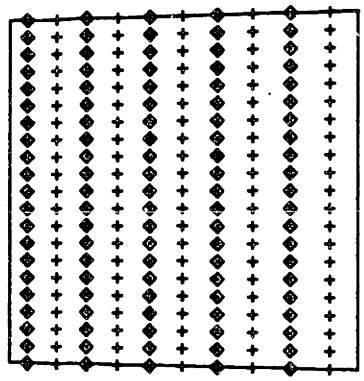

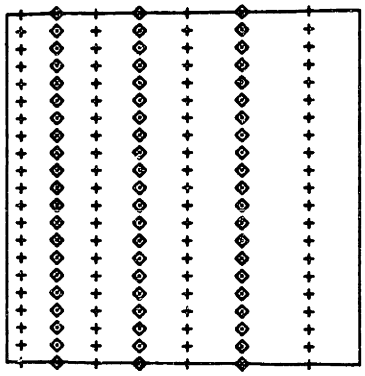

ANALYTICAL PREDICTIONS

+ - LIGHT FRINGE CENTERS

◇ - DARK FRINGE CENTERS

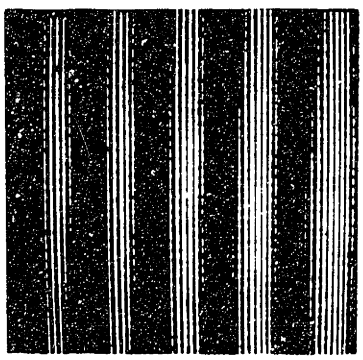

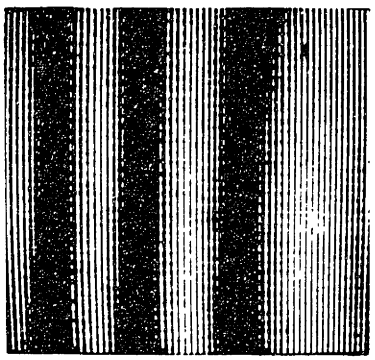

EXPERIMENTAL RESULTS

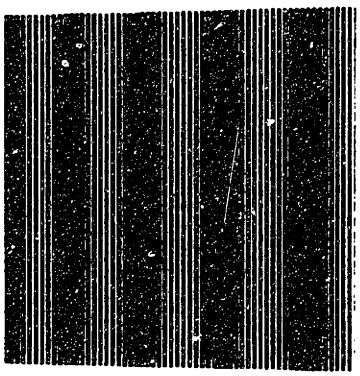

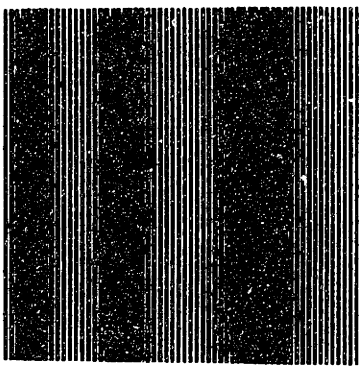

CAD BASED SIMULATIONS

ζ_{OBJ} = -10.0 deg

ζ_{OBJ} = -5.0 deg

FIGURE 5-4

FIGURE 5-5

Analytical Predictions, Experimental Results, and CAD Simulations for Moire Patterns on a Diffusely Reflecting Flat Object

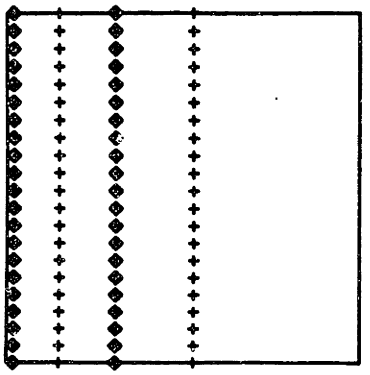

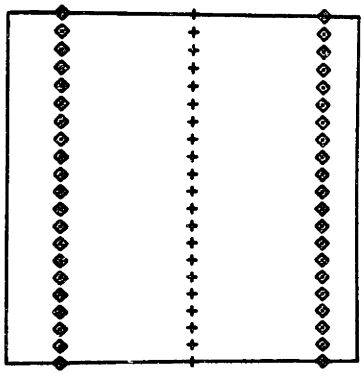

ANALYTICAL PREDICTIONS

+ - LIGHT FRINGE CENTERS
◇ - DARK FRINGE CENTERS

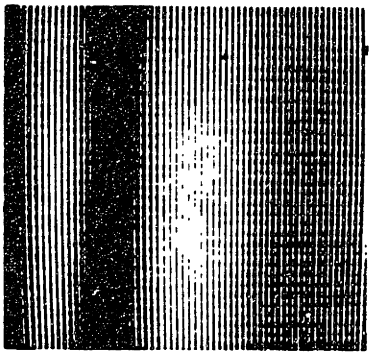

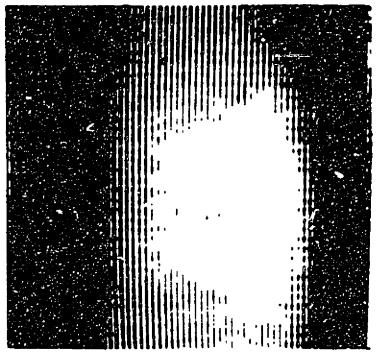

EXPERIMENTAL RESULTS

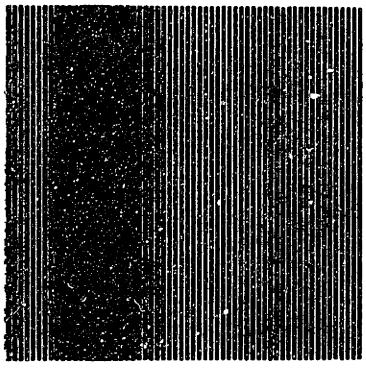

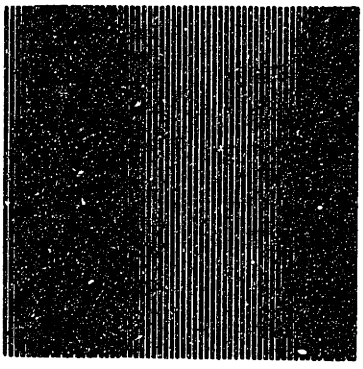

CAD BASED SIMULATIONS

ζ_{OBJ} = 0.0 deg

ζ_{OBJ} = 5.0 deg

FIGURE 5-6

FIGURE 5-7

Analytical Predictions, Experimental Results, and CAD Simulations for Moire Patterns on a Diffusely Reflecting Flat Object

It should be noted that although the cases shown in Figure 5-2 through 5-6 are simple, the relations used to produce them are applicable to objects of any shape. The technique is limited by the ability to conveniently represent complex shapes, but not the ability to compute the fringe pattern on that shape. Also, even though the fringe patterns produced on the flat object are straight for the cases considered here this will not generally be the case.

5.4 Verification of Approximate Relations for fringe Properties.

The relations developed in section 3.5 provide an approximate, closed form solution for certain local geometric properties of the moire fringe pattern. These relationships are unique in that these relationships directly calculate the local properties of the moire fringes observed for a particular interferometer and object configuration. Previous analyses do not compute the properties of the fringes directly. Accordingly, the validity of the relations of section 3.5 are experimentally verified. The results of this verification are presented in this section.

To verify the approximate relations, experimentally obtained fringe properties (using the apparatus described in Section 5.2) are compared against the values predicted using the approximate relations of section 3.5. This comparison is made over a range of object orientaions. Because there was no convenient way to vary the parameters of the interferometer, only changes in the object orientation were considered. As in section 5.3, changes in the orientation of the object were again restricted to rotations about the

Y'' axis (see Figure 5-3).

5.4.1 Obtaining Experimental Fringe Properties

As explained in section 5.2, the moire fringe pattern of the experimental interferometer was analysed using a computer vision system. Specifically, the pattern analysis software was used to identify the position and direction (angle) of individual fringe lines. The five local geometric fringe properties (outlined in section 3.5) were then calculated from the position and direction of the individual fringe lines. The specific steps used to calculate each of the fringe properties will be outlined briefly below:

FRINGE SPACING: At a specific object orientation, i.e. specific angle, ζ_{OBJ}, the pattern analysis software was used to obtain the position and angle of the centermost fringe lines. Using the two positions and the angle of the centermost fringe lines the perpendicular distance between the fringes was calculated . This distance was taken to be the fringe spacing.

FRINGE ANGLE: As indicated above, the angle of the fringe lines was measured directly with the pattern analysis software. The angle of the fringe closest to the center of the object was taken to be the fringe angle. The fringe angle was measured from the positive X_V axis on the image plane (positive counter clockwise).

FRINGE SPACING SENSITIVITY: To calculate the sensitivity of the fringe spacing to changes in the orientation (i.e. ζ_{OBJ}) of the object, the spacing for two different object orientations was compared. The spacing was first evaluated with the object at one

orientation. The object was then rotated one degree, and the spacing was again evaluated. The sensitivity was computed by first dividing the difference in spacing by the 1 degree rotation of the object (see Equ. 3-37), and then dividing by the fringe spacing for the unrotated object. Hence, the fringe spacing sensitivity is expressed as the fractional change in the spacing produced per degree object rotation. To evaluate the sensitivity of the spacing at a particular orientation it is desireable to have the object rotation used to perturb the spacing be a small as possible. One degree was the smallest rotation that produced detectable changes in spacing.

Fringe Angle Sensitivity: The sensitivity of the angle of the fringes to changes in the orientation was evaluated in a way similar to the fringe spacing sensitivity except that the fringe angle was evaluated using the pattern analysis software directly. The angle sensitivity was computed by dividing the change in fringe angle caused by a 1 degree rotation of the object by 1 degree (see Equ. 3-36).

Fringe Position Sensitivity: The sensitivity of the position of the fringe lines (i.e. the fringe shift) to a shift in the position (but not orientation) of the object was computed by comparing the location of a particular fringe line. The position of the centermost fringe line was first measured with the object unshifted. The position of the same fringe line was then measured after the object was shifted by 2.46 mm. The sensitivity was calculated by dividing distance between the unshifted and shifted fringe positions by the distance that the object was shifted.

5.4.2 Obtaining Analytical Predictions for Fringe Properties.

The analytical predictions for the fringe properties were obtained using the computer program implementation of the approximate relations that was described at the end of Section 3-5. The program is capable of computing and plotting the local geometric fringe properties for a given interferometer geometry and given object orientation. For comparison with the experimental res ults, the fringe properties were calculated for a range of object orientations. Again only rotations about the Y'' axis (see Figure 5-3) were considered.

PLOTTED RESULTS

Both the experimentally and the analytically obtained results for the fringe properties appear in Figures 5-8 through 5-12. The experimental data is indicated by diamond shape symbols. As seen in the figures, the experimental data was taken only over a limited range of object orientations. Outside of the range indicated on the plots the moire fringes were not clearly visible. At large negative values of ζ_{OBJ} the high inclination of the object plane causes the fringes to become so closely spaced that fringe pattern becomes confused with the viewing grid pattern. Also, for positive values of ζ_{OBJ} larger than about 7 degrees the spacing of the structured light pattern projected onto the object (as seen from the camera) became too small to be clearly resolved by the video camera. Subsequent processing of the blurred image produced poorly defined moire fringe lines.

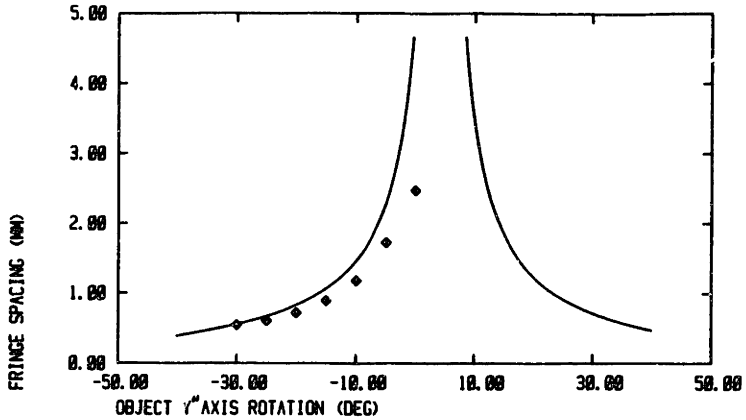

FIGURE 5-8 Analytical and Experimental Results for Fringe Spacing vs. Object Angle

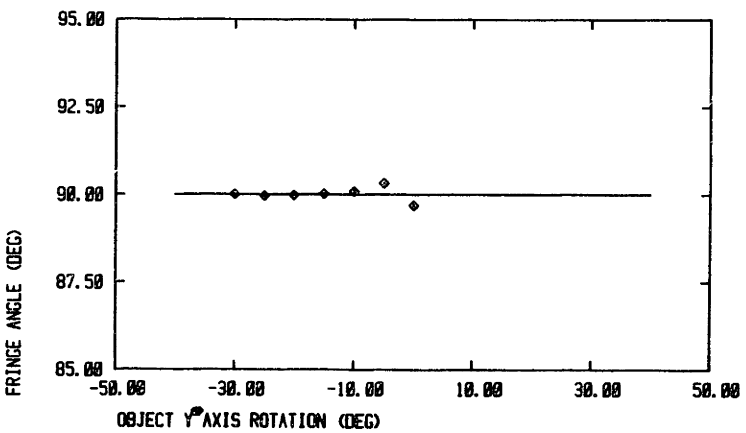

FIGURE 5-9 Analytical and Experimental Results for Fringe Angle vs. Object Angle

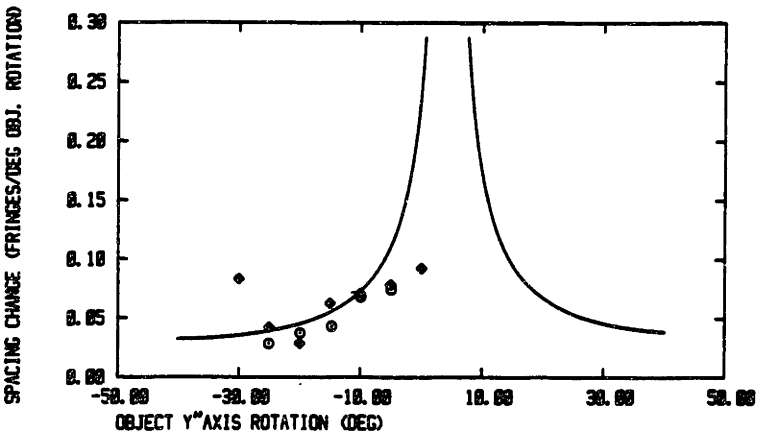

FIGURE 5-10 Analytical and Experimental Results for Fringe Spacing Sensitivity vs. Object Angle

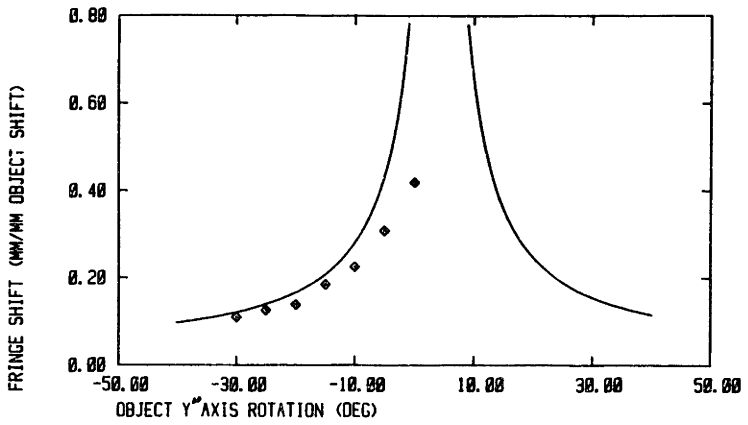

FIGURE 5-11 Analytical and Experimental Results for Fringe Angle Sensitivity vs. Object Angle

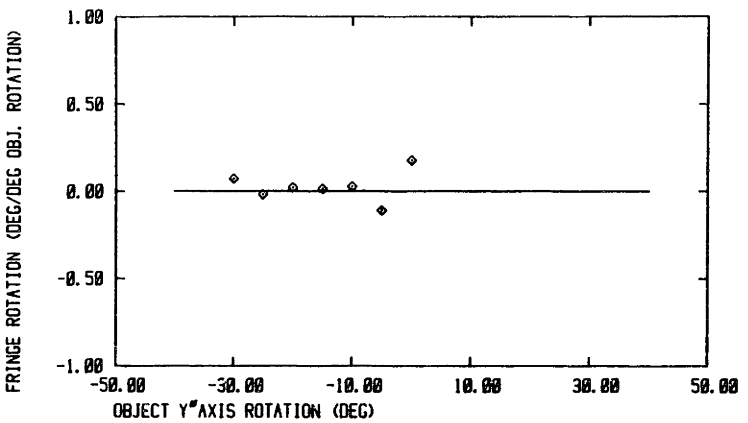

FIGURE 5-12 Analytical and Experimental Results for Fringe Position Sensitivity vs. Object Angle

In Figure 5-10 two sets of experimental data are shown. The diamond symbols denote the experimental values calculated using the method described above in subsection 5.4.1. It is clear from Figure 5-10 that the agreement betw een the original experimental results (diamond symbols) and analytical values for the spacing sensitivity is considerably worse than for the other fringe properties. Because of this the experimental fringe spacing sensitivity was evaluated by a second method.

The circular symbols in Figure 5-10 show the experimental values for the fringe spacing sensitivity evaluated using the experimental data from Figure 5-8 directly. From a smooth curve hand drawn to fit the experimental data for the fringe spacing, the sensitivity of the fringe spacing was evaluated by dividing the slope of the curve by the fringe spacing. As for the previous method, this yielded the fractional change in the fringe spacing per degree object rotation. Clearly the experimental data evaluated by this second method gives smoother results that show improved agreement with the analytical results.

Ideally, the two methods of evaluating the spacing sensitivity should yield the same results. Clearly this is not the case. The second method is not sensitive to noise in the measurement of the position of the individual fringes (because of the smoothly fit curve), and this is most likely the reason for the improvement of the results.

5.4.3 Interpreting the Results

It is clear from Figures 5-8 through 5-12 that there are significant differences between the experimentally and analytically obtained fringe properties. While for the fringe angle and the fringe angle sensitivity the results agree fairly well, there are clearly large and systematic differences in the results for the spacing, spacing sensitivity, and position sensitivity (fringe shift). To clearly understand why the results differ and what the differences mean to the validity of the closed form relations for fringe properties, it is necessary to interpret the results in terms of the equiorder surface concept (section 3.4).

The equiorder surfaces for the moire interferometer used in the experiments are shaped as illustrated in Figure 3-6 b. Thus, the equiorder surface for a particular order is slightly curved, with the concave side towards the camera and projector. Also, because the lines of the projecting and viewing grids are parallel, the shape of the equiorder surfaces does not change in the Y direction. This means that the cross section of an equiorder surface in any plane parallel to the X,Z plane is constant.

As described in section 3.4, the intersections of an object and the equiorder surfaces can be used to predict the moire fringe pattern. Specifically, a moire fringe on the camera image plane of a particular order corresponds to the perspective view of the line of intersection between the object and the equiorder surface of that order.

For the experiments both the equiorder surfaces and the object are of constant cross section for any value of Y (recall that the flat object is only allowed to rotate about the Y'' axis). Consequently, the intersections between the flat object and the equiorder surfaces will consist of straight lines that are parallel to the Y axis. The fringe lines (on the image plane) will, therefore, consist of straight lines that are parallel to the Y (or Y_V) axis (see Figures 5-4 through 5-7. Such equiorder surface/object intersections are illustrated in cross section in Figure 5-13.

In Figure 5-13 the intersections of the object with the equiorder surfaces (shown in cross section as a point) is shown to dictate the appearance of the moire fringe lines (also a point when shown in cross section) at a particular point on the viewing plane. The equiorder surface concept can also be applied to the analytical model provided the equiorder surfaces and the object accurately reflect the assumptions used in developing the model. Specifically, the equiorder surfaces associated with the analytical model must be flat and oriented perpendicular to the local normal vector for the actual equiorder surfaces. (The assumptions made for the equiorder surfaces for the analytical model are described in more detail in section 3.5). Figure 5-14 illustrates both the true curved equiorder surfaces and the flat approximations to the equiorder surfaces assumed for the analytical solutions. As in Figure 5-13, intersections between the object and the curved equiorder surfaces (dashed lines) indicate where moire fringe lines will be observed for for the actual moire interferometer. Intersections between the object and the flat equiorder surfaces indicate the moire fringe lines will be observed

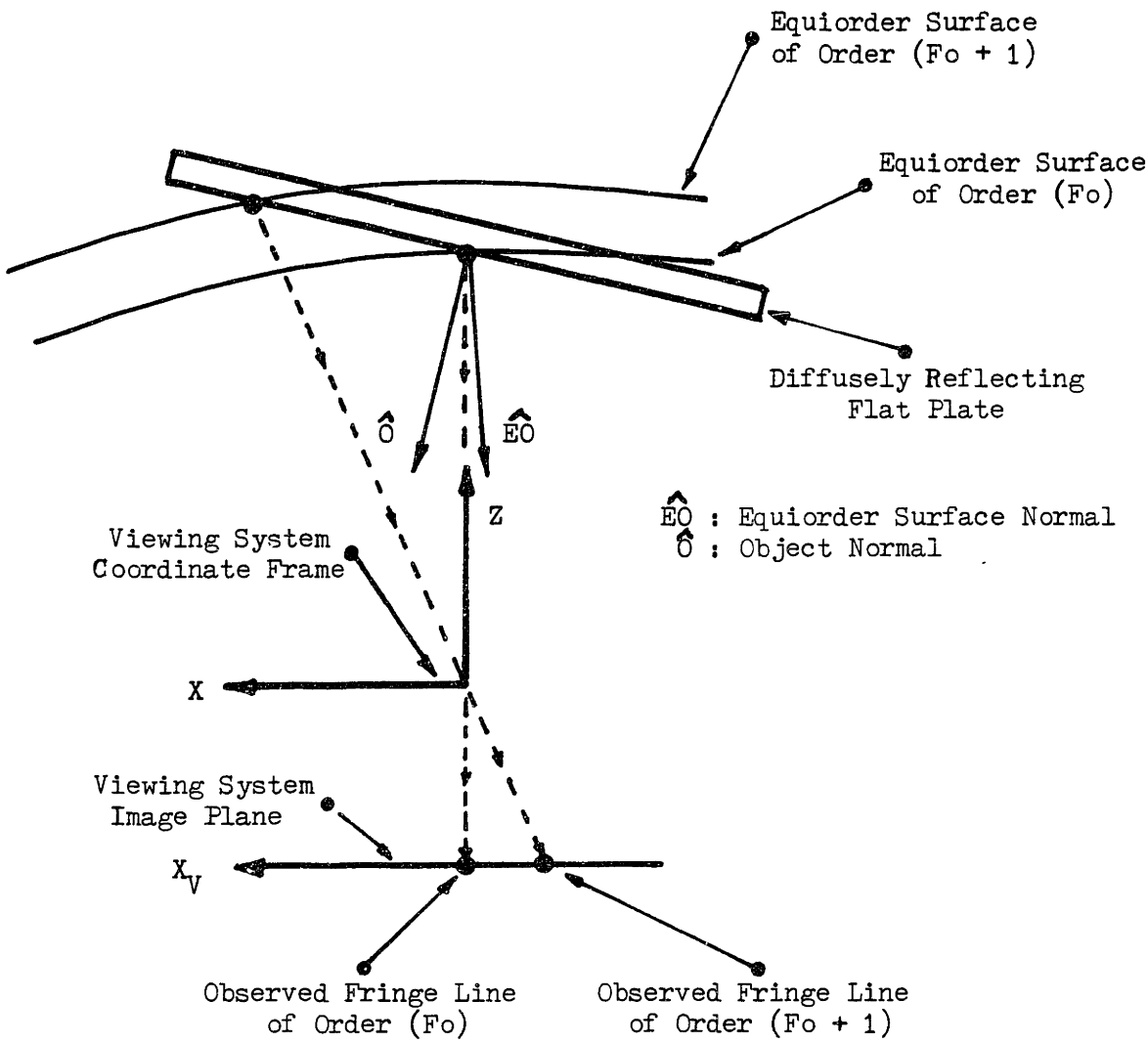

FIGURE 5-13 Cross Section of Equiorder Surface/Object Intersections

according to the approximate analytical techniques of section 3.5.

Now that the equiorder surface concept has been applied and illustrated for the experimental and analytically assumed equiorder surfaces, it can be used to interpret the validity and the accuracy of the analytical results. In discussing the results each of the fringe properties will be considered separately.

FRINGE ANGLE: The fringe angle is considered first because for the moire interferometer and object considered the relationship between fringe angle and object orientation angle (ξ_{OBJ}) is somewhat trivial. Recall that in developing the illustration for the equiorder surface/object intersections (Figure 5-13) it was stated that the cross sections of both the equiorder surfaces and the object did not change in the Y direction. This means that the equiorder surface/object intersections will be straight lines that are parallel to the Y axis. This is the case for both curved equiorder surfaces of the real interferometer and the planar equiorder surfaces assumed for the analytical solution.

The resulting fringe lines observed on the vision system image plane will also be straight lines that are parallel to the Y (or Y_V) axis. Consequently, from the equiorder surface concept one would expect that for both the experimental and the analytical results that the fringe angle would be constant at 90. From Figure 5-9 it is clear that the analytical and the experimental results both show the fringe angle to be constant at 90 degrees. There is some scatter in the experimental data, but this is attributed to noise due to processing the moire fringe pattern to determine the fringe angle.

FRINGE ANGLE SENSITIVITY: The relation between fringe angle sensitivity and object angle is also trivial for the object orientations. As discussed above the equiorder surface/object intersections indicate that the fringe angle will be constant at 90 degrees. This is true for both the curved equiorder surfaces of the actual interferometer and the planar equiorder surfaces assumed for the analytical solution. Thus, according to the equiorder surface concept the fringe angle sensitivity should be zero.

As seen in Figure 5-11 both the experimental and analytical results show zero fringe angle sensitivity, which is in agreement with the equiorder surface concept. The experimental results show some scatter, which is again attributed to processing errors.

FRINGE SPACING: The experimental and analytical results for fringe angle and fringe angle sensitivity were simple and the experimental and the analytical results were in clear agreement. The results for the fringe spacing, however, show significant and systematic differences between the experimental and analytical results (Figure 5-8). The reason for these differences can be explained by examining the illustration of the equiorder surface/object intersections of Figure 5-14.

By examining the equiorder surface/object intersections several observations can be made concerning the experimentally and analytically determined fringe spacing. These observations include:

1) Both the experimentally and analytically determined fringe spacing will increase (decrease) as the angle between the object normal and the equiorder surface normal is reduced (increased).

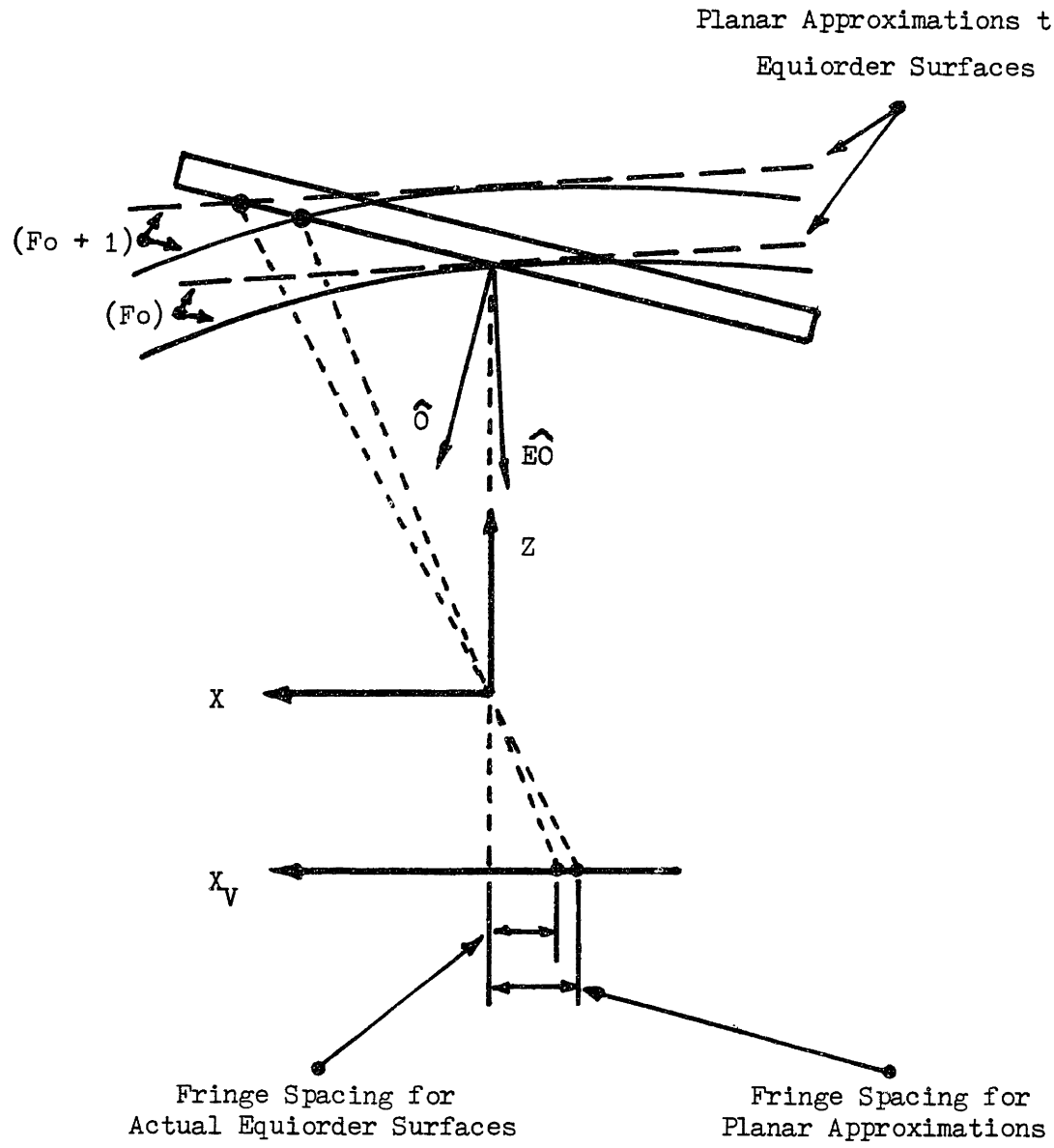

FIGURE 5-14 Effect of Planar Approximations for Equiorder Surfaces on Observed Fringe Spacing

2) The experimentally determined fringe spacing will in general be smaller than the analytically determined fringe spacing due to the shift of the equiorder surfaces.

3) At the orientation where the object normal vector aligns with the equiorder surface normal the analytically determined fringe spacing will become infinitely large, whereas the experimentally determined fringe spacing will remain finite.

Upon examining the actual results (Figure 5-8) it is clear that the above relationships (predicted using the equiorder surface concept) do appear.

FRINGE SPACING SENSITIVITY: The fringe spacing sensitivity is simply the rate of change of the fringe spacing with object orientation divided by the fringe spacing. From the geometry of the equiorder surface/object intersections, it is not obvious how the experimental and the analytical results should be related. The only observation that can be made is that the change in geometry between the equiorder surfaces and the object would indicate the fringe sensitivity would be a smooth and continuous function of object orientation. This is not true at the point where the object aligns with the equiorder surfaces. For both the analytical and the experimental results the point at which the object aligns with the equiorder surfaces is a point at which the fringe spacing is poorly defined.

Examining the results for the fringe spacing sensitivity (Figure 5-10) one can at least conlude that there are no contradictions between the results in the figure and the general characteristics predicted by the equiorder surface concept. The analytical results

are clearly continuous and smooth except where the object aligns with the equiorder surface. The experimental results (at least if only the circular symbols are considered) also appear to be smooth. Also, the trend (i.e. increasing fringe sensitivity as the object aligns with the equiorder surfaces) of the experimental and the analytical results agree.

Note that the experimental data represented by diamond symbols was ignored. The large fluctuations in this data is attributed to errors introduced by trying to determining small changes in fringe spacing directly with the vision system software. The experimental methods used to derive the data represented with the circular symbols, as described earlier in this section, is equally as valid, but less succeptable to measurement errors.

FRINGE POSITION SENSITIVITY: The equiorder surface concept can be used to visualize the shift produced in the moire fringes by a shift in the object, as illustrated in Figure 5-15. In the figure both the actual equiorder surfaces and the planar approximation to the surfaces are indicated. The figure is provided to illustrate the effect of object orientation on the fringe shift.

From the equiorder surface/object intersections illustrated in Figure 5-15 several observations can be made concerning the experimental and analytical results for shift. The important ones include:

1) The fringe shift for a given object shift will increase (decrease) as the angle between the object and the equiorder surfaces decreases (increases).

2) The analytically obtained fringe shift

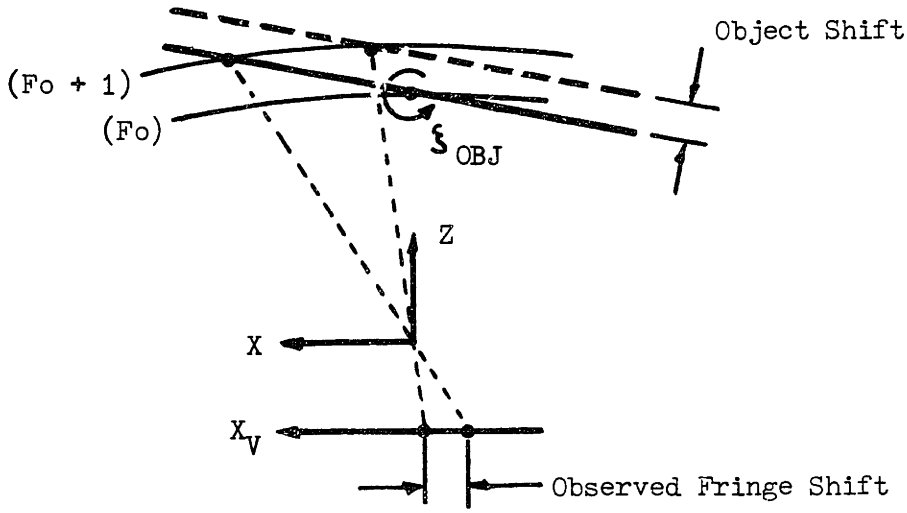

3-15 (a) Observed Fringe Shift for Small Object Angle

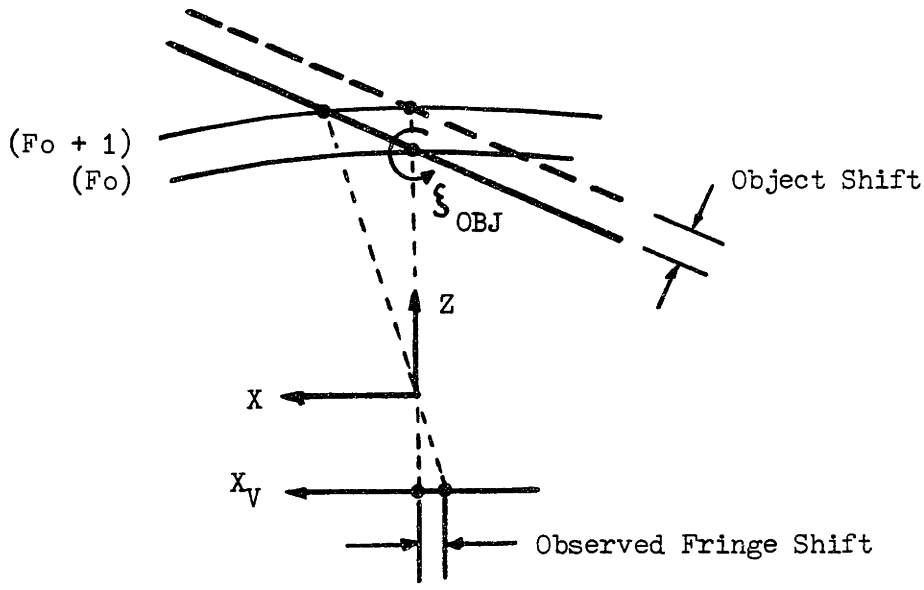

3-15 (b) Observed Fringe Shift for Larger Object Angle

FIGURE 3-15 Effect of Object Angle on Observed Fringe Shift

will be greater than the experimentally derived fringe shift for a given object orientation.

3) The analytically obtained fringe position sensitivity will be infinitely large for the object orientation that causes the object to align with the equiorder surfaces.

Upon examining the experimental and analytical results for the fringe shift (Figure 5-12) one can see that the results do agree with what was expected from the equiorder surface/object intersections.

5.4.4 Conclusions.

The experimental and analytical results have been examined in light of the equiorder surface concept. The results for all of the fringe properties agree without contradiction with what is expected from the equiorder surface/object intersections. Also, although quantitative comparisons were not made, the equiorder surface/object intersections accurately predict the differences between the experimental and the analytical results agrees.

Because the experimental and analytical results do make sense when analysed in terms of equiorder surfaces, the following conclusions were drawn:

1) The fringe properties for a real moire interferometer can be described using the concept of equiorder surface/object in intersections.

2) The relations of section 3.5, which were based on the assumption of flat equiorder surfaces and a flat object, give meaningful, although approximate, results for the fringe properties.

3) The differences between the experimental and analytical results in Figures 5-8 through 5-12 are a result of the assumption in the

analytical solution that the equiorder surfaces are flat. Also, the that errors in the values for the fringe properties predicted with the approximate relations can be significant.

Even though the material presented above showes the approximate relations to have shortcomings, the relations are still very useful for designing the properties of a moire interferometer. This utility is demonstrated in the next chapter through the desing of the properties of moire interferometers.

As mentioned, the inaccuracies of the approximate relations arise because the equiorder surfaces and the object are assumed to be flat. This assumption was made because it is very difficult to analyticlly represent curved surfaces of general shape. Significant improvements in the accuracy of the analytical relations would most likely be observed if the relations were expanded to facilitate equiorder surfaces and objects of simple shapes (such as cylinders, spheres, etc.).

Chapter 6. Example Design of Diffuse Moire Inspection Systems.

6.1 Introduction

The work of this thesis is directed to developing analytical methods that are useful in analysing and designing moire inspection systems. The analysis presented in Chapters 3 and 4 differs from previous work in that the fringe properties and the sensitivity of the fringes as observed on the image plane are calculated directly for a specific object and interferometer configuration. However, the utility of the local fringe properties for evaluating or designing inspection systems has not yet been established. Recall that previous moire methods concentrate primarily on the fringe map interpretation of moire fringes and do not consider the local changes in the fringe pattern from some nominal pattern.

In this Chapter two hypothetical inspection tasks serves to illustrate how object shape variations can be directly interpreted from changes in the local fringe properties and how the local fringe properties can be used to design the properties of the moire interferometer. The inspection tasks are very simple examples of the method and by no means establish a general method for object inspection or interferometer design. The tasks do exemplify, however, the utility of the analysis of Chapter 3 as a tool for design and evaluation of moire inspection systems.

The two example inspection tasks are illustrated in Figure 6-1, and involve detecting variations in the height and orientation of the top of a 1x2x1 inch block. The height of the center of the top face is to be inspected to 0.001" and the orientation is to be inspected to 0.1 degree. As indicated in Figure 6-1, to simplify the inspection tasks and the design procedures for the parameters of the moire interferometer, the height and orientation inspections are considered separately.

As a further simplification, for both tasks all of the parameters of a projection type moire interferometer are assumed to be specified except for the spatial frequency of the projecting and viewing patterns and the nominal object orientation. The assumed system configuration is illustrated in cross section in Figure 6-2 and corresponds to the special case interferometer configuration that produces flat equiorder surfaces (see Figure 3-5). The specific values of the parameters of the 4 by 4 coordinate transformation that locates the projecting system relative to the viewing system (recall Equation 3-2) are as follows:

$$X_o = 0 \qquad \theta = 0$$
$$Y_o = 50_{mm} \qquad \xi = 0$$
$$Z_o = 0 \qquad \psi = 0$$

This special case is chosen because it makes the object/equiorder surface intersections simpler to understand, and also since flat equiorder surfaces should yield good agreement between the approximate (planar model) relations of section 3.5 and the actual fringe properties.

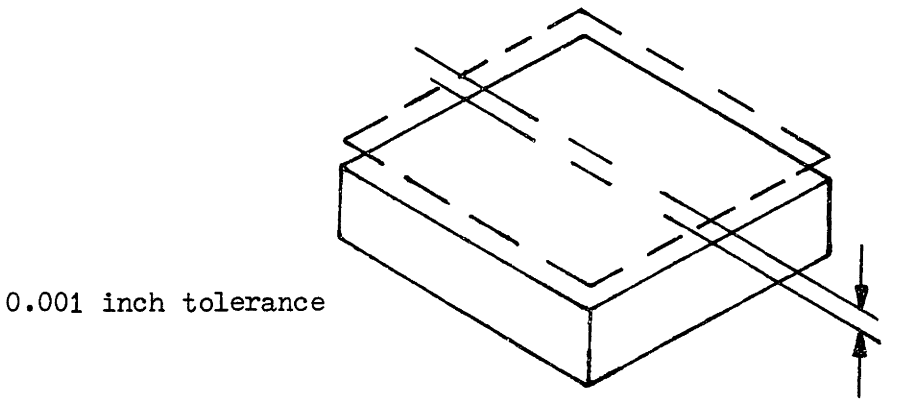

6-1 (a) Object Height Inspection Task

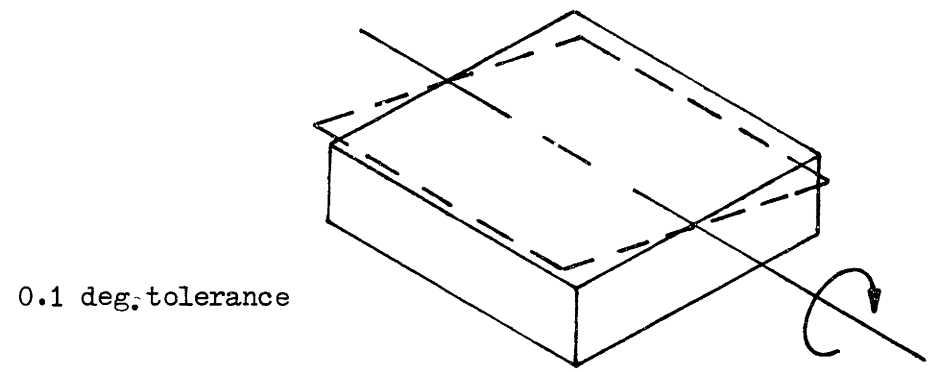

6-1 (b) Object Orientation Inspection Task

FIGURE 6-1 Hypothetical Inspection Tasks used in Example Interferometer Designs

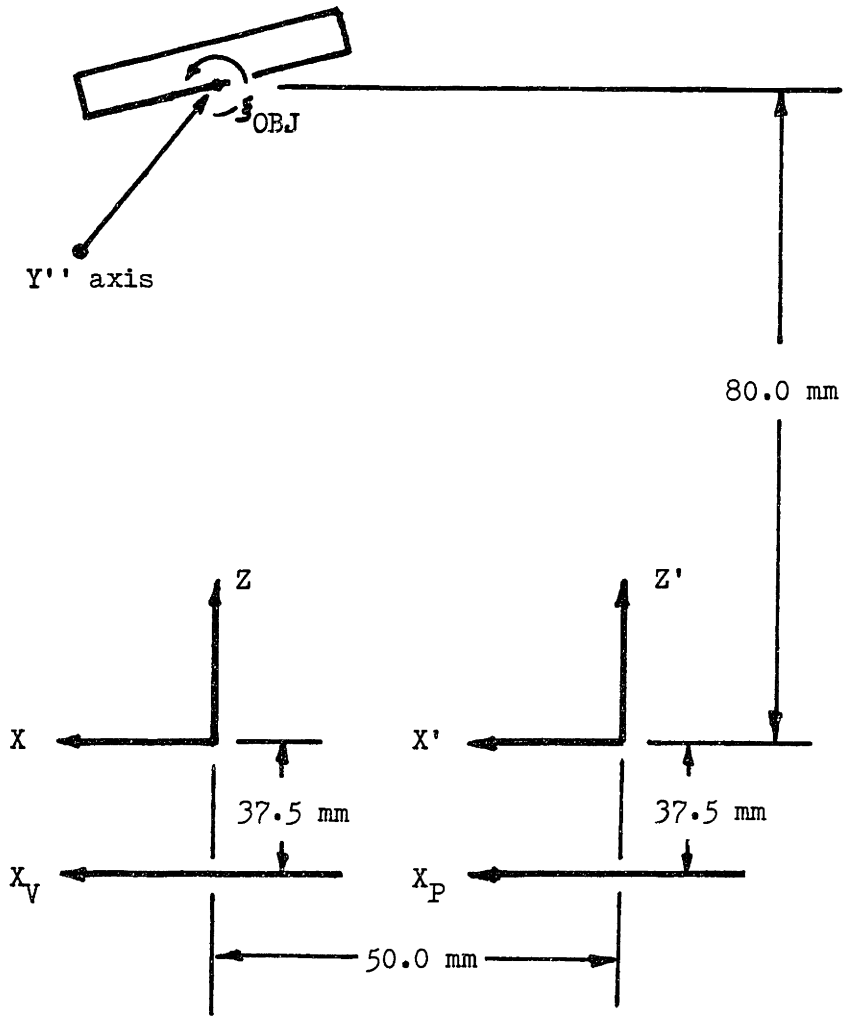

FIGURE 6-2 Configuration of the Projection and Viewing Systems used for Interferometer Design

The projecting and viewing patterns are assumed to have the same pitch pitch, P. Also, the nominal object orientation is constrained to consist only of rotations about the Y'' axis shown in Figure 6-2. With this assumption, the only system parameters that remain unspecified are the pitch of both patterns, P, and the Y'' axis rotation, ζ_{OBJ}, for the nominal object orientation. These parameters are specified using design procedures that are based on the closed form relations for local fringe properties of section 3.5.

The example design procedures consider both the inspection task requirements and the limitations of the vision system employed in the inspection system. These considerations are discussed in more detail in section 6-2. The design procedures for object height and orientation inspection are then developed and carried out in Sections 6-3 and 6-4, respectively. The success of the designs are then verified using analytically constructed fringe patterns for both nominal and displaced objects.

6.2 Considerations for Object Inspection Via Moire Fringes.

For the system configuration illustrated in Figure 6-2 the observed fringe pattern for the nominal object will consist of straight, parallel fringe lines with a nearly constant spacing (recall both the object and the equiorder surfaces do not vary in the Y direction). Variations in the height of the object will cause a lateral (X directed) shifting of the fringe lines from their nominal positions. Changes in the orientation of the top of the block (limited to small rotations about Y'') will cause the fringe spacing

to increase or decrease from its nominal value. In either case, for the changes of the nominal fringe pattern to be useful, the vision system employed must be able to first recognize the fringe lines and then resolve the differences between the nominal and varied fringe pattern. Accordingly, the shape, spacing and sensitivity of fringes must simultaneously satisfy the tolerances required for inspection task and the limitations of the vision system employed.

6.2.1 Vision System Limitations.

The only vision system limitations to be considered here are the spatial resolution of the sensor employed for the viewing system image plane and the basic requirments of currently available pattern recognition software used to process the fringe pattern. The imaging capabilities of the projection and viewing systems are ignored, as are the limits imposed by the method of producing the moire fringe patterns.

The spatial resolution of the image sensor is assumed to be 0.001 inches, which is comparable to that of the video camera employed for the experiments of Chapter 5. The size of the image plane is set at 0.5 inches square, again comparable to existing video cameras. To be detectable, it is assumed that the changes in position or spacing of the observed pattern (on the image plane) must be at least 0.001", which is 0.2% of the field of view.

The capabilities of the recognition software for image processing also imposes limits on the maximum spacing of the fringe pattern and the minimum detectable change in the fringe pattern. First, computer

based vision systems commonly use intensity thresholding to identify object boundaries. Consequently, to be recognizable the fringe lines must be bonded by adjacent fringes. For instance, to recognize the center of a dark fringe, the fringe spacing must be small enough so that a significant increase in intensity on either side of the dark fringe canter is detectable in the field of view. To insure easily recognized fringes the maximum fringe spacing should be limited to at most one third of the field of view. This insures that at least two fringe line centers that are well bounded by other fringes will be visible in the field of view. Second, specific points on a fringe, the fringe center for example, can only be recognized with finite accuracy. For changes in the fringe position to be detected with confidence the change should be a significant fraction of the fringe spacing. For the design presented in the next section it is assumed that the fringe spacing needs to change by 10 % to be detected accurately.

To summarize the limitations assumed to be imposed by the limitations of the vision system:

1) The minimum resolvable change in fringe position is 0.001" (on the image plane).

2) For accurate recognition the changes in fringe position should be at least 1/10 the nominal spacing.

3) For well defined fringes, the maximum fringe spacing is 1/3 the field of view.

These limites are very conservative estimates, and they are not intended to suggest the upper limmit on the performance that can be achieved. These limits are intended only as constraints for the design procedures of sections 6-3 and 6-4.

6.2.2 Tools for System Design.

The local fringe properties of fringe spacing and angle, the sensitivity of the spacing and angle to object orientation, and the sensitivity of the fringe positions to object position (fringe shift) are all functions of the projecting and viewing grid frequencies and the nominal object orientation. Plots of these relationships, developed with the approximate relations of Section 3.5, were given earlier in Figures 3-12 and 3-13. These plots show the approximate local fringe properties as a function of object orientation (3-12) and of the spatial frequency of the projecting and viewing grids (3-13). These and similar plots, developed with the relations of Section 3.5, can be used to isolate the nominal object orientation and grid pattern frequencies that will satisfy both the inspection task tolerances and the vision system limitations. Design procedures using such plots are developed in the next two sections for first the object height and then the object orientation inspection tasks.

6.3 Design for Object Height Inspection

As mentioned, for the system configuration illustrated in Figure 6-2 the nominal object will produce straight and nearly evenly spaced fringes. Variations in object height are manifest by a shift of the fringes from their nominal position. In this section a design procedure based on the relations of section 3.5 will be

developed to choose the nominal object orientation and grid frequencies that yield the fringe position sensitivity and fringe spacing that satisfy both the object height inspection task

requirements and the limitations of the vision system, as oulined in sections 6.1 and 6.2.

6.3.1 Design Considerations

Examining the plots of Figure 3-13 which correspond to the system configuration of Figure 6-2 with a fixed object rotation about the Y'' axis of 0.05 rad (2.7 deg), you can see that the fringe shift sensitivity (mm fringe shift/mm object shift) is independent of the grid pattern frequency. This independence allows the plot of 3-12 (a), which correspond to the correct system configuration except for a constant grid pitch of 0.0254 mm (0.01 inch), to be used to isolate the nominal object orientation (ξ_{OBJ}) that yields the necessary minimum fringe shift sensitivity. An acceptable grid frequency can then be determined using a plot of fringe spacing vs grid frequency, similar to 3-13 (a), that is developed for the object in the object orientation isolated from the minimum shift sensitivity.

6.3.2. Design Steps

The considerations discussed above can be used as the basis for designing the nominal object orientation and the grid frequencies for the object height inspection task outlined in Figure 6-1. The specific design steps to accomplish this are outlined below.

Step 1: Compute the Minimum Required Fringe Position Sensitivity.

The more severe restriction for the minimum fringe shift is imposed by the need for the fringe shift to be 1/10 th of the fringe spacing for the vision system to accurately resolve the fringe shift. The magnitude of the minimum required fringe position sensitivity is determined using the maximum allowable fringe spacing, which for this design is assumed to be 1/5 th the field of view, or 0.1 inches on the

image plane. The minimum resolvable fringe shift is then 0.01 inches. The minimum required fringe position sensitivity is found by dividing the minimum resolvable fringe shift by the object shift resolution required for the object height inspection, which is 0.001 inches.

$$\text{Fringe Position Sensitivity} = \frac{\text{Fringe Shift}}{\text{Object Shift}}$$

$$= \frac{0.01 \text{ inches}}{0.001 \text{ inches}}$$

$$= 10$$

Step 2: Isolate an acceptable nominal object orientation using closed form relation for fringe shift sensitivity.

Using the relations of Section 3.5, a plot of fringe shift sensitivity as a function of object orientation (Y'' axis rotation angle) was developed and is shown in Figure 6-3. From this plot, the maximum object rotation about the Y axis that will yield the required shift sensitivity is isolated as 2.69 degrees. Thus, the object would have to be inclined less than or equal to 2.69 degrees to achieve the required fringe shift sensitivity.

Step 3: Isolate minimum the grid frequency that yields the maximum acceptable fringe spacing.

Using the closed form relations for fringe spacing, a plot of the fringe spacing as a function of grid frequency can be generated for the object orientation isolated in Step 2 ($\xi_{OBJ} = 2.69$ deg). From this plot, which appears in Figure 6-4, the grid frequency that yields a fringe spacing of 0.1 inches (0.254 mm) can be determined. From the plot, the required grid frequency is found to be about 13.4 lines/mm (340 lines/inch).

6.3.3 Design Verification.

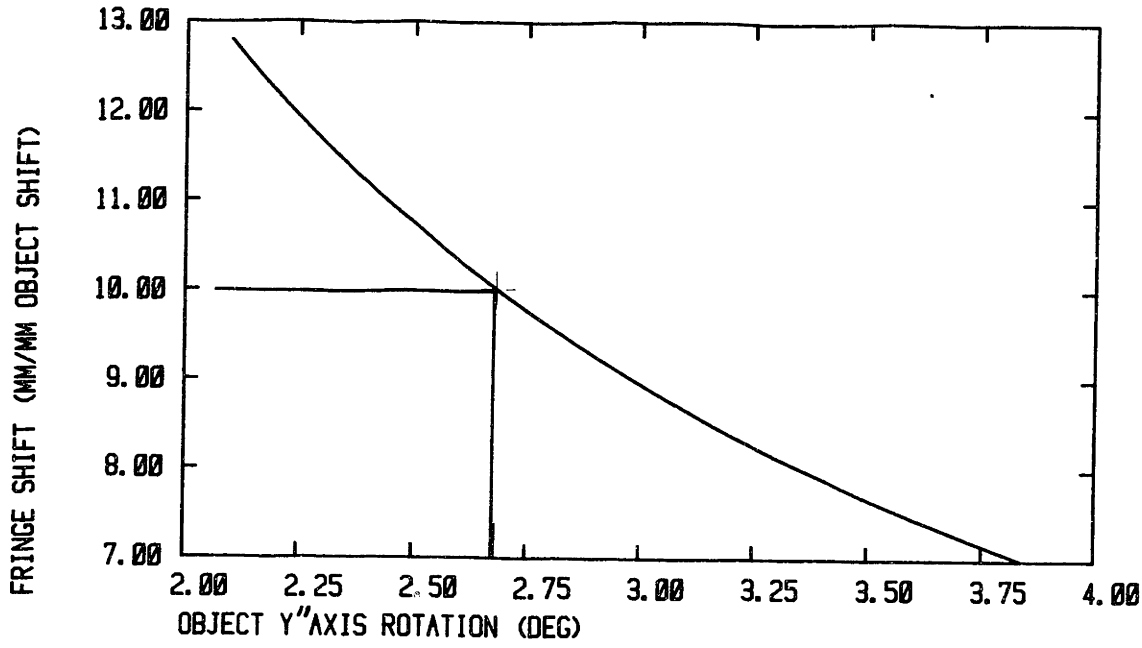

FIGURE 6-3 Sensitivity of Fringe Position vs. Object Angle for Object Height Inspection Task

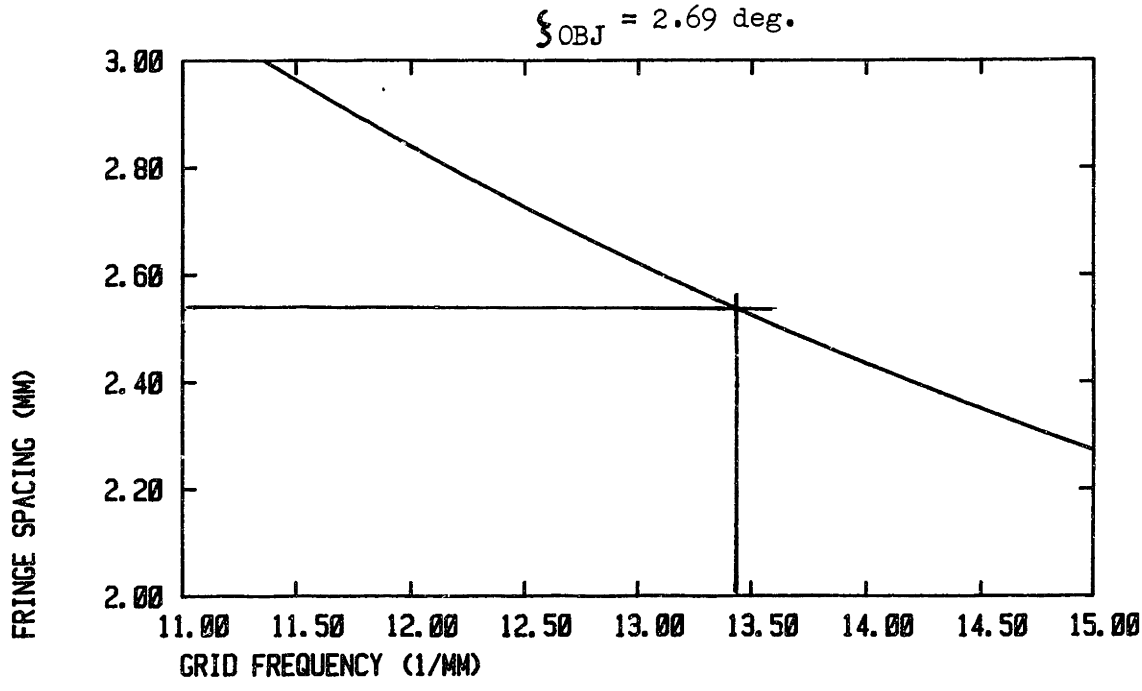

FIGURE 6-4 Fringe Spacing vs. Grid Frequency for Object Height Inspection Task

To verify the design performed through the steps above, the relations of section 3.3 were used to analytically construct the observed moire fringe pattern for both nominal object height and for the object shifted 0.001 inch in the direction of the surface normal. The nominal object orientation (from step 2) and the designed grid frequency (from step 3) were used for constructing the observed fringe patterns.

The top half of the nominally observed fringe pattern and the bottom half of the displaced fringe pattern appear in Figure 6-5. From a listing of the coordinates of the fringe centers, the average fringe shift and spacing of the center most fringes was computed to be 0.011 inches and 0.0998 inches, respectively. Clearly the design goals for fringe position sensitivity and spacing were closely met.

6.4 Design for Object Orientation Inspection.

For the system configuration adopted in Figure 6-2, variations in object orientation are manifested by changes in the observed fringe spacing. As for the object height inspection, plots of the fringe properties developed with the closed form relations of section 3.5 will be used to design the nominal object orientation and grid frequency that satisfy both the inspection tolerances and the assumed limitations of the vision system. The design steps are more complicated for the object orientation inspection task than for height inspection since the effect of variations of the object orientation on the fringe spacing needs to be considered.

6.4.1 Design Considerations

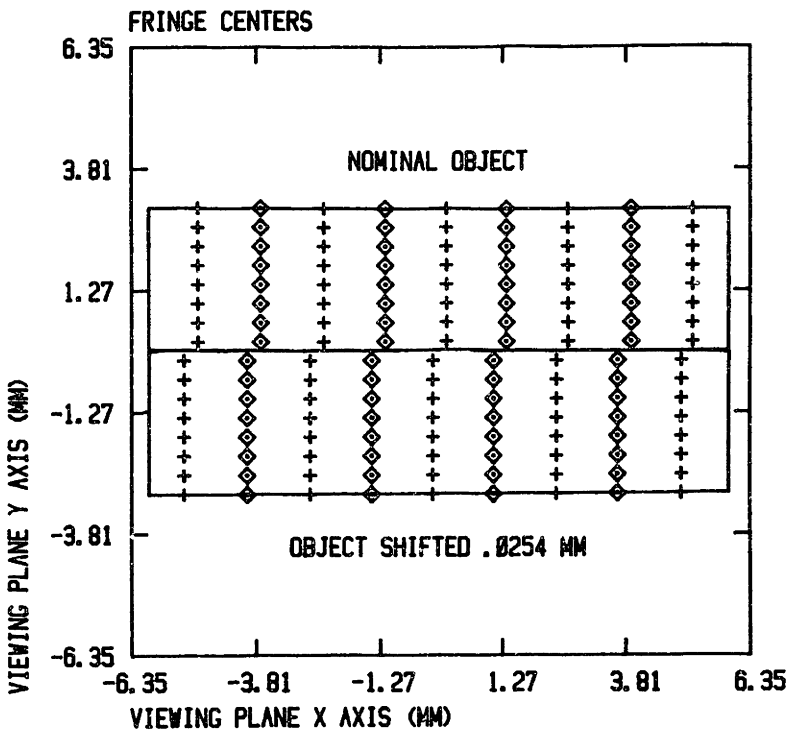

FIGURE 6-5 Fringe Shift Due to 0.001 Inch Shift in Height of Object

The designed interferometer must simultaneously satisfy a limit on the maximum fringe spacing and the minimum required spacing sensitivity. However, as shown in Figure 3-12 (a) and (c), the fringe spacing and the fringe spacing sensitivity are both strongly dependent on object orientation. The design steps must insure that the design requirements are met throughout the range of object orientations expected during operation.

From Figure 3-12 (a) and (c), you can note that for a given operating point object orientation variations in one direction cause an increase in both fringe spacing and fringe spacing sensitivity, whereas variations in the other direction cause a decrease in both properties. Consequently, the limits on the maximum fringe spacing and the maximum fringe spacing sensitivity will establish high and low boundaries for a range of object orientation that satisfy the design requirements.

The fringe spacing sensitivity is, at least for the approximate model of Section 3.5, constant for constant object orientation and for changing grid pattern frequencies. Therefore, plots of fringe spacing vs. object orientation can be used to isolate the maximum object rotation (ζ_{OBJ}) that will give the minimum fringe spacing sensitivity required for the inspection task. The object orientation isolated using the minimum fringe spacing is not the operating point but the limiting orientation into which the object is expected to vary.

The grid pattern frequency needs to be established by balancing the minimum acceptable operating range for object orientation against the maximum acceptable projecting grid frequency. The larger the range in object orientation, the higher the grid frequency required to satisfy the limit for maximum fringe spacing over that range. For this example the operating range is assumed to be 0.4 degrees with the nominal object orientation located in the center of this range. The required grid frequency is then calculated using a plot of fringe spacing generated with the object oriented at the lower bound for object Y'' axis rotation (minimum ξ_{OBJ}).

6.4.2 Design Steps

The considerations discussed above can be organized into specific design steps for isolating the nominal object orientation and the grid frequencies suitable for the object orientation inspection task. These design steps are carried out below.

Step 1: Compute the minimum required fringe spacing sensitivity.

The minimum fringe spacing sensitivity required for the inspection task needs to be expressed as the fraction increases or decrease in the fringe spacing per degree object rotation. The limitations of the vision system require that the spacing change by at least 10% for the spacing change to be accurately resolved. Accordingly, the minimum required sensitivity can be found as follows:

$$\text{minimum fringe sensitivity} = \frac{0.1 \text{ fringes}}{0.1 \text{ deg rotation}}$$

$$= 1. \text{ fringes/deg}$$

Step 2: Isolate minimum object orientation angle.

From a plot of the fringe spacing sensitivity vs. object orientation (developed with a grid pitch of 0.0254 mm), illustrated in Figure 6-6, the minimum object orientation angle to satisfy the minimum required fringe spacing sensitivity is found to be just less than one degree, taken to be 0.99 degrees.

Step 3: Isolate nominal object orientation.

The operating range is chosen as 0.4 degree. Recall that the upper limit on the object angle was found to be 0.99 deg. This establishes the operating point at 0.79 degree and the lower limit of object angle at 0.59 degrees.

Step 4: Isolate minimum required grid frequency.

The minimum acceptable grid frequency is determined from a plot of the fringe spacing vs. grid frequency (Figure 6-7) constructed for the lower bound of object angle, 0.59 degree. The grid frequency that lowers the fringe spacing to the maximum value of 1/3 the width of the viewing plane, or 1/3 x 0.5"= 0.165" (4.19 mm), is read to be 37.15 lines per mm (or 945 lines/inch).

6.4.3 Design Verification

As for the object height inspection task, the design for the object orientation inspection task is verified using analytically constructed fringe patterns. Fringe patterns corresponding to objects with orientations throughout the operating range are illustrated in Figure 6-8. As expected from the design, the maximum spacing occurs at the minimum object angle. From a listing of the coordinates for the fringe centers, the fringe spacing at the center of the object for the object orientation of 0.59 degrees was found to be 0.162 inches, which is close to the design maximum fringe spacing of 0.165 inches. Also, as the object orientation changes from 0.99 to 0.89 deg the fringe spacing (between the center most fringes) changes from 0.133 to 0.152 inches. This corresponds to a spacing sensitivity of the

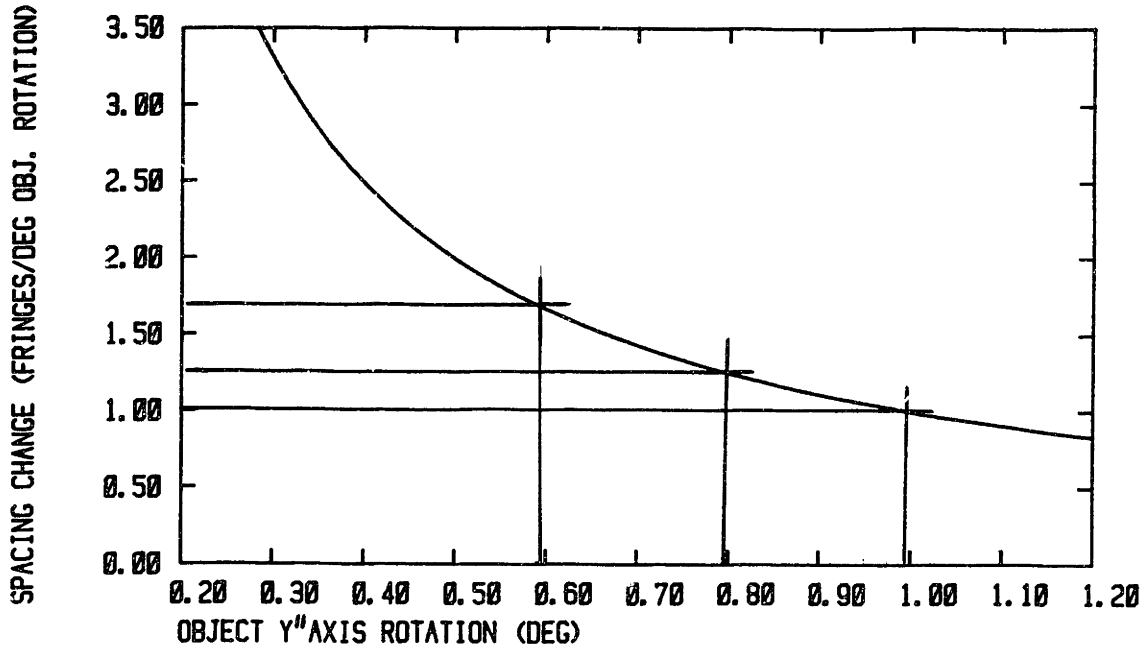

FIGURE 6-6 Sensitivity of Fringe Spacing vs. Object Angle for Object Orientation Inspection Task

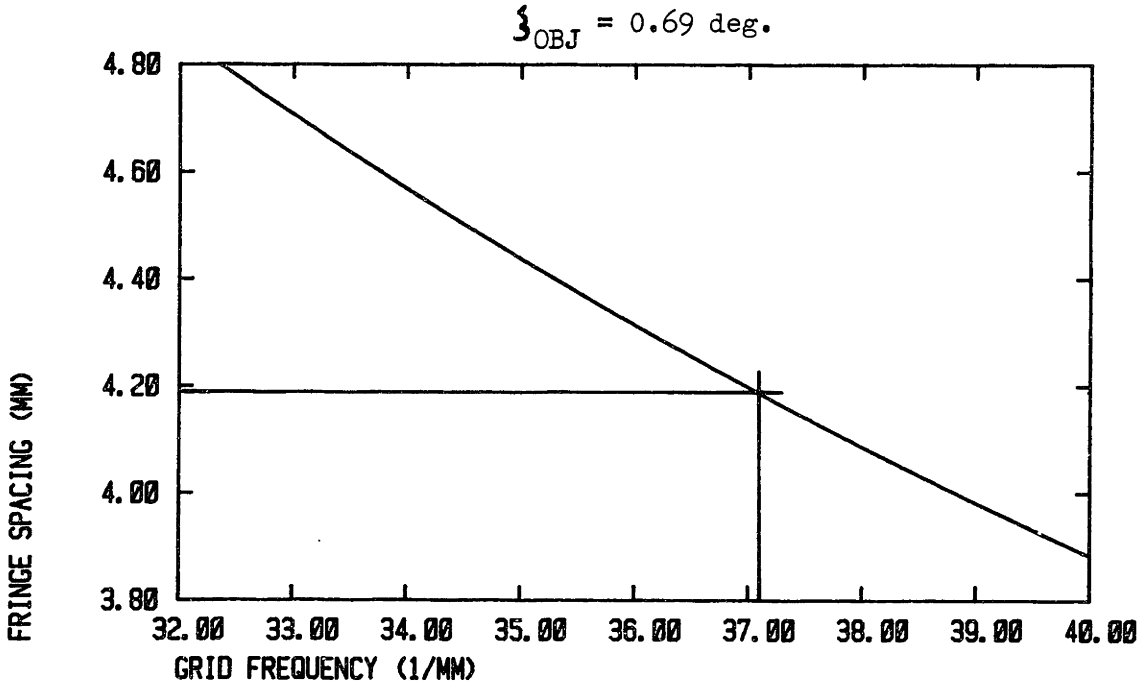

FIGURE 6-7 Fringe Spacing vs, Object Angle for the Object Orientation Inspection Task

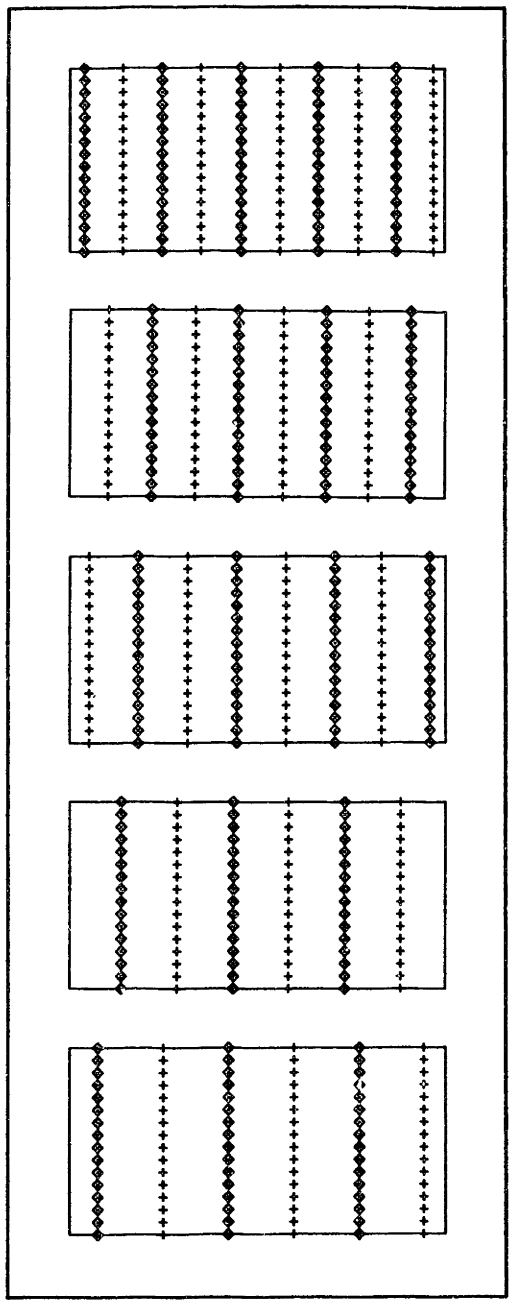

$\S_{OBJ}$ = 0.99 deg.

$\S_{OBJ}$ = 0.89 deg.

$\S_{OBJ}$ = 0.79 deg.

$\S_{OBJ}$ = 0.69 deg.

$\S_{OBJ}$ = 0.59 deg.

FIGURE 6-8 Change in Fringe Spacing Caused by a Change in Object Angle

fringes measured as the object orientation changes from 0.99 to 0.87 degree of 0.115, which meets the requirements of the inspection task. The fact that this is greater than the design sensitivity is expected since the spacing sensitivity increases as the object rotates from an object angle of 0.99 to 0.89 deg.

6.5 Discussion and Conclusions.

It is clear from the agreement between the design objectives and the resulting fringe patterns that the relationships of section 3.5 are useful for design. This very good agreement will be degraded, however, when system configurations are adopted that do not produce flat equiorder surfaces. Also, the relations for fringe properties as presented are only applicable approximate for non-flat objects and/or the use of non-straight line grids. In contrast, the technique for analytical fringe construction used in the previous two sections are applicable to objects of general shape. The algorythms developed for the plots shown in this thesis are relatively crude, drawing only the centers of the dark and light fringes. Even as the technique stands, it is a rapid and simple method for constructing observed fringe patterns.

Chapter 7. Moire Interferometry for Specular Objects.

7.1 Introduction

The work of Chapters 3 through 6 deals with moire interferometric methods for diffusely reflecting objects. This and the next chapter deal with moire interferometry for specularly reflecting objects.

As discussed in Chapter 1, moire interferometry for specular objects is fundamentally different from the methods for diffusive objects. A general schematic of a moire interferometer for specular objects is given in Figure 7-1. The process consists of a collimated light beam being reflected off a specular object through two transmittance grids that are spaced a small distance apart, and then onto a translucent screen. As the beam of light reflected off the object passes through the first transmittance grid (called the projecting grid), the straight lines of the grid structure the light into alternating sheets of light and shadow. As the light continues on and passes through the second grid (called the viewing grid) and onto the screen the light is further structured bu the second grid. If the shape of the structured light pattern produced by the projecting grid is similar but slightly different to the shape of the pattern created by the second grid, a moire fringe pattern will be observed on the translucent screen. For the work of this chapter the transmittance grids will again be considered to consist of evenly spaced straight lines. Also, the specular objects will be assumed to be nearly flat.

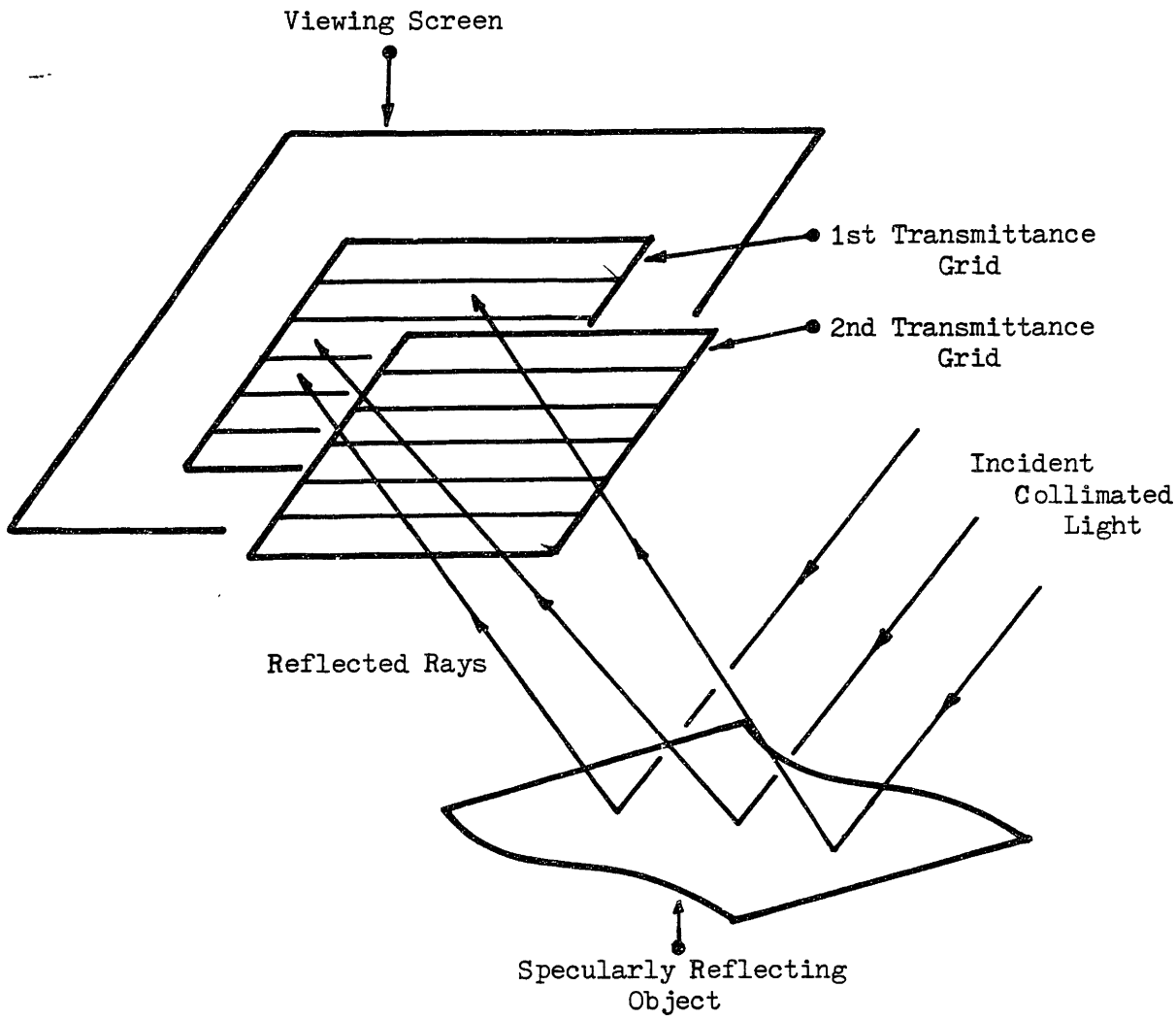

FIGURE 7-1 General Schematic for Specular Moire Interferometry

First consider the case of a perfectly flat specularly reflecting object. If the object is flat the rays reflected from the object are still collimated. The pattern on the screen formed when the reflected beam passes through the first straight line transmittance grid (i.e. the shadow of the grid) will still be straight and evenly spaced straight lines. Except for the special case when the lines of the projected pattern align with the lines of the analyzing grid (which is not considered), the moire fringes produced when the straight evenly spaced shadow of the projecting grid is further structured by the viewing grid will consist of straight evenly spaced fringe lines.

If the object is not flat then the reflected rays will no longer be collimated. The small variations in the direction of the rays will produce distortions in the nominally straight and evenly spaced shadow pattern cast by the projecting grid. These distortions in the shadow of the projecting grid will in turn produce distortions in the nominally straight evenly spaced moire fringe lines.

In illustration consider a perfectly flat specular object, the center section of which has been tilted. Such an object is illustrated in Figure 7-2 (a). The shadow produced from the light reflected off the tilted section of the object will appear shifted relative the the shadow produced with light reflecting off the rest of the object, as illustrated in Figure 7-2 (b). This shift in the shadwow will produce a corresponding shift in the fringe lines, as shown in Figure 7-2 (c).

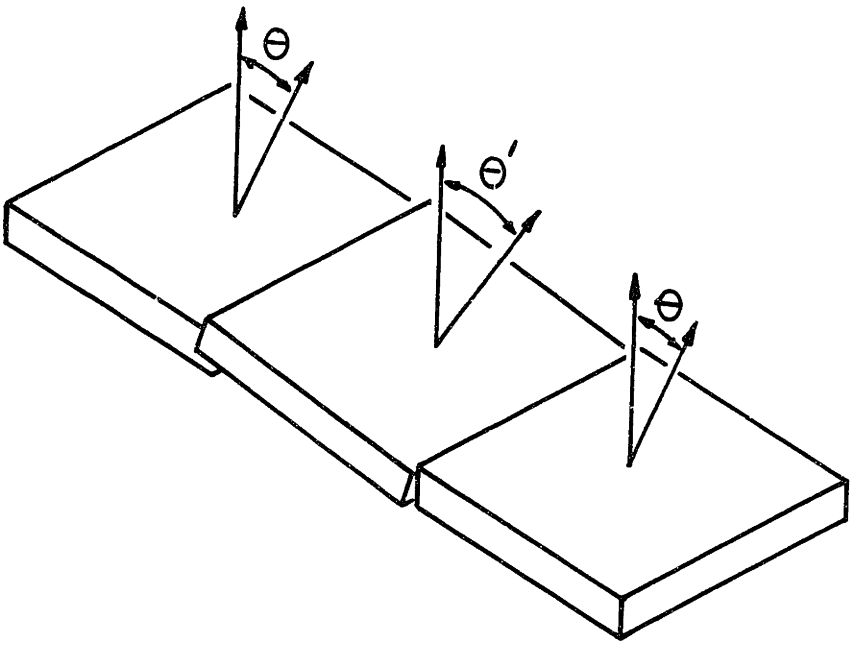

7-1 (a)
Hypothetical Specular Object

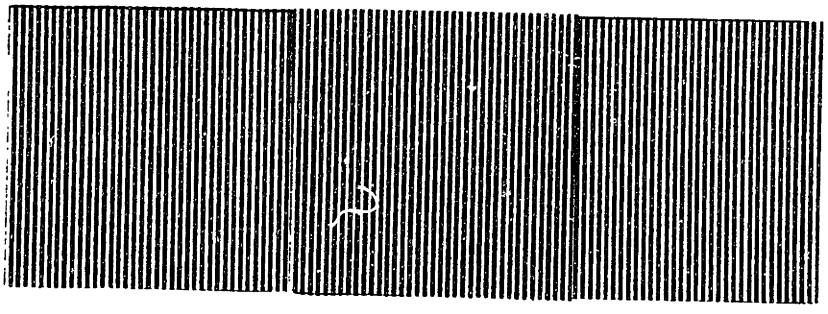

7-1 (b)
Corresponding Reflected Line Pattern

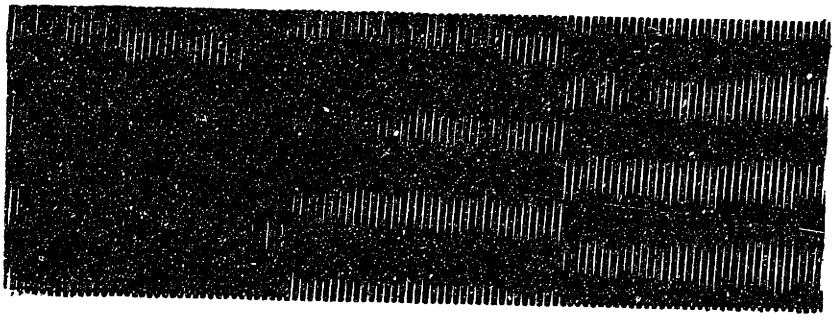

7-1 (c)
Corresponding Moire Fringe Pattern

FIGURE 7-2 Effect of Object Slope Change on the Moire Fringe Pattern

In this chapter it is assumed that the specular object is nearly flat and that the slope of the surface of the object varies continuously and smoothly across the object. These smooth variations in surface slope will produce corresponding smooth distortions in the moire fringe pattern.

As for moire methods for diffusive objects, a primary motivation for using moire methods for inspecting specular objects is the amplification observed between the distortions of the pattern projected onto the analyzing plane and the distortions of the resultant moire fringe pattern. Measurements of the large distortions of the fringe pattern can be used to deduce the small distortions of the projected pattern, which in turn indicate small distortions (changes in slope) of the object. Because the resolution of any measurement device is limited, greater accuracies can be achieved by measuring the fringe pattern than by directly measuring the projected pattern.

As discussed in Chapter 1, the moire techniques that have been applied to phase objects [20,21] seem promising for application to automated inspection of specular objects. Moire techniques for phase objects are similar to the techniques for specular objects except that instead of reflecting a collimated beam off a mirror like surface a collimated beam is passed through a transparent phase object. Distortions in the moire pattern are used to map the properties of the phase object (shape or index of refraction) that produce distortions in the direction of the rays that pass through the phase object.

The primary deficiency of the moire methods for phase objects, when considered for automated inspection of specular objects, is that the form of the relations used to analyze the distorted fringe pattern are only suitable for manual processing. To be valuable for automated inspection the relations used to analyze the fringe pattern must be expressed in terms of quantities that are available to an automated inspection system. Specifically, current analyses require the position of the nominal fringe lines to be estimated manually. The nominal fringe lines can be used in measuring the distortion of the moire fringe lines. In this chapter the distortion of the moire fringe lines is expressed analytically. The distortions of the object can then be expressed in terms of only the position and fringe order of the distorted fringe patten.

In this chapter an analysis of moire interferometry for specular objects is developed that is more suitable to automated shape inspection. In Section 7-2 the model that is adopted for moire interferometry is first introduced. Next, the fundamental relations that relate the direction of the reflected rays to the shape of the object are derived. These relations are developed in terms of the position and fringe order of points on the displaced fringe lines and the system parameters only. As in current analyses, the relations of section 7.2 are capable of determining only one component of the variations in reflected ray in one direction. In section 7.3 methods are suggested for obtaining complete knowledge (both components) of the variations in direction of the reflected rays. In section 7.4 the application of the relations of section 7.2 to real inspection tasks is discussed. Specifically, the need to exactly determine the fringe

order is discussed. Finally, in section 7.5 relations for the sensitivity of the position of the fringes to variations in the direction of the reflected rays are developed in terms of the system parameters. Such relations are useful for designing the parameters of a moire interferometer to yield a desired sensitivity to object surface slope variations. The validity and use of the relations derived in this chapter are then demonstrated experimentaly, as presented in Chapter 8.

7.2 Fundamental Relations for Specular Moire Interferometry.

7.2.1 Model for Specular Moire Interferometry

The model used in analysing moire interferometry for specular objects is shown in Figure 7.3. The nominally flat object is represented by the XY plane of the object coordinate system (X,Y,Z). The coordinate axes are arranged so that the rays of the collimated beam incident onto the object are parallel to the XZ plane. Accordingly, for perfect specular reflection off a nominally flat object, the reflected rays are also parallel to the XZ plane. The first transmittance grid (called the projecting grid) occupies the X' Y' plane (called the projecting plane) of a second coordinate system (X',Y',Z'). The Z' axis lies along the path of a ray that is reflected at the origin of the a hypothetical nominal object. The Y' axis is oriented parallel to the X axes of the object coordinate system. The second transmittance grid (called the analyzing grid) is located in the X'' Y'' plane (called the analyzing plane) of a third coordinate system, X'',Y'',Z''. The X'',Y'',Z'' coordinate system is oriented the same way as the X', Y', Z' coordinate systm except the

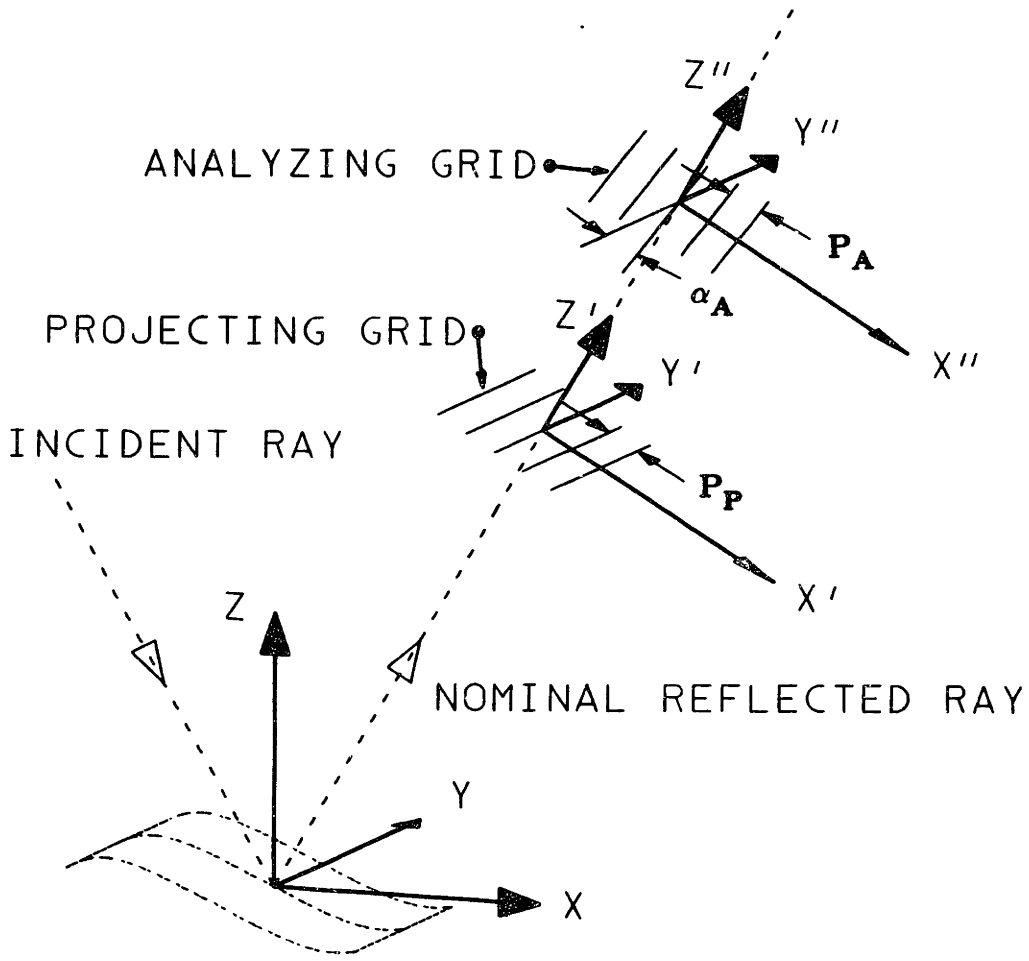

FIGURE 7-3 Analytical Model for Specular Moire Interferometer

origin of the X'',Y'',Z'' axis is farther out along the nominally reflected ray. The screen used for viewing the moire fringes is assumed to also occupy the X'' Y'' plane.

7.2.2 Analysing the Specular Moire Interferometer.

The equations for the straight line, evenly spaced grids are developed as discussed in Chapter 2. The equations for the projecting and analyzing grid expressed in their respective planes are given below:

$$\text{projecting grid} \quad X' = -Y' \tan \alpha_P + \frac{(n + \Phi)_P}{\cos \alpha_P} P_P \qquad (7\text{-}1)$$

$$\text{analyzing grid} \quad X'' = -Y'' \tan \alpha_A + \frac{(n + \Phi)_A}{\cos \alpha_A} P_A \qquad (7\text{-}2)$$

where α is the rotation of the lines of constant transmittance of the grids about the Z axis (positive by right hand rule), n is the profile number of the transmittance grid, ϕ is the offset of the line of zero profile number, P is the pitch of the grid, and the subscripts P and A denote the projecting and analyzing grids, respectively.

Variations in the direction of the reflected rays are modeled at the the projecting plane. As shown in Figure 7-4, variations in the reflected rays produce a displacement of the point where the rays from

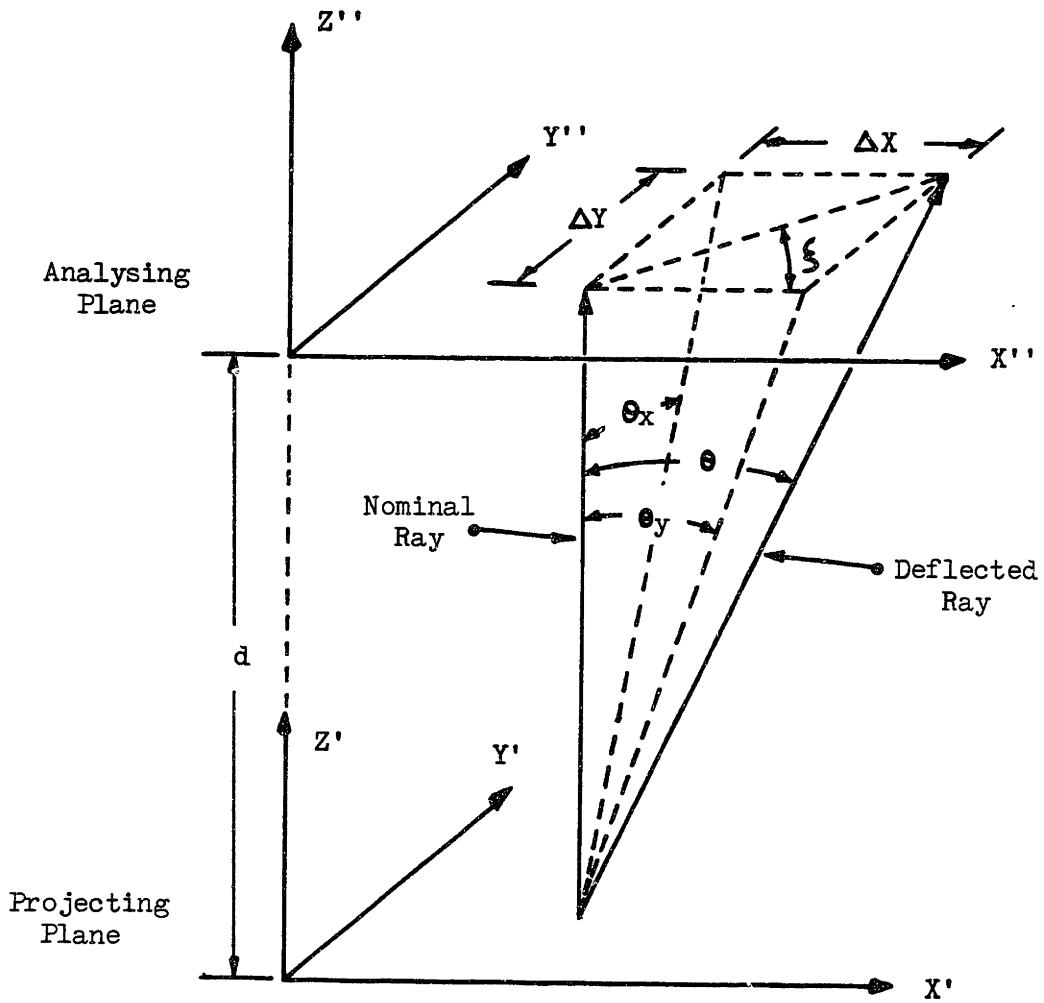

FIGURE 7-4 Effect of Reflected Ray Deflections on Point of Intersection on the Analysing Plane

the projecting plane fall on the analyzing plane relative to the nominal point of intersection. The deflection of the ray at a point X'', Y'' can be expressed in terms of the angle of the deflected ray, θ , relative to the nominal ray direction and the direction of the ray, ξ , which indicates the orientation of the projection of the deflected ray onto the X'', Y'' plane (see Figure 7-4). ξ is measured from the positive X'' axis, with positive rotations as shown in Figure 7-4. Equivalently, the deflection of the reflected rays can be expressed in terms of the component rotations about the X and Y rotation that are defined using the projections of the deflected ray onto the Z' Y' and Z' X' planes, respectively. The component rotations, θ_X and θ_Y, are measured from the positive Z axis, with the right hand rule sign convention. In Figure 7-4, θ_X is negative (for a positive Y) and θ_Y is positive (for a positive X).

For this chapter the displacement of the intersection of the reflected ray will be expressed using θ_X and θ_Y. However, θ and ξ will be used in the work of Chapter 3. The expressions for the X and Y components of the displacement in terms of the component rotations θ_X and θ_Y are:

$$\Delta X = d \tan [\theta_Y (X', Y')] \qquad (7\text{-}3\ a)$$

$$\Delta Y = - d \tan [\theta_X (X', Y')] \qquad (7\text{-}3\ b)$$

where d is the distance between the analyzing (X'', Y'') and the

projecting (X', Y') planes. As indicated in Equations 7-3 a and b, θ_X and θ_Y are functions of X' and Y'.

Using the expressions for X and Y a mapping from the points of origin of the rays passing through the projecting plane (X', Y') to the point of intersection with the analyzing plane (X'',Y'') can be written:

$$X'' = X' + d \tan [\theta_Y(X', Y')] \qquad (7\text{-}4\ a)$$

$$Y'' = Y' - d \tan [\theta_X (X', Y')] \qquad (7\text{-}4\ b)$$

Note that for the case when both θ_Y and θ_X are zero the mapping reduces to the nominal case of collimated projection parallel to the Z axis. For that case X'= X'' and Y'= Y''.

As described earlier, light reflected off the object is structured as it passes through a transmittance grid in the projecting plane. The grid lines in the projecting plane are straight and evenly spaced. The projection of the lines of the grid at the analyzing plane (i.e. the shadow of the grid) will in general not be straight lines because the reflected rays that project the lines are not in general collimated. For the special case of θ_X and θ_Y equal to zero or constant everywhere on the projecting plane, the reflecting rays are collimated and the projected grid on the analyzing plane will still consist of straight evenly spaced lines. However, if the components of the reflected ray direction, θ_X and θ_Y, vary over the projecting plane, the projected grid will consist of curved,

non-evenly spaced lines. Provided the ray deflections vary slowly and smoothly over the projecting plane, the projected grid lines will be well defined and continuous, and this condition is assumed.

By substituting for the coordinates X',Y' using the mapping of Equations 7-4 into Equation 7-2 you obtain the equation of the projection of the projecting grid on the analyzing plane.

$$X'' - d \tan [\theta_Y(X', Y')] = -\tan \alpha_p \left\{ Y'' + d \tan [\theta_X(X', Y')] \right\} + \frac{(n + \Phi)_p}{\cos \alpha_p} P_p \qquad (7\text{-}5)$$

Note that for θ_Y and θ_X equal to zero or a constant the lines of constant profile number of Equation 7-5 will be straight and evenly spaced.

The pattern represented by Equation 7-5 is a light intensity pattern (light and shadow). As the light of this pattern passes through the transmittance grid on the analyzing plane (analyzing grid) it is further structured. Provided the shadow pattern and the pattern of the analyzing grid are similar, a moire pattern will be observable in the intensity pattern emerging behind the transmittance grid. The moire pattern can be treated analytically using the fringe order, as discribed in Chapter 2. As discussed, the fringe order, which is defined as the difference between the profile numbers of the two interfering repeating patterns, can be used to determine the low frequency intensity fluctuations that are recognized as the moire pattern. The expression for the fringe order is found by first solving for the profile numbers, n_A and n_P, in Equations 7-2 and

7-5, and then forming the difference of the two quantities. The resulting equation for fringe order is given below:

$$Fo = \left\{\frac{\cos \alpha_A}{P_A} - \frac{\cos \alpha_P}{P_P}\right\} X'' + \left\{\frac{\sin \alpha_A}{P_A} - \frac{\sin \alpha_P}{P_P}\right\} Y'' + \left\{(\cos \alpha_P \tan [\Theta_Y(X', Y')] - \sin \alpha_P \tan [\Theta_X(X', Y')]\right\}\frac{d}{P_P} + (\Phi_P - \Phi_A) \tag{7-6}$$

The lines of constant average intensity of the moire pattern are also lines of constant fringe order, Fo, as discussed in Chapter 2. For instance, with the fringe order held constant at some integral value, Equation 7-6 is the equation of a bright fringe line (curve) in the X'', Y'' plane. Provided the position (X'', Y'') and order (Fo) are obtainable from measurement of the fringe pattern, Equation 7-6 can be rearranged to yield the unknown ray deflections in terms of the known position and order of a point on the fringe pattern and the system properties. Doing this yields the result:

$$\frac{d}{P_P}\left\{\sin \alpha_P \tan [\Theta_X(X', Y')] - \cos \alpha_P \tan [\Theta_Y(X', Y')]\right\} = \left[\frac{\cos \alpha_A}{P_A} - \frac{\cos \alpha_P}{P_P}\right] X'' + \left[\frac{\sin \alpha_A}{P_A} - \frac{\sin \alpha_P}{P_P}\right] Y'' + \left[\Phi_P - \Phi_A - Fo\right] \tag{7-7}$$

Note that with the fringe order of the distorted pattern, Fo, θ_X and θ_Y set to zero the expression of Equation 7-7 is the expression for the fringe order of the nominal fringe pattern at the point X'', Y''.

Thus, the difference between the observed fringe order and the fringe order for nominal (collimated rays, parallel to the Z' axis) projection at a point in the analyzing plane (X'', Y'') contains information about the deflection of the ray from the projecting plane that passes through that point.

Examining the left hand side of Equations 7-7 closely you can conclude that, excluding the pitch of the projected grid Pp, the left hand side represents only one component of the displacement of the point of intersection (with the analyzing plane) of the refected ray. The component is that component of the displacement that is perpendicular to the nominally projected grid lines, and the geometry is illustrated in Figure 7-5.

The correct way to interpret this is that only deflections in the direction of the reflected rays that produce visible distortions in the projected pattern, that is those that cause displacements perpendicular to the grid lines, will effect the moire pattern. This phenomena limits the information contained in the distortions of the moire fringe pattern to only one component of the variations in the direction of the reflected rays.

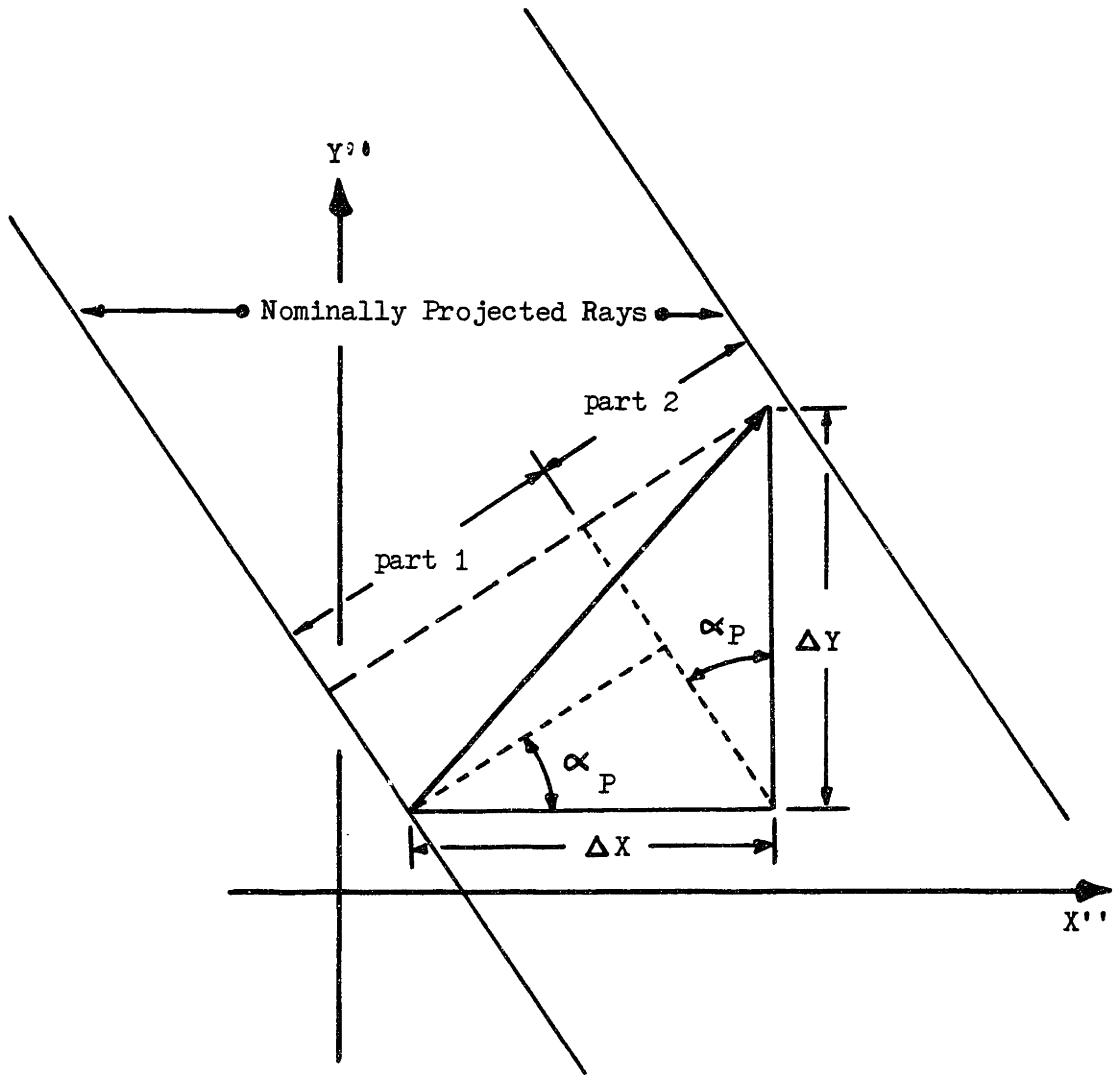

$$\text{part 1} = -d\ (\cos\alpha_P\ \tan(\theta_y(X',Y')))$$

$$\text{part 2} = \ d\ (\sin\alpha_P\ \tan(\theta_x(X',Y')))$$

FIGURE 7-5 Geometric Interpretation for Equation 7-7

An alternate way to show this is to consider the case when the projecting grid lines are aligned with the Y axis. For this case the angle α_P, is zero and Equation 7-7 reduces to

$$\frac{d}{P_P}\left\{-\tan\left[\theta_Y(X', Y')\right]\right\} = \left\{\frac{\cos\alpha_A}{P_A} - \frac{1}{P_P}\right\}X'' + \left\{\frac{\sin\alpha_A}{P_A}\right\}Y'' + \left\{\Phi_P - \Phi_A - Fo\right\} \tag{7-8}$$

Equation 7-8 could be rearranged to yield the component, θ_Y, of the reflected ray passing through the a point X'',Y''. For this case it is clear that knowledge of the location (X'',Y'') and fringe order (Fo) of a point on the distorted fringe pattern is sufficient to determine one and only one component of the reflected ray direction passing through that point.

7.3 Limitations of Specular Moire Interferometry.

The relations of section 7.2 are a contribution towards automating moire methods in that the analysis formulates the ray deflection in terms of the measurable fringe properties of the distorted fringe pattern. The relations of section 7.2 represent the nominal fringe pattern analytically, allowing the deflections of the moire pattern to be infered from knowledge of the distorted fringe pattern and the system parameters only. The relations developed in section 7.2 show that with knowledge of the coordinates and the fringe order at a point on the moire fringe pattern for a ne-arly flat specular object, then one component of the deflection of the ray passing through that point can be calculated. The assumed requirement of determining the fringe order and the restriction that only one

component of the reflected ray deflection is determined impose limitations to the application of the method to automated shape inspection. This section is devoted to discussing these limitations and to suggesting ways to avoid them.

7.3.1 Fringe Order Determination

The fringe order, as defined in Chapter 7, is assumed to be known exactly in Equations 7-7. Unfortunately, the value of the fringe order is difficult to determine. The average intensity of the fringe patter indicates only the fractional part of the fringe order. For instance, it is impossible from the intensity of the fringe pattern alone to determine if a fringe has a fringe order of 1.3, 2.3 or 10.3. Therefore, without a way to determine the integral part of the fringe order the value of the component of the ray deflection can not be determined exactly.

As for the case of diffuse moire interferometry, the fringe order of one fringe line could be determined, either by exact knowledge of the object at one point or by some means of direct measurement. The order of other points in the fringe pattern could then be determined relative to this known fringe line by indexing the fringe order up or down when an adjacent fringe is crossed. For istance, for the assumption of nearly flat objects the fringes will be well defined so that, in general, the fringe order increases in the positive Y'' direction.

It is not necessary to determine the fringe order exactly to gain useful information about the object. Regardless of the integral part of the fringe order, the shape of the fringes contain information about how the direction of the refected rays vary over the object. The distortions of the fringe pattern are sufficient to map the changes in one componenet of the direction of the reflected rays. For small deflection angles the equation for the angle of the reflected ray (7-7) is a linear function of fringe order. Provided the order of the fringes relative to each other is established correctly (by counting up or down across adjacent fringes) then the order of any one fringe can be assigned arbitrarily. Errors in the assigned value for fringe order simply adds or subtracts the same amount to every point for which the deflection of the reflected ray is evaluated. Thus, changes in the component of the ray deflection to which the interferometer is sensitive will still be determined correctly.

7.3.2 Object Shape from the Moire Fringe pattern.

The moire technique for specular objects is not directly sensitive to the shape of the object, but rather is sensitive to the direction of the rays reflected off of the object. Specifically, the fringes are sensitive to one componenet of the direction of the reflected rays, and distortions in the fringe pattern arise solely from the changes in this component. While the direction of the reflected rays do indicate directly the slope of the surface, they do not directly indicate the shape of (location of points on) the surface.

The insensitivity of the moire fringe pattern to object location is reflected by the lack of any object parameters in the equations of section 7.2. The physical explanation for this condition results from the fact that the projecting grid structures the light refected off of, as opposed to incident onto, the surface. Distortions of the light pattern produced by the projecting grid are caused only if the rays reflected are not collimated. Also, the distortions caused by variations of the direction of the reflected rays depends on the distance between the projecting grid and the analyzing grid and not the distance from the object to the grids. The distance from the object to the projecting grid will effect where the rays reflecting from a particular point on the object fall on the projecting and analyzing plane, but, unlike diffuse moire, this distance to the object is not directly obtainable from knowledge of the moire fringe pattern.

For many inspection tasks knowledge of the object shape is not required. For instance, for the case of nominally flat objects, the appearance of any distortions in the fringe pattern would indicate flaws in the object. Also, for a nominally flat object the exact fringe order is of little concern since small tilts in a truly flat object would just produce a shift in the nominal, straight and evenly spaced fringe pattern.

The fact that the fringes are only sensitive to one component of the reflected rays is not an important limitation to inspection tasks that can be accomplished using only the variations in the direction of the reflected rays. If knowledge of the variations of one component is not sufficient, a second measurement (that is independant of the

first) can be performed with a different system arrangement. In fact, the separate moire interferometers could be used simultaneously provided each was sensitive to the ray deflections caused by a different componenet of the slope of the surface.

For some applications (e.g. mapping the slope of an object) it may be desired to associate the ray defelctions mapped by the moire pattern with specific points on the object. To do this, the direction of the rays passing through specific points of the moire pattern (on the analyzing plane) must be known exactly. Also, the distance from the point on the moire to the object would need to be determined. If both the direction and the distance to the object are known than the deflections of a ray passing through a specific point on the viewing plane can be related back to a specific point on the object.

Because the distance to the object will only be known approximately (otherwise the exact object shape will already be known and there is no point to the inspection) there will be errors in determining the distance from object to the analysing plane. However, for nearly flat objects the error will be small since the object location is known fairly accurately.

To obtain the true direction of the reflected rays (as opposed to one component of the direction) the different components of the reflected rays need to be determined at the same point on the analyzing plane. To separate measurements using two interferometer arrangements are required. Furthermore, the ray deflections, and hence the fringe orders, must be determined exactly. Only if two different components of the reflected ray direction are known exactly

the components completely describe the direction of the ray.

7.4 Design Relations for Specular Moire Inspection Systems.

For any real inspection system the system parameters must be chosen to satisfy the tolerances of the inspection task and the limitations of the vision system employed to process the fringe pattern. In this section relations are developed that are valuable as design tools for choosing certain parameters of a specular moire interferometer.

For this thesis the only parameters that will be considered for design of a specular moire interferometer are the pitch of both the transmittance grids (P_A and P_P), the distance between the projecting plane and analyzing plane d , and the angle of the analyzing grid, alpa. Note, the angle of the projecting grid is assumed to be zero. Also, as pointed out in section 7.3, the specular moire interferometer is only sensitive to the componenets of the reflected rays that cause the lines of the projected grid to be displaced perpendicular to the lines of the nominally projected pattern. For the purposes of design only the component of the reflected rays to which the system is sensitive will be considered. For a projecting grid angle of zero this limits consideration to the X directed component (i.e. θ_Y of section 7.2). For simplicity this angle will simply be referred to as θ.

7.4.1 Criteria for Design.

As for the design procedures of Chapter 6, the design relations for the parameters of the specular moire interferometer consider both the sensitivity of the fringes and the limitations imposed by the capabilities of the vision system. As discussed in Chapter 6 the shifts in the fringe lines need to be large enough to be resolvable to the vision system. Also, to be processed accurately, the shift in the fringe pattern must be a significant fraction of the fringe spacing. Finally, the spacing of the fringe pattern must be small enough, and the distortions of the fringe pattern must be small and smooth enough, so that the software of the vision system can accurately recognize distinct fringe lines.

To design the parameters to meet these limitations relations are required for the sensitivity of the fringes to the distortions in the direction of the reflected ray and for the spacing of the nominal fringe pattern.

7.4.2 Pattern Sensitivity.

The sensitivity of the moire fringes will be expressed as the shift in the fringe pattern caused by a deflection of the reflected ray from its nominal direction. The shift of the fringe is expressed as the number of nominal fringe pitches that the fringes have moved. That is the distance the fringe has shifted divided by the nominal fringe pitch. The ray deflection is expressed in radians.

For simplicity the shift of the fringe pattern is not computed explicitly but is infered from the shift of the projected pattern lines. As illustrated in Figure 7-2, for overlapped straight line

patterns a shift in the projected pattern causes a shift in the fringe pattern that is proportionately larger by the ratio of the fringe pattern pitch to the projected pattern pitch. This correspondance is only approximately correct for non-straight line patterns. However, it will be assumed to hold for the small distortions produced in the projected pattern by nearly flat specular objects.

The relation between the shift in the projected pattern (pattern shift) and the shift in the fringe pattern (fringe shift) can be written:

$$\frac{\text{Pattern Shift}}{\text{Pattern Pitch}} = \frac{\text{Fringe Shift}}{\text{Fringe Pitch}} \qquad (7\text{-}9)$$

The pattern pitch (for nominal projection) is just Pp, the pitch of the projecting grid. The shift of the projected pattern can be expressed in terms of the reflected ray deflection as $d(\tan \theta)$, which for small angles can be approximated as $d(\theta)$ (see Figure 7-4). Substituting this into the expression for the sensitivity of the fringes yields:

$$\frac{\theta d}{P_p} = \frac{\text{Fringe Shift}}{\text{Fringe Pitch}} \qquad (7\text{-}10)$$

Note, the above expression for the fringe sensitivity is dimensionless, and only expresses the shift of the fringe pattern relative to the pitch of the fringe pattern.

7.4.3 Fringe Spacing

The pitch of the nominally observed fringe pattern is useful for design because for nearly flat objects the spacing of the distorted fringe lines will be of the same order of magnitude as the spacing of the nominal fringe lines. An expression for the spacing could be developed from an expression for the nominal constant fringe order lines (Equation 7-6 with θ_X and θ_Y equal to zero). However, if only the nominal case of straight line patterns are considered it is easier to develop a relation for the fringe spacing directly from the geometry of the interfering pattern lines.

A small section of two interfering line patterns is shown in Figure 7-6. As depicted in Figure 7-6 the straight lines of constant and integral fringe order correspond to the lines connecting closest adjacent intersection points of the integral profile number lines. This can be verified at the intersection points by evaluating the fringe order using the profile nubers for the intersecting lines ($Fo = n_A - n_p$).

The spacing of the fringe pattern (i.e. the perpendicular distance between adjacent fringe lines) is indicated in the Figure with the symbol FSP.

The intersection angle of the line patters, α , will be equal to the angle of the analyzing grid, α_A , for the case of nominal projection and zero projecting grid angle ($\alpha_p = 0$). As shown in the figure, the pitches of the line patterns are simply the pitch of the projecting and analyzing grid, P_A and P_p.

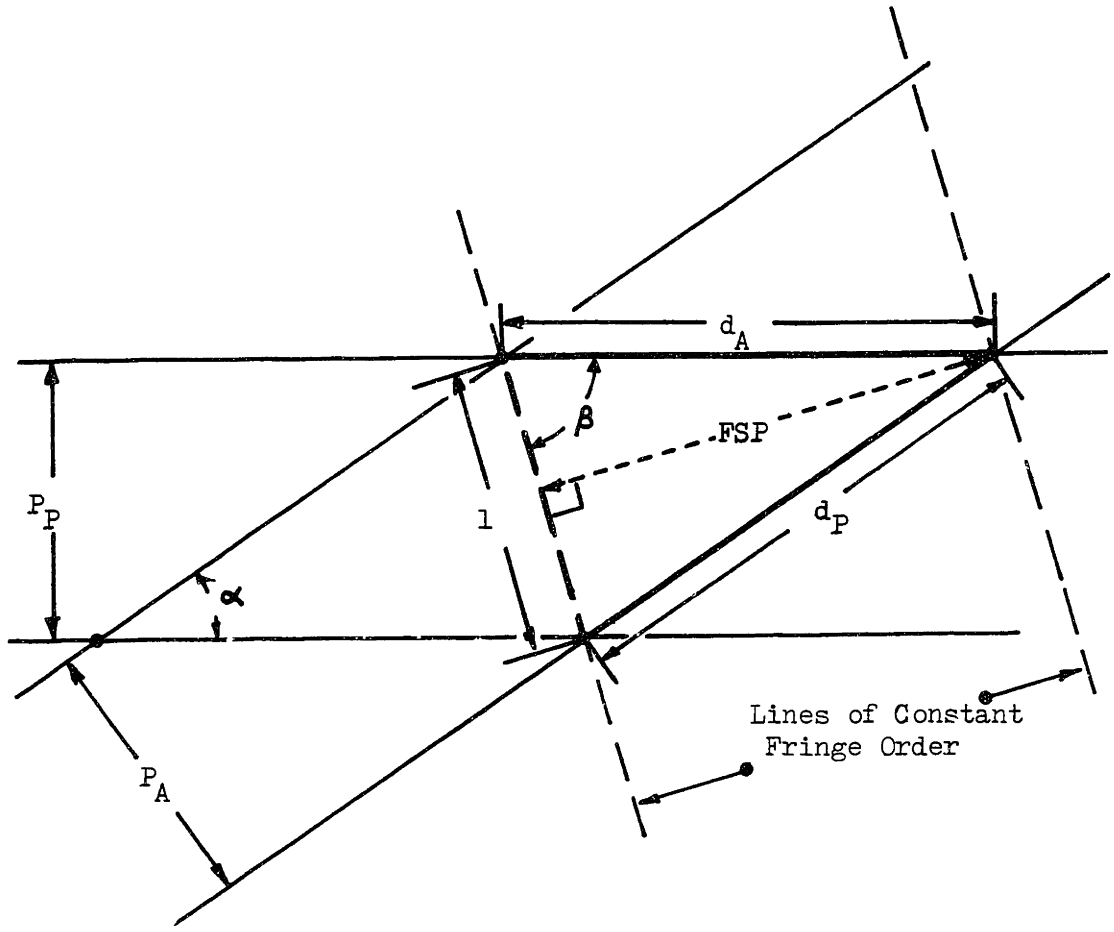

FIGURE 7-6 Interfering Staight Line Patterns

From inspection of the geometry of the intersecting lines, the the following simple geometric relations can be recognized to hold:

$$d_P \text{ SIN } \alpha = P_P \tag{7-11}$$

$$d_A \text{ SIN } \alpha = P_A \tag{7-12}$$

$$d_A \text{ SIN } \beta = FSP \tag{7-13}$$

Using the law of sines, the sin term in Equation 7-13 can be expressed in terms of the parameters β , l , and dP as follows:

$$\text{SIN } \beta = \frac{d_P}{\ell} \text{ SIN } \alpha \tag{7-14}$$

Next, the length, l , can be expressed in terms of d_A, d_P, and α using the law of cosines:

$$\ell^2 = d_P^2 + d_A^2 - 2d_P d_A \text{ COS } \alpha \tag{7-15}$$

Equations 7-11 through 7-15 can be solved easily for the fringe spacing, FSP, in terms of the pitch of the transmittance grids, P_A and P_p, and the angle of the analysing grid, α_A (which equals α for $\alpha_P = 0$). The resulting expression for the fringe spacing is:

$$FSP = \frac{P_A P_P}{\sqrt{P_P^2 + P_A^2 + 2P_P P_A \text{ COS } \alpha}} \tag{7-16}$$

A useful special case of Equation 7-16 arises when the pitch of the two patterns is equal, i.e. $P_A = Pp = P$. For this case Equation 7-16 reduces to:

$$FSP = \frac{P}{\sqrt{2 - 2 \cos \alpha}} \qquad (7\text{-}17)$$

In conclusion, Equations 7-10 and 7-17 are developed under the assumption of a perfectly flat object. They can be used to design the parameters of the moire interferometer to tune the spacing and sensitivity of the nominal fringe pattern to suit the requirements of a specific inspection task.

In Chapter 8 an experimental demonstration of moire interferometry for specular objects is used to explore the feasibility of the implimenting the suggested system arrangement and to verify the validity of the analyses presented in this chapter. The parameters for the experimental apparatus were chosen using relations 7-10 and 7-17 to estimate the spacing and sensitivity of the fringe pattern. This work, which appears in section 8.2, serves to demonstrate how the relations of this section can be used to scale the parameters of a specular moire inspection system.

Chapter 8 Demonstration and Verification of the Specular Moire Technique.

8.1 Introduction

In this chapter the validity of the analysis for specular moire interferometry developed in Chapter 7 will be demonstrated experimentally. The work of this chapter also serves to demonstrate the use of the design relations developed in section 7.4.

Verification of the relations of chapter 7 involves both analytical and expermental methods. First a specific system configuration and a specific specular object were chosen. The specular object was chosen so that the shape of the surface of the object could be modeled analytically. Next the moire interferometric process was both emulated using computer aided design (CAD) based simulations and implimented experimentally. The moire fringe patterns obtained from the simulations and the experiments were then analyzed using the relations of Chapter 7. In each case the results of the analyses, which are one component of the reflected ray destortion at specific analyzing plane locations, were compared with the results predicted from the theoretical model for the specular surface.

The specular object and its model, and the choice of parameters for the specular moire interferometer are discussed in section 8.2. The procedures and the comparison of the results for the CAD simulations and the experiments will be discussed in sections 3.3 and 8.4, respectively. In general, the results of the comparisons do

verify the validity of the relations of Chapter 7. The implications of the results for automated inspection are discussed in section 8.5.

8.2 Choosing the Object and System Parameters.

For comparison and simplicity the same specular object and interferometer configuration will be used for both the CAD simulations of section 3.3 and the experiments of section 8.4. In this section the object and its analytical representation, and the design of the parameters for the specular moire interferometer are discussed. An effort is made to clearly indic ate the motivation for the choices made for the object and the parameters.

8.2.1 Specular Objects

As mentioned above, verification of the analysis for specular moire interferometry involves comparing measured and actual values, for one component of the distortions in the rays reflected off a specular object. Instead of measuring the actual deflections by a proven method to determine the 'true' values the 'true' ray deflections were calculated from an analytical model of the object shape. This choice was also motivated by the fact that an object that could be represented analytically could relatively easily be simulated by CAD methods.

The object was chosen to be disk made of thin steel plate. As indicated in Figure 8-1, a 3-dimensional object is created by deforming the disk. With the disk simply supported at a given radius, a, from the center of the disk, a force applied over a small area at

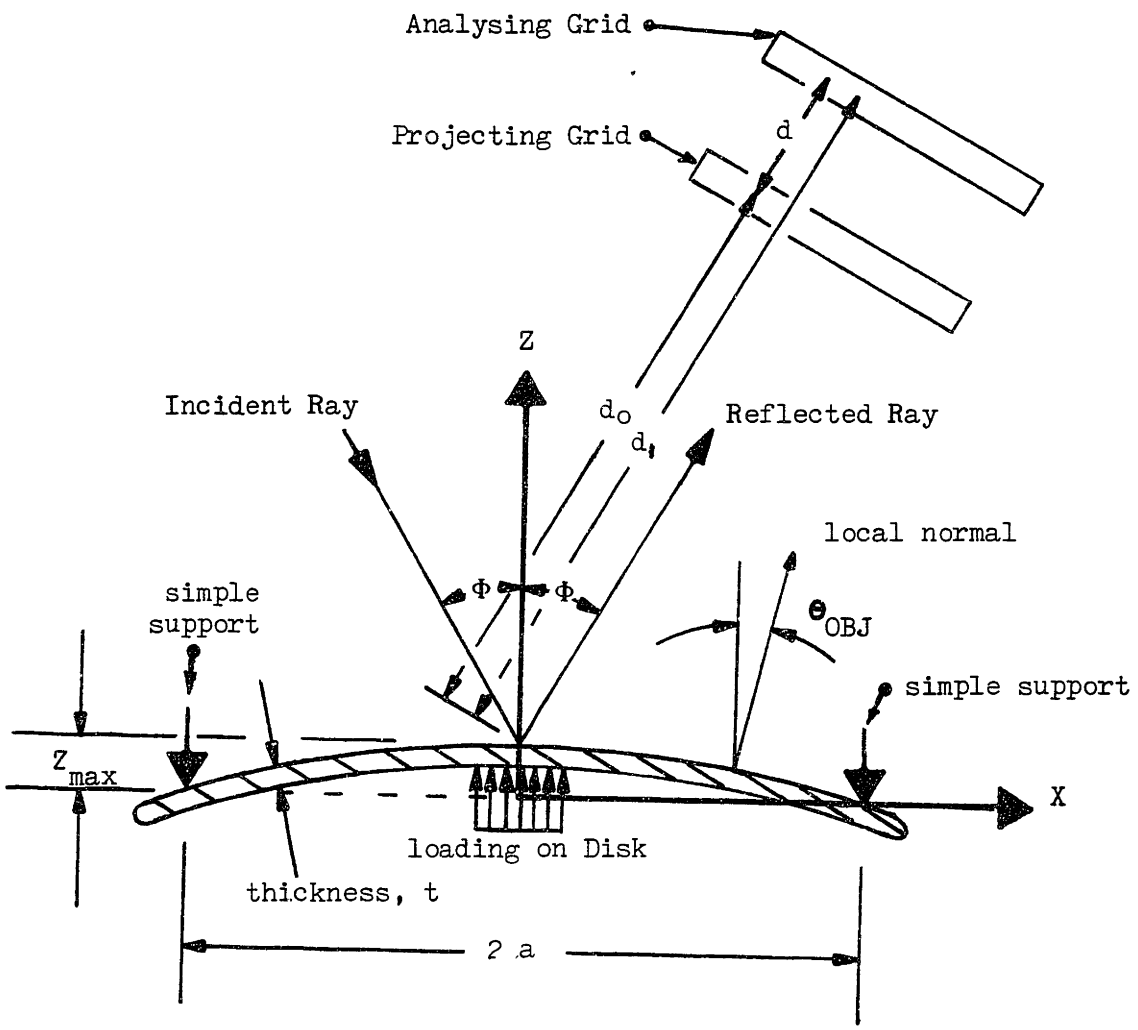

FIGURE 8-1 Cross Section of Steel Disk in a Specular Moire Interferometer

the center of the disk will displace the disk. The shape of the surface created by this loading can be modeled using solid mechanics, and th e solution for this configuration was readily available [32]. The solution for the slope (i.e. angle of deflection), θ_{OBJ} (radians), of the disk as a function of radial distance from the center of the disk, R (inches), is repeated below:

$$\theta_{OBJ} = C \frac{R}{4\Pi} \left(\frac{1}{1+\upsilon} + \ln \left(\frac{a}{R}\right)\right) \qquad (8\text{-}1)$$

where

$$C = Z_{max} \frac{16\ \Pi}{9^2} \left(\frac{1+\nu}{3+\nu}\right) \qquad (8\text{-}2)$$

In the above equations Zmax is the displacement of the disk at the center (inches), a (inches) is the radius from the disk center at which the disk is simply supported, and ν is poissons ratio for steel (takens as 0.285). Steel was chosen as the material for the disk since steel polishes well, and provided a good specular surface.

The properties of the disk, including the diameter, the thickness, the displacement at the center, and the radius at which the disk was to be supported, were chosen so that hardware implimentation would be relatively simle. This is discussed in more detail later.

8.2.2 Modeling Reflected Rays.

As stated before, the exact (or true) values for the deflection of the reflected rays for both the simulations and the experiments are based on the theoretical shape (i.e. equ. 8-1) of the deformed disk. The direction of the reflected rays at the disk surface are calculated from knowledge of the direction of the incident rays and the local slope of the surface assuming perfectly specular reflection. The intersection point of the reflected rays with the analyzing plane is then calculated using the distance between the surface and the analyzing plane, the direction of the reflected rays, and the point of origin of the reflected ray on the disk surface.

In developing the expressions describing the direction of the reflected rays the disk is assumed to be oriented such that the undeflected disk would coincide with the XY plane of the system model for the specular moire interferometer (recall Figure 7-2). With the disk configured in this way, the deflection of the surface (θ in Equation 8-1) can be considered to be the deflection of the local normal direction of the disk away from the positive Z axis, as indicated in in Figure 8-1. Because of the symmetry of the deflected disk, the projecton of the normal vector at any point onto the XY plane will be a line directed radially outward from the disk center. Also, it is assumed that the deflection of the position of the disk is insignificant; thus, when calculating where the rays reflected from a point on the disk will intersect the analysing plane it is assumed that the rays originate on the X Y plane.

The direction of the reflected ray at a given point is computed from the surface normal and the known incident ray direction under the assumption that the object exhibits perfect specular reflection. This assumption implies that the incident ray, the surface normal, and the reflected ray will all be coplanar. Furthermore, the angle between the reflected ray and the surface normal is equal to the angle between the incident ray and the surface normal.

The reflected ray direction will be calculated assuming that the incident rays lie in the X Z plane at an angle ϕ from the Z axis (as shown in Figure 3-1). The steps involved in calculating the direction of the deflected ray will be omitted as they involve only simple geometry. The resulting relations for the components, θ_X and θ_Y (see Figure 7-3) of the deflection, θ, of the reflected ray are:

$$\theta_X = 2\,\theta_{OBJ}\,\text{COS}\,\zeta\,\text{COS}\,\Phi \qquad (8\text{-}3\ a)$$

$$\theta_Y = 2\,\theta_{OBJ}\,\text{SIN}\,\zeta \qquad (8\text{-}3\ b)$$

where ζ = tan (X/Y), where X and Y are the coordinates of the point on the disk surface.

The intersection of the reflected rays with the analyzing plane can be computed using the ray directions determined from Equations 8-3 a and b and the distance from the point X,Y on the object plane to the analyzing plane. By simple geometry the point of intersection X'',Y'' can be expressed as:

$$X'' = X \cos \Phi + \Theta_Y (d_1 - X \sin \Phi) \qquad (8\text{-}4\ a)$$

$$Y'' = Y - \Theta_X (d_1 - X \sin \Phi) \qquad (8\text{-}4\ b)$$

where d_1 is the distance (inches) from the origin of the object coordinate system (X,Y,Z) to the origin of the analysing plane along the Z' axis.

In subsequent sections when the theoretical values for the direction and location of the reflected rays are presented it was Equations 8-3 and 8-4 that were used to calculate these values. Also, as is dscussed in section 3.3, these equations are used in the CAD emulation of the moire process.

8.2.3 Choosing System Parameters/Interferometer Design

The parameters for the components of the moire interferometer and the steel disk were chosen primarily to insure that the hardware implimentaton of proccess would be feasible. The parameters that need to be chosen for the disk itself are the thickness, the diameter, the radius for the simple support and the magnitude of the deflection at the center of the disk. After choosing the diameter of the disk (2.36 inches) and the radius to the simple support (0.984 inches) to be of reasonable size, the thickness and maximum deflection were chosen so that detectably large ray deflections would be produced with a small loading force. By trial and error application of Equations 8-1, 8-2 and the equation for the load (see [32]), the thickness and displacement were chosen as 0.016 inches and 0.0075 inches,

respectively. The maximum deflection θ_{OBJ} (which occurs at the support) was acceptably large (0.5 deg) and the force on the disk was acceptably small (1.5 lbf).

After arbitrarily choosing the angle of incidence of the collimated beam to be 30 deg, the distance to the first transmittance grid, d_o, was chosen as the smallest value that would still leave sufficient room so that the projecting grid did not interfer with the collimated beam incident onto the disk. This distance was chosen as 50 mm (1.968 inches)(see Figure 8-1).

The parameters that remain to be choosen for the interferometer include the pitch of the transmittance grids, P, (recall it was assumed that the the pitch of both grids the is same), the orientation of the grids (α_A and α_P), and the distance between the grids, d.

First, to simplify the implimentation and interpretation of the process the angle of the projecting grid, alpp, is assumed to be zero. The lines of the projecting grid will therefore align with the Y, Y' and Y'' axes. Also, the interferometer will consequently be sensitive only to X directed (i.e the θ_Y component in the equations of Chapter 7) deflectons in the reflected rays.

The three remaining parameters, P, α_P and d were chosen to produce an acceptable spacing and sensitivity for the moire fringe lines. The design relations for the spacing and sensitivity presented in section 7.4 were used to help choose acceptable values for P, α_P and d.

As discussed in section 7.4 the limitations of the vision system used to process the fringe pattern require that the fringe lines are well bounded and that they are sensitive enough to indicate the expected reflected ray deflections. To insure that the fringes are well bounded the spacing of the fringe pattern was limited to be about 1/10th the expected field of view. The field of view was assumed to be equal to the diameter of the disk between the supports, or 1.97 inches, making the desired fringe spacing about 0.2 inches. In choosing the desired fringe sensitivity it was assumed that it would be easy to recognize the distortion in the fringe lines if the largest deflections of the reflected rays produced a shift in the fringe lines were on the order of 3 times the pitch of the nominal fringe pattern. Using the relations 7-7 and 7-10 to express the limits interms of the grid parameters yields:

$$\text{FRINGE SPACING:} \qquad 0.2 = \frac{P}{\sqrt{2 - 2\cos\alpha_P}} \qquad (8\text{-}5)$$

$$\text{FRINGE SENSITIVITY:} \qquad 3 = \frac{d\Theta_{max}}{P} \qquad (8\text{-}6)$$

Note that the pitch, P, is the pitch of both transmittance grids. Also, Θ_{max} is the maximum deflection angle of the reflected rays. Recall that the parameter chosen for the disk produces a maximum deflection of the disk of 0.5 deg. (0.0087 rad). The maximum ray deflections Θ_{max} will be about twice the maximum disk deflection, or about 1 deg (0.0174 rad).

The two expressions above are not sufficient to determine the three unknown parameters, but they do express conditions that must be met. By trial and error it was not difficult to choose values for the parameters that provided an acceptabl fringe spacing and fringe sensitivity, and that also were convenient to impliment (for instance the pitch was chosen to correspond to a commercially available size ronchi ruling). The resulting parameter choices were:

$$P = 0.01 \text{ inches}$$
$$\alpha = 3 \text{ deg.}$$
$$d = 1.18 \text{ inches (30 mm)}$$

Unless otherwise noted, the parameters for the object and the orientation, pitch and, angles of the transmittance grids listed in this section are used both in the CAD simulations and the experiments of sections 3.3 and 3.4.

8.3 CAD Simulation of Specular Moire Interferometry.

In this section the validity of the analysis presented in Chapter 7 is verified using computer generated simulations of the moire fringe pattern produced on the analyzing plane.

Calculations of the magnitude of the x directed component, Θ_Y, of the reflected ray deflections are made using the relations of Chapter 7. The calculated deflections are then compared with the exact (as given by Equations 8-1 through 8-4) ray deflections, that are used in constructing the simulated fringe pattern. As is shown subsequently, the values predicted with the relations derived in Chapter 7 and the theoretical values correspond closely.

8.3.1 CAD Simulation Techniques

The comuter based simulation of the specular moire interferometer (and the diffuse simulation of Chapter 5) were developed here at MIT by a colleague, Ron Leonard [29]. The techniques, which utilize the geometric modeling capabilities of a CAD system, emulate the moire process by analytically tracing the path of rays reflected from the surface of the disk through the projecting grid to determine where the individual dark shadow lines of the projected pattern fall on the analyzing plane. Calculation of the direction and point of intersection with the analyzing plane of individual rays was based on relatons 3-1 through 3-4. For each projecting grid line several rays were traced to the analysing plane. The projected grid line (or line of shadow) was approximated by drawing a splined line through the these points of intersection.

The interference between the lines of the projected pattern and the lines of the transmittance grid is simulated by superimposing the splined line pattern and a CAD based representation of the analyzing grid. This could be done either on a monitor or on a high precision pen plotter. A moire fringe pattern for the specular object and system parameters of section 8.2 (produced with the plotter) is illustrated in Figure 3.2. Note that the figure is drawn 2.5 times larger than actual.

Analysis of the Simulated Moire Pattern

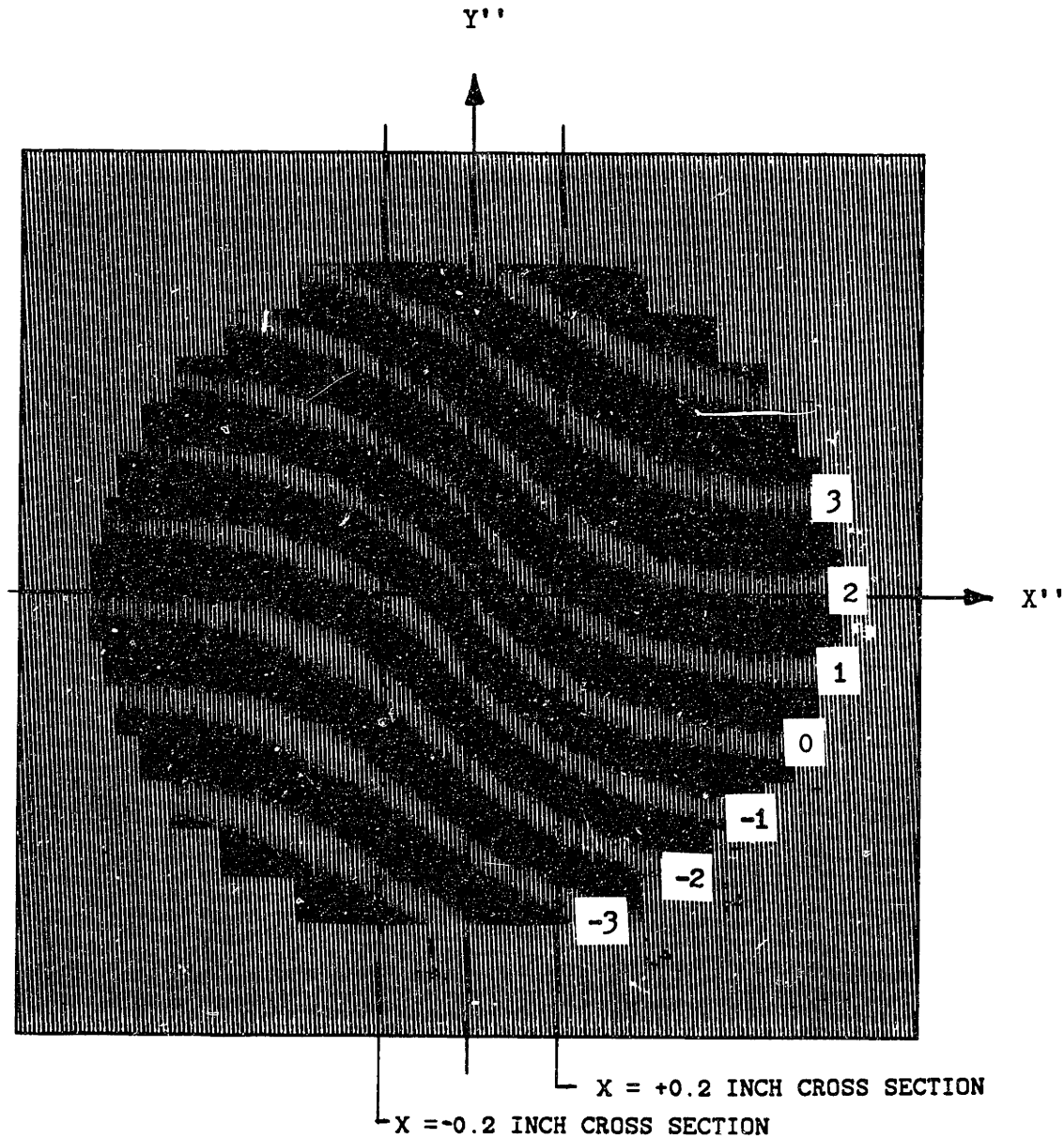

FIGURE 8-2 CAD simulation of Moire Fringe Pattern Produced On Steel Disk with 0.0075 Inch Center Displacement

The distortions of the moire fringe pattern are analyzed by applying equaton 7-8 at specific points on the fringe pattern. The two cross sections indicated on the moire pattern of Figure 8-2 were arbitrarily chosen as paths along which relation 7-8 would be applied. The properties that must be be measured (by hand in this case) to apply Equation 7-8 are the analyzing plane coordinates, X'', Y'', and the fringe order of specific points along the cross section.

Measuring the coordinates can be accomplished simply by the use of scales. Determining the fringe order is, however, a bit more involved. As discussed in Chapter 7, Equation 7-8 yields the correct deflection angle, Θ_Y, only if the exact fringe order is known. However, the fractional part only of the fringe pattern can be determined from the average intensity of the fringe lines. In this case it is convenient to determine only the points of maximum and minimum intensity on the fringe lines which corresponds to intergral (fractional part of zero) or intergral plus 1/2 (fractional part of 0.5) fringe orders, respectively. The intergral part of the fringe order at points along the cross section was determined by realizing that the rays reflected off the center of the disk are undeflected. Therefore, the fringe order at the center of the analyzing plane will be the same as the fringe order for the nominal fringe pattern, and can be determined from Equation 7-9 with the deflection, Θ_Y, set to zero. As can be seen in 7-8, if (as it was for the simulations)the offset, ϕ, of both the grids is set to zero, the order at the center of the analyzing plane will be zero. Thus, everywhere along the same (maximum intensity) fringe line the order will be zero. This allows the order of one of the maximum intensity points along each cross

section to be determined exactly (i.e. the point with a fringe order of 0.0). The order of adjacent points of maximum (and/or minimum) intensity fringe lines can be found by counting up or down as adjacent fringes are crossed. The fringe orders indicated on the simulation (Figure 8-2) were determined in this way.

The coordinates of each point of maximum intensity, i.e. points with intergral fringe order, on the two cross sections indicated in Figure 8-2 were measured, and then Equation 7-8 was used to calculate the X directed component of the reflected ray, θ_Y. The results for points along each cross section are indicated by small diamond symbols in Figure 8-3 and 8-4. The results of the analysis are plotted against the theoretical values (solid line) for θ_Y. The theoretical values were determined from the analytical representation of the disk, or Equations 8-1 through 8-4. In fact, the algorithms used to isolate the theoretical values for points along the cross section were the same as the algorithms used by the CAD simulation in constructing the projected pattern.

The very good agreement between the results indicates that the equation of Chapter 7 are indeed capable of predicting one component of the deflections of the reflected rays from the distortion of the moire fringe pattern. The small errors that do exist can be attributed to errors in estimating and measuring the point of maximum intensity on the fringe pattern. The measurements were made on a fringe pattern identical to the pattern of Figure 8-2, except drawn to a scale 5 times larger than actual size. If the error in estimating and measuring the Y'' coordinate of the fringe centers is estimated to be + or - 1/50th of an inch, the corresponding error in the angle of

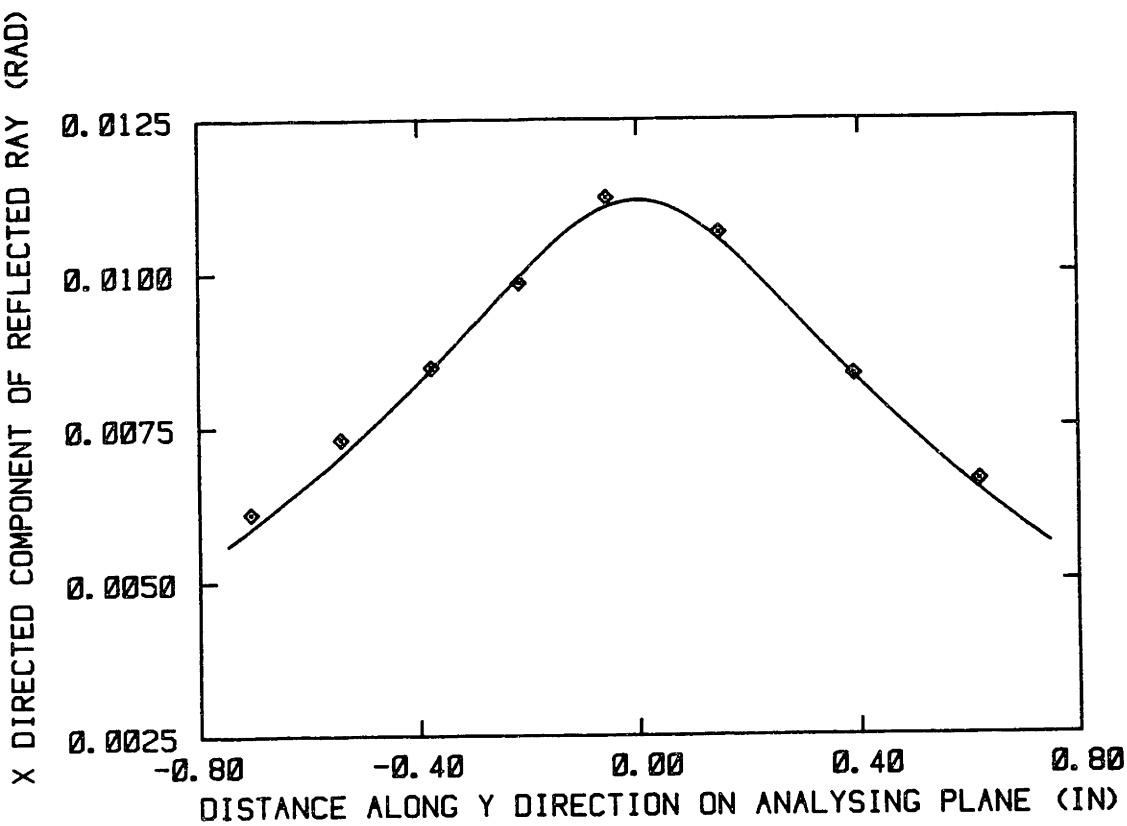

FIGURE 8-3 Results of Theory and Anslysis of CAD Simulated Moire Fringe Pattern for 0.2 Inch Cross Section

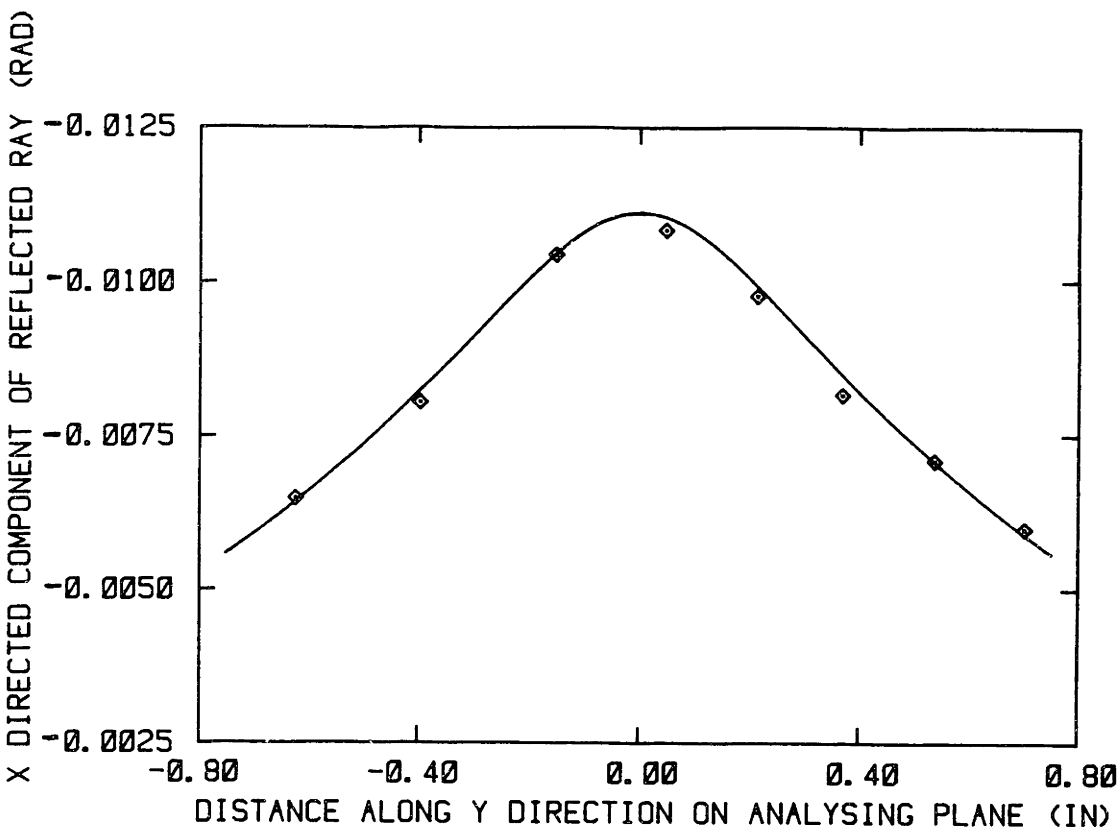

FIGURE 8-4 Results of Theory and Analysis of CAD Simulated Moire Fringe Pattern for -0.2 Inch Cross Section

deflection is +/- 0.0017 rad. On the plot this is approximately +/- 1/15 of the large divisions on the plot, or about 30% larger than the size of the diamond plotting symbol. All but two points on either plot fall within this estimated band of error.

Very good agreement should be expected between the results of analysis of the CAD simulation and the theoretical results, as the same equations that are used to produce the CAD simulation are used to compute the theoretical values.

8.4 Experimental Verification of Specular Moire Interferometry.

The specular moire interferometric process that was simulated in the last section was implimented experimentally, and the schematic for the apparatus is shown in Figure 8-5. The apparatus was designed and built to match the specifications for the specular object and the system configuration specified in Section 8.2. The motivation for the experiments was both to verify the analysis of Chapter 7 and to explore the feasibility of the suggested configuration for nearly flat specular objects.

As in section 8.3, the fringe pattern produced on the analysing plane is analysed to determine one component of the deflections of the rays reflected from the disk. The results are again compared with the deflections predicted from theory. This comparison is not a true verification of the process, however, because the experimental results are not compared with measurements of the actual ray deflections. The theoretical values infered from Equations 8-1 through 8-3 can only be considered to be approximately correct. The comparison does indicate,

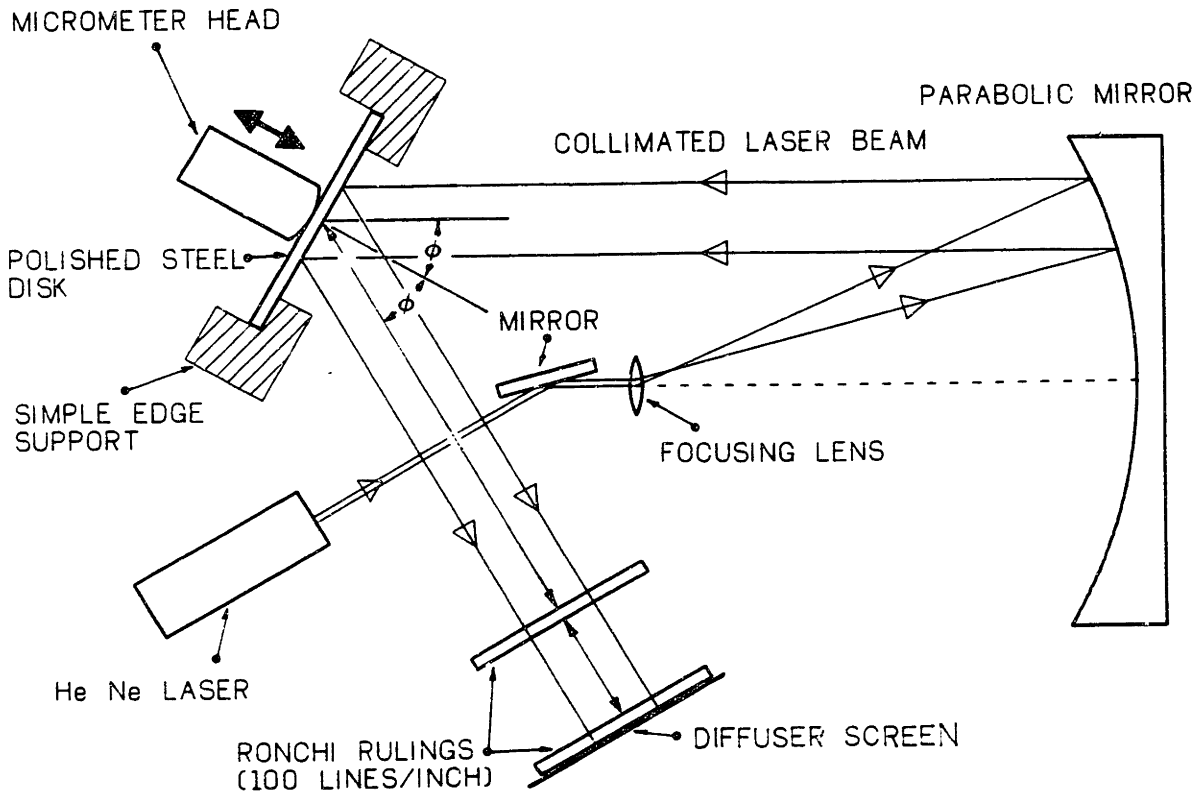

FIGURE 8-5 Schematic for Experimental Apparatus for Specular Moire Interferometry

however, that the specular moire technique yields reasonable quantitative results.

8.4.1 Experimental Apparatus

As indicated in Figure 8-5 the collimated beam incident onto the disk is produced by expanding the beam of a 5 milliwatt output HeNe laser. The beam of the laser is first passed through a focusing lens (18 mm, f=1.8 lens) and then onto a parabolic mirror (6 inch ,f=6). The lens is oriented so that the focal point of the lens is at the focal point of the parabolic mirror. When aligned properly in this configuration the beam divergance of the expanded laser beam will be minimized, and will be smaller than the divergance of the unexpanded beam by the ratio of the focal lengths of the lens and parabolic mirror. By this reasoning, the divergence of the expanded beam was approximately 0.02 milliradians. The beam divergence is important as it limits the clarity of the shadow created by the projecting grid.

Alignment of the lens and mirror was accomplished in several steps. First the optical axes of the mirror was isolated by aligning the laser beam and small mirror so that the beam from the small flat mirror reflected off the center of the parabolic mirror, and then back along its path into the laser. Note that the small flat mirror (flat to 1/4 wave length of light) was used only to make the apparatus more compact. Next, the lens was placed in the path of the beam so that the expanded beam was centered on the mirror. The distance from the lens to the mirror was adjusted for best collimation by finding the position which cast the most clear shadow of a 100 line/inch ronchi ruling. The laser itself was then moved so that the beam reflected

off the edge of the parabolic mirror, as depicted in Figure 8-5.

As indicated in Figure 8-5, the polished steel disk was deflected at its center by using the blunted tip of a micrometer. The disk was pressed against a cylindrical hole (machined in aluminum, with a diameter of 50 mm) that provided the simple support for the disk. Alignment of the supporting block for the disk to the proper angle relative to the collimated light beam (30 deg.) was accomplished using a flat mirror (flat to 1/4 wave) mounted in the supporting block. After mounting the mirror flush against the edge that would support the disk, the supporting block was oriented so that the combined angle of incidence and reflection of the incident collimated beam was 60 degrees.

The micrometer head that deflects the center of the disk was mounted on an aluminum post. The deflection of the disk could then be read directly from the scale of the micrometer. The supporting block and the micrometer post were built to be very rigid so that there would be only small deflections (i.e. significantly less less than the deflection of the disk) in the block and the post.

As for diffuse moire interferometry, ronchi rulings were used as the transmittance grids. The square glass ronchi rulings measured 2" by 2" by 1/8" with a spatial frequency of 100 lines/inch. The rulings were mounted on flat aluminum plates (1/4" thick), with the center of the plates removed to allow a path for the light. Each of the plates were then mounted onto a common set of guide rails. The guide rails fit tightly (slight clearence) through holes that were drilled perpendicular to the face of the plates. The plates were fabricated

using identical steps so that when mounted on the guide rails the plates, and therefore the rulings, would be close to parallel.

The rulings were aligned by hand to be perpendicular to the rays reflected off the reference mirror by adjusting the orientation of the guide rails. The position of the rulings could then be adjusted by moving the aluminum plates along the rails. The spacing between the rulings was adjusted to the specified distance (30 mm, or 1.18 inches). Also, the distance from the center of the undeflected disk to the first ruling was adjusted to be 50 mm.

The translucent diffuser screen was used to form a real image of the moire pattern that is visible to an observer (or a camera) placed behind the diffuser screen. The screen used for the experiments was rear projection screen of the type commonly used for slide projectors and large television screens. A 2" x 2" square of the screen was attached directly to the back of the 2nd ronchi ruling (analysing grid).

To establish a visible reference for the X'', Y'' coordinate frame a wire crosshair was inserted in the path of the collimated beam between the parabolic mirror and the disk. Accordingly, the shadow of the cross hairs were used to indicate the X'', Y'' axis during analysis of the fringe pattern. The center of the crosshairs was aligned to reflect off the center of the disk.

The orientation the first ronchi ruling was adjusted so that the lines of the ruling were parallel to the Y'' axis. The orientation of the second ruling was then adjusted so that the angle of the lines, α_p, was 3 degrees. This was accomplished by observing the fringe

pattern observed with the reference (flat) mirror, and adjusting the spacing of the fringes to equal the designed spacing (0.19 inches).

A 35 mm camera (50 mm, f=2 lens) placed behind the diffuser screen was used to record the fringe patterns. Standard color slide film was used. Typical exposure times with ASA 200 film were 1/125th and 1/250th of a second.

The steel disk itself was made from 1/64 inch thick precision ground stock. One surface of the disk was polished to produce a highly specular (mirror like) surface. After polishing the average thickness of the disk was accurately measured using a micrometer to be 0.0164 inches.

8.4.2 Experimental Results

The three moire fringe patterns that will be analyzed are shown in Figures 3-6 through 8-8. What is presented in the figures are color xerox reproductions made from the photographs taken during the experiments. Figure 8-6 shows the moire fringe pattern produced with the flat reference mirror held against the supporting block for the disk. Figure 8-7 shows the fringe pattern produced with the steel disk deflected 0.0075 inches (7.5 mills), and Figure 8-8 shows the fringe pattern produced with the disk deflected 0.004 inches (4.0 mills).

Originally it was planned to only use a disk deflection of 7.5 mills. However, during the experiments the fringe patterns produced with a disk deflection of 7.5 mill were visibly unsymetrical, and the shape of the pattern did not compare well with the shape of the

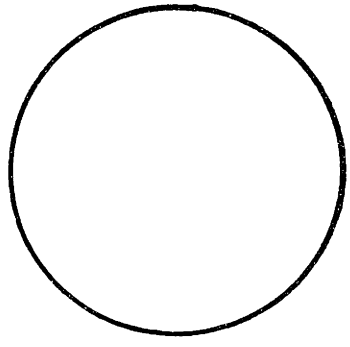

FIGURE 8-6
(see following page)

Moire Fringe Pattern Produced using Flat Reference Mirror

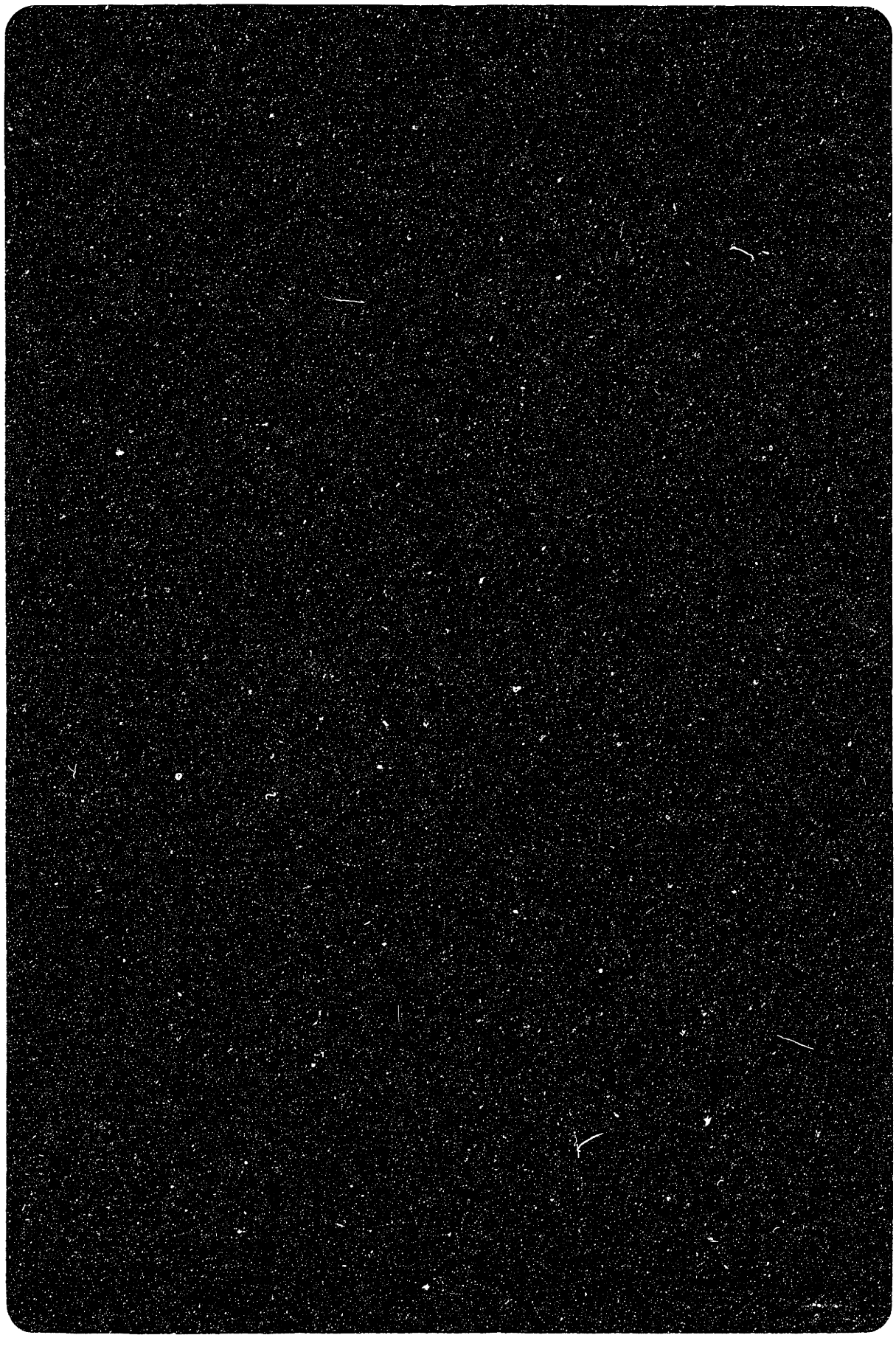

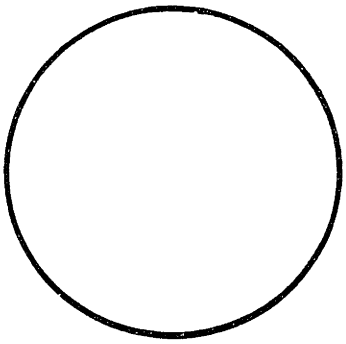

FIGURE 8-7

(see following page)

Moire Fringe Pattern Produced using a Steel Disk with a 0.0075 Inch Center Displacement

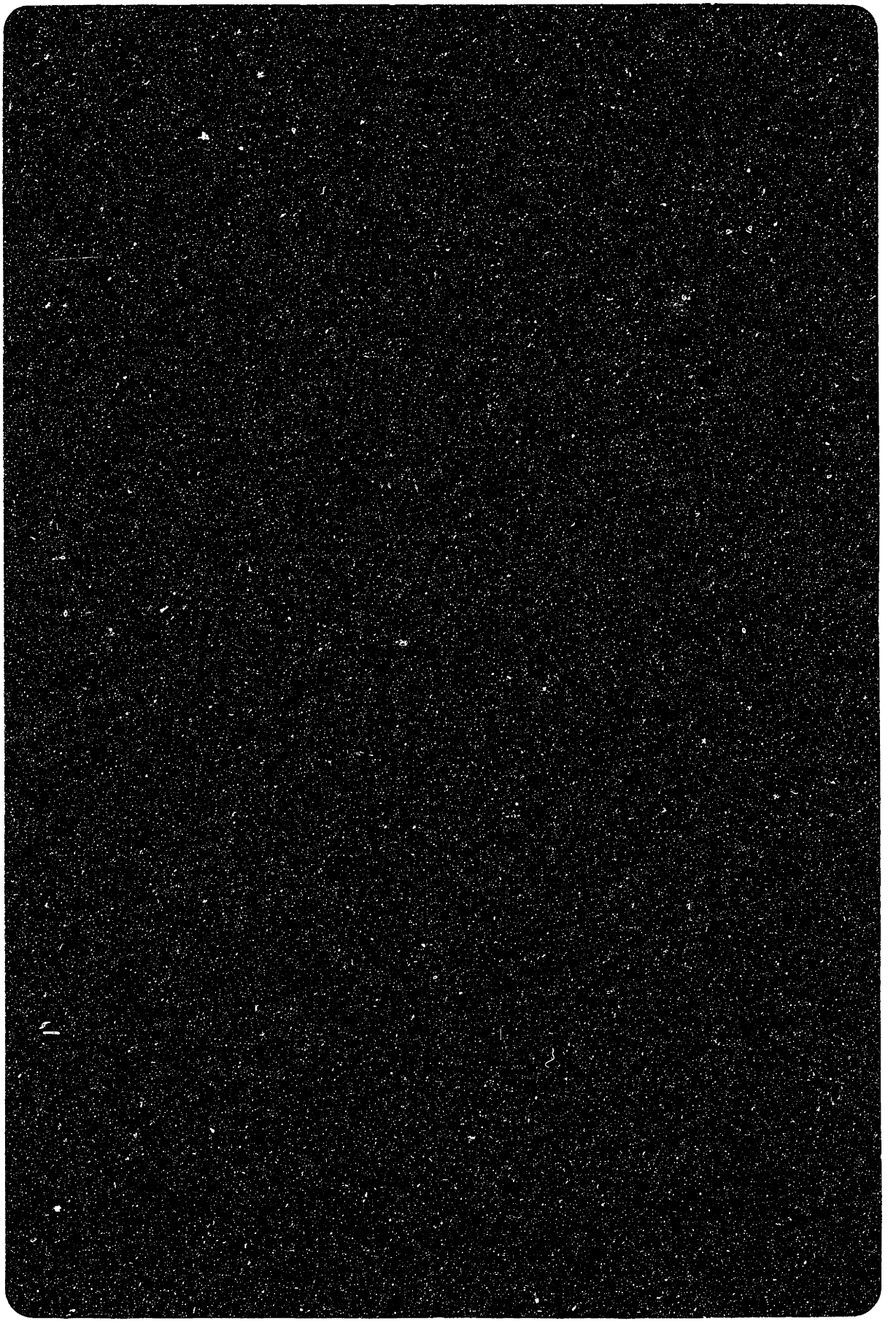

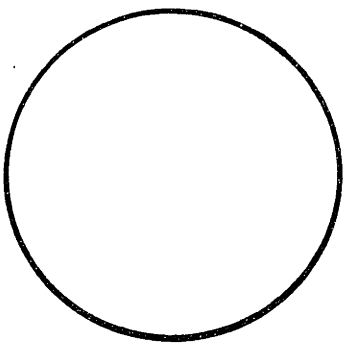

FIGURE 8-8
(see following page)

Moire Fringe Pattern Produced using a Steel Disk with a 0.004 Inch Center Displacement

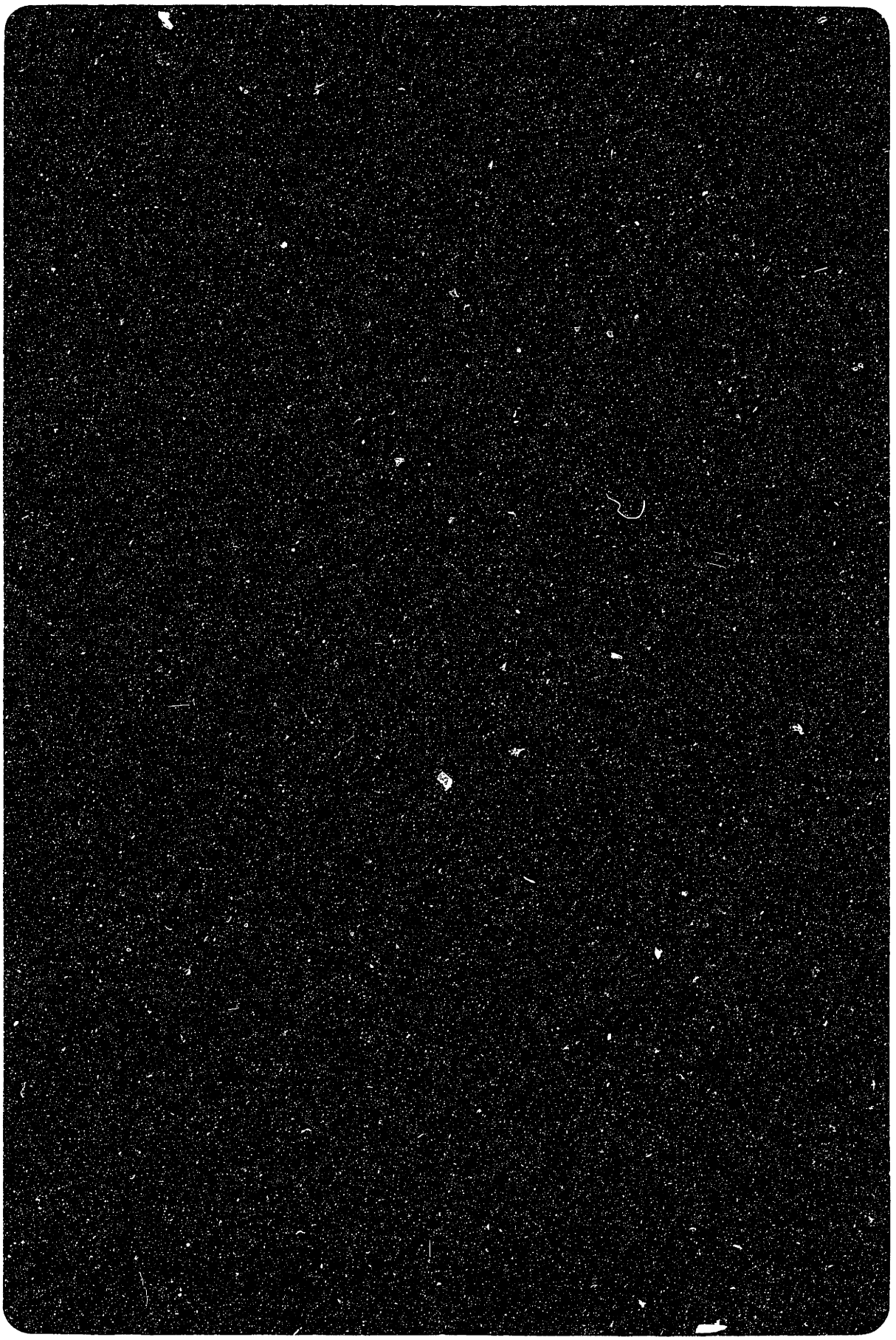

simulated moire patterns. Also, the shape of the fringe pattern changed significantly with the orientation of the disk in the support. This indicated that the disk was not behaving elastically, as was assumed. The fringe patterns produced with smaller deflections seemed to compare more favorably with the simulated fringe pattern, so a deflection of 4.0 mills was included in the experiment.

8.4.3 Analysis of the Experimental Fringe Patterns.

All three of the fringe patterns presented above were analyzed using Equation 7-8 to determine the X directed component of the reflected light rays, θ_Y. The analysis of the experimental fringe pattern is very similar to the analysis of the simulated moire fringe pattern. As in section 3.3, the deflection of the reflected rays is evaluated along cross sections on the analyzing plane at X'' = 0.2 and X'' = -0.2 inches.

To evaluate Equation 7-8 the it was necessary to determine the position and fringe order along the cross sections. Obtaining these quantities for the experimental fringe patterns was similar, but more involved than for the simulated fringe patterns of section 8.3. The position of the centers of the light fringes (along each cross section) were measured using scales. To make the measurments more accurate the fringe patterns (which were recorded on 35 mm color slide film) were projected onto a large piece of paper. The projected fringe pattern (which was significantly enlarged) was sketched onto the paper, and could then be measured more conveniently. As discussed in section 8.3, the shadow of a wire crosshair that had been inserted into the path of the collimated beam was used to keep track of the X''

and Y'' axes on the diffuser plane.

Determining the fringe order of the center of the light fringe lines was again based on the assumption that the reflected ray deflection is zero at the center of the disk (or mirror). However, for the experimental fringe patterns the assignment of fringe order to the light fringe lines is complicated by the fact that the zero order (bright) fringe will not necessarily pass through the origin of the analyzing plane coordinate systems.

Recall that for the simulation the offsets of the projected and analyzing grids (ϕ_P and ϕ_A) were set to zero. This ensured that the zero order fringe would pass through the origin provided the projecting grid was projected by undeflected rays. For the experiments, however, the grid positions were not precise, so that ϕ_P and ϕ_A will not be zero. The effect of non-zero grid offsets on the fringe pattern is to shift the zero order bright fringe line away from the analyzing plane origin. Equation 7-8 still applies at every point on the fringe pattern, but the offsets of the grids need to be determined if the ray reflections are to be calculated exactly. The effect of ignoring the offsets, or determining the offsets incorrectly, would simply be to add or subtract a constant value to the values for the ray deflections.

The offsets for the fringe patterns were determined by applying Equation 7-8 at the analyzing plane origin with the deflection of the reflected ray assumed to be zero. The equation was simply rearranged to yield the $\phi_A - \phi_P$ term. To do this however, the fringe order at the origin had to be known. The fractional part of the fringe

order was estimated by assuming that fringe order between adjacent bright fringe centers was a linear function of distance. After being evaluated the offsets were used in Equation 7-8 to evaluate the ray deflection, θ_Y, at along the X'' = 0.2 inch and the X'' = -0.2 inch cross sections.

In assigning the integral portion of the fringe order to the center of the light fringe lines it was important that the assumption as to which fringe line was the zero order fringe was consistent with the assumptions made in evaluating the offsets. As for the simulations, the fringe orders along the cross sections were assigned relative to the zero order fringe line by counting up or down when adjecent fringe lines were crossed.

8.4.4 Results of Analysis.

The results of the analysis for the three moire fringe patterns are shown in Figure 8-9 through 8-11. The figures show the experimentally determined (diamond symbols) and the theoretically predicted (solid line) values for the deflections of the reflected rays. The ordinate of Figures 8-9 through 8-11 is the X directed component of the deflections of the reflected rays, θ_Y. Part a of all three figures shows the results along the cross section at X'' = 0.2 inches, and part b shows the results along the X'' = -0.2 inch cross section.

Figure 8-9 shows the results for the moire fringe produced with the flat reference mirror. The theoretical prediction for the deflection of the rays reflected off the flat mirror is zero, provided

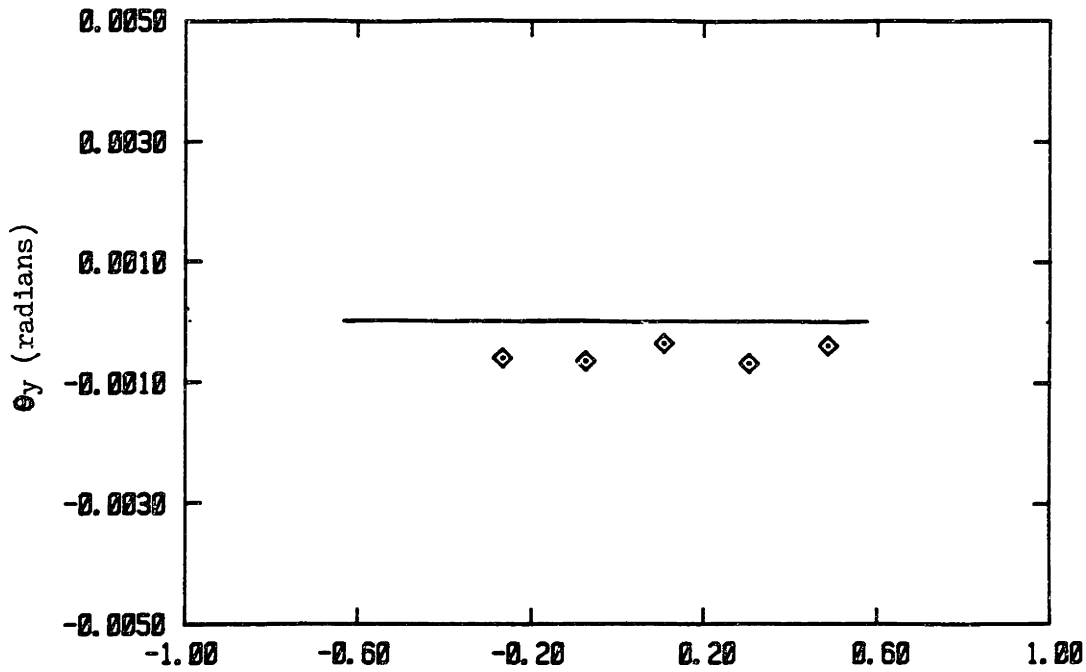

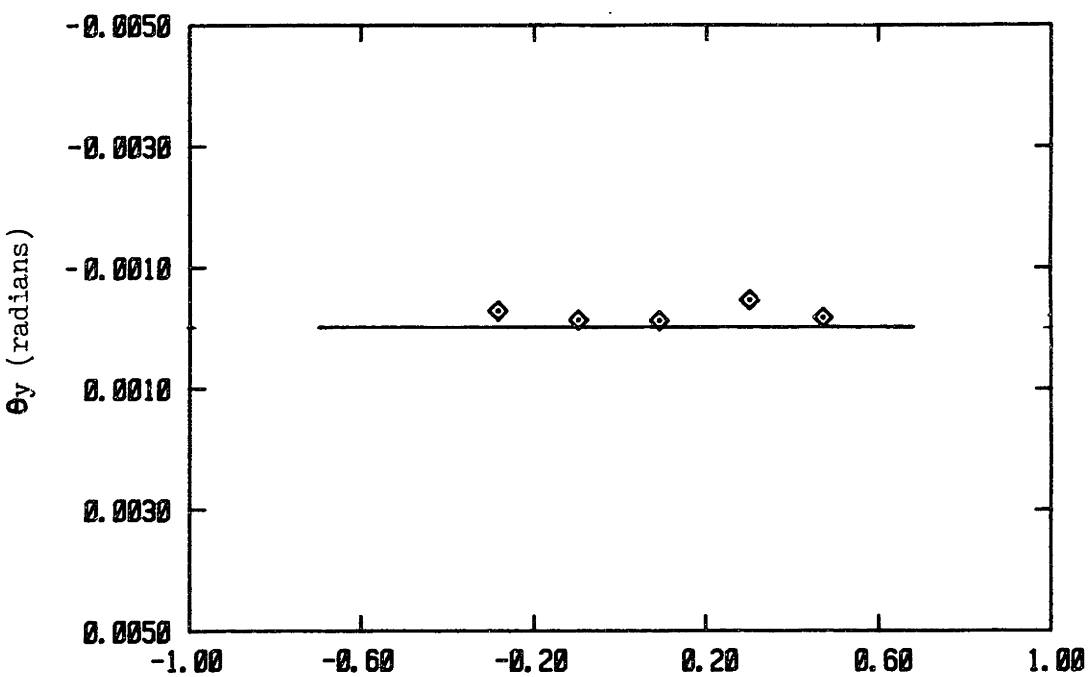

FIGURE 8-9 Results of Theory and Analysis of Moire Fringe Pattern for Flat Mirror

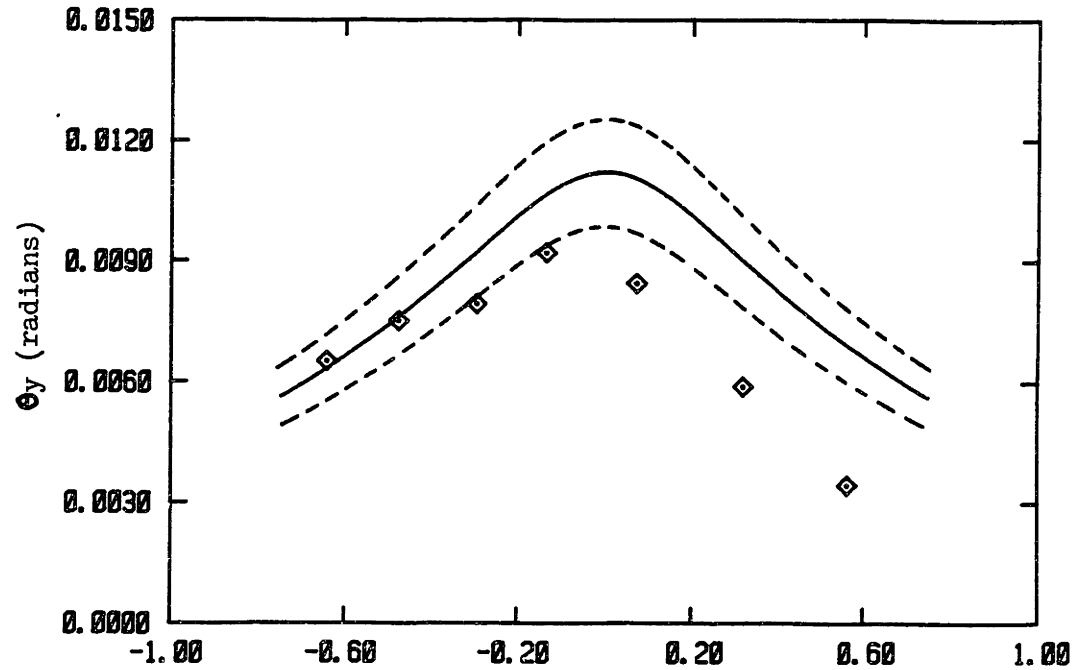

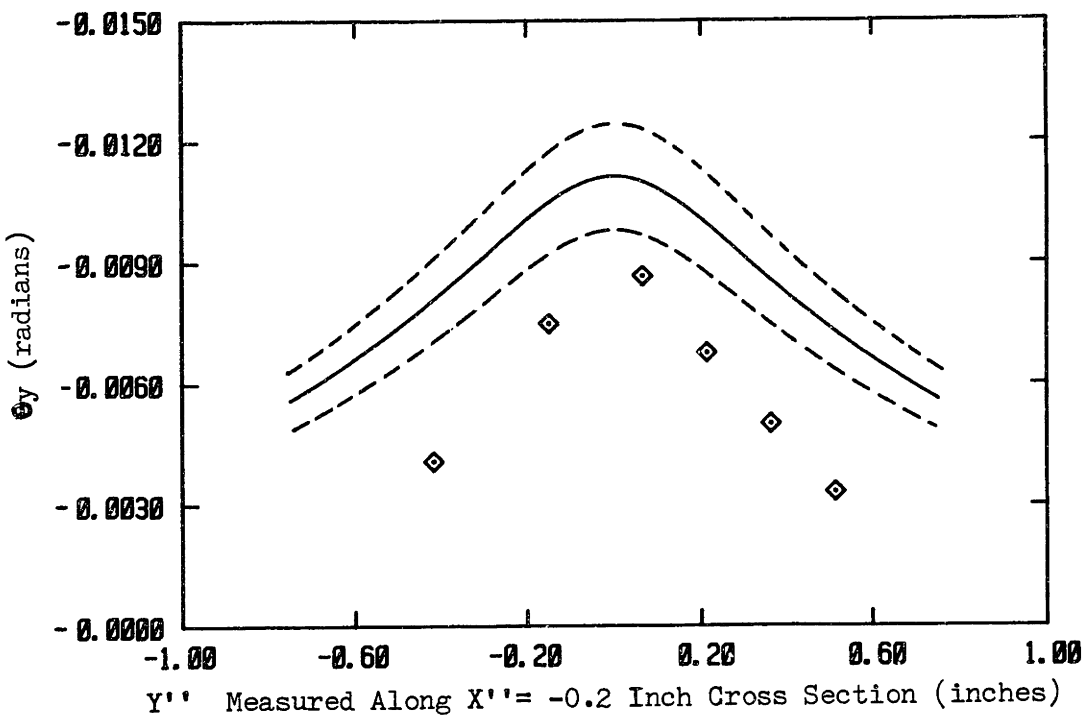

FIGURE 8-10 Results of Theory and Analysis of Moire Fringe Pattern for Disk Displaced 0.0075 Inches

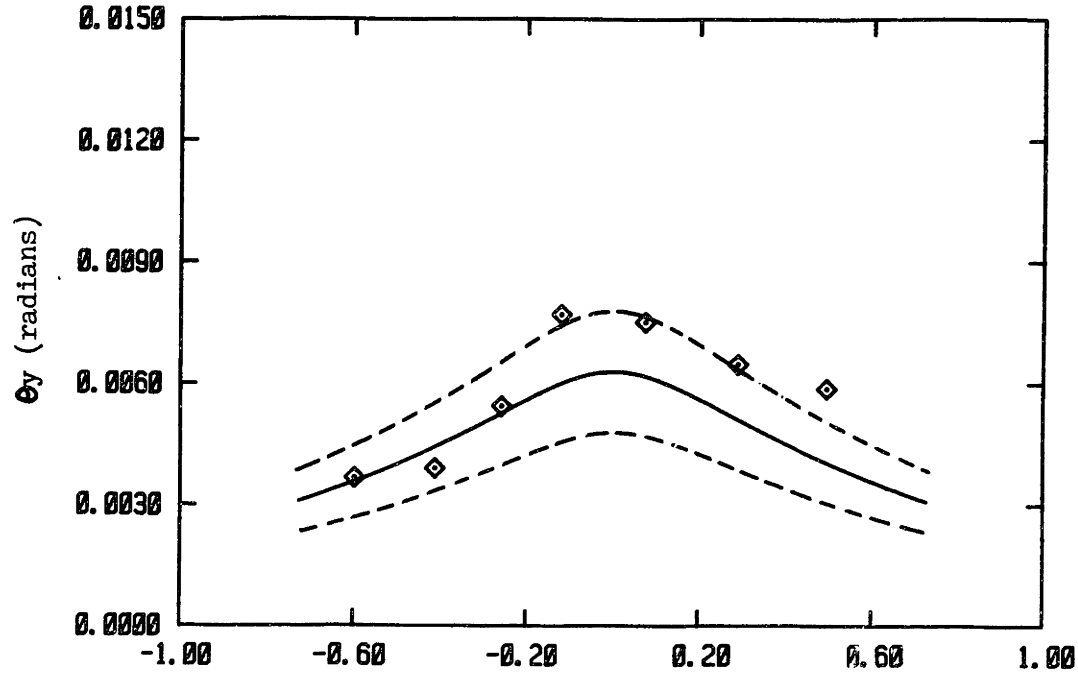

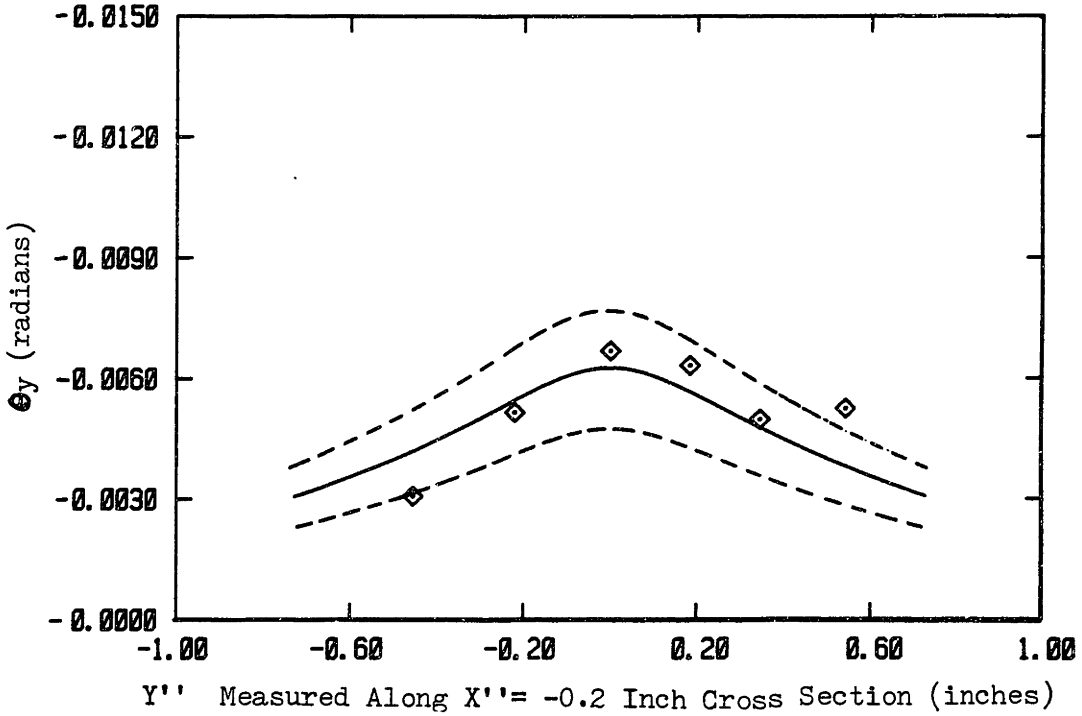

FIGURE 8-11 Results of Theory and Analysis of Moire Fringe Pattern for Disk Displaced 0.004 Inches

the mirror is flat to 1/4 wavelength of light (as specified by manufacturer). The experimental data seems to agree well with the theoretical data except that the experiments data for the +0.2 inch cross section appears to have an offset. A probable cause for this systematic error is that the offset of the grids used in Equation 7-8 was not correct. As the results are plotted, an error in the offset of the grids would shift the experimental data points up on one plate and down on the other.

Figures 8-10 a and b show the experimental results for the fringe pattern produced with a 7.5 mill displacement of the steel disk. Clearly, the theoretical predictions for the ray deflections do not agree well with the results from analysis of the experimental fringe pattern. Although the shape of the experimental data, agrees with the shape of the theoretical data the experimental values are significantly lower than theory would predict.

The dashed lines in Figures 8-10 and 8-11 that are above and below the solid line show the theoretical values for a disk displcement that is + or - 1 mill from the nominal disk displacement. These lines give an indication of the sensitivity of the ray deflections to the deflection of the steel disk.

It is clear that the theoretical and experimental values do not agree well. However, it should be remembered that the true shape of the disk is not represented by the theoretical predictions. It was clear just from comparing qualitatively the simulated (Figure 8-2) and the experimental (Figure 8-7) fringe patterns that the shape of the actual fringe pattern does not match the shape predicted by the

simulation. From this it was expected that the experimental and simulation values would disagree. Unfortunately there is not enough information from the experiments and or the simulations of Chapter 7 to conclude decisively what is the source of the discrepancy.

One likely source for the discrepency is of course that the actual disk is not the shape that is predicted by the theoretical model. While performing the experiments (which were originally designed for a 7.5 mill disk deflection) it was observed that smaller disk deflections produced moire fringe patterns that were more smooth and symmetrical than the patterns for larger disk deflections. Specifically, for disk deflections below about 4.0 mills the moire fringes looked much more similar in shape to the simulations. For disk displacements above these values the fringes were not smoothly curved lines and the fringe pattern was not symmetric.

The theory used to model the shape of the disk assumes isotropic and elastic behavior of the steel disk. The observations described above indicated that a 7.5 mill deflection may be outside of the range for which these assumptions are appropriate. This may be the reason for the relatively poor agreement between the experimental and theoretical results in Figure 3-10.

To ascertain if this was the case the experiment was repeated for a 4.0 mill disk deflection. The results of the experiment are shown in Figure 8-11. Clearly, the experimental and theoretical results for this case agree better than for the 7.5 mill case. The differences are still significant, but the magnitudes and the shape of the experimental data agree to, at worst, within about 25% of the

theoretically predicted values.

8.5 Discussion and Conclusions.

The results of the simulation of section 8.3 and of the experiments of section 8.4 were presented as a verification for the analysis of specular moire interrerometry presented in Chapter 7. To correctly draw conclusions form these results about the validity of the analysis it is helpful to separate the analysis into two areas. The simulation can be shown to offer verification for the first of these areas, and the experiments the second. The two plenomena that are modeled in the analysis can be separated into the following two functional areas:

1) the relationship between the distortions of the shadow of the projecting grid and the distortion of the fringe pattern.

2) the relationship between the distortion of a specularly reflecting object and the distortions of the shadow of the projecting grid.

Included in the first area is the analysis developed in Chapter 2 (specifically Equation 2-7) that relates the fringe order to the interfering patterns. Included in the second area is the analysis in Chapter 7 that relates the angle of the reflected rays to the distortion of the lines (Equation 7-4), and the analysis summarized in Chapter 3 that relates the orientation of the surface to the angle of the reflected rays (Equation 8-3).

The results for the simulated moire pattern presented in section 8-3 can be used to draw conclusions about the validity of only the first area of the analysis. That is, the very good agreement in the results obtained for the simulated moire pattern and the results obtained from analysis of the simulated moire pattern tend to verify the relations used to analyse the moire pattern (i.e. Equation 2-7) only. The reason for this is that the same analytical model is used to relate the ray deflections to the distortion of the projected pattern for both the simulations and experiments. Consequently, any discrepancies between the ray deflections used to construct the simulated line pattern and the ray deflections obtained by analyzing the moire pattern are not likely to arise from the relation between the ray deflections and the grid pattern distortions.

What is really being tested by first constructing and then analyzing a fringe pattern in section 3.3 is the analytical method for determining the line pattern distortions from the moire fringe pattern. Specifically, if Equation 7-4 were incorrect than the results of Figures 8-4 and 8-5 would not corresopond as well as they do. The results of the simulation are, therefore, a positive statement for the validity of only the first area (as listed above) of the analysis.

The experiments described in section 8.4, on the other hand, compare both areas of the analysis. For the theoretical predictions and the experimental results to match both areas of the analysis must correctly model the experiments. Unfortunately, the experiments are not a decisive test of the analysis because the true shape of the deflected disk is not known.

In designing the experiments it was sought to avoid measuring the actual shape of the disk with proven method by using an object that could be analytically represented. The disk used in the experiments was designed to be such an object. However, the analytical representation assumes that the disk:

1) the disk behaves elastically and isotropically

2) the disk is loaded uniformly at the center and around its edges

3) the deflection of the disk is known accurately.

Even though these criterion were considered in the design of the experiment, it is not clear that they were satisfied. In fact, as described in section 3.4, the lack of symmetry observed in the experimental fringe pattern suggested that the above criterion were not met.

Consequently, the true shape of the disk, and hence the true ray deflections, are not accurately known. It is not conclusive, therefore, that differences between the theoretical predictions and the experimental results constitute errors.

The object is known exactly for one case. This is the case for which the flat mirror is used to produce the moire pattern. This case can not be used to test both areas of the analysis, however, since there are no reflected ray deflections. Because the projected grid for this case is not deformed, this case can be used to check only whether or not the analysis correctly models the distortion (or lack there of) of the projected grid. Thus, the results for the reference mirror (Figures 3-9 a and b) are, as for the CAD simulations, a test of only the ability to relate the fringe patterns to the projected

pattern.

With all of the likely sources of error considered, the experiments do give a positive indication of the validity of the analysis. For all of the experiments the gross shape of the theoretical results and the experimental results agree. Also, even though true shape of the disk is not known, the theoretical predictions do at least give an indication of the magnitude of the ray deflections that should be observed. In every case the experimental results are comparable in magnitude. Although this is not concrete evidence for the validity of the analysis, it does indicate that there are no major flaws within the analysis.

Clearly the analysis yields sensible results. This indicates that the fundamental models are correct, although significant discrepancies do exist. It is not conclusive whether or not these discrepancies represent are atributabl e to the analysis. Before this can be decided, more careful experiments need to be designed and performed. The experiments need to provided a conclusive test, with the shape of the object (or more specifically the deflection of the light rays) accurately known.

Chapter 9 Summary and Conclusions

The analyses presented in this thesis for both diffusely reflecting and specularly reflecting objects relate the geometry of the object to the observed moire fringe pattern. For diffuse moire interferometry the 3-dimensional coordinates of points on the visible surface of the object are related to the properties (position and fringe order) of the observed moire fringe pattern. For specular objects the direction of rays of light reflected off the object are related to the properties (position and fringe order) of the observed moire fringe pattern. For both diffuse and specular moire interferometry only the case where straight line, evenly spaces grid patterns are used for structuring light is considered. Both the analysis for diffuse moire interferometry and spacular moire interferometry were developed specifically to be useful as tools for the analysis and design of moire interferometric based shape inspection systems.

The analysis for diffusive objects produced:

1) Relations for the coordinates of the object surface as a function of fringe order and position of the observed moire fringes (suitable for computing object shape),

2) Relations for the fringe order and positon of the moire fringes as a function of the object surface (suitable for computing the moire fringe pattern),

3) Relations for the approximate local properties (direction, spacing, and sensitivity) of the fringe lines as a function of the orientation and position of the object (assumed to be flat) and the parameters of the moire interferometer.

The second and third (2 and 3 above) analytical developments for diffuse moire interferometry were verified experimentally using fringe patterns produced on a flat diffusely reflecting object. The results of the experiments show that the analytical relations are capable of accurately predicting the shape of the fringe pattern and capable of predicting approximately the properties of the observed fringe lines. Also, the analytically predicted fringe patterns are shown to compare well with simulated moire fringe patterns generated with a CAD based emulation of a diffuse moire interferometer.

The analysis for specular moire interferometry produced relations for the direction of the rays reflected off the surface of the object as a function of the order and position of the observed fringe pattern. These relationships are suitable determining one component of the local slope of the specular surface from any one measurement (i.e. fringe pattern). The analysis for specular moire interferometry was verified through both experimentation and CAD simulations. The results indicate that the relations give reasonably accurate results.

For both analyses, relations suitable for designing the characteristics (i.e. the sensitivities shape of the moire fringes to changes in the shape of the object) of the moire interferometer are developed. These relations should prove to be useful tools for the analysis and design of moire inspection systems.

REFERENCES

1 Idesawa, M., Yatagai,T., Soma.,T. "Scanning Moire Method and Automated Measurement of 3-D Shapes. Applied Optics, Vol. 16, No. 8, August 1977. pg 2152.

2 Tou, J. T. "Automated Parts Inspection Via Moire Topography". proceedings of SME and AUTOFACT, Vol. 1 Anaheim, CA. 1980

3 Post, Daniel. "Moire Grid-analyser Method for Strain Analysis". Experimental Mechanics, Nov. 1965, pg 1965.

4 Weissman, Eric M. and D. Post, "Moire Interferometry Near the Theoretical Limit," Applied Optics, Vol. 21, No. 9, May, 1982, pg. 1621.

5 Meadows, D.M., Johnson,W. O., and Allen, J.B. "Generation of Surface Contours by Moire Patterns." Applied Optics, Vol. 9, No. 4, April 1970. pg 942.

6 Takasaki, H. "Moire Topography". Applied Optics, Vol. 9, No. 6, June 1970. pg 1467.

7 Takasaki, H. "Moire Topography". Applied Optics, Vol. 12, No. 4, April 1973. pg 845.

8 Chiang, Chung. "Moire Topography". Applied Optics, Vol. 14, No. 1, January 1975. pg 177.

9 Sheperd, R. and L. McD. Wensley, "The Moire-Fringe Method of Displacement Measurement Applied to Indirect Structural-model Analysis," Experimental Mechanics, June, 1965, pg. 168.

10 Burch, J. M. and C. Forno, "A High Sensitivity Moire Grid Technique for Studying Deformation in Large Objects," Optical Engineering, Vol. 14, No. 2, March 1975, pg. 178.

11 Gasvik, K. J., "Moire Technique by Means of Digital Image Processing," Applied Optics, Vol. 22, No. 23, Dec. 1983, pg. 3543.

12 Halioua, M., Krishnamurthy, R. S., Liu, H. and Chiang, F. P. "Projection Moire With Moving Gratings for Automated 3-D Topograghy". Applied Optics, Vol. 22, No. 6, March 1983

13 Livnat, A. and O. Kafri, "Fringe Addition in Moire Analysis," Applied Optics, Vol. 22, No. 19, Oct. 1983, pg. 3013.

14 Livnat, A. and O. Kafri, "Finite Fringe Shadow Moire Slope Measurement of Diffusive Objects," Applied Optics, Vol. 22, No. 20, Oct. 1983, pg. 3232.

15 Brooks, R., and Heflinger,L. "Moire Gauging Using Optical Interference Patterns". Applied Optics, Vol. 8, No. 5, May 1969. pg 935.

16 Sikora, J. "Deflection of Rotating Marine Propellers Using Projected Grating Moire Techniques". Experimental Mechanics, December 1981. pg 456.

17 Funnell, W. R. J., "Image Processing Applied to the Interactive Analysis of Interferometric Fringes," Applied Optics, Vol. 20, No. 18, Sept. 1981, pg. 3245

18 Livnat, A., Kafir,O. and Erez,G. "Hills and Valleys Analysis in Optical Mapping and Its Application to Moire Contouring". Applied Optics, Vol. 19, No. 19, October 1980. pg 3396.

19 Schemm, J. B. and Charles M. Vest, "Fringe Pattern Recognition and Interpolation Using Nonlinear Regression Analysis," Applied Optics, Vol. 22, No. 18, Sept. 1983, pg. 2850.

20 Mertz, L., "Real Time Fringe-Pattern Analysis," Applied Optics, Vol. 22 No. 10, May 1983.

21 Perrin, J. C. and Thomas,A. "Electronic Processing of Moire Fringes: Application to Moire Topography and Comparison Photogrammetry". Applied Optics, Vol. 18, No. 4, February 1979.

22 Breslow, T., "Sensitivity of Moire Fringes," interdepartmental report, not published.

23 Breslow, T., "Moire Fringe Interferometry," interdepartmentsl report, not published.

24 Yokozeki, S. and S. Mihara, "Moire Interferometry," Applied Optics, Vol. 18 No. 8, April 1979, pg. 1275.

25 Kafri, O., "Noncoherent Method for Mapping Phase Objects," Optical Letters, Vol. 5 No. 12, Dec. 1980, pg. 555.

26 Kafri, O., A. Livnat and E. Keren, "Infinite Fringe Moire Deflectometry," Applied Optics, Vol. 21 No. 21, Nov. 1982, pg. 3884.

27 Kafri, O. and A. Livnat, "Second and Third Optical Differentiation by Double Moire Interferometry," Applied Optics, Vol. 22 No. 14, July 1983.

28 Moore, D. and Truax,B. "Phase-Locked Moire Fringe Analysis for Automated Contouring of Diffuse Surfaces," Applied Optics, Vol. 18, No. 1, January 1979. pg 91.

29 Leonard, Ron J., "Application of Moire Techniques to Manufacturing Inspection," Masters of Science Thesis, Deptatrment of Mechanical Engineering, Massachusettes Institute of Technology, Dec., 1984.

30 Denavit, J. and Hartenberg, R.S., "A Kinematic Notation for Lower-Pair Mechanisms Based on Matricies," ASME Journal of Applied Mechanisms, June, 1955.

31 Paul, Richard P., Robot Manipulators: Mathematics, Programing, and Control., 3rd. ed., Massachusettes Institute of Technology Press, Cambridge, MA., 1982

32 Roark, Raymond J., and Warren C. Young, Formulas for Stress and Strain, 5th ed., McGraw-Hill, 1975

33 Spiegel, Murray R., "Vector Analysis and an Introduction to Tensor Analysis," McGraw-Hill, New York, 1959.

34 The Third Annual Applied Machine Vision Conference Proceedings (Feb. 27 - March 1, 1984, Chicago Ill.), Society of Manufacturing Engineers, Dearborn, Mich., 1984.

35 13 th Annual Symposium on Industrial Robots and Robots 7 Conference Proceedings, (April 17-21, 1983, Chicago Ill.), Society of Manufacturing Engineers, Dearborn, Mich., 1983.

*** APPENDIX A ***

LISTING FOR PROGRAM THAT CALCULATES
AND PLOTS FRINGE PROPERTIES

The following listing is of the fortran program that was developed to compute and plot the properties of the moire fringe lines produced on a flat diffusely reflecting object. The program is based on the approximate relations for fringe local properties developed in section 3.5.

```
C$$$$$$$$$$$$$$$$$$$$$$$$$$$$$$$$$$$$$$$$$$$$$$$$$$$$$$$$$$$$$$$$$$$$$$$$
C
C                              DIFFUSE.FTN
C
C          PROGRAM FOR CALCULATING THE E.O. SURFACE NORMAL
C          THE E.O. SURFACE SPACING, THE FRINGE SHIFT SEN-
C          SITIVITY, AND THE FRINGE SPACING AND ANGLE SEN-
C          SITIVITIES FOR A GIVEN DIFFUSE PROJECTION MOIRE
C          ARRANGEMENT
C
C          Author: J. Wander
C          Date: Aug., 1984
C
C$$$$$$$$$$$$$$$$$$$$$$$$$$$$$$$$$$$$$$$$$$$$$$$$$$$$$$$$$$$$$$$$$$$$$$$$
C
C
        DIMENSION PLT0(701),PLT1(701),PLT2(701),PLT3(701)
        DIMENSION SHSEN(50),ANSEN(50),SPSEN(50),
     1  EANGLE(50),ESPACE(50),ESHIFT(50)
        COMMON /UPLOT/ IDEV,POS(4),USCALE(4),LABX(80),LABY(80),
     1  LABT(80),NTKX,NTKY,ITM,MARK,CHWD,CHHT,PTWD,FMTX(6),
     2  FMTY(6)
        BYTE LABX,LABY,LABT,FMTX,FMTY
        COMMON /PROJEC/ T21,T22,T23,T24,T25,T26,T27,T28,T29,
     1  T2X,T2Y,T2Z,PIP,IMP,PIV,IMV,CAL,SAL
        COMMON /OBJECT/ T31,T32,T33,T34,T35,T36,T37,T38,T39,
     1  T3X,T3Y,T3Z,OBSIZE,T41,T42,T43,T44,T45,T46,T47,T48,T49
        COMMON /PARAMP/THETAP,ZETAP,PSIP,T1X,T1Y,T1Z,PP,SP,
     1  PV,SV,ALF
        COMMON /PARAMO/ PSIO,ZETAO,X,Y,Z,PSID,ZETAD,
     1  XV,YV,FO
        COMMON /PARAEO/ EX,EY,EZ,EOSPC
        COMMON /OBJNRM/ OX,OY,OZ,OXD,OYD,OZD
        COMMON /FLAGS/ FLAG,FLAGD
        COMMON /FLINE/ FX,FY,FZ
C
        REAL OBANG(50)
        REAL MAX0,MIN0,MAX1,MIN1,MAX2,MIN2,MAX3,MIN3
```

```
      REAL PIP,IMP,PIV,IMV

C
C
C$$$$$$$$$$$  ENTER THE PROJECTION SYSTEM GEOMETRY  $$$$$$$$$$$$
C
C
      TYPE*,'ENTER INITIAL VALUES FOR PROJECTOR PARAMETERS;'
   1  TYPE*,'ENTER PROJ. SYSTEM TRANSFORM ANG., THETA, ZETA,
     1    PSI'
      ACCEPT*, THETAP, ZETAP, PSIP
      TYPE*,'ENTER XO,YO,ZO FOR THE PROJ. SYSTEM'
      ACCEPT*,T1X,T1Y,T1Z
      TYPE*,'ENTER PP AND PV, THE GRID PITCHES'
      ACCEPT*,PP,PV
      TYPE *,'ENTER THE IMAGE DISTANCES; SP,SV'
      ACCEPT*,SP,SV
      TYPE*,'ENTER ALF, THE VIEW. GRID ANG. FROM THE Y AXIS'
      ACCEPT*,ALF
C
      TYPE *,'ENTER THE OBJECT LOCATION, X,Y,Z'
      ACCEPT *,X,Y,Z
   2  TYPE *,' WOULD YOU LIKE TO CHANGE SYSTEM PARAMETERS,
     1    1=Y,0=N'
      ACCEPT*,CHOICE
      IF(CHOICE.EQ.1)THEN
        GO TO 1
      ELSE
      END IF
C
C$$$$$$$$$$$$  INITIALIZE THE PLOTTING PARAMETERS  $$$$$$$$$$$$$$
C
C

      POS(1)=2000.
      POS(2)=2000.
      POS(3)=9400.
      POS(4)=6400.
      NTKX=10
      NTKY=5
      ITM=0
      CHWD=.2
      CHHT=.4
      PTWD=.2
      FMTX(1)='F'
      FMTX(2)='7'
      FMTX(3)='.'
      FMTX(4)='2'
      FMTY(1)='F'
      FMTY(2)='8'
      FMTY(3)='.'
      FMTY(4)='2'
```

```
        MARK = 0
C
C
C$$$$$$$$$$$$$$$$$$$$$$$$$$$$$$$$$$$$$$$$$$$$$$$$$$$$$$$$$$$$$$$$$$$$
C$$$$$$$$$$$$$$$$$$$  MAIN  PROGRAM  $$$$$$$$$$$$$$$$$$$$$$$$$$$$$$$$
C$$$$$$$$$$$$$$$$$$$$$$$$$$$$$$$$$$$$$$$$$$$$$$$$$$$$$$$$$$$$$$$$$$$$
C
        TYPE *,'ENTER THE NOMINAL Z AXIS ROT. FOR OBJECT, PSI'
        ACCEPT *,PSIO
        TYPE*,'ENTER PLOTTER, 0,HP2648A 1,HP9872S'
        ACCEPT*,IDEV

C


C
        PI = 3.141592654
        PSID = 0.
        ZETAD=0.00005

C
        TYPE*,'ENTER ZETA START AND ZETA STOP'
        ACCEPT*,ZETMIN,ZETMAX
        ZETSTP = (ZETMAX-ZETMIN)/700
C
        TYPE*,'WOULD YOU LIKE TO SKIP SENSITIVITIES, 1=Y,0=N'
        ACCEPT*,SKIP
        IF(SKIP.EQ.1)THEN
          GO TO 290
        ELSE
        END IF
C
        DO 100 N=1,701
        ZETAO = (N-1)*ZETSTP + ZETMIN
C
C$$$$$$$$$$$$$$$  EVALUATE FRINGE PROPERTIES  $$$$$$$$$$$$$$$$$$$
C
C


        CALL PTRAN
        CALL COMPFO
        CALL EONORM
        CALL EOMAG
        CALL OBTRAN
        CALL OBNORM
        CALL FRDEL(FRSHIF,DELANG,DELSPC,FRSPC)

C
C
        PLTO(N) = ZETAO*180./PI
C
        IF((FLAG.EQ.1).OR.(FLAGD.EQ.1))THEN
         GO TO 100
```

```
        ELSE
        CALL FRSEN(FRSHIF,DELANG,DELSPC,FRSPC,
     1                SHISEN,ANGSEN,SPCSEN)
        PLT1(N) = ABS(SHISEN)
        PLT2(N) = ANGSEN
        PLT3(N) = ABS(SPCSEN)
        END IF
C
  100   CONTINUE
C
        TYPE*,'WILL WE BE PLOTTING EXPERIMENTAL DATA, 0=NO,1=YES'
        ACCEPT*,EXPLT
C
        IF(EXPLT.EQ.1)THEN
C
          OPEN (UNIT=4, FILE='SEN.DAT',STATUS='OLD')
          PLFLAG=1
          READ(4,*)NEPTS
          DO 110 N=1,NEPTS
          READ(4,*)OBANG(N),SHSEN(N),ANSEN(N),SPSEN(N)
  110     CONTINUE
          CLOSE (UNIT=4,STATUS='SAVE')
C
        ELSE
C
          TYPE*,'WOULD IT GIVE YOU PLEASURE TO SCALE THE PLOTS,
     1      0=NO,1=Y'
          ACCEPT*,PLFLAG
C
          IF(PLFLAG.EQ.0)THEN
            DO 200 N=1,700
            CALL SORT(N,PLT0(N),MAX0,MIN0)
            CALL SORT(N,PLT1(N),MAX1,MIN1)
            CALL SORT(N,PLT2(N),MAX2,MIN2)
            CALL SORT(N,PLT3(N),MAX3,MIN3)
  200       CONTINUE
          ELSE
          END IF
        END IF
C
        TYPE *,'PLOTING SHIFT SENSITIVITY VS OBJ ANGLE'
        CALL BOX(PLFLAG, MIN0,MIN1,MAX0,MAX1)
        CALL GEDPLT(PLT0,PLT1,700,1)
        IF(EXPLT.EQ.1)THEN
          MARK = 4
          CALL GEDPLT(OBANG,SHSEN,NEPTS,1)
          MARK = 0
        ELSE
        END IF
        CALL GEDCLR
C
        TYPE *,'PLOTTING ANGLE SENS. VS OBJ ANGLE'
```

```
        IF((MAX2.LE..1).AND.(MIN2.GE.-.1))THEN
        MIN2=-.833333333
        MAX2=.833333333
        ELSE
        END IF
        CALL BOX(PLFLAG, MIN0,MIN2,MAX0,MAX2)
        CALL GEDPLT(PLT0,PLT2,700,1)
        IF(EXPLT.EQ.1)THEN
          MARK = 4
          CALL GEDPLT(OBANG,ANSEN,NEPTS,1)
          MARK = 0
        ELSE
        END IF
        CALL GEDCLR
C
        TYPE *,'PLOTING SPACING SENS. VS OBJ ANGLE'
        CALL BOX(PLFLAG, MIN0,MIN3,MAX0,MAX3)
        IF(EXPLT.EQ.1)THEN
          MARK=4
          CALL GEDPLT(OBANG,SPSEN,NEPTS,1)
          MARK=0
        ELSE
        END IF
        CALL GEDPLT(PLT0,PLT3,700,1)
        CALL GEDCLR
C
C$$$$$$$$$$$$$$$$$$$$$$$$$$$$$$$$$$$$$$$$$$$$$$$$$$$$$$$$$$$$$$$$$$$
C
 290    TYPE*,' DO YOU WANT TO SKIP FRING PROPERTIES, 1=Y,0=N'
        ACCEPT*,SKIP
        IF(SKIP.EQ.1)THEN
          GO TO 500
        ELSE
        END IF
C
C$$$$$$$$$$$$$$ EVALUATE AND PLOT FRINGE PROPERTIES $$$$$$$$$$$$$
C
        DO 300 N=1,701
        ZETAO = (N-1)*ZETSTP+ZETMIN
        CALL PTRAN
        CALL COMPFO
        CALL EONORM
        CALL EOMAG
        CALL OBTRAN
        CALL OBNORM
        CALL PERSP(OX,OY,OZ,FVX,FVY,AVX,AVY)
        IF(FLAG.EQ.1)THEN
          FRSPC = 1000
          FRSHIF = 1000
          GO TO 250
        ELSE
          CALL FRCOMP(FVX,FVY,AVX,AVY,FRANG,FRSPC)
```

```
          CALL SHIFT(OX,OY,OZ,FVX,FVY,FRSHIF)
        END IF
C
C
  250   PLT0(N) = ZETAO*180/PI
        PLT1(N)=ABS(FRSHIF)
        PLT2(N)=FRANG
        PLT3(N)=ABS(FRSPC)
  300   CONTINUE
C
        TYPE*,'WILL WE BE PLOTTING EXPERIMENTAL DATA, 0=NO,1=YES'
        ACCEPT*,EXPLT
C
        IF(EXPLT.EQ.1)THEN
C
          OPEN (UNIT=4, FILE='FRG.DAT',STATUS='OLD')
          PLFLAG=1
          READ(4,*)NEPTS
          DO 310 N=1,NEPTS
          READ(4,*)OBANG(N),ESHIFT(N),EANGLE(N),ESPACE(N)
  310     CONTINUE
          CLOSE (UNIT=4,STATUS='SAVE')
C
        ELSE
C
          TYPE*,'WOULD IT GIVE YOU PLEASURE TO SCALE THE PLOTS,
     1     0=NO,1=Y'
          ACCEPT*,PLFLAG
C
          IF(PLFLAG.EQ.0)THEN
            DO 400 N=1,700
            CALL SORT(N,PLT0(N),MAX0,MIN0)
            CALL SORT(N,PLT1(N),MAX1,MIN1)
            CALL SORT(N,PLT2(N),MAX2,MIN2)
            CALL SORT(N,PLT3(N),MAX3,MIN3)
  400       CONTINUE
          ELSE
          END IF
        END IF
C
        TYPE *,'PLOTTING FRINGE SHIFT VS OBJ ANGLE'
        CALL BOX(PLFLAG, MIN0,MIN1,MAX0,MAX1)
        CALL GEDPLT(PLT0,PLT1,700,1)
        IF(EXPLT.EQ.1)THEN
          MARK = 4
          CALL GEDPLT(OBANG,ESHIFT,NEPTS,1)
          MARK = 0
        ELSE
        END IF
        CALL GEDCLR
C
        TYPE *,'PLOTING FRINGE ANGLE VS OBJ ANGLE'
```

```
        TEMP1=PLFLAG
        IF(MAX2.EQ.MIN2)THEN
          WRITE(5,*)'THE FRINGE ANGLE IS CONSTANT AT ',MIN2
          PLFLAG=1
        ELSE
        END IF
        CALL BOX(PLFLAG, MIN0,MIN2,MAX0,MAX2)
        PLFLAG=TEMP1
        CALL GEDPLT(PLT0,PLT2,700,1)
        IF(EXPLT.EQ.1)THEN
          MARK = 4
          CALL GEDPLT(OBANG,EANGLE,NEPTS,1)
          MARK = 0
        ELSE
        END IF
        CALL GEDCLR
C
        TYPE *,'PLOTTING FRINGE SPACING'
        CALL BOX(PLFLAG, MIN0,MIN3,MAX0,MAX3)
        IF(EXPLT.EQ.1)THEN
          MARK=4
          CALL GEDPLT(OBANG,ESPACE,NEPTS,1)
          MARK=0
        ELSE
        END IF
        CALL GEDPLT(PLT0,PLT3,700,1)
        CALL GEDCLR

C
C$$$$$$$$$$$$$$$$$$$$$$$$$$$$$$$$$$$$$$$$$$$$$$$$$$$$$$$$$$$$$$$$$$$$$$
C
  500   TYPE*,'WOULD YOU LIKE TO REPLOT, 1=YES, 0=NO'
        ACCEPT*, REPLT
        IF(REPLT.EQ.1) GO TO 2
C
        STOP
        END
C
C$$$$$$$$$$$$$$$$$$$$$$$$$$$$$$$$$$$$$$$$$$$$$$$$$$$$$$$$$$$$$$$$$$$$$$
C$$$$$$$$$$$$$$$$$$$$   SUBROUTINES   $$$$$$$$$$$$$$$$$$$$$$$$$$$$$$$$$
C$$$$$$$$$$$$$$$$$$$$$$$$$$$$$$$$$$$$$$$$$$$$$$$$$$$$$$$$$$$$$$$$$$$$$$
C
C$$$$$$$$$$$$$$$$$$$$$$$$$$$$$$$$$$$$$$$$$$$$$$$$$$$$$$$$$$$$$$$$$$$$$$
C            COMPUTE PROJECTION SYSTEM TRANSFORM
C$$$$$$$$$$$$$$$$$$$$$$$$$$$$$$$$$$$$$$$$$$$$$$$$$$$$$$$$$$$$$$$$$$$$$$
C
        SUBROUTINE PTRAN
C
        COMMON /PARAMP/ THETAP,ZETAP,PSIP,T1X,T1Y,T1Z,PP,SP,
     1  PV,SV,ALF
        COMMON /PROJEC/ T21,T22,T23,T24,T25,T26,T27,T28,T29,
     1  T2X,T2Y,T2Z,PIP,IMP,PIV,IMV,CAL,SAL
```

```
      REAL PIP,IMP,PIV,IMV
      COMMON /PRIN/ PRINT
C
      PIP = PP
      IMP = SP
      PIV = PV
      IMV = SV
      CAL = COS(ALF)
      SAL = SIN(ALF)
      CPSP=COS(PSIP)
      SPSP=SIN(PSIP)
      CZEP=COS(ZETAP)
      SZEP=SIN(ZETAP)
      CTHP=COS(THETAP)
      STHP=SIN(THETAP)
C
C COMPUTE THE TRANSFORM ELEMENTS FOR THE PROJ. FRAME
C
      T21=CPSP*CZEP
      T22=SPSP*CZEP+CPSP*SZEP*STHP
      T23=SPSP*STHP-CPSP*SZEP*CTHP
      T24=-SPSP*CZEP
      T25=CPSP*CTHP-SPSP*SZEP*STHP
      T26=CPSP*STHP+SPSP*SZEP*CTHP
      T27=SZEP
      T28=-CZEP*STHP
      T29=CZEP*CTHP
      T2X=-(T21*T1X+T22*T1Y+T23*T1Z)
      T2Y=-(T24*T1X+T25*T1Y+T26*T1Z)
      T2Z=-(T27*T1X+T28*T1Y+T29*T1Z)
C

      RETURN
      END
C
C$$$$$$$$$$$$$$$$$$$$$$$$$$$$$$$$$$$$$$$$$$$$$$$$$$$$$$$$$$$$$$$$$$$$$$$
C          COMPUTE OBJECT TRANSFORM ELEMENTS
C$$$$$$$$$$$$$$$$$$$$$$$$$$$$$$$$$$$$$$$$$$$$$$$$$$$$$$$$$$$$$$$$$$$$$$$
C
      SUBROUTINE OBTRAN
C
      COMMON /PARAMO/ PSIO,ZETAO,X,Y,Z,PSID,ZETAD,
     1  XV,YV,FO
      COMMON /OBJECT/ T31,T32,T33,T34,T35,T36,T37,T38,T39,
     1  T3X,T3Y,T3Z,OBSIZE,T41,T42,T43,T44,T45,T46,T47,T48,T49
      COMMON /PRIN/ PRINT
C
      CPSO=COS(PSIO)
      SPSO=SIN(PSIO)
      CZEO=COS(ZETAO)
      SZEO=SIN(ZETAO)
C
```

```
C
C COMPUTE TRANSFORM ELEMENTS FOR NOMINAL OBJECT FRAME
C
C
        T31=CPSO*CZEO
        T32=-SPSO
        T33=CPSO*SZEO
        T34=SPSO*CZEO
        T35=CPSO
        T36=SPSO*SZEO
        T37=-SZEO
        T38=0.
        T39=CZEO
        T3X=X
        T3Y=Y
        T3Z=Z
C
C COMPUTE TRANSFORM TO DEFLECT OBJECT
C
        CPSD = COS(PSID)
        SPSD = SIN(PSID)
        CZED = COS(ZETAD)
        SZED = SIN(ZETAD)
C
        T41=CPSD*CZED
        T42=-SPSD
        T43=CPSD*SZED
        T44=SPSD*CZED
        T45=CPSD
        T46=SPSD*SZED
        T47=-SZED
        T48=0.
        T49=CZED
C
        RETURN
        END
C
C$$$$$$$$$$$$$$$$$$$$$$$$$$$$$$$$$$$$$$$$$$$$$$$$$$$$$$$$$$$$$$$$$$$
C         COMPUTATION OF THE FRINGE ORDER AT A POINT X,Y,Z
C$$$$$$$$$$$$$$$$$$$$$$$$$$$$$$$$$$$$$$$$$$$$$$$$$$$$$$$$$$$$$$$$$$$
C
        SUBROUTINE COMPFO
C
        COMMON /PROJEC/ T21,T22,T23,T24,T25,T26,T27,T28,T29,
     1  T2X,T2Y,T2Z,PIP,IMP,PIV,IMV,CAL,SAL
        COMMON /PARAMO/ PSIO,ZETAO,X,Y,Z,PSID,ZETAD,
     1  XV,YV,FO
        REAL PIP,IMP,PIV,IMV
        COMMON /PRIN/ PRINT
C
C COMPUTE CORRESPONDING COORDS. ON VIEWING PLANE
        XV=-X*IMV/Z
```

```
        YV=-Y*IMV/Z
C
C TRANSfORM POINT TO PROJ. FRAME & TRACE TO PROJ. PLANE
        XPRO=T21*X+T22*Y+T23*Z+T2X
        YPRO=T24*X+T25*Y+T26*Z+T2Y
        ZPRO=T27*X+T28*Y+T29*Z+T2Z
        XP=-XPRO*IMP/ZPRO
        YP=-YPRO*IMP/ZPRO
C
C COMPUTE THE FRINGE ORDER
C
        FO = (XV*CAL-YV*SAL)/PIV - XP/PIP
C
        RETURN
        END
C
C$$$$$$$$$$$$$$$$$$$$$$$$$$$$$$$$$$$$$$$$$$$$$$$$$$$$$$$$$$$$$$$$$$$$$
C           COMPUTE THE E. O. SURFACE UNIT NORMAL
C$$$$$$$$$$$$$$$$$$$$$$$$$$$$$$$$$$$$$$$$$$$$$$$$$$$$$$$$$$$$$$$$$$$$$
C
        SUBROUTINE EONORM
C
        COMMON /PROJEC/ T21,T22,T23,T24,T25,T26,T27,T28,T29,
     1  T2X,T2Y,T2Z,PIP,IMP,PIV,IMV,CAL,SAL
        COMMON /PARAMO/ PSIO,ZETAO,X,Y,Z,PSID,ZETAD,
     1  XV,YV,FO
        COMMON /PARAEO/ EX,EY,EZ,EOSPC
        REAL I,MAG
        REAL PIP,IMP,PIV,IMV
        COMMON /PRIN/ PRINT
C
C ASSIGN VALUES TO EXPRESSIONS
C
C
        A = -T2Z*CAL*PIP/(IMP*PIV)
        B = -T2Z*SAL*PIP/(IMP*PIV)
        C = T2Z*FO*PIP/IMP-T2X
        D = -T27*CAL*PIP/(IMP*IMV*PIV)
        E = -T28*SAL*PIP/(IMP*IMV*PIV)
        F = -(T27*SAL+T28*CAL)*PIP/(IMV*IMP*PIV)
        G = (T27*FO+T29*CAL)*PIP/(IMP*PIV)-T21/IMV
        H = (T28*FO+T29*SAL)*PIP/(IMP*PIV)-T22/IMV
        I = T23-T29*FO*PIP/IMP
C
C
C FOR R = <X,Y,Z>, COMPUTE PARTIALS WITH RESPECT TO XV & YV $$$
C
C
        V=D*XV*XV+E*YV*YV+F*XV*YV+G*XV+H*YV+I
C
C
C FIRST PARTIAL WITH RESPECT TO XV...
```

```
C
C
        AAX=((A*XV*XV+B*XV*YV+C*XV)*(2*D*XV+F*YV+G)-
     1          (2*A*XV+B*YV+C)*V)/IMV
C
        AAY=((A*XV*YV+B*YV*YV+C*YV)*(2*D*XV+F*YV+G)-
     1          (A*YV)*V)/IMV
C
        AAZ=((A*V)-(A*XV+B*YV+C)*(2*D*XV+F*YV+G))
C
C
C FIRST PARTIAL WITH RESPECT TO YV...
C
C
        BBX=((A*XV*XV+B*XV*YV+C*XV)*(2*E*YV+F*XV+H)-
     1          (B*XV)*V)/IMV
C
        BBY=((A*XV*YV+B*YV*YV+C*YV)*(2*E*YV+F*XV+H)-
     1          (A*XV+2*B*YV+C)*V)/IMV
C
        BBZ=((B*V)-(A*XV+B*YV+C)*(2*E*YV+F*XV+H))
C
C
C COMPUTE THE NORMAL DIRECTION FROM CROSS PRODUCT $$$$
C
C
        DIRX=(AAY*BBZ-BBY*AAZ)
        DIRY=(BBX*AAZ-AAX*BBZ)
        DIRZ=(AAX*BBY-BBX*AAY)
C
        MAG = SQRT(DIRX*DIRX+DIRY*DIRY+DIRZ*DIRZ)
C
        EX=DIRX/MAG
        EY=DIRY/MAG
        EZ=DIRZ/MAG
C
C
        RETURN
        END
C
C
C$$$$$$$$$$$$$$$$$$$$$$$$$$$$$$$$$$$$$$$$$$$$$$$$$$$$$$$$$$$$$$$$$$$$$$
C   COMPUTE THE E. O. SURFACE SPACING OR MAG OF ORDER GRADIENT
C$$$$$$$$$$$$$$$$$$$$$$$$$$$$$$$$$$$$$$$$$$$$$$$$$$$$$$$$$$$$$$$$$$$$$$
C
        SUBROUTINE EOMAG
        COMMON /PRIN/ PRINT
C
        COMMON /PROJEC/ T21,T22,T23,T24,T25,T26,T27,T28,T29,
     1  T2X,T2Y,T2Z,PIP,IMP,PIV,IMV,CAL,SAL
        COMMON /PARAMO/ PSIO,ZETAO,X,Y,Z,PSID,ZETAD,
     1  XV,YV,FO
```

```
      COMMON /PARAEO/EX,EY,EZ,EOSPC
      REAL PIP,IMP,PIV,IMV
C
C
      A = -T2X-(CAL*XV+SAL*YV)*T2Z*PIP/(PIV*IMP)
      B = (T23-T21*XV/IMV-T22*YV/IMV)+
     1  (T29-T27*XV/IMV-T28*YV/IMV)*(CAL*XV+SAL*YV)*PIP/(IMP*PIV)
      C = -T2Z*PIP/IMP
      D = (T29-T27*XV/IMV-T28*YV/IMV)*PIP/IMP
C
C
C COMPUTE Z COMPONENT BETWEEN FRINGES
C
      DELTZ = (A*D-B*C)/(B*B-(2*FO+1)*B*D+(FO*FO+FO)*D*D)
C
C
      EOSPC= DELTZ/EZ
C
C
      RETURN
      END
C
C$$$$$$$$$$$$$$$$$$$$$$$$$$$$$$$$$$$$$$$$$$$$$$$$$$$$$$$$$$$$$$$$$$$$
C       COMPUTE NOMINAL AND DEFLECTED OBJECT UNIT NORMAL
C$$$$$$$$$$$$$$$$$$$$$$$$$$$$$$$$$$$$$$$$$$$$$$$$$$$$$$$$$$$$$$$$$$$$
C
      SUBROUTINE OBNORM
C
      COMMON /OBJECT/ T31,T32,T33,T34,T35,T36,T37,T38,T39,
     1  T3X,T3Y,T3Z,OBSIZE,T41,T42,T43,T44,T45,T46,T47,T48,T49
      COMMON /OBJNRM/ OX,OY,OZ,OXD,OYD,OZD
      COMMON /PRIN/ PRINT
C
C COMPUTE NOMINAL OBJECT NORMAL
C
      OX = T33
      OY = T36
      OZ = T39
C
C COMPUTE DEFLECTED OBJECT UNIT NORMAL
C
      OXD = T31*T43 + T32*T46 + T33*T49
      OYD = T34*T43 + T35*T46 + T36*T49
      OZD = T37*T43 + T38*T46 + T39*T49
C
      RETURN
      END
C
C$$$$$$$$$$$$$$$$$$$$$$$$$$$$$$$$$$$$$$$$$$$$$$$$$$$$$$$$$$$$$$$$$$$$
C            COMPUTE SHIFT AND ANGLE SENSITIVITY
C$$$$$$$$$$$$$$$$$$$$$$$$$$$$$$$$$$$$$$$$$$$$$$$$$$$$$$$$$$$$$$$$$$$$
C
```

```
C
      SUBROUTINE FRDEL(FRSHIF,DELANG,DELSPC,FRSPC)
C
      COMMON /PROJEC/ T21,T22,T23,T24,T25,T26,T27,T28,T29,
     1  T2X,T2Y,T2Z,PIP,IMP,PIV,IMV,CAL,SAL
      COMMON /OBJECT/ T31,T32,T33,T34,T35,T36,T37,T38,T39,
     1  T3X,T3Y,T3Z,OBSIZE,T41,T42,T43,T44,T45,T46,T47,T48,T49
      COMMON /PARAMP/ THETAP,ZETAP,PSIP,T1X,T1Y,T1Z,PP,SP,
     1  PV,SV,ALF
      COMMON /PARAMO/ PSIO,ZETAO,X,Y,Z,PSID,ZETAD,
     1  XV,YV,FO
      COMMON /PARAEO/ EX,EY,EZ,EOSPC
      COMMON /OBJNRM/ OX,OY,OZ,OXD,OYD,OZD
      REAL PIP,IMP,PIV,IMV
      COMMON /FLINE/ FX,FY,FZ
      COMMON /FLAGS/ FLAG,FLAGD
      COMMON /PRIN/ PRINT
C
      CALL PERSP(OX,OY,OZ,FVX,FVY,AVX,AVY)
      IF(FLAG.EQ.1)THEN
        FLAGD = 1
      ELSE
        FLAGD = 0
      END IF
      CALL PERSP(OXD,OYD,OZD,FVXD,FVYD,AVXD,AVYD,FLAGD)


C
      IF((FLAG.EQ.1).OR.(FLAGD.EQ.1))THEN
        DELANG =1000
        DELSPC =1000
      ELSE
C
        CALL SHIFT(OX,OY,OZ,FVX,FVY,FRSHIF)
        CALL FRCOMP(FVX,FVY,AVX,AVY,FRANG,FRSPC)
        CALL FRCOMP(FVXD,FVYD,AVXD,AVYD,FRANGD,FRSPCD)
C
        DELANG = FRANGD-FRANG
        DELSPC = FRSPCD-FRSPC
C
      END IF
      RETURN
      END
C
C$$$$$$$$$$$$$$$$$$$$$$$$$$$$$$$$$$$$$$$$$$$$$$$$$$$$$$$$$$$$$$$$$$$$
C                      COMPUTE SENSITIVITIES
C$$$$$$$$$$$$$$$$$$$$$$$$$$$$$$$$$$$$$$$$$$$$$$$$$$$$$$$$$$$$$$$$$$$$
C
C
      SUBROUTINE FRSEN(FRSHIF,DELANG,DELSPC,FRSPC,
     1                 SFTSEN,ANGSEN,SPCSEN)
C
```

```
      COMMON /PARAMO/ PSIO,ZETAO,X,Y,Z,PSID,ZETAD,
     1  XV,YV,FO
      COMMON /PRIN/ PRINT
      COMMON /FLAGS/ FLAG,FLAGD

C
      PI = 3.141592654
C

      IF((FLAG.EQ.1).OR.(FLAGD.EQ.1))THEN
      GO TO 10
      ELSE
      SFTSEN = FRSHIF/FRSPC
      ANGSEN = DELANG/ZETAD
      SPCSEN = DELSPC*PI/(ZETAD*FRSPC*180)
      END IF
C
   10 RETURN
      END
C
C$$$$$$$$$$$$$$$$$$$$$$$$$$$$$$$$$$$$$$$$$$$$$$$$$$$$$$$$$$$$$$$$$$$$$$
C             COMPUTE THE POSITION SENSITIVITY
C$$$$$$$$$$$$$$$$$$$$$$$$$$$$$$$$$$$$$$$$$$$$$$$$$$$$$$$$$$$$$$$$$$$$$$
C
      SUBROUTINE SHIFT(OX,OY,OZ,FVX,FVY,FRSHIF)
      COMMON /FLINE/ FX,FY,FZ
      COMMON /PARAEO/ EX,EY,EZ,EOSPC
      COMMON /PROJEC/ T21,T22,T23,T24,T25,T26,T27,T28,T29,
     1  T2X,T2Y,T2Z,PIP,IMP,PIV,IMV,CAL,SAL
      COMMON /PARAMO/ PSIO,ZETAO,X,Y,Z,PSID,ZETAD,
     1  XV,YV,FO
      COMMON /FLAGS/ FLAG,FLAGD
      REAL PIP,IMP,PIV,IMV

C
      DISP = 1
      IF(FLAG.EQ.1)THEN
        SAX = 0
        SAY = 0
        SAZ = 0
        FRSHIF = 1000
      ELSE
        SAX = DISP*(FY*EZ-FZ*EY)/
     1     (EX*(OY*FZ-OZ*FY)+EY*(OZ*FX-OX*FZ)+EZ*(OX*FY-OY*FX))
C
        SAY = SAX*(FZ*EX-FX*EZ)/(FY*EZ-FZ*EY)
C
        SAZ = (SAX*EX+AY*EY)/-EZ
C
C
        SAVX = IMV*(X*SAZ - Z*SAX)/(Z*Z + Z*SAZ)
        SAVY = IMV*(Y*SAZ - Z*SAY)/(Z*Z + Z*SAZ)
```

```
C
          FRSHIF = (SAVX*FVY + SAVY*-FVX)/(SQRT(FVX*FVX+FVY*FVY))
        END IF
C
        RETURN
        END
C
C$$$$$$$$$$$$$$$$$$$$$$$$$$$$$$$$$$$$$$$$$$$$$$$$$$$$$$$$$$$$$$$$$$$
C         COMPUTE THE PERSPECTIVE VIEW OF FRINGE VECTORS
C$$$$$$$$$$$$$$$$$$$$$$$$$$$$$$$$$$$$$$$$$$$$$$$$$$$$$$$$$$$$$$$$$$$
C
        SUBROUTINE PERSP(OX,OY,OZ,FVX,FVY,AVX,AVY)
C
        COMMON /PROJEC/ T21,T22,T23,T24,T25,T26,T27,T28,T29,
     1  T2X,T2Y,T2Z,PIP,IMP,PIV,IMV,CAL,SAL
        COMMON /PARAMO/ PSIO,ZETAO,X,Y,Z,PSID,ZETAD,
     1  XV,YV,FO
        COMMON /PARAEO/ EX,EY,EZ,EOSPC
        REAL PIP,IMP,PIV,IMV
        COMMON /FLAGS/ FLAG,FLAGD
        COMMON /FLINE/ FX,FY,FZ
        COMMON /PRIN/ PRINT
C
        FTMPX = OY*EZ - OZ*EY
        FTMPY = OZ*EX - OX*EZ
        FTMPZ = OX*EY - OY*EX
C
        IF((FTMPX.EQ.0).AND.(FTMPY.EQ.0).AND.(FTMPZ.EQ.0))THEN
C
C
        FVX=0
        FVY=0
        AVX=0
        AVY=0
        FLAG=1
        GO TO 10
C
C
        ELSE
C
        FLAG = 0
        FMAG = SQRT(FTMPX*FTMPX+FTMPY*FTMPY+FTMPZ*FTMPZ)
C
        FX = FTMPX/FMAG
        FY = FTMPY/FMAG
        FZ = FTMPZ/FMAG
C
        FVX = IMV*(X*FZ - Z*FX)/(Z*Z + Z*FZ)
        FVY = IMV*(Y*FZ - Z*FY)/(Z*Z + Z*FZ)
C
        AX = EOSPC*(FY*OZ-FZ*OY)/(
     1     EX*(FY*OZ-OY*FZ)+EY*(OX*FZ-FY*OZ)+EZ*(OY*FX-OX*FY))
```

```
C
      AY = AX*(FZ*OX-FX*OZ)/(FY*OZ-FZ*OY)
C
      AZ = (OX*AX+OY*AY)/-OZ
C
C
      AVX = IMV*(X*AZ - Z*AX)/(Z*Z + Z*AZ)
      AVY = IMV*(Y*AZ - Z*AY)/(Z*Z + Z*AZ)
C
   10 END IF
C
      RETURN
      END
C
C$$$$$$$$$$$$$$$$$$$$$$$$$$$$$$$$$$$$$$$$$$$$$$$$$$$$$$$$$$$$$$$$$$$$$$$
C     COMPUTE PERSPECTIVE PLANE FRINGE ANGLE & SPACING
C$$$$$$$$$$$$$$$$$$$$$$$$$$$$$$$$$$$$$$$$$$$$$$$$$$$$$$$$$$$$$$$$$$$$$$$
C
      SUBROUTINE FRCOMP(FVX,FVY,AVX,AVY,FRANG,FRSPC)
      COMMON /FLAGS/ FLAG,FLAGD
      COMMON /PRIN/ PRINT
C
      PI = 3.141592654
      IF(FLAG.EQ.1)THEN
        FRSPC = 1000
      ELSE
        FRSPC  = (AVX*FVY + AVY*-FVX)/(SQRT(FVX*FVX+FVY*FVY))
      END IF
C
      IF(FVX.EQ.0.)THEN
        FRANG=90.
      ELSE
        FRANG= ATAN(FVY/FVX)*180/PI
      END IF
      RETURN
      END
C
C
C$$$$$$$$$$$$$$$$$$$$$$$$$$$$$$$$$$$$$$$$$$$$$$$$$$$$$$$$$$$$$$$$$$$$$$$
C              SORT ARRAY TO SCALE PLOT BOX
C$$$$$$$$$$$$$$$$$$$$$$$$$$$$$$$$$$$$$$$$$$$$$$$$$$$$$$$$$$$$$$$$$$$$$$$
C
      SUBROUTINE SORT(N,VALUE,MAX,MIN)
      REAL MAX,MIN,MAXOLD,MINOLD
C
      IF(N.EQ.1)THEN
      MAX = VALUE
      MIN = VALUE
C
      ELSE
      MAXOLD = MAX
      MINOLD = MIN
```

```
C
        IF(VALUE.GE.MAXOLD)MAX = VALUE
        IF(VALUE.LE.MINOLD)MIN = VALUE
C
        END IF
C
        RETURN
        END
C
C
C$$$$$$$$$$$$$$$$$$$$$$$$$$$$$$$$$$$$$$$$$$$$$$$$$$$$$$$$$$$$$$$$$$$$$$
C                       DRAW  PLOT BOX
C$$$$$$$$$$$$$$$$$$$$$$$$$$$$$$$$$$$$$$$$$$$$$$$$$$$$$$$$$$$$$$$$$$$$$$
C
        SUBROUTINE BOX(PLFLAG, XMIN,YMIN,XMAX,YMAX)
C
        COMMON /UPLOT/ IDEV,POS(4),USCALE(4),LABX(80),LABY(80),
     1  LABT(80),NTKX,NTKY,ITM,MARK,CHWD,CHHT,PTWD,FMTX(6),
     2  FMTY(6)
        BYTE LABX,LABY,LABT,FMTX,FMTY
C
        TYPE *,'ENTER THE X AXIS LABLE.'
        READ(5,1)LABX
    1   FORMAT(80A1)
        TYPE *, 'ENTER THE Y AXIS LABLE.'
        READ(5,2)LABY
    2   FORMAT(80A1)
        TYPE *, 'ENTER THE PLOT TITLE.'
        READ(5,3)LABT
    3   FORMAT(80A1)
C
C
        IF(PLFLAG.EQ.1)THEN
         TYPE*,'ENTER XMIN,YMIN,XMAX,YMAX AND NTKX,NTKY FOR PLOT'
         ACCEPT*,USCALE(1),USCALE(2),USCALE(3),USCALE(4),NTKX,
     1           NTKY
        ELSE
C
          USCALE(1)=XMIN-.1*(XMAX-XMIN)
          USCALE(2)=YMIN-.1*(YMAX-YMIN)
          USCALE(3)=XMAX+.1*(XMAX-XMIN)
          USCALE(4)=YMAX+.1*(YMAX-YMIN)
C
        END IF
C
        CALL GEDBOX
C
        RETURN
        END
C
C
C$$$$$$$$$$$$$$$$$$$$$$$$$$$$$$$$$$$$$$$$$$$$$$$$$$$$$$$$$$$$$$$$$$$$$$
```

*** APPENDIX B ***

LISTING FOR PROGRAM THAT COMPUTES AND PLOTS ANALYTICALLY CONSTRUCTED FRINGE PATTERNS

The following is the listing for the program that was developed to compute and the fringe pattern observed on a flat diffusely reflecting object. The program was developed based on the relations derived in section 3.3.

```
C$$$$$$$$$$$$$$$$$$$$$$$$$$$$$$$$$$$$$$$$$$$$$$$$$$$$$$$$$$$$$$$$$$$
C
C                          FRINGEPLT.FTN
C
C        PROGRAM FOR DRAWING THE MOIRE FRINGES OBSERVED
C        ON THE VIEWING PLANE OF A PROJECTION MOIRE SYSTEM
C        FOR A PLANAR OBJECT.C
C
C        Author: J. Wander
C        Date: Aug., 1984
C
C$$$$$$$$$$$$$$$$$$$$$$$$$$$$$$$$$$$$$$$$$$$$$$$$$$$$$$$$$$$$$$$$$$$
C
C
         DIMENSION PLTX1(601),PLTY1(601),PLTX2(601),PLTY2(601),
     1   FO1(600),FO2(600)
         COMMON /FIRST/ SV
         COMMON /UPLOT/ IDEV,POS(4),USCALE(4),LABX(80),LABY(80),
     1   LABT(80),NTKX,NTKY,ITM,MARK,CHWD,CHHT,PTWD,FMTX(6),
     2   FMTY(6)
         BYTE LABX,LABY,LABT,FMTX,FMTY
         COMMON /TTOO/ T11,T12,T13,T14,T15,T16,T17,T18,T19,
     1   T1X,T1Y,T1Z
         COMMON /TTDD/ T21,T22,T23,T24,T25,T26,T27,T28,T29,
     1   T2X,T2Y,T2Z
         COMMON /FFOO/T1,T2,T3,T4,T5,T6,T7,T8,T9,SP,PV,PP,
     1   CAL,SAL,XPO,YPO,ZPO
         COMMON /THIRD/ OLDMSS,DRWFLG
         COMMON /FORTH/ OLDMSX,DRWFLX
         COMMON /TMP/ NOPLT
         COMMON /PHASE/ PHASEP,PHASEV
C
C
C
C
C$$$$$$$$$$$  ENTER THE PROJECTION SYSTEM GEOMETRY  $$$$$$$$$$$
C
C
     1   TYPE*,'ENTER PROJ. SYSTEM TRANSFORM ANG., PSI,ZETA,
      1        THETA'
         ACCEPT*,PSIP,ZETP,THEP
         TYPE*,'ENTER XPO,YPO,ZPO FOR THE PROJ.SYSTEM'
```

```
      ACCEPT*,XPO,YPO,ZPO
      TYPE*,'ENTER ALF, THE VIEW. GRID ANG. FROM THE Y AXIS'
      ACCEPT*,ALF
      TYPE*,'ENTER PP AND PV, THE GRID PITCHES'
      ACCEPT*,PP,PV
      TYPE *,'ENTER THE IMAGE DISTANCES; SV,SP'
      ACCEPT*,SV,SP
      TYPE *,'ENTER THE PHASE FOR THE PROJ. AND VIEW. GRIDS,
     1          0-1'
      ACCEPT*,PHASEP,PHASEV
    2 TYPE*,'WOULD YOU LIKE TO CHANGE THE PARAMETERS Y=1,
     1        0=N'
      ACCEPT*,CHANGE
      IF (CHANGE.EQ.1)GO TO 1
C
      SAL=SIN(ALF)
      CAL=COS(ALF)
      CPSP=COS(PSIP)
      SPSP=SIN(PSIP)
      CZEP=COS(ZETP)
      SZEP=SIN(ZETP)
      CTHP=COS(THEP)
      STHP=SIN(THEP)
C
C
C$$$$  COMPUTE THE TRANSFORM ELEMENTS FOR THE PROJ. FRAME  $$$$
C
C
      T1=CPSP*CZEP
      T2=SPSP*CTHP+CPSP*SZEP*STHP
      T3=SPSP*STHP-CPSP*SZEP*CTHP
      T4=-SPSP*CZEP
      T5=CPSP*CTHP-SPSP*SZEP*STHP
      T6=CPSP*STHP+SPSP*SZEP*CTHP
      T7=SZEP
      T8=-CZEP*STHP
      T9=CZEP*CTHP
C
C
C$$$$$$$$$  ENTER THE GEOMETRY FOR THE OBJECT PLANE  $$$$$$$$$
C
C
      IF(REPEAT.EQ.0)THEN
   4  TYPE*,'ENTER THE OBJECT PLANE WIDTH AND HEIGHT, (MM)'
      ACCEPT*,WIDTH,HEIGHT
      TYPE*,'ENTER THE OBJECT SYSTEM ORIGIN LOCATION, XL,YL,
     1        ZL'
      ACCEPT*,XL,YL,ZL
      TYPE*,'ENTER NOMINAL OBJECT FRAME ROTATIONS, PSI, ZETA'
      ACCEPT*, PSIO,ZETO
      TYPE*,'ENTER THE OBJECT SHIFT THEN ZETA DEFLECTION'
      ACCEPT*,OBSFT,ZETAD
      ELSE
      TYPE*,'WOULD YOU LIKE TO CHANGE THE OBJECT, 1=Y,0=N'
      ACCEPT*,OBJCHG
```

```
        IF(OBJCHG.EQ.1)GO TO 4
        END IF
C
        CZEO=COS(ZETO)
        SZEO=SIN(ZETO)
        CPSO=COS(PSIO)
        SPSO=SIN(PSIO)
C
C
C$$$$$$$$  COMPUTE TRANSFORM ELEMENTS FOR OBJECT FRAME  $$$$$$$
C
C
        T11=CPSO*CZEO
        T12=-SPSO
        T13=CPSO*SZEO
        T14=SPSO*CZEO
        T15=CPSO
        T16=SPSO*SZEO
        T17=-SZEO
        T18=0.
        T19=CZEO
        T1X = XL
        T1Y = YL
        T1Z = ZL
C
C$$$$$$$$$ COMPUTE TRANSFORM FOR OBJECT DEFLECTION  $$$$$$$$$$
C
        CZED = COS(ZETAD)
        SZED = SIN(ZETAD)
C
        T21 = CZED
        T22 = 0.
        T23 = SZED
        T24 = 0.
        T25 = 1.
        T26 = 0.
        T27 = -SZED
        T28 = 0.
        T29 = CZED
        T2X = 0.
        T2Y = 0.
        T2Z = OBSFT
C
C$$$$$$$$$$$$  INITIALIZE THE PLOTTING PARAMETERS  $$$$$$$$$$$$
C
C
        TYPE *,'DO YOU WANT PLOTTING TERMINAL OR HARD COPY, 0,1.'
        ACCEPT *,QUEST
        IDEV=QUEST
        POS(1)=2000.
        POS(2)=2000.
        POS(3)=7000.
        POS(4)=7000.
        NTKX=5
        NTKY=5
```

```
        ITM=0
        CHWD=.18
        CHHT=.36
        PTWD=.22
        FMTX(1)='f'
        FMTX(2)='6'
        FMTX(3)='.'
        FMTX(4)='2'
        FMTY(1)='f'
        FMTY(2)='6'
        FMTY(3)='.'
        FMTY(4)='2'
C
C
C$$$$$$$$$$$$ SCAN OBJECT AND DRAW FRINGE LINES  $$$$$$$$$$$$$$
C
C
        TYPE*,'ENTER THE SEARCH INCREMENT ON OBJECT (MM)'
        ACCEPT*, OBJSTP
        TYPE *,'ENTER THE FRINGE ERROR TOLERANCE'
        ACCEPT*,DELT
        TYPE*,'ENTER THE NUMBER OF STEPS ON Y AXIS'
        ACCEPT*, YSTEPS
        TYPE *,'ENTER PLOTING CHOICE, PLOT = 1, NO PLOT = 0'
        ACCEPT *, NOPLT
C
C$$$$   DRAW OBJECT
        CALL OBJDRW(WIDTH,HEIGHT)
C
C$$$    SCAN PTS, TEST PT, TRANSFORM PT, DRAW PT
        DRWFLG = 1
        DRWFLX = 1
        OLDMSS = 1
        OLDMSX = 1
C
        AAAA=WIDTH/OBJSTP
        REPEAT=NINT(AAAA)
        DELTX=WIDTH/REPEAT
        DELTY=HEIGHT/YSTEPS
        J = 1
        K = 1
C
        DO 20 I=1,YSTEPS+1
        DO 10 N=1,REPEAT+1
        YO=-HEIGHT/2+DELTY*(I-1)
        XO=-WIDTH/2+DELTX*(N-1)
        CALL TRANSO(XO,YO,XS,YS,ZS)
        CALL COMPFO(XS,YS,ZS,XV,YV,FO)
C
        CALL TESDRA(DELT,FO,TEST)
        FOX = FO + .5
        CALL TESDRX(DELT,FOX,TESTX)
C
C$$$$$$$ AS OPTION PRINT SEARCH DATA INSTEAD OF PLOTTING $$$$$$
C
```

```
        IF(NOPLT.EQ.0)THEN
        WRITE(6,*)'-------------- I,N,DELTX,DELTY-------------'
        WRITE(6,*)I,N,DELTX,DELTY
        WRITE(6,*)'-------------XO,YO,XS.YS,ZS----------------'
        WRITE(6,*)XO,YO,XS,YS,ZS
        WRITE(6,*)'-----------------XV,YV,FO----------------'
        WRITE(6,*)XV,YV,FO
        WRITE(6,*)'-------------PREOLD,PREM,TEST------------'
        WRITE(6,*)PREOLD,PREM,TEST
        ELSE
C
C$$$$$$$$$$$$$$$$$$$$ STORE FRINGE CENTERS $$$$$$$$$$$$$$$$$$
C
          IF (TEST.EQ.0)GO TO 9
          FO1(J) = FO
          PLTX1(J) = XV
          PLTY1(J) = YV
          J = J+1
    9     IF(TESTX.EQ.0)GO TO 10
          FO2(K) = FO
          PLTX2(K) = XV
          PLTY2(K) = YV
          K = K+1
        END IF
   10   CONTINUE
   20   CONTINUE
        IPLT1 = J-1
        IPLT2 = K-1
   30   CONTINUE
        MARK = 1
        CALL GEDPLT(PLTX1,PLTY1,IPLT1,1)
        MARK = 4
        CALL GEDPLT(PLTX2,PLTY2,IPLT2,1)
        CALL GEDCLR
C
C$$$$$$$$$$$$ AS OPTION PRINT THE FRINGE CENTER DATA $$$$$$$$$$
C
        TYPE*,'DO YOU WANT TO PRINT FRINGE POINTS 1=Y,0=N'
        ACCEPT*, PRTFRI
        IF(PRTFRI.EQ.1)THEN
        WRITE(6,*)' '
        WRITE(6,*)'--------- bright fringe centers ----------'
        WRITE(6,*)' '
        WRITE(6,*)'-----------*---------*---------*----------'
        WRITE(6,*)'          order    xv (mm)   yv (mm)       '
        WRITE(6,*)'-----------*---------*---------*----------'
        DO 50 N=1,IPLT1
        WRITE(6,45)FO1(N),PLTX1(N),PLTY1(N)
   45   FORMAT(6X,3F10.3)
   50   CONTINUE
        WRITE(6,*)'-----------*---------*---------*----------'
        WRITE(6,*)' '
        WRITE(6,*)' '
        WRITE(6,*)'---------  dark fringe centers  ----------'
        WRITE(6,*)' '
```

```
      WRITE(6,*)'-----------*---------*---------*----------'
      WRITE(6,*)'          order    xv (mm)   yv (mm)       '
      WRITE(6,*)'-----------*---------*---------*----------'
      WRITE(6,*)' '
      DO 60 N=1,IPLT2
      WRITE(6,55)FO2(N),PLTX2(N),PLTY2(N)
   55 FORMAT(6X,3F10.3)
   60 CONTINUE
      WRITE(6,*)'-----------*---------*---------*----------'
C
      ELSE
      END IF
      TYPE*,'WOULD YOU LIKE TO DO IT AGAIN... Y = 1, N = 0'
      ACCEPT *, REPEAT
      IF(REPEAT.EQ.1)GO TO 2
      STOP
      END
C
C$$$$$$$$$$$$$$$$$$$$$$$$$$$$$$$$$$$$$$$$$$$$$$$$$$$$$$$$$$$$$$$$
C                        SUBROUTINES
C$$$$$$$$$$$$$$$$$$$$$$$$$$$$$$$$$$$$$$$$$$$$$$$$$$$$$$$$$$$$$$$$
C
C$$$$$$$$$  TRANSFORM OBJECT COORD. TO SYSTEM COORD.  $$$$$$$$$
C
C
      SUBROUTINE TRANSO(XO,YO,XS,YS,ZS)
      COMMON /TTOO/ T11,T12,T13,T14,T15,T16,T17,T18,T19,
     1 T1X,T1Y,T1Z
      COMMON /TTDD/ T21,T22,T23,T24,T25,T26,T27,T28,T29,
     1 T2X,T2Y,T2Z
      COMMON /UPLOT/ IDEV,POS(4),USCALE(4),LABX(80),LABY(80),
     1 LABT(80),NTKX,NTKY,ITM,MARK,CHWD,CHHT,PTWD,FMTX(6),
     2 FMTY(6)
      BYTE LABX,LABY,LABT,FMTX,FMTY
C
C
      ZO = 0.
      XOD=T21*XO+T22*YO+T23*ZO+T2X
      YOD=T24*XO+T25*YO+T26*ZO+T2Y
      ZOD=T27*XO+T28*YO+T29*ZO+T2Z
C
      XS=T11*XOD+T12*YOD+T13*ZOD+T1X
      YS=T14*XOD+T15*YOD+T16*ZOD+T1Y
      ZS=T17*XOD+T18*YOD+T19*ZOD+T1Z
C
      RETURN
      END
C
C
C$$$$  COMPUTATION OF THE FRINGE ORDER AT A POINT XS,YS,ZS  $$$$
C
C
      SUBROUTINE COMPFO(XS,YS,ZS,XV,YV,FO)
      COMMON /FIRST/ SV
      COMMON /FFOO/T1,T2,T3,T4,T5,T6,T7,T8,T9,SP,PV,PP,
```

```
     1  CAL,SAL,XPO,YPO,ZPO
        COMMON /PHASE/ PHASEP,PHASEV
C
C$$$    COMPUTE CORRESPONDING COORDS. ON VIEWING PLANE
        XV=-XS*SV/ZS
        YV=-YS*SV/ZS
C
C$$$    TRANSFORM POINT TO PROJ. FRAME & TRACE TO PROJ. PLANE
        XSP=((XS-XPO)*T1+(YS-YPO)*T2+(ZS-ZPO)*T3)
        ZSP=((XS-XPO)*T7+(YS-YPO)*T8+(ZS-ZPO)*T9)
        XP=-XSP*SP/ZSP
C
C$$$    COMPUTE FRINGE ORDER
        FO = ((XV*CAL-YV*SAL)/PV+PHASEV) - (XP/PP+PHASEP)
C
        RETURN
        END
C
C
C$$$$$$$$$$$$$  TEST IF XV,YV,FO  IS ON A FRINGE  $$$$$$$$$$$$$
C
C
        SUBROUTINE TESDRA(DELT,FO,TEST)
        REAL OLDMSS
C
        COMMON /THIRD/ OLDMSS,DRWFLG
        TEST=0
        FON = NINT(FO)
        FMISS = ABS(FON - FO)
        IF(FMISS.GT.0.2)THEN
          DRWFLG = 1
        ELSE
        END IF
        IF(FMISS.GE.DELT)GO TO 10
        IF(FMISS.LT.OLDMSS)GO TO 10
        IF(DRWFLG.EQ.0)THEN
          TEST = 0
          GO TO 20
          ELSE
          TEST=1
          DRWFLG = 0
          GO TO 20
        END IF
   10   TEST=0
   20   OLDMSS = FMISS
        RETURN
        END
C
C
        SUBROUTINE TESDRX(DELT,FOX,TESTX)
        REAL OLDMSX
C
        COMMON /FORTH/ OLDMSX,DRWFLX
        TESTX=0
        FONX = NINT(FOX)
```

```
        FMISSX = ABS(FONX - FOX)
        IF(FMISSX.GT.0.2)THEN
          DRWFLX = 1
        ELSE
        END IF
        IF(FMISSX.GE.DELT)GO TO 10
        IF(FMISSX.LT.OLDMSX)GO TO 10
        IF(DRWFLX.EQ.0)THEN
          TESTX = 0
          GO TO 20
          ELSE
          TESTX=1
          DRWFLX = 0
          GO TO 20
        END IF
   10   TESTX=0
   20   OLDMSX = FMISSX
        RETURN
        END
C
C
C$$$$$$$$ DRAW THE OBJECT PLANE ON THE VIEWING PLANE $$$$$$$$$
C
C
        SUBROUTINE OBJDRW(WIDTH,HEIGHT)
C
        DIMENSION XXO(5),YYO(5),ZZO(5),XXS(5),YYS(5),ZZS(5),
     1  XXV(10),YYV(10)
        COMMON /FIRST/ SV
        COMMON /UPLOT/ IDEV,POS(4),USCALE(4),LABX(80),LABY(80),
     1  LABT(80),NTKX,NTKY,ITM,MARK,CHWD,CHHT,PTWD,FMTX(6),
     2  FMTY(6)
        BYTE LABX,LABY,LABT,FMTX,FMTY
        COMMON / TMP/ NOPLT
        XXO(1)=-WIDTH/2
        XXO(2)=WIDTH/2
        XXO(3)=WIDTH/2
        XXO(4)=-WIDTH/2
        XXO(5)=-WIDTH/2
        YYO(1)=-HEIGHT/2
        YYO(2)=-HEIGHT/2
        YYO(3)=HEIGHT/2
        YYO(4)=HEIGHT/2
        YYO(5)=-HEIGHT/2
C
        DO 10 N=1,5
        CALL TRANSO(XXO(N),YYO(N),XXS(N),YYS(N),ZZS(N))
        XXV(N)=-XXS(N)*SV/ZZS(N)
        YYV(N)=-YYS(N)*SV/ZZS(N)
   10   CONTINUE
C
        TYPE*,'THIS IS WHAT IS SENT/RETURNED TO TRANSO IN
     1        OBJDRW'
        DO 11 K=1,5
        WRITE(5,12)XXO(K),YYO(K),XXS(K),YYS(K),ZZS(K)
```

```
   12    FORMAT(2X,5F13.4)
   11    CONTINUE
C
C
         MARK=0
         CALL BOX
         IF(NOPLT.EQ.0)GO TO 1
         CALL GEDPLT(XXV,YYV,5,1)
    1    RETURN
         END
C
C
C$$$$$$$$$$$$$$$$$  DRAW INITIAL PLOT BOX  $$$$$$$$$$$$$$$$$$$
C
C
         SUBROUTINE BOX
         COMMON /UPLOT/ IDEV,POS(4),USCALE(4),LABX(80),LABY(80),
     1   LABT(80),NTKX,NTKY,ITM,MARK,CHWD,CHHT,PTWD,FMTX(6),
     2   FMTY(6)
         BYTE LABX,LABY,LABT,FMTX,FMTY
         COMMON /TMP/ NOPLT

C
         TYPE *,'ENTER THE PLOT SIDE LENGHT'
         ACCEPT *,SCALE
         USCALE(1)=-SCALE/2
         USCALE(2)=-SCALE/2
         USCALE(3)=SCALE/2
         USCALE(4)=SCALE/2
         TYPE *,'ENTER THE X AXIS LABLE.'
         READ(5,1)LABX
    1    FORMAT(80A1)
         TYPE *, 'ENTER THE Y AXIS LABLE.'
         READ(5,2)LABY
    2    FORMAT(80A1)
         TYPE *, 'ENTER THE PLOT TITLE.'
         READ(5,3)LABT
    3    FORMAT(80A1)
C
         IF(NOPLT.EQ.0)GO TO 4
         CALL GEDBOX
C
    4    RETURN
         END
C
C
C$$$$$$$$$$$$$$$$$$$$$$$$$$$$$$$$$$$$$$$$$$$$$$$$$$$$$$$$$$$$$$$$
C$$$$$$$$$$$$$$$$$$$$$$$$$$$$$$$$$$$$$$$$$$$$$$$$$$$$$$$$$$$$$$$$
C$$$$$$$$$$$$$$$$$$$$$$$$$$$$$$$$$$$$$$$$$$$$$$$$$$$$$$$$$$$$$$$$
```